UNIVERSIDADE DE LISBOA
INSTITUTO SUPERIOR TÉCNICO

In situ resource utilization on Mars using non-equilibrium plasmas

Polina Ogloblina

Supervisor: Doctor Vasco António Dinis Leitão Guerra
Co-supervisors: Doctor Luís Paulo Da Mota Capitão Lemos Alves
Doctor Olivier Guiatella

Thesis approved in public session to obtain the PhD Degree in
Technological Physics Engineering

Jury final classification: **Pass With Distinction**

2020

UNIVERSIDADE DE LISBOA
INSTITUTO SUPERIOR TÉCNICO

In situ resource utilization on Mars using non-equilibrium plasmas

Polina Ogloblina

Supervisor: **Doctor Vasco António Dinis Leitão Guerra**
Co-supervisors: **Doctor Luís Paulo Da Mota Capitão Lemos Alves**
Doctor Olivier Guiatella

Thesis approved in public session to obtain the PhD Degree in
Technological Physics Engineering

Jury final classification: **Pass With Distinction**

Jury

Chairperson:

Doctor Vítor João Rocha Vieira, Instituto Superior Técnico, Universidade de Lisboa

Members of the Committee:

Doctor Vasco António Dinis Leitão Guerra, Instituto Superior Técnico, Universidade de Lisboa

Doctor Nikolay Britun, Center for Low-temperature Plasma Sciences, Nagoya University, Japan

Doctor Carlos Daniel Diogo Matias Pintassilgo, Faculdade de Engenharia, Universidade do Porto

Doctor Mário António Prazeres Lino da Silva, Instituto Superior Técnico, Universidade de Lisboa

Funding institution - Fundação para a Ciência e a Tecnologia

2020

Abstract

Human colonisation on Mars is one of the hottest topics nowadays and is in the focus of space agencies like NASA and ESA, and of private companies such as SpaceX. Since the 1960s, robotic exploration has provided valuable knowledge about the conditions on the planet. Nevertheless, human exploration has not yet been achieved. Ambitious plans of space agencies and private companies promise the first crewed missions to Mars in 2020s and 30s. *In Situ* Resource Utilization (ISRU) can provide materials for life support and propellants, thereby reducing the mass and cost of space exploration missions.

The main component of the Martian atmosphere is carbon dioxide (almost 96%) and it has been proposed to dissociate it to produce oxygen, which can serve as fuel and breathable gas. An experiment based on solid oxide electrolysis is being prepared for a future NASA mission. In this thesis we propose an alternative approach: to use non-equilibrium plasmas for CO_2 dissociation and oxygen production. It is argued that non-equilibrium plasmas can be the most efficient medium to produce oxygen from carbon dioxide and can be applied locally on Mars, where the atmospheric pressure and temperature are auspicious for CO_2 reforming. To do so, one specific vibrational mode of the CO_2 molecule should be pumped, with subsequent climbing into the higher vibrational levels during the relaxation process, in a process that favours dissociation. Changing the gas temperature, plasma density and other parameters of the discharge allows controlling the electron energy and the vibrational distribution functions and, therefore, the oxygen yield.

This work covers a theoretical, experimental and numerical investigation of carbon dioxide plasma-decomposition in low-pressure DC glow-discharges, addressing the electron and vibrational kinetics, the chemistry of the discharge, the influence of the gas temperature and of other species in the plasma, always ensuring an experimental validation of the models. Along the thesis we created an experimental setup with operating conditions of temperature and pressure close to ones observed on Mars; performed an experimental characterization of CO_2 and CO_2-CO plasmas; developed a complete and consistent electron impact cross section set for CO; validated a self-consistent model of CO_2 discharges, including possible reactions with products of decomposition, *e.g.* CO, O_2 and O; and investigated the role of carbon monoxide and oxygen on the vibrational non-equilibrium of CO_2. The ensemble of results obtained builds a strong case in favour of ISRU on Mars using non-equilibrium plasmas and contributes to the definition of a *reaction mechanism*, in the sense of a set of reactions and rate coefficients validated against benchmark experiments, for CO_2 plasmas.

Keywords: In situ resource utilisation, CO_2 dissociation, plasma, oxygen production, glow discharge

Resumo

A colonização de Marte é presentemente um tópico em voga, estando na mira tanto de agências espaciais como a NASA e a ESA como de empresas privadas como a SpaceX. A exploração robótica, iniciada nos anos sessenta do século XX, tem fornecido conhecimento valioso sobre as condições existentes no planeta vermelho. No entanto, nenhum humano chegou ainda a Marte. Os planos mais ambiciosos das agências espaciais e empresas privadas preveem a realização das primeiras missões tripuladas nas décadas de 2020 e 30. A utilização *in-situ* de recursos naturais ("*in-situ* resource utilization," ou ISRU) pode fornecer materiais para o apoio à vida e o fabrico de combustíveis, reduzindo assim o peso e o custo das missões de exploração espacial.

O dióxido de carbono é o principal componente da atmosfera marciana, contribuindo com com quase 96% do total. Existem propostas de o decompor de modo a produzir oxigénio, que pode ser utilizado na produção de combustíveis ou como gás respirável. Uma experiência baseada em electrolisadores de óxido sólido está presentemente a ser preparada para uma missão futura da NASA com este fim. Nesta tese propõe-se uma abordagem alternativa: a utilização de plasmas de não-equilíbrio para a dissociação do CO_2 e a produção de oxigénio. Argumenta-se que os plasmas de não-equilíbrio podem ser o meio mais eficiente de produzir oxigénio a partir do dióxido de carbono e que podem ser utilizados localmente em Marte, onde as condições atmosféricas de pressão e temperatura são auspiciosas para a reciclagem do CO_2. Para o conseguir, um modo vibracional específico do CO_2 deve ser excitado, favorecendo-se em seguida, ao longo do processo de relaxação da energia, uma transferência de energia para os níveis vibracionais mais elevados, num processo que globalmente favorece a dissociação. O ajuste da temperatura do gás, da densidade do plasma, bem como de outros parâmetros da descarga, permite o controlo da função de distribuição da energia dos electrões e da função de distribuição vibracional e, consequentemente, da taxa de produção de oxigénio.

Este trabalho consite numa investigação experimental, teórica e de simulação numérica da decomposição do dióxido de carbono por plasmas em descargas luminescentes, debruçando-se sobre as cinéticas electrónica e vibracional, a química da descarga, e a influência da temperatura do gás e de outras espécies que não o CO_2 na descarga, assegurando sempre uma validação experimental dos modelos. No decorrer da tese foi criada uma montagem experimental capaz de operar em condições de temperatura e pressão semelhantes àquelas observadas em Marte; foi levada a cabo uma caracterização experimental de plasmas de CO_2 e CO_2-CO; foi desenvolvido um conjunto completo e consistente de secções eficazes de colisão por impacto electrónico para o CO; foi validado um modelo auto-consistente para descargas em CO_2, incluindo as reacções envolvendo os produtos da decomposição do CO_2, *e.g.* CO, O_2 e O; e foi investigado o papel do monóxido de carbono e do oxigénio no não-equilíbrio vibracional das moléculas de CO_2. O conjunto de resultados obtido constrói um caso forte a favor da ISRU em Marte usado plasmas de não-equilíbrio e contribui para a definição de um *mecanismo de reacção* – no sentido de obter um conjunto de reacções e coeficientes de reacção validados por comparação de simulações com experiências de referência – para plasmas de dióxido de carbono.

Palavras-chave: Utilização in-situ de recursos naturais, dissociação do CO_2, plasma, produção

de oxigénio, descarga luminescente

Acknowledgements

First of all, I would like to thank my supervisor Vasco Guerra. I am extremely grateful for your help with any difficulty I encountered and your support not only as a supervisor but also as a friend. Your acknowledgment and appreciation of small achievements to milestones have been very supportive throughout the Ph.D. Thank you for the guidance throughout my PhD and always finding the time for me. This thesis would not have been made without your lead and support during these four years.

I would like to express my sincere appreciation to Dr Olivier Guiatella, my co-supervisor. You have encouraged me to work harder while maintaining a healthy work-life balance. Your assessment and evaluation of the results has been crucial for the thesis work. Thanks for the experimental freedom you gave me while making sure the CO levels remained within tolerable levels. It was a real pleasure working with you.

I would like to thank Dr Luís Lemos Alves, my co-supervisor. Thank you for welcoming me into N-PRiME team and safe-guarding the scientific progress of my PhD project.I consider myself fortunate to work under your supervision and learn from your expertise. I am extremely grateful for your willingness to discuss difficulties I encountered throughout my research.

I am also deeply indebted to Ana Sofia Morillo-Candas for all the assistance and support you offered with the experimental setup. Thank you for sharing your knowledge and helping me solve countless problems along the way. I would also like to thank Tiago Silva for the help you provided and many direct and indirect contributions you made to this thesis and to the team. I have learnt a great deal with you. I thank my fellow lab- and officemates Loann Terras, Alejandro Alvarez Laguna, Constance Lapous and Florian Marmuse. I would like to thank you all for the emotional support and guidance you provided into my french life.

Thank you, Jihane Kamil, for experiencing Paris together with Parisian chic and showing what our true strengths are. Thank you my dear friends, Domenica and Ridhima, for being always by my side and experiencing many happy memories together. Thank you for making me laugh even during the hard times.

And finally, I would like to thank my family. My mother, who always believed in me and pushed me into hardships to teach me. And Eugene, who supported me during these years, pulled into the adventures and let us both pursue our dreams.

Contents

Contents vii

List of Figures ix

List of Tables xvi

1 General introduction and state of the art 1
- 1.1 Motivation . . . 1
  - 1.1.1 *In situ* resource utilization on Mars . . . 1
  - 1.1.2 Solid Oxide Electrolysis (SOEC) . . . 3
- 1.2 Non-equilibrium CO_2 plasma for oxygen production on Mars . . . 5
  - 1.2.1 CO_2 molecule and ways to dissociate it . . . 5
  - 1.2.2 Why using non-thermal plasmas on Mars . . . 7
  - 1.2.3 Advantages of the non-equilibrium plasma over SOEC for oxygen production on Mars . . . 8
- 1.3 Overview of CO_2 reforming from modeling point of view . . . 9
- 1.4 Objectives . . . 11
- 1.5 Original contributions . . . 12
- 1.6 Outline . . . 12

Bibliography . . . 14

2 The case for *in situ* resource utilization 21
- 2.1 Introduction . . . 22
- 2.2 Results and discussion . . . 23
- 2.3 Conclusions . . . 26

Bibliography . . . 28

3 CO cross section and CO_2/CO electron kinetics 31
- 3.1 Introduction . . . 32
- 3.2 Description of the electron cross section set in CO . . . 34
  - 3.2.1 Overview . . . 34
  - 3.2.2 Elastic and rotational excitation cross sections . . . 34
  - 3.2.3 Other inelastic cross sections . . . 40
- 3.3 Validation . . . 41
- 3.4 Electron kinetics in CO_2 - CO mixtures . . . 45
  - 3.4.1 Electron energy distribution functions . . . 46
  - 3.4.2 Electron impact rate coefficients . . . 48
  - 3.4.3 Power balance . . . 50
- 3.5 Conclusions . . . 52

Bibliography . . . 53

4 *In situ* oxygen and propellant production on Mars 59
4.1 Introduction . . . 60
4.2 Experiment . . . 61
4.3 Model . . . 62
4.4 Results and Discussion . . . 64
4.4.1 CO_2 plasma chemistry at Mars and Earth temperature conditions . . . 65
4.4.2 CO_2 vibrational kinetics at Mars and Earth temperature conditions . . . 72
4.4.3 Synthetic Martian atmosphere . . . 74
4.5 Conclusions . . . 77
Bibliography . . . 79

5 Influence of carbon monoxide on CO_2 plasma 85
5.1 Introduction . . . 86
5.2 Experimental setup . . . 87
5.3 Model . . . 88
5.4 Results and discussion . . . 88
5.4.1 Influence of the current and pressure on CO_2/CO plasmas . . . 88
5.4.2 Influence of the CO concentration . . . 93
5.4.3 Importance of the oxygen atoms and wall reactions on vibrational temperatures of CO_2 . . . 95
5.5 Conclusions . . . 99
Bibliography . . . 100

6 Conclusions 103

A Appendix - Input files 107
A.1 CO_2 reactions . . . 107
A.2 O_2 and O reactions . . . 108
A.3 CO reactions . . . 109
A.3.1 Flow . . . 109
A.3.2 Electron-impact . . . 109
A.4 CO_2 vib wall deactivation reactions . . . 109
A.5 CO_2-O VT reactions . . . 109
A.6 CO_2-O_2 VT reactions . . . 109
A.7 CO_2-CO_2 VT reactions . . . 109
A.8 CO_2-CO_2 VV reactions . . . 112

List of Figures

1.1 Curiosity rover "selfie" on its mission taken in location nicknamed "Glen Etive". Image is taken from [1]. 1

1.2 Reactions across a SOEC cell. Image is taken from [2] 3

1.3 Two SOEC stacks with 11 cell each. A center voltage tab (green) separates the two stacks. Image is taken from [2] 4

1.4 Schematic outline of MOXIE subsystems (top). MOXIE design (bottom left) and its location on the Mars 2020 Perseverance rover (bottom right). Images are taken from [3, 4]. 5

1.5 Vibrational modes of a CO_2 molecule. a) Symmetric stretching mode, characterized by quantum number ν_1. b) Asymmetric stretching mode of vibration, with quantum number ν_3. c) Bending mode ν_2 with vibrations in two orthogonal planes. The figure is taken from [5]. 6

1.6 Schematic representation of the potential curve of the O=CO bond and electronic and vibrational levels of CO_2 molecule. Two dissociation mechanisms are shown: electron impact dissociation and vibrational ladder-climbing mechanism. The figure is taken from [6]. 6

1.7 Summary of the CO_2 conversion, χ, and energy efficiency, η, results obtained in the literature using different plasma sources. Here E_s correspond to constant specific energy input - the energy spent for dissociation of one CO_2 molecule in the discharge. The figure is taken from [7]. 10

2.1 Time evolution of the gas (– ·) and the T_3 characteristic temperature for a DC pulsed discharge at p = 5 Torr, I = 50 mA, Δt = 5 ms: (—) Earth; (– –) Mars; (···) the same as "Mars," but with $n_e = 5.5 \times 10^9$ cm^{-3}; (—) Earth without VV up-pumping; (– –) Mars without VV up-pumping. 24

2.2 Logarithm of the normalised densities of the first level of the symmetric stretching, bending and asymmetric stretching modes, for a DC pulsed discharge at p = 5 Torr, I = 50 mA, Δt = 5 ms: on (—) Mars; on (– –) Earth. 25

2.3 Time evolution of the ratio of different characteristic temperatures on a DC pulsed discharge at p = 5 Torr, I = 50 mA, Δt = 5 ms: (—) T_3/T_g; (– –) T_{12}/T_g; (···) T_3/T_{12} for discharges on Mars and Earth. 26

3.1 Summary of the IST-Lisbon set of electron-impact cross sections for CO, as a function of the electron kinetic energy. Here, for mere representation purposes, both the rotational and the vibrational cross sections are total cross sections, calculated as the sum of contributions from the individual levels, weighted by their populations for a Boltzmann distribution at T_g = 300 K. 37

3.2 (a) 0→1 rotational cross section calculated from the Born approximation with μ = $4.4 \cdot 10^{-2}$ (– –) and $1.5 \cdot 10^{-2}$ (···), proposed in the calculations from [59] (▲), [60] (– –), [62] (– –), and used in this work (—); (b) Proposed elastic cross section (—) , effective momentum transfer cross section from [38] (···) and total rotational excitation cross section (– –) assuming that the populations of the rotational states follow a Boltzmann distribution with temperature T_{rot} = 300 K. 39

3.3 Vibrational excitation cross section for the first 5 transitions $v_i = 0 \rightarrow v_f = 1 - 5$ [40]. The dotted line represents the near threshold region of the 0→1 cross section proposed by Phelps [41] (included in the IST-Lisbon set). 41

3.4 Calculated and measured reduced electron mobility in CO as a function of E/N for T_{gas} = 300 K (a) and T_{gas} = 77 K (b); the symbols are experimental data from ■ [69], • [70], ▲ [71], ♦ [72],▼ [73]; the solid curves are calculations performed with the current cross section set; dashed lines replace the cross section for the excitation of the first vibrational level with that proposed in [40] (without the contribution from non-resonant excitation); dotted curves neglect the rotational excitation/deexcitation processes; black/red curves consider the elastic momentum transfer cross section from the current set or replace it with the effective momentum transfer cross section from [42]. 42

3.5 Calculated and measured characteristic energy in CO as a function of E/N, for: (a) T_{gas} = 300 K with experimental results from [72] and (b) T_{gas} = 77 K with experimental results from [74]. The curves are as in fig. 3.4. 43

3.6 Calculated and measured reduced ionization coefficient in CO, as a function of E/N. The symbols represent experimental data from: ■ [75]; • [76]; and ▲ [77]. The lines are calculations obtained with the IST-Lisbon (—), IST-Lisbon with $a'\ ^3\Sigma^+$ cross section from Sawada [51] (– –) and the "effective" [42](—) data sets. 44

3.7 The ratio of the anisotropic (f_1) and isotropic (f_0) components of the electron velocity distribution function, as a function of the electron energy, for different values of E/N. 45

3.8 Electron Energy Distribution Functions in pure CO (a) and pure CO_2 (b), for E/N = 0.01 (—), 1 (—), 10 (—) and 50 Td (—), accounting (—) and neglecting (– –) superelastic collisions from vibrationally excited states, for T_{CO} = 3000 K (a) and T_{12} = 1500 K and T_3 = 4000 K (b). 46

3.9 Electron Energy Distribution Functions for E/N = 1 (—), 10 (—) and 50 Td (—): for different values of the vibrational temperatures in pure CO (a) in pure CO_2 (b) and in a CO_2-CO mixture (c). 47

3.10 Electron impact rate coefficients for excitation of the first level of CO_2 asymmetric stretching mode (a) and excitation of the first level of the CO_2 bending mode (b), CO_2 dissociative attachment (c) and CO_2 dissociation (d) as a function of E/N for three different combinations of values of vibrational temperatures (T_{12}, T_3, T_{CO}) in K [(—) (500, 1000, 1000); (—) (1000, 3000, 3000); (—) (1500, 4000, 5000)], and the following CO_2-CO mixture compositions: 100% CO_2 (—), 50% CO_2 (– –) and 10% CO_2 (···). Dissociation (e) electron impact rate coefficients as a function of the CO_2 percentage in CO_2-CO mixture, for the same combination of values of vibrational temperatures as before, and the following E/N values in Td: 10 (—), 50 (– –), 100 (···). Ionization (f) electron impact rate coefficients of CO (—), CO_2 (—) and combined ionization rate coefficient in the mixture (—) as a function of the CO_2 percentage in the CO_2-CO mixture and vibrational temperatures T_{12} = 1000 K, T_3 = 3000 K, T_{CO} = 3000 K and the following E/N values in Td: [80, 100, 200]. 49

3.11 (a) Absolute power per electron of unit gas density, transferred to rotational excitation/de-excitation of CO and vibrational excitation/de-excitation of CO and CO_2, for $T_{CO} = T_{12} = T_3 = T_g$ = 300 K, in pure CO (—) and 50%CO_2-50%CO (– –). (b) Relative (to the power absorbed by the electric field, P_E) net power transfered to different mechanisms, for T_{12} = 500 K and $T_3 = T_{CO}$ = 1000 K and the following CO_2-CO mixtures: 0% CO_2 - 100% CO (—), 10% CO_2 - 90% CO (–·–), 50% CO_2 - 50% CO (– –), 100% CO_2 - 0% CO (···). (c) Relative (to the power absorbed by the electric field, P_E) net power transfered to the total excitation of vibrational levels in CO and CO_2 (—), as well as in the excitation of the first bending (—) and first asymmetric stretching (—) levels of CO_2, for T_{12} = 1000 K and $T_3 = T_{CO}$ = 3000 K and the same mixture composition as in (b). (d) Relative (to the power absorbed by the electric field, P_E) net power transfer in the excitation of the first bending (—) and first asymmetric stretching (—) levels of CO_2 and in dissociation by direct electron impact (—) in pure CO_2, for the following values of (T_{12}, T_3) in K: (···) (500, 1000), (– –) (1000, 3000), (—) (1500, 4000). 51

4.1 Schematic representation of the discharge reactor placed in the sample compartment of the FTIR spectrometer. 62

4.2 Discharge reactor immersed into a mixture of dry ice and ethanol and positioned in the sample compartment of the FTIR when the plasma is OFF (left) and ON (right). 63

4.3 Reduced electric field, E/N, as a function of NR product, when a pure CO_2 discharge is ignited in Mars and Earth background temperatures at currents I = 20 mA (left panel) and I = 50 mA (right panel): experiment (•), self-consistent calculation (—). 66

4.4 CO_2 dissociation fraction when a pure CO_2 discharge is ignited in Mars and Earth background temperatures at currents I = 20 mA (left panel) and I = 50 mA (right panel): experiment (•), model calculations by including (—) and excluding (···) the vibrational kinetics. 67

4.5 Relative contribution (in %) of the main mechanisms of creation and destruction of CO($X\ ^1\Sigma^+$) when a pure CO_2 discharge at p = 5 Torr and I = 50 mA is ignited in Mars and Earth background temperatures, including (colored bars) and neglecting (grey bars) the vibrational kinetics.The reactions are identified in Table 4.1. 68

4.6 Relative density of the dominant species when a pure CO_2 discharge is ignited in Mars and Earth background temperatures at currents I = 20 mA (left panel) and I = 50 mA (right panel). The symbols correspond to experimental data for CO_2 (•) and CO (∘). 69

4.7 Relative density of various electronically excited states and of ozone, when a pure CO_2 discharge is ignited in Mars and Earth background temperatures at currents I = 20 mA (left panel) and I = 50 mA (right panel). 69

4.8 Relative density of various charged particles, when a pure CO_2 discharge is ignited in Mars and Earth background temperatures at currents I = 20 mA (left panel) and I = 50 mA (right panel). 70

4.9 Relative contribution (in %) of the main mechanisms of creation and destruction of $O_2(X\ ^3\Sigma_g^-)$ when a pure CO_2 discharge is ignited at p = 5 Torr and I = 50 mA in Mars and Earth background temperatures, including (colored bars) and neglecting (grey bars) the vibrational kinetics. The reactions are identified in Table 4.1. . . 71

4.10 Relative contribution (in %) of the main mechanisms of destruction of $CO(a\ ^3\Pi_r)$ when a pure CO_2 discharge is ignited at p = 5 Torr and I = 50 mA in Mars and Earth background temperatures, including (colored bars) and neglecting (grey bars) the vibrational kinetics. The reactions are identified in Table 4.1. 71

4.11 Experimental value of the gas temperature T_g (· ⋄ ·), together with the measured (symbols) and calculated (lines) vibrational temperatures of the asymmetric stretching mode T_3 (•, – –) and the common temperature of the bending and symmetric modes T_{12} (⋆, —) and CO vibrational temperature T_{CO} (*square*), when a pure CO_2 discharge is ignited in Mars and Earth background temperatures at currents I = 20 mA (left panel) and I = 50 mA (right panel). 72

4.12 Measured (symbols) and calculated (lines) ratios T_3/T_g (—,⋆) and T_{12}/T_g (···, •) when a pure CO_2 discharge is ignited in Mars and Earth background temperatures at currents I = 20 mA (left panel) and I = 50 mA (right panel). 73

4.13 Reduced electric field, E/N, as a function of NR product, measured when pure CO_2 (•) and 96%CO_2-2%Ar-2%N_2 (∘) discharges are ignited in Mars and Earth background temperatures at currents I = 20 mA (left panel) and I = 50 mA (right panel). 74

4.14 Experimental values of the gas temperature T_g (◆, ◇), the vibrational temperature of the asymmetric stretching mode T_3 (•, ∘) and the common vibrational temperature of the bending and symmetric modes T_{12} (⋆, ⋆) and CO vibrational temperature T_{CO} (■,□), when pure CO_2 (—, closed symbols) and 96%CO_2-2%Ar-2%N_2 (···, open symbols) discharges are ignited in Mars background temperature at currents I = 20 mA (left panel) and I = 50 mA (right panel). 75

4.15 Experimental values of the ratios T_3/T_g (⋆, ⋆) and T_{12}/T_g (•, ∘), when pure CO_2 (—, closed symbols) and 96%CO_2-2%Ar-2%N_2 (···, open symbols) discharges are ignited in Mars background temperature at currents I = 20 mA (left panel) and I = 50 mA (right panel). 75

4.16 Experimental CO_2 dissociation fraction when pure CO_2 (-•-) and 96%CO_2-2%Ar-2%N_2 (· ∘ ·) discharges are ignited in Mars and Earth background temperatures at currents I = 20 mA (left panel) and I = 50 mA (right panel) 76

4.17 Electron Energy Distribution Functions calculated for the experimental values of E/N, T_{12}, T_3 and T_{CO} at p = 3 Torr (left panel) and p = 5 Torr (right panel), I = 50 mA, and Mars background temperature, for pure CO_2 (—) and 96%CO_2-2%Ar-2%N_2 (– –). Additional curves for 96%CO_2-4%Ar (—); 96%CO_2-4%N_2 (—) are calculated for the same conditions as in the CO_2-Ar-N_2 mixture. 77

5.1 Reduced electric field as a function of NR for currents I = 20-50 mA and CO_2/CO initial mixtures 90/10% (left) and 50/50% (right). The symbols correspond to the experimental data, the lines to the self-consistent calculations. 89

5.2 Calculated (lines) and measured (points) relative densities of the main species in the discharge, for currents I = 20 (– –,∘) and 50 (—,•) mA and CO_2/CO initial mixtures 90/10% (left) and 50/50% (right). 90

5.3 Creation and destruction rates of CO(X) molecules as a function of pressure, for a current I = 40 mA and a CO_2/CO initial mixture 50/50%. The reactions that contribute to the creation and loss of CO(X) from/to the excited state CO(a) are indicated with dotted lines (···). Additionally, the (- -) line corresponds to the reaction CO(a)+O_2 → CO_2+ O, that does not destroy CO(X), but removes molecules from the CO manifold. 90

5.4 Relative density of excited species and carbon atom and ozone as a function of pressure, for currents I = 20 (– –) and 50 (—) mA and CO_2/CO initial mixtures 90/10% (left) and 50/50% (right). 91

5.5 Relative densities of various charged particles as a function of pressure, for currents I = 20 (– –) and 50 (—) mA and CO_2/CO mixtures 90/10% (left) and 50/50% (right) in the initial gas input. 91

5.6 Experimental values of the gas temperature, T_g, together with the measured (symbols) and calculated (lines) vibrational temperatures of the bending and symmetric stretching mode, T_{12}, when a discharge is ignited in 90/10% (left) and 50/50 % (right) CO_2/CO mixtures. 92

5.7 Measured (symbols) and calculated (lines) vibrational temperatures of the asymmetric stretching modeof CO_2, T_3, and CO vibrational temperature, T_{CO}, when a discharge is ignited in 90/10% (left) and 50/50% (right) CO_2/CO mixtures. . 93

5.8 Variation of the conversion parameter α at pressure 2 torr and current 40 mA (closed symbols) and 0 mA (open symbols), as a function of the input ratio α_i or CO % (see text) in the gas mixture. 94

5.9 Relative contribution of the main mechanisms of creation and destruction of CO(X) as a function of the input ratio α_i, for pressure p = 2 Torr and current = 40 mA. The reactions that contribute to the creation and loss of CO(X) from/to the excited state CO(a) are indicated with dotted lines (···). Additionally, the (- -) line correspond to the reaction CO(a)+O_2 → CO_2+ O, that does not destroy CO(X), but removes molecules from the CO manifold. 94

5.10 Relative contribution of the main mechanisms of creation and destruction of O(^3P) as a function of the initial CO fraction in the mixture α_i, for pressure p = 2 Torr and current = 40 mA. The reactions that contribute to the creation and loss of O(^3P) from/to the excited state O(^1D) are indicated with dotted lines (···). 96

5.11 Experimental value of the gas temperature, together with measured (symbols) and calculated (lines) vibrational temperatures of the joint symmetric stretching and bending mode T_{12} and the asymmetric stretching mode T_3 (left), and the ratio of T_3/T_g (right) of CO_2, as a function of the input CO fraction α_i, for pressure p = 2 Torr and current I = 40 mA. The different curves correspond to modelling results for the base model (—), chemistry without CO_2-O VT processes (-··-), without vibrational quenching on the wall (- -) and with a varying γ_O (···). 97

5.12 Fitted variation of the wall recombination probability for atomic oxygen, γ_O, as a function of the [O]/[CO] ratio in CO_2/O_2 plasmas [17], measured at p = 2 Torr and I = 40 mA, and extrapolated for CO_2/CO plasmas. 98

List of Tables

1.1 Mars' atmosphere composition [9] 2
1.2 Mars' atmosphere conditions [9] 4

3.1 Summary of the cross section set proposed in this work: elastic collisions, excitations of vibrational states from $CO(X, v = 0)$, excitation of electronic states, ionization, dissociative attachment and dissociation from the ground state CO. . 35
3.2 Summary of the cross section set proposed in this work (cont.): rotational excitation 36
3.3 Summary of the cross section set proposed in this work (cont.): stepwise vibrational excitation 36

4.1 List of some important reactions mentioned in the text. 65
4.2 Measured gas temperature (K) deduced from rotational temperature of CO and CO_2 in pure CO_2 plasmas 66

Chapter 1

General introduction and state of the art

1.1 Motivation

1.1.1 *In situ* resource utilization on Mars

Human colonisation of Mars is one of the hottest topics nowadays and is in the focus of space agencies such as National Aeronautics and Space Administration (NASA) and European Space Agency (ESA) and companies as SpaceX. Since 1960s humankind was driven to explore this planet by sending probes and rovers. Though many failed, there have been eight long-operating rovers and landers on the surface of Mars, two of those still working at the time of writing this thesis [10] (see Curiosity rover in figure 1.1). Robotic exploration allowed to gain valuable

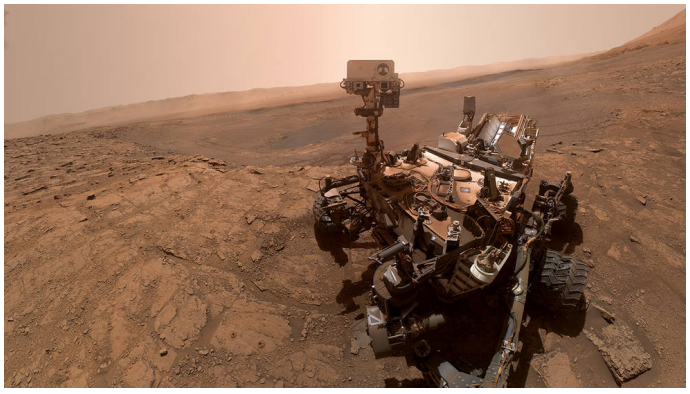

Figure 1.1: Curiosity rover "selfie" on its mission taken in location nicknamed "Glen Etive". Image is taken from [1].

information about the weather, climate and geology of the planet and encouraged the preparation for future human exploration. Each year more and more Mars-realted proposals from space agencies are announced. For example, the ExoMars program launched by ESA is planning to land the first European rover by 2023, while NASA is going to create a base camp on the Earth's moon by the end of 2020s as a stepping stone to a Mars expedition planned for 2030s [11]. Private companies, such as SpaceX, are further encouraging the space race by promising first crewed flights in 2024 and successfully performing intermediate steps [12]. The Chinese National Space

Table 1.1: Mars' atmosphere composition [9]

Carbon dioxide (CO_2)	95.32 - 96 %
Nitrogen (N_2)	1.9 - 2.6 %
Argon (Ar)	1.6 - 1.9 %
Oxygen (O_2)	0.174 %
Carbon monoxide (CO)	0.0747 %
Water vapour	0.03 % (variable)

Administration, Japan Aerospace Exploration Agency, United Arab Emirates Space Agency, Russian Roscosmos, Blue Origin, Virgin Galactic and Boeing have all expressed their interest in Mars landing and, therefore, are creating a competitive environment. All of these initiatives and the accelerating development of space technologies are a clear indicator that in the near future humans will most likely step on Mars.

A manned trip to Mars brings many of dangers to the crew. Just considering the surface of the planet, explorers will face extreme levels of UV radiation, greatly reduced atmospheric pressure, decreased surface gravity, toxic soil, and an atmosphere filled almost completely with carbon dioxide. To function in this hostile environment or create a colony, people would need different basic support utilities. Resources to create a habitable environment, solar panels and food should be brought from Earth. To decrease the load and the cost of any mission to Mars, a future colony should consider using the resources that can be found locally, *i.e. in situ* on Mars. *In Situ* Resource Utilization (ISRU) can provide materials for life support and production of propellants. It will minimise risks to the crew and the mission, by reducing logistics, enabling to increase the space-craft shielding and providing increased self-sufficiency. Moreover, it will reduce costs by reducing the number of launched vehicles to complete the mission.

ISRU is probably the only way to successfully complete a manned mission to Mars [13, 14]. Therefore, it pushes the scientific community to develop new creative ways to use Martian resources. For example, there have been proposals for using the martian soil as a building material [15, 16], "mining" water from the polar ice caps [17] and fertilizing soil to grow plants [18].

Another promising candidate for ISRU is carbon dioxide which is abundant in the Martian atmosphere (96%) with smaller percentages of Ar (1.9%), N_2 (2.6%) and other gases (see table 1.1). A pioneering paper [19] proposes producing propellants from CO_2 and water, trapped in the upper layers of the surface. From the water it is proposed to produce hydrogen (H_2), which will react with CO_2 to form methane via the Sabatier process:

$$CO_2 + 4H_2 \rightarrow CH_4 + 2H_2O. \tag{1.1}$$

which then leads to oxygen through electrolysis process:

$$2H_2O \rightarrow 2H_2 + O_2 \tag{1.2}$$

which then to be used as methane/oxygen propellant. Another paper [20] proposes to convert CO_2 into carbon monoxide (CO) and oxygen (O_2) and to use CO/O_2 propellant for a reusable "hopper" vehicle. Boiron and Cantwell [21] discuss the possibility of hybrid rocket propulsion systems, based on a combination of a liquid oxidizer and a solid fuel, where the oxidizer is acquired through decomposition of carbon dioxide on the surface of Mars. A review of the state-of-the-art on Mars ISRU was published in 2015 by Sanders et al. [14].

Stancati proposed to use solid oxide electrolysis (SOEC) to generate oxygen from the Martian atmosphere back in the late 1970s [22]. But the technology was very new back then and only

in 1995 the design of Stancati was proven to be working and gave promising results [23]. Over the years the idea of using SOEC led to engineering the Mars Oxygen ISRU Experiment (MOXIE) proposed by Hecht [2, 24, 25], that will be tested in February 2021 during NASA's 2020 Mars mission. It is claimed that MOXIE can produce oxygen at a rate 10g/hour for a power of 300 W.

1.1.2 Solid Oxide Electrolysis (SOEC)

In the SOEC of carbon dioxide, a solid state yttria-stabilized zirconia (YSZ) ion conductor is used, which conducts electricity through negatively charged oxygen ions according to equation 1.3. The doped crystal lattice contains "holes," allowing ions to propagate through the lattice when an electric field is applied across it according to equation 1.4. This results in the total net chemical reaction shown in equation 1.5.

$$2CO_2 + 4e^- \rightarrow 2CO + 2O^{2-} \tag{1.3}$$

$$2O^{2-} \rightarrow O_2 + 4e^- \tag{1.4}$$

$$2CO_2 \rightarrow 2CO + O_2 \tag{1.5}$$

The electric field is generated by mounting porous metallic electrodes on each side of the YSZ, where a potential difference is applied [26]. This forms one SOEC cell, the base unit of the SOEC stack (see details in figures 1.2 and 1.3).

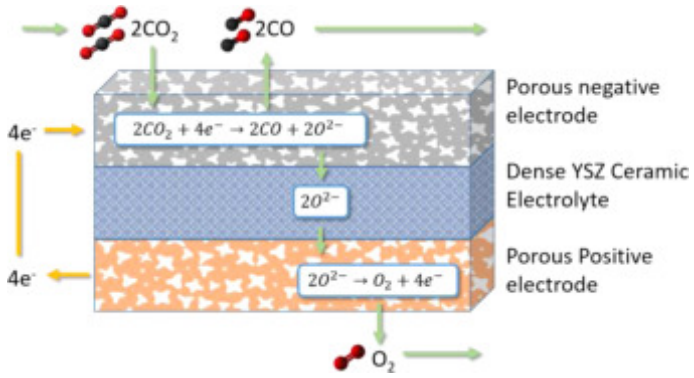

Figure 1.2: Reactions across a SOEC cell. Image is taken from [2]

Solid state electrolysis is very appealing, but appears to have several technical challenges for operation in the Martian atmosphere, as discussed in the next few paragraphs.

First, the ionic conductivity of YSZ has a maximum at around 800-1200^{o}C. Even for typical operation temperatures in the range 500-700 ^{o}C a degradation of conductivity is already observed [27]. And for Mars surface teperature, on everage 210 K [9] (see table 1.2), an external heating element and thermal insulation would be required occupying valuable space and increasing the launching load.

Second, the technology is working very well only when a sufficient amount of CO_2 is available on the inlet, *i.e.* SOEC operates at terrestrial atmospheric pressure. Therefore, the incoming gases need to be pressurized to 1 Earth atmosphere by the MOXIE scroll pump. The atmospheric pressure of Mars fluctuates depending on altitude and season, with an average annual pressure of 4.5 torr [9] (see table 1.2). Variations in the inlet pressure affect the pump performance.

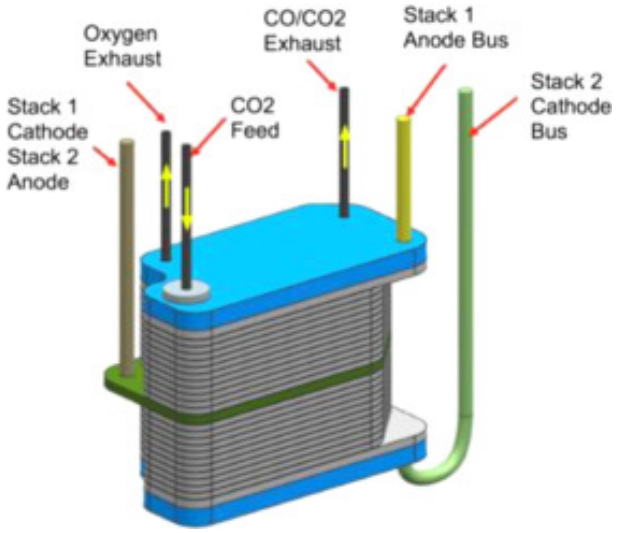

Figure 1.3: Two SOEC stacks with 11 cell each. A center voltage tab (green) separates the two stacks. Image is taken from [2]

Table 1.2: Mars' atmosphere conditions [9]

	Temperature	Pressure
Average	210 K	4.5 torr
Min registered	~ 150 K	0.3 torr
Place and time	South Pole, winter	South Pole, winter
Max registered	~ 300 K	7.5 torr
Place and time	Equator, noon	Utopia Planitia, late spring

Third, there is a chance of coking of the cathode for high utilization rates or high voltages. A risk in solid oxide electrolysis is that the process is driven too far, and oxygen is split from CO molecules, producing carbon, that is deposited on the cathode and therefore decreases the performance of the reaction.

Finally, and probably the most difficult challenge, scalability for Mars exploration purposes is far from trivial. MOXIE is only 0.5% of the scale needed to produce oxygen for future human missions on Mars [2, 3, 24]. Scaling the system means increasing the surface area of the SOEC cells and a scaled up orbiting scroll pump with a mass of around 18 kg occupying a volume of almost 4000 cm^3 for maintaining the required flow rate. Nasr *et al* express their concerns about the ability to maintain the same level of control and robustness over a much bigger system in [3].

All in all, solid oxide electrolysis is a strong candidate for oxygen production on Mars and will be tested in real conditions with the launch of MOXIE, but there is plenty of room for improvement and for the development of complementary or alternative technologies.

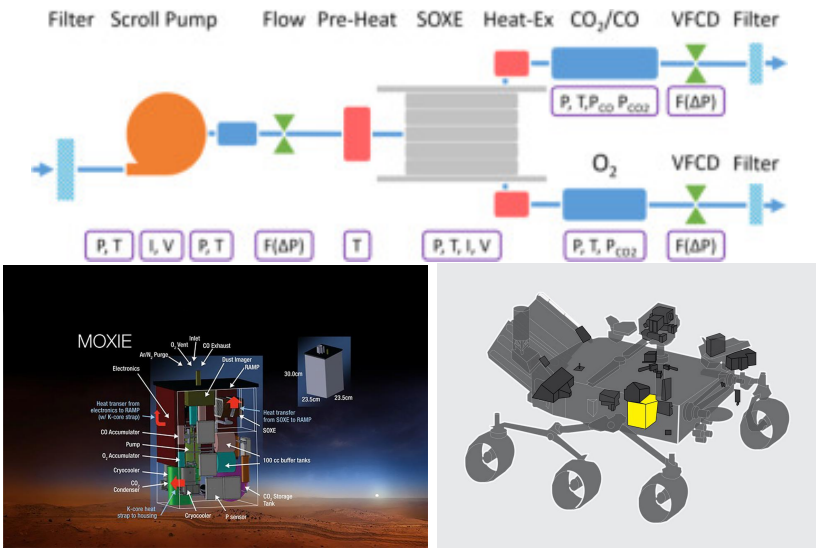

Figure 1.4: Schematic outline of MOXIE subsystems (top). MOXIE design (bottom left) and its location on the Mars 2020 Perseverance rover (bottom right). Images are taken from [3, 4].

1.2 Non-equilibrium CO_2 plasma for oxygen production on Mars

Each year Earth's atmosphere suffers from larger and larger amounts of carbon dioxide pollution. The increasing concentration of CO_2 in the atmosphere due to anthropogenic emissions is widely established to be a major cause of global warming [28]. This means that our planet needs a practical solution for reducing carbon dioxide emissions and decompose it.

The interest of non-equilibrium plasmas for CO_2 dissociation on Earth started in the 1970s and 1980s [29, 30] but did not gain much attention until much later, after publishing of the book by A. Fridman in 2008 [31] where these former results are shown and caused a huge wave of investigation on CO_2 conversion in recent years [6, 32–46].

This section reviews recent efforts of the scientific community to achieve plasma reforming of CO_2 on Earth and discusses similarities and differences with Martian conditions in the process, to assess the interest of exploring the applicability of non-equilibrium plasma technologies for ISRU on Mars.

1.2.1 CO_2 molecule and ways to dissociate it

CO_2 is a triatomic molecule with a carbon atom in its centre double bonded to both oxygen atoms on its sides. In its vibrational ground state CO_2 has a linear configuration. The molecule has four degrees of freedom for vibration, which gives the following vibrational modes: the symmetric stretch mode, characterized by quantum number ν_1, one double-degenerated bending mode, ν_2, and the asymmetric stretch mode, ν_3 (see figure 1.5). The level of vibrational excitation can be specified in the form CO_2 (ν_1 $\nu_2^{l_2}$ ν_3), where l_2 is a quantum number associated with the angular momentum used to characterize the degeneration of the bending vibration. l_2 can take the values $l_2 = \nu_2, \nu_2 - 2, \nu_2 - 4, ...1$ or 0, depending on the parity of ν_2 [40].

Dissociation of CO_2 can be done thermally, but due to the relatively strong carbon–oxygen bonds it requires temperatures in the range 2500–3500 K [47]. This can give high dissociation

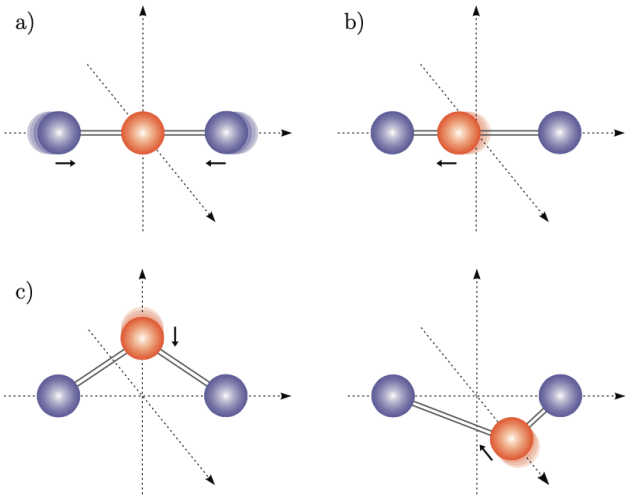

Figure 1.5: Vibrational modes of a CO_2 molecule. a) Symmetric stretching mode, characterized by quantum number ν_1. b) Asymmetric stretching mode of vibration, with quantum number ν_3. c) Bending mode ν_2 with vibrations in two orthogonal planes. The figure is taken from [5].

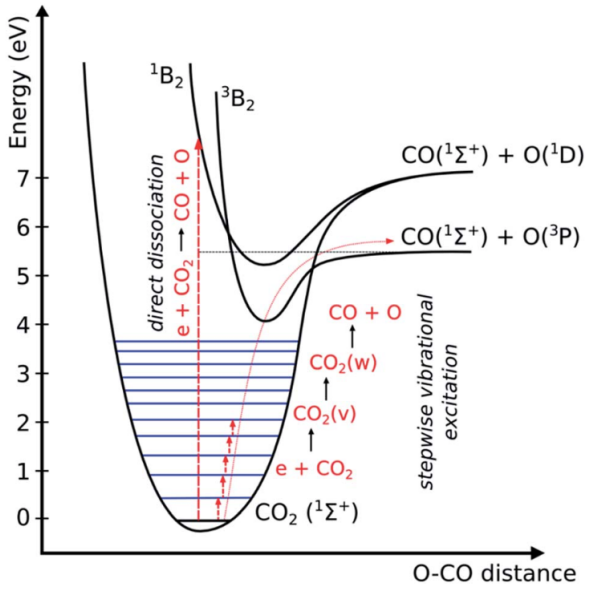

Figure 1.6: Schematic representation of the potential curve of the O=CO bond and electronic and vibrational levels of CO_2 molecule. Two dissociation mechanisms are shown: electron impact dissociation and vibrational ladder-climbing mechanism. The figure is taken from [6].

rates but quite low energy efficiency.

In non-thermal plasmas, with electron temperatures typically around 1 eV, the major portion of the discharge energy is transferred from plasma electrons to CO_2 vibrational excitation. A significant part of the energy absorbed by the electrons is transmitted to the excitation of the vibrational levels of the CO_2 asymmetric mode [31]:

$$CO_2(0,0^0,0) + e^- \rightarrow CO_2(0,0^0,1) + e^-, \tag{1.6}$$

And the population of highly excited vibrational levels takes place as a consequence of vibrational–vibrational (VV) exchange reactions :

$$CO_2(\nu_1,\nu_2^{l_2},\nu_3) + CO_2(\nu_1,\nu_2^{l_2},\nu_3) \rightarrow CO_2(\nu_1,\nu_2^{l_2},\nu_3+1) + CO_2(\nu_1,\nu_2^{l_2},\nu_3-1). \tag{1.7}$$

By selectively exciting this asymmetric stretch mode up to level 21 we can reach the dissociation energy at 5.5 eV, in a process known as stepwise vibrational excitation and often called as vibrational ladder climbing (right path on figure 1.6) [6, 29, 31, 32]. However, other collisional processes can influence the vibrational energy transfers involving the CO_2 molecule and hinder the ladder climbing mechanism. Vibrational energy can be further transferred through collisions to the translation energy of neutrals, which is referred to as vibrational-translational (VT) relaxation. To prevent the loss of CO_2 asymmetric vibration and the onset of reverse reaction mechanisms giving back CO_2 from the produced CO, a fast adiabatic cooling of the plasma may preserve the distribution achieved at higher temperature (ideal quenching) or even induce the formation of a new CO molecule from vibrationally excited CO_2 and O (super-ideal quenching) [31]. The overall energy efficiency of the process results from a complex interplay between mixture composition, gas dynamics, temperature and pressure.

Another less efficient way of dissociating CO_2 molecule is through direct electron impact:

$$CO_2 + e^- \rightarrow CO + O + e^-. \tag{1.8}$$

One example of this process is represented by the vertical arrow in figure 1.6. Dissociation by direct electron impact into neutral fragments always leads to at least one of the products in an electronically excited stated. Dissociation with a combination of both methods is also possible when electrons collide with vibrationally excited CO_2 causing dissociation.

1.2.2 Why using non-thermal plasmas on Mars

There are several reasons why Mars seems to have excellent conditions for ISRU by plasma. First, Mars has a CO_2 atmosphere and, if oxygen is to be produced locally on Mars, then there is no other available oxygen source than the atmospheric CO_2. Actually, the idea of using non-equilibrium CO_2 plasma for oxygen production on Mars was first proposed by Outlaw and colleagues back in the 1990s [48–50]. They studied oxygen permeation through an Ag 0.05Zr membrane (operating as the anode) with glow-discharge assisted dissociation, with an energy efficiency of about 25% and dissociation up to 75% for only 5mA discharge current. Silver is known to be uniquely more permeable to oxygen than other gases. Their research has shown that atomic oxygen generated by a glow discharge in a molecular oxygen stream bypasses the dissociative adsorption and increases the upstream surface concentration of oxygen atoms significantly [49]. Recently, Premathilake [51] has performed a similar experiment with a solid Ag rod cathode and a much thinner Ag membrane anode and confirmed that the oxygen flux through the Ag membrane is proportional to $1/d$, where d is the thickness of the membrane.

Second, the atmospheric pressure on Mars is on the correct range for plasma reforming. Working at much higher pressures leads to a higher VT-relaxation rates, faster gas heating, a

decrease in the degree of VT non-equilibrium and, finally, to lower values of energy efficiency for the CO_2 dissociation. [31, 33, 34, 52]. Indeed, the pressure on the surface of Mars fluctuates around the annual average of ≈ 4.5 torr with lowest 0.3 and highest 7.5 torr [9], meaning that there is no need to use compressors or pumps to operate effectively the plasma.

Third, the cold atmosphere (~ 210 K) may induce a stronger vibrational up-pumping than what can be achieved on Earth which is the most favourable way to reach dissociation as we have seen in section 1.2.1. Additionally, lower temperatures will significantly freeze the chemistry, preventing back reactions and giving enough time for the separation of products [31].

Fourth, traces of Ar and N_2 can only help. Several works have been done on plasmas where CO_2 was diluted with Ar [44–46] and N_2 [38, 44, 53]. A DC discharge was studied in a laboratory simulation of the Martian ambient $CO_2/Ar/N_2$ [54, 55]. The presence of Ar is expected to shift the Electron Energy Distribution Function (EEDF) to higher energies [56] and the presence of N_2 induces transfers of vibrational energy from nitrogen to carbon dioxide molecules [38].

Finally, the required power for discharge operation is typically ≈ 100 W and can be as low as ≈ 20 W, perfectly feasible on Mars (e.g., the Mars Exploration Rover solar arrays generate, when fully illuminated, about 140 watts of power for up to four hours per sol) [57].

1.2.3 Advantages of the non-equilibrium plasma over SOEC for oxygen production on Mars

The downsides of the SOEC, mentioned in section 1.1.2, are in fact the areas where non-equilibrium plasmas will thrive.

- Plasma discharges do not need additional heating. Silver membranes, used in [48–51] are required to be heated up to 450 - 650^{o}C, which is much lower than the 800 - 1200^{o}C necessary for ionic conductivity. Additionally, the search for new membranes and their activation by plasma continues [58] and it is not impossible that an external heating source will not be needed at all.

- As it was already mentioned, the plasma technology will not need additional pumping for the inlet gas. However, a pressure drop for oxygen penetration through the membrane and a compressor for oxygen collection at the outlet is required for both technologies.

- Deposition of carbon C is unlikely to happen in low-temperature discharges at Martian pressures. If some carbon is created by dissociation of CO, it will be subsequently and rapidly oxidized back to CO [5, 8].

- The scalability of the plasma reactors is relatively cheap since it does not require scarce materials and it does not bring any additional challenges associated with its implementation.

- There is no information about the effect of radiation on SOEC or on MOXIE, whereas for plasmas the CO_2 molecule is more likely to get vibrationally excited due to absorbed UV radiation, with a positive effect in the plasma operation [59].

- Figure 1.7 summarizes the conversion/energy efficiency obtained in microwave (MW), dielectric barrier (DB), radio-frequency (RF) and gliding arc (GA) discharges. Existing plasma technologies can reach up to 60% conversion efficiency when used together with a catalyst [7, 36]. At 300 W this corresponds to the production of 35g of O_2 per hour, at an energy cost of 10 eV/molecule. A decrease in performance of about 50%, to account

for unexpected difficulties and the uncertainties in the development of new technology, brings these numbers to approximately 20 g of O_2 per hour, at an energy cost of 18 eV per molecule and 31% energy efficiency. The anticipated throughput of the MOXIE experiment is 10g/hour for a power of 300 W. This rough estimation outperforms the most optimistic predictions of MOXIE by 100% and brings further evidence in favor of the plausibility and significance of plasma ISRU on Mars as a complementary technology to SOEC.

Despite these advantages, it is worth noticing that the gas separation is at the core of SOEC technology, while gas separation for low-temperature plasmas will be a specific system which will require additional control and understanding of the gas-surface coupling. Nevertheless, the silver membranes used in [49–51] showed significant enhancement in dissociation comparing to the similar discharge without membrane. Moreover, the link between plasma and ion conducting membranes for product separation has also started to be followed at the Dutch Institute For Fundamental Energy Research (DIFFER) and the promising results can provide the impetus for developing easily fabricated electrochemical reactors for sustainable, large-scale chemistry [58].

It can be concluded that the increased interest in the plasma technology for Earth indicates that it can be an alternative or even a better technology than SOEC for oxygen production on Mars. However, it is not possible to ignore the fact that MOXIE system will be tested on the surface of Mars in February 2021 if NASA's Mars 2020 mission will be successful, while there is still a long way for constructing and deploying working prototype for oxygen production on Mars using non equilibrium plasma.

1.3 Overview of CO_2 reforming from modeling point of view

Ever since the review paper by Rusanov [29, 30] resurfaced in the western academic community, CO_2 reforming became a very active research topic, due to the importance of developing synthetic fuels. Modelling of non-equilibrium plasmas can be a strong tool for understanding and predicting connections between main discharge parameters and the performance of the reactor.

The detailed modelling of any plasma discharge requires addressing several aspects, such as electron, vibrational and ion kinetics, chemistry and surface processes. However, a significant fraction of modelling studies on CO_2 plasmas focuses on the vibrational kinetics. A complete vibrational kinetics model would include all the levels and all of the corresponding VV and VT transitions between them, which would need an important computational power. Simplified schemes, where only a few vibrational levels are taken into account are extensively used in plasma models. For instance, 0D kinetic models with state-to-state (STS) approach are used to study MW and DB discharges, describing low-lying levels and effective level that represents the sum of the higher symmetric stretch (n00) and bending (0n0) modes [60]. Kozak and Bogaerts [34] have developed more extensive model including low-lying symmetric stretching and bending mode levels and all the levels (total of 21) in the asymmetric mode, up to the dissociation energy (5.5 eV). This formulation of the vibratinal kinetics was later adopted by several other authors [35, 39, 61–63]. A very extended model of vibrational kinetics was used by Armenise and Kustova [32] for calculating re-entry conditions for Mars' and Venus' atmospheres where several thousand vibrational levels were included. A somewhat intermediate formulation accounting for ~ 500 vibraitonal levels, but that neglects or lumps mixed levels, was proposed by Annaloro and Bultel [64]. Alternatively to STS, individual vibrational levels are replaced by a continuum and described by Fokker-Planck equation [65, 66].

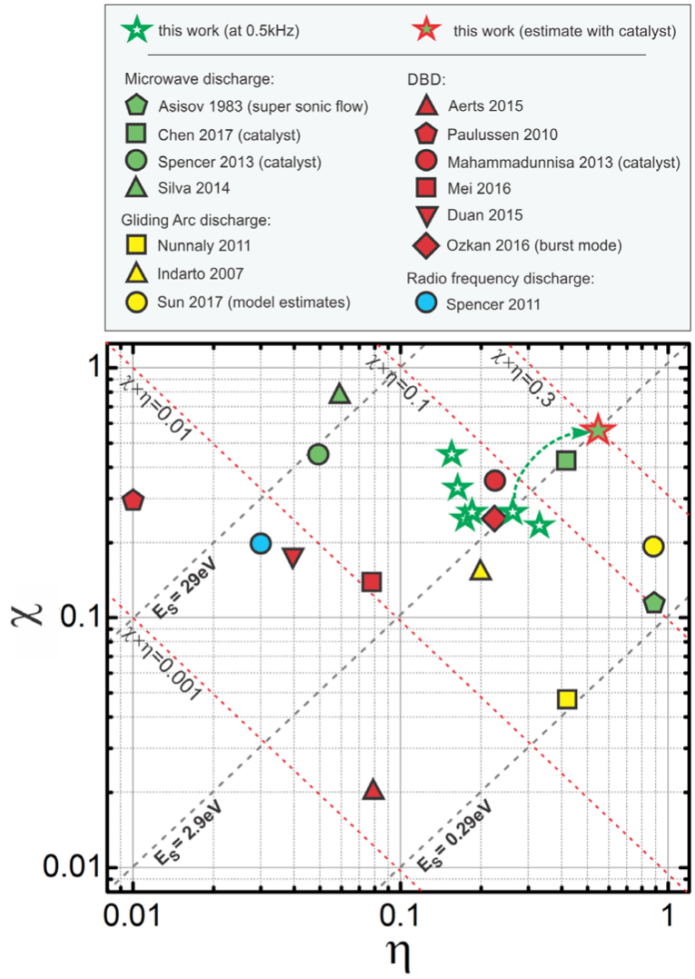

Figure 1.7: Summary of the CO_2 conversion, χ, and energy efficiency, η, results obtained in the literature using different plasma sources. Here E_s correspond to constant specific energy input - the energy spent for dissociation of one CO_2 molecule in the discharge. The figure is taken from [7].

The coupling between the electron and vibrational kinetics was done by Silva and Grofulović [40, 41] with the model that includes low-lying vibrational levels (in a total of 72 levels), including the levels corresponding both to the normal modes and to the mixed modes, by coupling the system of rate balance equations describing the vibrational kinetics to the electron Boltzmann equation. The populations of the low vibrational levels, calculated in their study are in good agreement with the ones obtained experimentally. Capitelli and Pietanza [39, 61, 62] used similar strategy in their time-dependant model describing MW and DB and nanosecond repetitively pulsed (NRP) discharges. They study in detail the influence of superelastic collisions with vibrationally and electronically excited states in the electron energy distribution function and the importance of some state-specific chemical reactions. The coupling between electron and heavy-species kinetics was recently done and validated by A. Silva [67] in "vibrationally cold" plasmas, so that the vibrational kinetics was not included in the model.

Depending on the configuration and the objectives of the work, 0D[40, 41, 47, 58, 68, 69], fluid models [35, 70] and particle-in-cell (PIC) [71] codes have been used in the modelling of

CO_2 kinetics.

1.4 Objectives

There are many open challenges and directions for research on plasma reforming of CO_2 on Earth with large potential for successful implementation on Mars. The goal of this thesis is by using the reliable and consistent data widen the understanding of different kinetic processes, investigate the influence of the discharge parameters on the different kinetics and, ultimately, proof the concept for plasma-assisted CO_2 dissociation for ISRU on Mars. This thesis presents a fundamental study, rather than a guide to achieve high energy or dissociation efficiency. To pursue its objective, this work establishes reliable and consistent data that can be used for modelling, brings new developments into existing kinetic models and undertakes and experimental characterisation of CO_2 plasmas in Martian conditions.

The present works intend to fill several gaps in pursue of the developing 0D detailed self-consistent kinetic model and first steps of experimental and numerical proof of ISRU for oxygen production. From a modelling point of view, the previous section shows that there is still a need for a model that binds together vibrational and electron kinetics and heavy-species chemistry. This thesis intends to give a step forward in this direction. Moreover, a reliable model should be based on valid input data. Therefore, special attention is given to the input data used such as electron-neutral scattering cross sections and reaction rates. The present work only uses data that were verified against experiment.

Many different types of discharges have been studied in the last years, mainly trying to find the proper regime and optimal plasma parameters for efficient CO_2 dissociation. Microwave, radiofrequency and dielectric barrier discharges, possibly coupled with catalysts, are strong candidates for CO_2 dissociation with high energy efficiency, dissociation efficiency and/or robustness, and ease of operation. However, neither of them is simple to describe using numerical models nor to characterise experimentally, due to non-homogeneity, transient phenomena and complex physics. For fundamental studies, DC glow discharges present several advantages, such as the simple geometry, straightforward determination of the electric field, homogeneity of the positive column and reproducibility of the results. This makes them accessible to many diagnostics otherwise difficult to apply, like Fourier transform infrared spectroscopy (FTIR), which is very useful in the study of CO_2 plasmas [42]. Furthermore, it allows the comparison of experimental data with the results of 0D models, ideally placed for the investigation of complex plasma chemistries. Therefore, DC glow discharges are the aim of this study.

Following a step-by-step model validation strategy being pursued at the N-PRiME team (N-Plasmas Reactive: Modelling and Engineering) of the Instituto de Plasmas e Fusão Nuclear (IPFN) from Instituto Superior Técnico (IST) since 2016 [38, 40, 41, 72], to which this work also contributes, a DC glow discharge is the system of study here. Additionally, MW discharges can be described by 0D models to a good approximation, so the results obtained here can also provide guidelines for the operation of the most promising discharges for CO_2 reforming [53].

To complement the modelling investigation, we experimentally investigate the influence of the current and pressure on the CO_2 and CO vibrational temperatures, CO_2 dissociation using *in-situ* FTIR. The plasma is studied under different conditions in which we replicated the average temperature on Mars and Earth. The pressure was varied between 0.5 and 6 Torr which is close to the average pressure found on Mars (see table 1.2) and also has relevance to some applications [73]. To our knowledge, this is the first time that Mars' atmospheric conditions were replicated for plasma discharge studies.

1.5 Original contributions

A significant part of the contents of this thesis has been presented at international conferences and is published as journal papers and conference proceedings. The main original contributions of this work can be summarized as follows.

Through a modelling study, it was found that a more efficient up-pumping of vibrational quanta into the asymmetric stretching mode and a higher degree of non-equilibrium in the plasma, generally assumed to contribute to efficient CO_2 dissociation, can be obtained in typical conditions on Mars than on Earth. The results are essentially published as journal papers [52, 74] and presented at at international conference [75].

A serious inconsistency was found in most electron impact cross section sets for CO available in the literature, related to the high value of the rotational excitation/deexcitation cross sections at low electron energies, surpassing the effective momentum transfer cross-section. The present work presents a complete and consistent electron impact cross section set for CO that corrects for this inconsistency. The proposed set of cross sections includes all the main collisional processes and provides swarm calculations in very good agreement with the experimental data over the full range of reduced electric fields considered, 10^{-4} - 10^{3} Td. The results are essentially published in a journal paper [76] and were resented at international conferences as poster contributions [77–79].

CO_2-CO plasma was investigated both numerically and experimentally, since CO is an important product of dissociation and its presence modifies the properties of a "pure" CO_2 plasma. A study of the electron kinetics of CO_2-CO plasma with different mixture composition is published in a journal paper [76] and was presented at an international conference [79] as a poster and at an international workshop [80] as an oral presentation. The experimental investigation of CO_2-CO mixture was presented at an international conference [81] and the workshop [80]. It was shown, that CO concentration in the initial CO_2-CO mixture changes the [O]/[CO] balance and therefore change the degree of the vibrational non-equilibrium in the system (due to the importance of VT collisions with O atoms).

A setup to operate a DC discharge in conditions simulating Mars' atmosphere low-temperature conditions was built. The experimental results furnish a characterisation of CO_2 plasmas in realistic Martian conditions. To the best of our knowledge, these results constitute the first determination of the dissociation degree and vibrational temperatures in these conditions. A dissociation of nearly ~30% was observed. The experimental results were published in [82] and presented at the conferences [80, 83] as oral presentations. A kinetic model was later developed to describe and interpret the experimental data. A journal paper with the modelling results is currently in preparation.

1.6 Outline

This thesis includes a theoretical and numerical simulation study, performed at IST, and a series of experimental campaigns done at Laboratoire de Physique des Plasmas (LPP), Ecole Polytechnique, France. The joint experimental-modelling effort allows to identify and understand the main mechanisms underlying CO_2 dissociation by plasmas for the conditions of interest, that will ultimately lead to an optimisation of the process. Each chapter constitutes a part of a coherent ensemble fulfilling the global objectives of the thesis, but it is written in a way that facilitates its reading in a standalone fashion.

Before addressing the detailed modelling and discussing the elaborate experimental setup that recreates Martian conditions, some preliminary work is presented in chapter 2, where the

concept of this thesis is described and tested. In this chapter, a single-pulsed DC discharge is described with a self-consistent model coupling the electron and vibrational kinetics, as presented in [40, 41, 84]. Here, the energy input into the vibrational channels is tracked for pressure and temperature representative of Mars conditions and compared with the results obtained for the same discharge operating under Earth's atmosphere temperature and the same pressure as on Mars. In this system only the first few vibrational levels get excited, no significant CO_2 dissociation takes place and, accordingly, the kinetics of CO molecules and O atoms is not taken into account.

Electron kinetics is one of the main components of discharge modeling for any gas discharge, since it is essential to understand how the energy gained by the electrons from the applied electric field is transferred to the internal degrees of freedom and to the different heavy-particles. Electron kinetics in pure CO_2 was studied by Grofulović *et al*, who published an electron-impact cross section set for CO_2 [72], freely available at the IST-Lisbon database with LXCat [85]. The cross sections for O and O_2 are also known and freely available at the same database. However, electron cross sections in carbon monoxide (CO) have never been addressed by the N-PRiME team, hence a new cross section set for CO is derived and proposed in chapter 3. The cross sections are validated by comparing swarm parameters calculated using the two-term Boltzmann solver with available experimental data. The new cross section set is already available at the IST-Lisbon database. Moreover, since a discharge ignited in pure CO_2 can contain significant amounts of CO, the influence of CO on the CO_2 electron kinetics is worthy of consideration, thus the CO_2-CO electron kinetics is also studied in detail in chapter 3. We investigate the changes on the EEDF, the dissociation and ionization rate coefficients, and the power balance for different concentrations of CO in the discharge.

Chapters 4 and 5 of this thesis present experimental results as well as a kinetic model of CO_2 plasmas, subsequently used to interpret the experimental data. Although there have been experiments performed in the past under conditions mimicking the Martian mixture of atmosphere gases [54], to our knowledge there is no experimental characterization of plasmas created in a realistic Martian environment where low-temperature conditions are recreated. In chapter 4 low-temperature Martian conditions are achieved by immersing the plasma reactor in a bath of dry ice and ethanol. The discharge pressure is varied between 0.5 and 5 Torr, which are typical for the atmosphere of Mars. The experiments are conducted both in pure CO_2 and in synthetic Martian atmosphere, corresponding to a mixture of 96% CO_2 with 2% of Ar and 2% of N_2.

Oxygen production on Mars suggests oxygen extraction from the plasma, leaving a higher concentration of carbon-containing species. In chapter 5 the influence of mixture composition in CO_2/CO DC glow discharges is experimentally studied using FTIR. The mixing ratio was varied between 33 and 100 % of CO_2 concentration, the experimental results are compared with the simulations. The enlarged "parameter space" provided by different CO_2-CO ratios provide further validation of the model and additional insight into the main mechanisms ruling the kinetics of CO_2 plasmas [80, 81].

Finally, chapter 6 summarizes the main results and presents the general conclusions of the thesis.

Bibliography

[1] NASA, "New Selfie Shows Curiosity, the Mars Chemist," 2019. [Online]. Available: https://www.nasa.gov/feature/jpl/new-selfie-shows-curiosity-the-mars-chemist

[2] F. Meyen, M. Hecht, and J. Hoffman, "Thermodynamic Model of Mars Oxygen ISRU Experiment (MOXIE)," *Acta Astronaut.*, vol. 129, pp. 82–87, 2016.

[3] M. Nasr, F. Meyen, and J. Hoffman, "Scaling the Mars Oxygen ISRU experiment (MOXIE) for mars sample return," *IEEE Aerospace Conference Proceedings*, vol. 2018-March, pp. 1–7, 2018.

[4] NASA, "Mars 2020 Perseverance rover." [Online]. Available: https://mars.nasa.gov/mars2020/spacecraft/instruments/moxie/

[5] M. Grofulovic, "Energy storage and transfer in non-equilibrium CO_2 plasmas," Ph.D. dissertation, 2019.

[6] A. Bogaerts, T. Kozák, K. van Laer, and R. Snoeckx, "Plasma-based conversion of CO_2: current status and future challenges," *Faraday Discuss.*, pp. 217–232, 2015.

[7] N. Britun, T. Silva, G. Chen, T. Godfroid, J. Van Der Mullen, and R. Snyders, "Plasma-assisted CO_2 conversion: Optimizing performance via microwave power modulation," *Journal of Physics D: Applied Physics*, vol. 51, no. 14, 2018.

[8] A.-S. Morillo-Candas, "Investigation of fundamental mechanisms of CO_2 plasmas," Ph.D. dissertation, 2019.

[9] R. M. Haberle, *Solar System/Sun, Atmospheres, Evolution of Atmospheres: Planetary Atmospheres: Mars*. Elsevier, 2015, vol. 5, no. 1.

[10] NASA, "Chronology of Mars Exploration," 2020. [Online]. Available: https://nssdc.gsfc.nasa.gov/planetary/chronology_mars.html

[11] NASA, "Moon to Mars," 2020. [Online]. Available: https://www.nasa.gov/specials/moontomars/index.html

[12] SpaceX, "Missions to Mars," 2020. [Online]. Available: https://www.spacex.com/mars

[13] NASA, "In-situ Resource Utilization (ISRU)," Tech. Rep., 2016.

[14] G. B. Sanders, A. Paz, L. Oryshchyn, K. Araghi, A. C. Muscatello, T. Peters, D. L. Linne, and J. E. Kleinhenz, "Mars ISRU for production of mission critical consumables – options, recent studies, and current state of the art," in *AIAA SPACE Conference and Exposition*, 2015, pp. 0–31.

[15] B. J. Chow, T. Chen, Y. Zhong, and Y. Qiao, "Direct Formation of Structural Components Using a Martian Soil Simulant," *Scientific Reports*, vol. 7, no. 1, pp. 1–8, 2017.

[16] D. Karl, F. Kamutzki, A. Zocca, P. Lima, O. Goerke, and J. Guenster, "Ceramics from wet-processing of Martian soil simulant using slip casting or Additive Manufacturing for in-situ resource utilization on Mars," in *8th European Conference for Aeronautics and Space Science(EUCASS)*, 2019, pp. 1–8.

[17] S. J. Hoffman, A. Andrews, B. K. Joosten, and K. Watts, "A water rich mars surface mission scenario," *2017 IEEE Aerospace Conference*, pp. 1–21, 2018.

[18] G. W. Wamelink, J. Y. Frissel, W. H. Krijnen, and M. R. Verwoert, "Crop growth and viability of seeds on Mars and Moon soil simulants," *Open Agriculture*, vol. 4, no. 1, pp. 509–516, 2019.

[19] R. L. Ash, W. L. Dowler, and G. Varsi, "Feasibility of rocket propellant production on Mars," *Acta Astronautica*, vol. 5, no. 9, pp. 705–724, 1978.

[20] G. A. Landis and D. L. Linne, "Mars rocket vehicle using in situ propellants," *J. Spacecraft Rockets*, vol. 38, no. 5, pp. 730–735, 2001.

[21] A. J. Boiron and B. J. Cantwell, "Hybrid rocket propulsion and in-situ propellant production for future mars missions," in *49th AIAA/ASME/SAE/ASEE Joint Propulsion Conference*, San Jose, CA, 2013, p. 3899.

[22] M. L. Stancati, J. C. Niehoff, W. C. Wells, and R. L. Ash, "In situ propellant production: a new potential for round trip spacecraft," in *AIAA Conference on Advanced Technology for Future Space Systems*, no. 79-0906, 1979.

[23] K. R. Sridhar, "Mars sample return mission with in-situ resource utilization," *Journal of Propulsion and Power*, vol. 11, no. 6, pp. 1356–1362, 1995.

[24] J. Hartvigsen, S. Elangovan, D. Larsen, J. Elwell, M. Bokil, L. Frost, and L. M. Clark, "Challenges of Solid Oxide Electrolysis for Production of Fuel and Oxygen From Mars Atmospheric CO_2," *ECS Transactions*, vol. 68, no. 1, pp. 3563–3583, 2015.

[25] M. Hecht and J. Hoffman, "The Mars Oxygen ISRU Experiment MOXIE on the Mars 2020 Rover," in *3rd International Workshop on Instrumentation for Planetary Mission*, 2016, p. 4130.

[26] D. Rapp, *Use of Extraterrestrial Resources for Human Space Missions to Moon or Mars*, 2018.

[27] B. Butz, "Yttria-Doped Zirconia as Solid Electrolyte for Fuel-Cell Applications," Ph.D. dissertation, 2009.

[28] G. A. Schmidt, R. A. Ruedy, R. L. Miller, and A. A. Lacis, "Attribution of the present-day total greenhouse effect," *Journal of geophysical research*, vol. 115, p. D20106, 2010.

[29] V. D. Rusanov, "The physics of a chemically active plasma with nonequilibrium vibrational excitation of molecules," *Soviet Physics Uspekhi*, vol. 24, no. 6, p. 447, 1981.

[30] R. Azizov, A. Vakar, V. Zhivotov, and M. Krotov, "Non-equilibrium plasma-chemical process of CO_2 decomposition in a supersonic microwave discharge," *Proc. USSR Acad. Sci*, vol. 1, p. 271, 1983.

[31] A. Fridman, *Plasma Chemistry*. New York: Cambridge University Press, 2008.

[32] I. Armenise and E. V. Kustova, "State-to-state models for CO_2 molecules: From the theory to an application to hypersonic boundary layers," *Chem. Phys.*, vol. 415, pp. 269–281, 2013.

[33] G. van Rooij, D. van den Bekerom, N. den Harder, T. Minea, G. Berden, W. Bongers, R. Engeln, M. Graswinckel, E. Zoethout, and M. van de Sanden, "Taming microwave plasma to beat thermodynamics in CO_2 dissociation," *Faraday discussions*, vol. 183, pp. 233–248, 2015.

[34] T. Kozák and A. Bogaerts, "Splitting of CO_2 by vibrational excitation in non-equilibrium plasmas: a reaction kinetics model," *Plasma Sources Sci. Technol*, vol. 23, no. 4, p. 045004, 2014.

[35] S. Ponduri, M. M. Becker, S. Welzel, M. C. Van De Sanden, D. Loffhagen, and R. Engeln, "Fluid modelling of CO_2 dissociation in a dielectric barrier discharge," *J. Appl. Phys.*, vol. 119, no. 9, 2016.

[36] S. Heijkers, R. Snoeckx, T. Kozák, T. Silva, T. Godfroid, N. Britun, R. Snyders, and A. Bogaerts, "CO_2 conversion in a microwave plasma reactor in the presence of N_2: Elucidating the role of vibrational levels," *J. Phys. Chem. C*, vol. 119, no. 23, pp. 12 815–12 828, 2015.

[37] T. Silva, N. Britun, T. Godfroid, and R. Snyders, "Optical characterization of a microwave pulsed discharge used for dissociation of CO_2," *Plasma Sources Sci. Technol.*, vol. 23, no. 2, 2014.

[38] L. Terraz, T. Silva, A. Morillo-Candas, O. Guaitella, A. Tejero-del Caz, L. L. Alves, and V. Guerra, "Influence of N_2 on the CO_2 vibrational distribution function and dissociation yield in non-equilibrium plasmas," *Journal of Physics D: Applied Physics*, vol. 53, no. 9, 2019.

[39] M. Capitelli, G. Colonna, G. D'Ammando, and L. D. Pietanza, "Self-consistent time dependent vibrational and free electron kinetics for CO_2 dissociation and ionization in cold plasmas," *Plasma Sources Sci. Technol*, vol. 26, no. 5, 2017.

[40] M. Grofulović, T. Silva, B. Klarenaar, A. Morillo Candas, O. Guaitella, R. Engeln, C. Pintassilgo, and V. Guerra, "Kinetic study of CO_2 plasmas under non-equilibrium conditions. II.Input of vibrational energy," *Plasma Sources Sci. Technol*, vol. 27, p. 115009, 2018.

[41] T. Silva, M. Grofulović, B. Klarenaar, A. Morillo-Candas, O. Guaitella, R. Engeln, C. Pintassilgo, and V. Guerra, "Kinetic study of low-temperature CO_2 plasmas under non-equilibrium conditions. I. Relaxation of vibrational energy," *Plasma Sources Sci. Technol.*, 2017.

[42] B. Klarenaar, R. Engeln, D. van den Bekerom, M. van De Sanden, A. Morillo Candas, and O. Guaitella, "Time evolution of vibrational temperatures in a CO_2 glow discharge measured with infrared absorption spectroscopy," *Plasma Sources Sci. Technol.*, vol. 26, no. 11, p. 115008, 2017.

[43] S. H. M. Wandurraga, "Reduced reaction kinetics model for CO_2 dissociation in non-thermal microwave discharges," Ph.D. dissertation, Delft University ofTechnology, 2015.

[44] D. Ray, R. Saha, and C. Subrahmanyam, "DBD plasma assisted CO_2 decomposition: Influence of diluent gases," *Catalysts*, vol. 7, no. 244, pp. 1–11, 2017.

[45] Q. Huang, D. Zhang, D. Wang, K. Liu, and A. W. Kleyn, "Carbon dioxide dissociation in non-thermal radiofrequency and microwave plasma," *J. Phys. D*, vol. 50, no. 29, p. 4001, 2018.

[46] M. S. Moss, K. Yanallah, R. W. Allen, and F. Pontiga, "An investigation of CO_2 splitting using nanosecond pulsed corona discharge: Effect of argon addition on CO_2 conversion and energy efficiency," *Plasma Sources Science and Technology*, vol. 26, no. 3, 2017.

[47] D. C. Van Den Bekerom, J. M. Linares, T. Verreycken, E. M. Van Veldhuizen, S. Nijdam, G. Berden, W. A. Bongers, M. C. Van De Sanden, and G. J. Van Rooij, "The importance of thermal dissociation in CO_2 microwave discharges investigated by power pulsing and rotational Raman scattering," *Plasma Sources Science and Technology*, vol. 28, no. 5, 2019.

[48] R. L. Ash, D. Wu, and R. A. Outlaw, "A study of glow-discharge and permeation techniques for extraterrestrial oxygen beneficiation," *Adv. Space Res.*, vol. 14, no. 6, pp. 259–263, 1994.

[49] D. Wu, R. A. Outlaw, and R. L. Ash, "Extraction of oxygen from CO_2 using glow-discharge and permeation techniques," *J. Vac. Sci. Technol. A*, vol. 14, no. 2, pp. 408–414, 1996.

[50] R. A. Outlaw, "O_2 and CO_2 glow-discharge-assisted oxygen transport through Ag," *Journal of Applied Physics*, vol. 68, no. 3, pp. 1002–1004, 1990.

[51] D. Premathilake, R. A. Outlaw, R. A. Quinlan, and C. E. Byvik, "Oxygen generation by carbon dioxide glow discharge and separation by permeation through ultrathin silver membranes," *Earth and Space Science*, vol. 6, no. 4, pp. 557–564, 2019.

[52] V. Guerra, T. Silva, P. Ogloblina, M. Grofulović, L. Terraz, M. da Silva, C. Pintassilgo, L. Alves, and O. Guaitella, "The case for in situ resource utilisation for oxygen production on Mars by non- equilibrium plasmas," *Plasma Sources Sci. Technol.*, vol. 26, 2017.

[53] R. Snoeckx, S. Heijkers, K. V. Wesenbeeck, S. Lenaertsb, and A. Bogaertsa, "No CO_2 conversion in a dielectric barrier discharge plasma: N_2 in the mix as a helping hand or problematic impurity?" *Energy Environ. Sci.*, vol. 9, pp. 999–1011, 2016.

[54] G. Garcia-Cosio, H. Martinez, M. Calixto-Rodriguez, and A. Gomez, "DC discharge experiment in an $Ar/N_2/CO_2$ ternary mixture: A laboratory simulation of the Martian ionosphere's plasma environment," *Journal of Quantitative Spectroscopy and Radiative Transfer*, vol. 112, no. 18, pp. 2787–2793, 2011.

[55] H. L. Manning, I. L. Ten Kate, S. J. Battel, and P. R. Mahaffy, "Electric discharge in the Martian atmosphere, Paschen curves and implications for future missions," *Advances in Space Research*, vol. 46, no. 10, pp. 1334–1340, 2010.

[56] A. Janeco, N. R. Pinhão, and V. Guerra, "Electron kinetics in $He/CH_4/CO_2$ mixtures used for methane conversion," *J. Phys. Chem. C*, vol. 119, no. 1, pp. 109–120, 2015.

[57] G. A. Landis, T. W. Kerslake, P. Jenkins, and D. Scheiman, "Mars solar power," *Collection of Technical Papers - 2nd International Energy Conversion Engineering Conference*, vol. 1, no. November 2004, pp. 376–385, 2004.

[58] A. P. Goede, "CO_2 neutral fuels," *EPJ Web of Conferences*, vol. 189, p. 00010, 2018.

[59] A. Morillo-Candas, C. Drag, J.-P. Booth, T. Dias, V. Guerra, and O. Guaitella, "Oxygen atom kinetics in CO_2 plasmas ignited in a DC glow discharge," *Plasma Sources Sci. Technol*, vol. 28, no. 7, p. 075010, 2019.

[60] R. Aerts, T. Martens, and A. Bogaerts, "Influence of vibrational states on CO_2 splitting by dielectric barrier discharges," *J. Phys. Chem. C*, vol. 116, no. 44, pp. 23 257–23 273, 2012. [Online]. Available: http://pubs.acs.org/doi/abs/10.1021/jp307525t

[61] L. D. Pietanza, G. Colonna, G. D'Ammando, A. Laricchiuta, and M. Capitelli, "Vibrational excitation and dissociation mechanisms of CO_2 under non-equilibrium discharge and post-discharge conditions," *Plasma Sources Science and Technology*, vol. 24, no. 4, p. 42002, 2015. [Online]. Available: http://dx.doi.org/10.1088/0963-0252/24/4/042002

[62] L. D. Pietanza, G. Colonna, G. D'Ammando, A. Laricchiuta, and M. Capitelli, "Non equilibrium vibrational assisted dissociation and ionization mechanisms in cold CO_2 plasmas," *Chemical Physics*, vol. 468, pp. 44–52, 2016. [Online]. Available: http://dx.doi.org/10.1016/j.chemphys.2016.01.007

[63] J. F. de la Fuente, S. H. Moreno, A. I. Stankiewicz, and G. D. Stefanidis, "A new methodology for the reduction of vibrational kinetics in non-equilibrium microwave plasma: application to CO_2 dissociation," *React Chem Eng*, vol. 1, pp. 540–554, 2016. [Online]. Available: http://dx.doi.org/10.1039/C6RE00044D

[64] J. Annaloro and A. Bultel, "Vibrational and electronic collisional-radiative model in CO_2-N_2-Ar mixtures for Mars entry problems," *Physics of Plasmas*, vol. 26, p. 103505, 2019.

[65] P. Diomede, M. C. Van De Sanden, and S. Longo, "Insight into CO_2 dissociation in plasma from numerical solution of a vibrational diffusion equation," *Journal of Physical Chemistry C*, vol. 121, no. 36, pp. 19 568–19 576, 2017.

[66] P. Viegas, M. C. Van De Sanden, S. Longo, and P. Diomede, "Validation of the Fokker-Planck Approach to Vibrational Kinetics in CO_2 Plasma," *Journal of Physical Chemistry C*, vol. 123, no. 37, pp. 22 823–22 831, 2019.

[67] A. F. Silva, A. S. Morillo-Candas, A. Tejero-del Caz, L. L. Alves, O. Guaitella, and V. Guerra, "A reaction mechanism for vibrationally cold CO_2 plasmas," *In preparation*, 2020.

[68] A. Berthelot and A. Bogaerts, "Modeling of plasma-based CO_2 conversion: lumping of the vibrational levels," *Plasma Sources Sci. Technol.*, vol. 25, no. 4, p. 045022, 2016. [Online]. Available: http://stacks.iop.org/0963-0252/25/i=4/a=045022?key=crossref.c20e4eb36e1a507bb594fd0b8e5e98c4

[69] T. Kozák and A. Bogaerts, "Evaluation of the energy efficiency of CO_2 conversion in microwave discharges using a reaction kinetics model," *Plasma Sources Sci. Technol.*, vol. 24, no. 1, p. 015024, 2014. [Online]. Available: http://stacks.iop.org/0963-0252/24/i=1/a=015024?key=crossref.6ddb8a33aa4ce58fca197f080841e769

[70] N. den Harder, D. C. van den Bekerom, R. S. Al, M. F. Graswinckel, J. M. Palomares, F. J. Peeters, S. Ponduri, T. Minea, W. A. Bongers, M. C. van de Sanden, and G. J. van Rooij, "Homogeneous CO_2 conversion by microwave plasma: Wave propagation and diagnostics," *Plasma Processes and Polymers*, vol. 14, no. 6, pp. 1–24, 2017.

[71] D. Levko, M. Pachuilo, and L. L. Raja, "Particle-in-cell modeling of streamer branching in CO_2 gas This," *J. Phys. D: Appl. Phys.*, vol. 50, no. 35, p. 354004, 2017.

[72] M. Grofulović, L. L. Alves, and V. Guerra, "Electron-neutral scattering cross sections for CO_2: a complete and consistent set and an assessment of dissociation," *J. Phys. D: Appl. Phys.*, vol. 49, p. 395207, 2016.

[73] G. J. van Rooij, H. N. Akse, W. Bongers, and M. van de Sanden, "Plasma for electrification of chemical industry: a case study on CO_2 reduction," *Plasma Physics and Controlled Fusion*, vol. 60, p. 014019, 2017.

[74] V. Guerra, T. Silva, P. Ogloblina, M. Grofulović, L. Terraz, M. L. D. Silva, C. D. Pintassilgo, L. L. Alves, and O. Guaitella, "Reply to Comment on 'The case for in situ resource utilisation for oxygen production on Mars by non-equilibrium plasmas'," *Plasma Sources Science and Technology*, vol. 27, no. 2, pp. 15–17, 2018.

[75] T. Silva, V. Guerra, P. Ogloblina, M. Grofulovic, L. Terraz, M. L. da Silva, O. Guaitella, C. D. Pintassilgo, and L. L. Alves, "Living On Mars: How to produce oxygen and fuel to get home," in *Gordon Research Conferences*, 2018.

[76] P. Ogloblina, A. Tejero-Del-Caz, V. Guerra, and L. L. Alves, "Electron impact cross sections for carbon monoxide and their importance in the electron kinetics of CO_2-CO mixtures," *Plasma Sources Science and Technology*, vol. 29, no. 1, 2020.

[77] P. Ogloblina, A. Tejero-del Caz, V. Guerra, and L. L. Alves, "Cross sections for electron collisions with carbon monoxide," in *21st International colloquim on plasma processes CIP*, 2017.

[78] P. Ogloblina, A. Tejero-del Caz, V. Guerra, and L. L. Alves, "Cross sections for electron collisions with carbon monoxide," in *International conference on phenomena in ionized gases ICPIG*, 2017.

[79] P. Ogloblina, A. Tejero-del Caz, V. Guerra, and L. L. Alves, "Electron and vibration kinetics in CO_2/CO mixtures," in *Europhysics Conference on the Atomic and Molecular Physics of Ionized Gases ESCAMPIG*, 2018.

[80] P. Ogloblina, V. Guerra, S.-A. Candas-Morillo, and O. Guaitella, "Effect of the gas temperature and CO content on vibrational kinetics in CO_2 plasma," in *PREMiERE - CO2 Plasmas: a fRIendly MEdium for Renewable Energy Workshop*, 2018.

[81] P. Ogloblina, V. Guerra, A. S. M. Candas, and O. Guaitella, "Influence of carbon monoxide on CO_2 plasma," in *24th International simposium on plasma chemistry*, 2019.

[82] P. Ogloblina, V. Guerra, S.-A. Candas-Morillo, and O. Guaitella, "Plasma reforming for oxygen production on Mars," in *8th European Conference for Aeronautics and Space Science(EUCASS)*, 2019, pp. 1–5.

[83] P. Ogloblina, T. Silva, M. Grofulović, L. Terraz, V. Guerra, A. Morillo-Candas, and O. Guaitella, "CO_2 plasmas: from solar fuels to oxygen production on Mars," in *International Symposium on Plasma Chemistry*, 2019.

[84] A. Tejero-del Caz, V. Guerra, D. Goncalves, M. L. da Silva, L. Marques, N. Pinhão, C. D. Pintassilgo, and L. L. Alves, "The LisbOn KInetics Boltzmann solver," *Plasma Sources Sci. Technol.*, vol. 28, p. 043001, 2019.

[85] L. Alves, "The IST-LISBON database on LXCat," *J. Phys.: Conf. Ser.*, vol. 565, p. 012007, 2014. [Online]. Available: www.lxcat.net/IST-Lisbon

[86] V. Guerra, T. Silva, and O. Guaitella, "Living on mars: how to produce oxygen and fuel to get home," *Europhys. News*, vol. 49, no. 3, pp. 15–18, 2018.

[87] G. Chen, T. Silva, V. Georgieva, T. Godfroid, N. Britun, R. Snyders, and M. P. Delplancke-Ogletree, "Simultaneous dissociation of CO_2 and H_2O to syngas in a surface-wave microwave discharge," *Int. J. Hydrog. Energy*, vol. 40, no. 9, pp. 3789–3796, 2015. [Online]. Available: http://dx.doi.org/10.1016/j.ijhydene.2015.01.084

[88] R. D. Hake and A. V. Phelps, "Momentum-transfer and inelastic-collision cross sections for electrons in O_2, CO, and CO_2," *Phys. Rev.*, vol. 158, no. 1, pp. 70–84, 1967.

[89] L. D. Pietanza, G. Colonna, G. D'Ammando, A. Laricchiuta, and M. Capitelli, "Electron energy distribution functions and fractional power transfer in "cold" and excited CO_2 discharge and post discharge conditions," *Phys. Plasmas*, vol. 23, p. 013515, 2016. [Online]. Available: http://dx.doi.org/10.1063/1.4940782

[90] L. S. Polak and D. I. Slovetsky, "Electron impact induced electronic excitation and molecular dissociation," *Int. J. Radiat. Phys. Chem.*, vol. 8, pp. 257–282, 1976.

[91] V. Guerra and J. Loureiro, "Kinetic model of a low-pressure microwave discharge in O_2-N_2 including the effects of O^- ions on the characteristics for plasma maintenance," *Plasma Sources Science and Technology*, vol. 8, no. 1, pp. 110–124, 1999.

Chapter 2

The case for *in situ* resource utilization

In this chapter it is argued that Mars has nearly ideal conditions for CO_2 decomposition by non-equilibrium plasmas. It is shown that the pressure and temperature ranges in the ~ 96% CO_2 Martian atmosphere favour the vibrational excitation and subsequent up-pumping of the asymmetric stretching mode, which is believed to be a key factor for an efficient plasma dissociation, at the expense of the excitation of the other modes. Therefore, gas discharges operating at atmospheric pressure on Mars are extremely strong candidates to produce O_2 efficiently from the locally available resources. [1]

[1]The results presented here were published as *The case for in situ resource utilisation for oxygen production on Mars by non-equilibrium plasmas*, Vasco Guerra, Tiago Silva, Polina Ogloblina Marija Grofulović, Loann Terraz, Mário Lino da Silva, Carlos D Pintassilgo, Luís L Alves and Olivier Guaitella 2016 Plasma Sources Sci. Technol. 26 11LT01.

2.1 Introduction

Mankind is exploring space for decades, stimulating the imagination and expanding the horizons of knowledge and Mars is the next step of the voyage into the universe. The red planet has resources that can be used for a sustainable settlement. In particular, the local production of oxygen from martian atmosphere may help solving the problems of manufacturing fuel for coming back on Earth and of creating a breathable environment for a future outpost. Such ISRU will diminish the needs of additional launch or lander mass. Accordingly, it will minimise risks to the crew and mission, contribution to reduce logistics, making it possible to increase the space-craft shielding and providing increased self-sufficiency. Moreover, it will reduce costs by demanding the launching of less vehicles to complete the mission [1–4].

Plasma reforming of CO_2 on Earth is also a growing field of research, prompted by the problems of climate change and production of solar fuels [5, 6]. Indeed, low-temperature plasmas constitute one of the best media for CO_2 dissociation, both by direct electron impact and, specially, by transferring electron energy into vibrational excitation [6–10]. As emphisized in previous chapter, the direct electron impact dissociation has an energy threshold above 7 eV, producing CO and O.

The latter mechanism of vibrational up-pumping takes advantage of the non-equilibrium nature of low-temperature plasmas, with the activation of the plasma at relatively low energy-cost, because it is possible to benefit from the energy stored in the vibrational levels. As a matter of fact, an efficient excitation of the vibrational levels can be achieved with a non-thermal plasma source with low mean electron energy (1-2 eV) [8]. Most of the discharge energy is carried by low energy electrons, which effectively transfer it to vibrational excitation of CO_2 and other molecules. If the electron energy can be selectively channelled into the asymmetric stretching mode, it will minimise the losses on the excitation of the other vibration modes and on gas heating. The subsequent VV up-pumping on the asymmetric stretching mode provides a unique way to efficiently break the C=O bond and dissociate the CO_2 molecule [7, 8].

For the characterization of the degree of the CO_2 vibrational excitation it is beneficial to introduce the concept of the characteristic temperatures of each mode of CO_2. From the populations of the excited levels related to the different modes of vibration three characteristic temperatures T_1, T_2 and T_3 can be defined, associated with the symmetric, bending, and asymmetric modes, respectively. It is often found that the characteristic temperatures T_1 and T_2 are very similar and the symmetric and bending modes can be described with a common temperature, T_{12} [11, 12]. Accordingly, to create vibrational imbalance, or vibrational non-equilibrium, the asymmetric stretching mode should be significantly more excited, *e.i.* heated. Therefore, one important parameter to assess the efficiency of CO_2 dissociation seems to be the ratio T_3/T_g, where T_g is the gas temperature, characterising the degree of vibrational non-equilibrium of the plasma [13]. By the same reasoning, the ratio T_3/T_{12}, where T_{12}, is another interesting parameter to maximize.

The knowledge acquired from these investigations on Earth can be transposed to a large extent to ISRU on Mars, with the additional benefit of not requiring carbon capture. Besides, there are several other reasons that were mentioned in chapter 1 why Mars seems to have excellent conditions for ISRU by plasma. In this context, CO_2 vibrational kinetics plays an important role, to the extent that the energy stored in the vibrationally excited states activates the plasma and contributes to an increase in dissociation efficiency, helping low-temperature plasmas to surpass the competing technologies, such as electrolysis and thermo-chemistry. The conjecture of an exceptional VV up-pumping and subsequent CO_2 dissociation on Mars is supported by the opposite dependences of the VT and VV energy transfer rate coefficients when the gas temperature goes down: on the one hand, the VT reaction rates decrease and, accordingly, VT

deactivation is likely to be hindered; on the other hand, the near resonant VV rates *increase* as a result of the long-range attractive forces [14], favouring the VV up-pumping. The purpose of this chapter is to start building a case for *in situ* resource utilisation on Mars using non-equilbrium plasmas, by investigating the similarities and differences of the vibrational energy input and relaxation in CO_2 plasmas for typical conditions on Earth and on Mars.

2.2 Results and discussion

Pulsed DC discharges constitute an ideal system for fundamental studies, since their simple geometry and homogeneity makes them accessible to a series of diagnostics and suitable to the development of 0D self-consistent kinetic models accounting for very complex vibrational and chemical kinetics. CO_2 pulsed discharges have been recently investigated, both experimentally [15, 16] and theoretically [17–19], for a Pyrex cylindrical plasma reactor (23 cm length, 2 cm diameter), operated under flowing conditions in the millibar range, with a pulsed 10-50 mA plasma current at 5/10 ms on/off. In particular, the time-resolved populations of the vibrational levels $\nu_1 \leq 2$, $\nu_2 \leq 6$ and $\nu_3 \leq 5$ – where ν_1, ν_2 and ν_3 correspond to the quanta of vibration in the symmetric stretching, bending and symmetric stretching modes, respectively – were measured by IR absorption [15, 16] and calculated from a detailed self-consistent kinetic model accounting for eV, VT and VV transfers involving ~ 70 vibrational levels [18, 19], whose predictions are in excellent agreement with the experimental results.

Herein the model developed in [17–19] where the self-consistent coupling between the electron and vibrational kinetics is made as described in [20], of non-equilibrium plasmas to efficiently up-pump CO_2 vibrational quanta on Martian conditions. The model couples the electron Boltzmann equation, using the usual two-term expansion approximation, and a system of rate balance equations describing the creation and loss of both the low vibrational levels of CO_2 and of CO_2^+ ions. The model was validated through the comparison of the calculated time-dependent concentrations of several individual vibrational levels of CO_2 with the experimental results obtained in a millisecond pulsed glow discharge as described in [17–19]. To this purpose, we focus on a similar DC pulsed discharge operating at discharge current I = 50 mA, pulse length Δt = 5 ms and gas pressure p = 5 Torr, corresponding to one of the conditions for CO_2 reforming on Earth reported in [15, 17] and to the relevant pressure on Mars taken for both "Earth simulations" and "Mars simulations". The gas temperature profile for the Earth simulations was taken from experiment [15]. The same profile was assumed for Mars, simply shifted down by 100 K, as a consequence of a similar shift in the temperature boundary condition. This assumption was shown to be valid by later measuring the rotational temperature of CO_2 in the DC discharge ignited to simulate the Martian atmosphere. Therefore, the simulations take as input the discharge geometry (R), the discharge operating parameters (I, Δt and p) and, additionally the temporal profile of the gas temperature (T_g). The self-consistently calculated reduced electric fields are $E/N \simeq 63.5$ Td and $E/N \simeq 59.5$ Td, respectively for Earth and for Mars, corresponding to electron temperatures of about 1.7 and 1.6 eV, respectively, with calculated electron densities $n_e = 5.5 \times 10^9$ cm^{-3} and $n_e = 7.1 \times 10^9$ cm^{-3}, respectively. Here, E is the applied electric field and N is the total gas density.

It is worth noting that the system under analysis corresponds to a low excitation regime, where only the first few vibrational levels get excited, no significant CO_2 dissociation takes place [17–19] and, accordingly, the kinetics of CO molecules and O atoms plays a negligible role. Although it might seem strange to adopt these cnditions to assess the efficiency of the plasma-assisted up-pumping of vibrational quanta in CO_2, this is indeed a perfect arrangement to study the input of electron energy into the vibrational levels and its initial redistribution

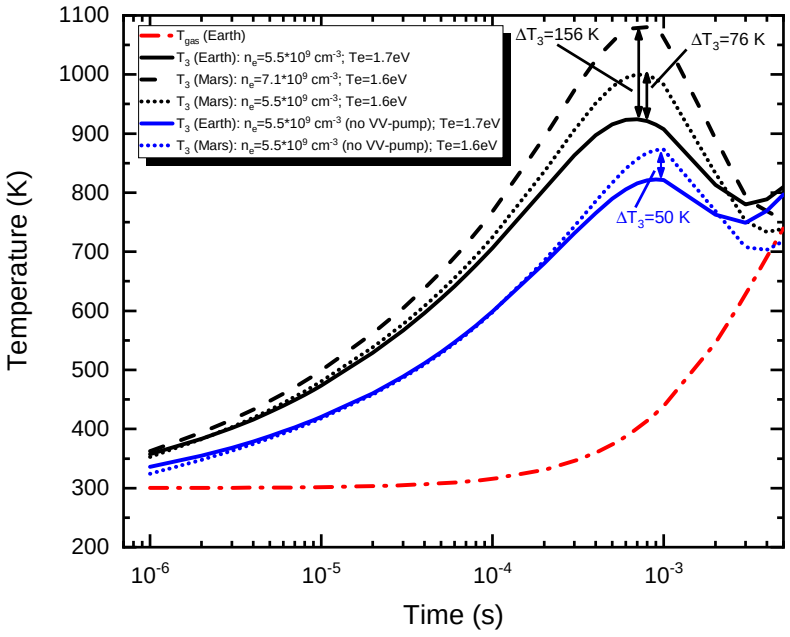

Figure 2.1: Time evolution of the gas (– ·) and the T_3 characteristic temperature for a DC pulsed discharge at p = 5 Torr, I = 50 mA, Δt = 5 ms: (—) Earth; (– –) Mars; (···) the same as "Mars," but with $n_e = 5.5 \times 10^9$ cm^{-3}; (—) Earth without VV up-pumping; (– –) Mars without VV up-pumping.

among the lower levels, that are crucial to determine T_3 and the ratios T_3/T_g and T_3/T_{12} [13].

Figure 2.1 shows the calculated effective vibrational temperature between the first vibrational level of the asymmetric stretching mode ν_3 and the ground state, T_3, as function of time, for a DC pulsed discharge in the conditions described above. The full and dashed black curves reveal that T_3 is strongly enhanced on Mars during the discharge pulse in comparison to the same discharge made on Earth. However, at the end of the discharge pulse this effect vanishes (see however figure 2.3 and respective discussion), which suggests that pulsing appropriately the discharge may maximise the vibrational temperature T_3. The black dotted curve corresponds to the same conditions as in the calculation for Mars, with the exception of the value of the electron density, which is taken the same as on Earth, $n_e = 5.5 \times 10^9$ cm^{-3}. This curve shows that the increase in T_3 on Mars is not due solely to the slightly larger electron density and an enhancement of electron impact vibrational excitation (e-V processes), but it is also an outcome of the complex vibrational kinetics strongly influenced by the gas temperature. This is further confirmed by inspecting behavior of the blue curves in figure 2.1, corresponding to simulations performed without taking into account VV energy exchanges. As it can be seen, in this case the temperatures T_3 for the conditions on Earth and on Mars remain very close and much lower than the actual values, which demonstrates the important role of the VV transfers in the buildup of T_3.

The time-evolution of the densities of the first level of each of the vibration modes during the pulse – denoted here, according to Herzberg's notation [21], as (10^00) for the symmetric

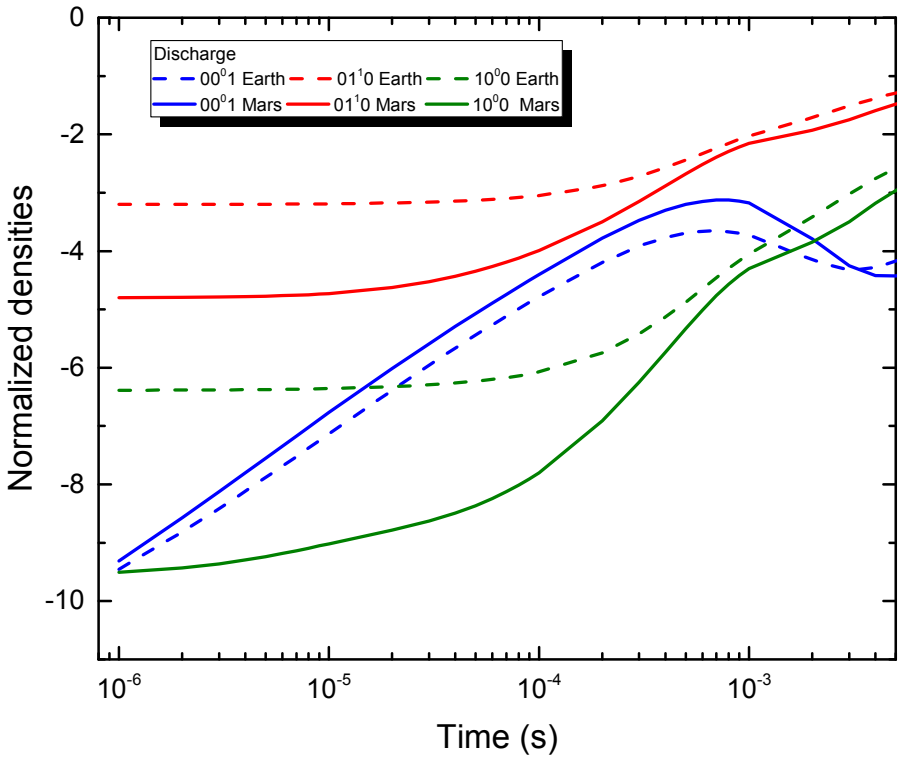

Figure 2.2: Logarithm of the normalised densities of the first level of the symmetric stretching, bending and asymmetric stretching modes, for a DC pulsed discharge at p = 5 Torr, I = 50 mA, Δt = 5 ms: on (—) Mars; on (– –) Earth.

stretching mode (green curves), (01^10) for the bending mode (red curves), and (00^01) for the asymmetric stretching mode (blue curves) – is shown in figure 2.2, depicting the logarithm of the normalised populations with respect to the ground state (00^00), divided by the corresponding statistical weight. This figure discloses a very interesting effect. Besides the efficient pumping of the asymmetric-stretching mode, verified by the higher population of the (00^01) level on Mars than on Earth, the Martian conditions promote as well a stronger internal non-equilibrium, since, contrarily, both levels (10^00) and (01^10) are more populated on Earth than on Mars. Accordingly, advantageous conditions for using non-equilibrium plasmas for CO_2 dissociation can be fulfilled easier on Mars.

For completeness, figure 2.3 represents the non-equilibrium parameter T_3/T_g, suggested in [13] as an important measure of the impact of vibrational kinetics to dissociation, as well as the ratios T_{12}/T_g and T_3/T_{12}, where T_{12} is the characteristic temperature of the symmetric and bending modes. It can be immediately verified that a discharge under Martian atmospheric conditions is very suitable to induce vibrational non-equilibrium, with a larger difference between T_3 and both T_g and T_{12}, anticipating a positive impact on CO_2 dissociation. As noted in figure 2.1, the strongest non-equilibrium is verified for an on-time ~ 0.5 ms, decreasing for longer times. Nevertheless, the ratio T_3/T_g remains higher for Mars than for Earth even at the end of the 5 ms pulse.

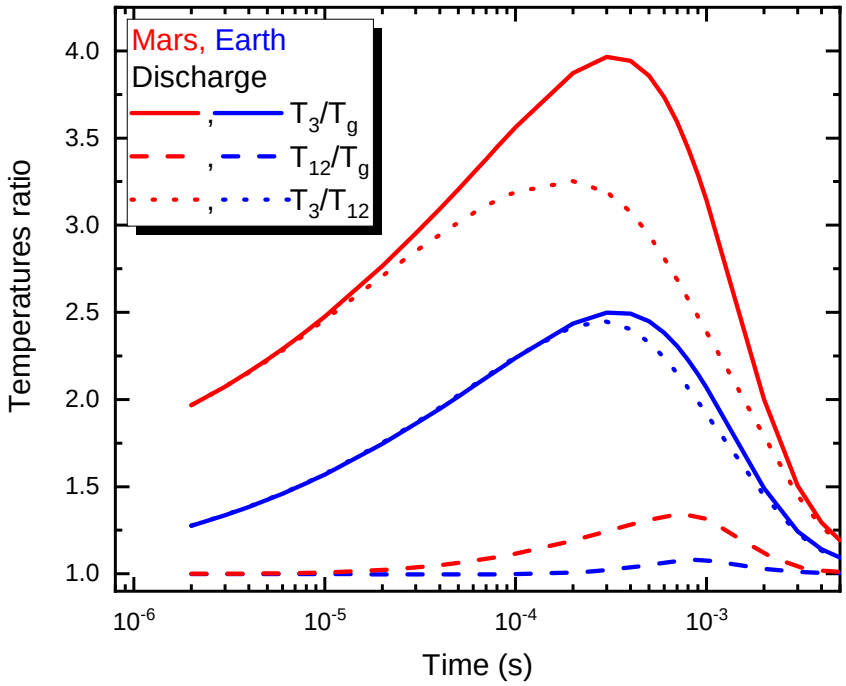

Figure 2.3: Time evolution of the ratio of different characteristic temperatures on a DC pulsed discharge at p = 5 Torr, I = 50 mA, Δt = 5 ms: (—) T_3/T_g; (– –) T_{12}/T_g; (···) T_3/T_{12} for discharges on Mars and Earth.

2.3 Conclusions

The present analysis strongly suggests the possibility of an efficient CO_2 plasma dissociation from the Martian atmosphere, as the low-temperature and low-pressure on Mars allow to obtain a more efficient up-pumping of vibrational quanta into the asymmetric stretching mode and higher ratios T_3/T_g and T_3/T_{12} than under typical conditions on Earth. These simulation predictions are also observed experimentally, as it will be shown in chapter 4. Accordingly, the reasonableness of using non-equilibrium plasmas for efficient oxygen production on Mars is established.

Plasma technologies for CO_2 reforming on Earth are already competitive nowadays with SOEC. Our investigation evinces that a non-equilibrium plasma process can probably perform better than SOEC, the technology proposed by the exciting MOXIE programme [22], for oxygen production on Mars. In fact, while the efficiency of plasma dissociation of CO_2 on Mars is likely to increase as compared to that on Earth, as demonstrated in this chapter, the efficiency of solide oxide electrolysis is likely to decrease, because extra energy is necessary to heat the gas up to ~ 1100 K and to compress it up to ~ 1 atm [22]. In addition, any estimation based on typical gas flows and CO_2 conversion rates obtained on Earth [6] points out that the throughput anticipated by the MOXIE experiment, of about 10 g per hour for a power of 300 W, is perfectly within reach of an optimised plasma device, as debated in chapter 1 (subsection 1.2.3).

Evidently there are still many open challenges and directions for research that will be answered later in the thesis. Nevertheless, the current indications are already extremely promising and are enough to justify further theoretical and experimental research, constituting the first

step to build a case for non-equilibrium plasma *in situ* resource utilisation on Mars.

Bibliography

[1] G. A. Landis and D. L. Linne, "Mars Rocket Vehicle Using In Situ Propellants," *Journal of Spacecraft and Rockets*, vol. 38, no. 5, pp. 730–735, 2001.

[2] J. J. Hartvigsen, S. Elangovan, D. Larsen, J. Elwell, M. Bokil, L. Frost, and L. M. Clark, "Challenges of solid oxide electrolysis for production of fuel and oxygen from mars atmospheric CO_2," *ECS Transactions*, vol. 68, pp. 3563–3583, 2015.

[3] G. B. Sanders, A. Paz, L. Oryshchyn, and K. Araghi, "Mars ISRU for Production of Mission Critical Consumables – Options , Recent Studies , and Current State of the Art," *SPACE Conferences and Exposition*, pp. 1–14, 2015.

[4] NASA, "In-situ Resource Utilization (ISRU)," Tech. Rep., 2016.

[5] A. P. Goede, W. A. Bongers, M. F. Graswinckel, R. M. van de Sanden, M. Leins, J. Kopecki, A. Schulz, and M. Walker, "Production of solar fuels by CO_2 plasmolysis," *EPJ Web of Conferences*, vol. 79, p. 01005, 2014.

[6] G. J. van Rooij, D. C. M. van den Bekerom, N. den Harder, T. Minea, G. Berden, W. A. Bongers, R. Engeln, M. F. Graswinckel, E. Zoethout, and M. C. M. van de Sanden, "Taming microwave plasma to beat thermodynamics in CO_2 dissociation," *Faraday discussions*, vol. 183, pp. 233–248, 2015. [Online]. Available: http://pubs.rsc.org/en/Content/ArticleHTML/2015/FD/C5FD00045A

[7] P. Capezzuto, F. Cramarossa, R. D'Agostino, and E. Molinari, "Contribution of vibrational excitation to the rate of carbon dioxide dissociation in electrical discharges," *J. Phys. Chem.*, vol. 80, pp. 882–888, 1976.

[8] A. Fridman, *Plasma Chemistry*. Cambridge University Press, 2008.

[9] T. Kozák and A. Bogaerts, "Splitting of CO_2 by vibrational excitation in non-equilibrium plasmas: a reaction kinetics model," *Plasma Sources Science and Technology*, vol. 23, p. 045004, 2014. [Online]. Available: http://stacks.iop.org/0963-0252/23/i=4/a=045004?key=crossref.ae2245ca0b3f38b3e8652fc96aea2549

[10] L. D. Pietanza, G. Colonna, G. D'Ammando, A. Laricchiuta, and M. Capitelli, "Vibrational excitation and dissociation mechanisms of CO_2 under non-equilibrium discharge and post-discharge conditions," *Plasma Sources Sci. Technol.*, vol. 24, p. 042002, 2015.

[11] T. Silva, M. Grofulović, B. Klarenaar, A. Morillo-Candas, O. Guaitella, R. Engeln, C. Pintassilgo, and V. Guerra, "Kinetic study of low-temperature CO_2 plasmas under non-equilibrium conditions. I. Relaxation of vibrational energy," *Plasma Sources Sci. Technol.*, 2017.

[12] M. Grofulović, T. Silva, B. Klarenaar, A. Morillo Candas, O. Guaitella, R. Engeln, C. Pintassilgo, and V. Guerra, "Kinetic study of CO_2 plasmas under non-equilibrium conditions. II.Input of vibrational energy," *Plasma Sources Sci. Technol*, vol. 27, p. 115009, 2018.

[13] P. Diomede, M. C. M. van de Sanden, and S. Longo, "Insight into CO_2 dissociation in plasmas from numerical solution of a vibrational diffusion equation," arXiv:1705.10144 [physics.chem-ph], 2017.

[14] R. T. Pack, "Analytic estimation of almost resonant molecular energy transfer due to multipolar potentials. VV processes involving CO_2," *J. Chem. Phys.*, vol. 72, pp. 6140–6152, 1980.

[15] B. L. M. Klarenaar, R. Engeln, M. A. Damen, M. C. M. van de Sanden, A. S. Morillo-Candas, P. Auvray, and O. Guaitella, "Measuring vibrational excitation of CO_2 in a pulsed glow discharge," in *Proceedings of the ISPC23 (International Symposium on Plasma Chemistry)*, Montréal, Canada, 2017.

[16] B. L. M. Klarenaar, R. Engeln, D. C. M. van den Bekerom, M. C. M. van de Sanden, A. S. Morillo-Candas, and O. Guaitella, "Time evolution of vibrational temperatures in a CO_2 glow discharge measured with infrared absorption spectroscopy," *Plasma Sources Sci. Technol.*, vol. 26, p. 115008, 2017.

[17] T. Silva, M. Grofulović, B. L. M. Klarenaar, O. Guaitella, R. Engeln, C. D. Pintassilgo, and V. Guerra, "Understanding the electron and vibration kinetics in CO_2 plasmas," in *Proceedings of the ICPIG XXXIII (International Conference on Phenomena in Ionized Gases)*, Estoril, Portugal, 2017.

[18] T. Silva, M. Grofulović, L. Terraz, C. D. Pintassilgo, and V. Guerra, "Modelling the input and relaxation of vibrational energy in CO_2 plasmas," *J. Phys. D: Appl. Phys.*, vol. 51, p. 464001, 2018.

[19] T. Silva, M. Grofulović, B. L. M. Klarenaar, O. Guaitella, R. Engeln, C. D. Pintassilgo, and V. Guerra, "Kinetic study of CO_2 plasmas under non-equilibrium conditions. I. Relaxation of vibrational energy," *Plasma Sources Sci. Technol.*, vol. 27, p. 015019, 2018.

[20] C. D. Pintassilgo, V. Guerra, O. Guaitella, and A. Rousseau, "Study of gas heating mechanisms in millisecond pulsed discharges and afterglows in air at low pressures," *Plasma Sources Sci. Technol.*, vol. 23, p. 025006, 2014.

[21] G. Herzberg, *Molecular Spectra and Molecular Structure - II: Infrared and Raman Spectra of Polyatomic Molecules.* D. van Nostrand, 1951.

[22] M. H. Hecht, D. R. Rapp, , and J. A. Hoffman, "The Mars Oxygen ISRU experiment (MOXIE)," https://ssed.gsfc.nasa.gov/IPM/PDF/1134.pdf.

Chapter 3

CO cross section and CO_2/CO electron kinetics

This chapter proposes a complete and consistent set of cross sections for electron impact collisions with carbon monoxide (CO), to be published in the IST-Lisbon database with LXCat. The set is validated by comparing swarm parameters calculated using the two-term LisbOn Kinetics Boltzmann solver LoKI-B with available experimental data. A severe inconsistency between the total rotational and effective cross sections reported in the literature for low values of the electron energy ($\epsilon < 0.1$ eV) is pointed out. It is shown that inelastic and superelastic collisions involving rotationally excited levels, as well as superelastic collisions with the first vibrational excited level, have to be taken into account in order to accurately calculate the EEDF. The relevance of these mechanisms implies a dependence of the effective momentum transfer cross section with the gas and the vibrational temperatures and suggesting that it would be better replaced by an elastic momentum transfer cross section. The electron kinetics in CO_2-CO mixtures is also discussed in detail, namely the influence of vibrational excitation and of the CO_2/CO ratio on the EEDF, rate coefficients and power transfer. The vibrational temperatures of both CO and the different vibrational modes of CO_2 have a marked influence on the results, due to the importance of superelastic collisions with the vibrationally excited states of both gases. The presence of CO in the mixture modifies the energy transfer pathways and, at moderate reduced electric fields ($\sim 30 - 100$ Td), vibrational excitation of CO can become the dominant energy loss mechanism, affecting the input of electron energy into the asymmetric stretching mode of CO_2.[1]

[1]The results presented here were published as *Electron impact cross sections for carbon monoxide and their importance in the electron kinetics of CO_2–CO mixtures*, Polina Ogloblina, Antonio Tejero-del-Caz, Vasco Guerra and Luis L. Alves, 2020 Plasma Sources Sci. Technol. 29 015002.

3.1 Introduction

Carbon monoxide (CO) is one of the main constituents of the atmospheres of Venus and Mars [1–3] and is the most abundant molecule observed in the interstellar space after hydrogen. Electron collisions with CO play an important role in the study of various processes occurring in planets and comets, in the physics of spacecraft reentries into the Venusian and Martian atmospheres [4–9] and in the deployment of ISRU for oxygen production on Mars [10–12]. CO is also relevant in laboratory gas discharges for the production of gas lasers [13, 14], syngas [15–17] and the reforming of CO_2 [18–33]. The latter subject has received much attention in recent years, essentially because CO_2 is one of the main greenhouse gases and global warming is becoming a growing challenge to face. The interest of low-temperature plasmas in this context lies in the fact that the electron energy can be channelled to efficiently dissociate CO_2 into oxygen and carbon monoxide, a necessary step to produce syngas and to create hydrocarbons for energy storage from renewable energy sources.

The study of the electron kinetics is essential in all the aforementioned applications, allowing to understand how the energy gained by electrons is transferred to the different heavy-particles. CO is typically one of the main components of the gas mixture in any CO_2-containing plasma, since it is a stable product resulting from CO_2 dissociation. Therefore, electron collisions with CO play an important role in shaping the EEDF and, accordingly, in the understanding of the energy pathways in these plasmas. As a prior requirement for an accurate calculation of the EEDF and the subsequent modelling of CO and CO_2 plasmas, a reliable set of electron impact cross sections for electron-CO collisions is necessary.

The purpose of this chapter is twofold. First, we present a complete and consistent set of electron-neutral scattering cross sections for carbon monoxide, included in the IST-Lisbon database [34] with LXCat. Second, since CO is a product of dissociation of CO_2 and is present in a CO_2-CO mixture, we study in some detail the electron kinetics in CO_2-CO mixtures. Herein all the calculations are made using the free two-term LisbOn KInetics Boltzmann solver (LoKI-B) [35, 36] which handles simulations for molecular gases in a user-friendly way, namely by accounting for the excitation and de-excitation of electronic, vibrational and rotational degrees of freedom.

The cross section set proposed here is considered *complete* because it includes all the necessary energy and momentum-transfer processes, allowing the calculation of an EEDF using a kinetic code, namely the elastic momentum transfer, inelastic losses, non-conservative processes (ionization and attachment) and all the relevant superelastic gains. Moreover, the set is *consistent* because it allows reproducing the experimentally measured electron transport parameters by using kinetic simulations.

The present IST-Lisbon cross section set is constructed based essentially on the works of Itikawa [37], Land [38], Hake and Phelps [39], Laporta *et al.* [40] and Phelps [41]. Itikawa has collected previous experimental results of cross sections for electron collisions with carbon monoxide [37]. His compilation is one of the largest collections of cross sections to date, which presents also a valuable discussion about the data available from calculations, yet giving preference to cross sections determined experimentally. However, no verification of the consistency of the cross section set with experimentally obtained transport coefficients is made. In this regard, notice that the cross section set available from Phelps' database with LXCat [42] is not complete, since it does not include rotational excitation. Nevertheless, it can be used for calculations at mid and high reduced electric fields ($E/N \gtrsim 10$ Td), where the contribution from these processes is not very important.

The data from [37, 38] are used to define the elastic momentum transfer cross section and the cross sections for the excitation of the electronically excited levels. The cross sections for

dissociation, dissociative attachment and ionization are taken from [37]. Hake and Phelps [39] published a theoretical study on rotational excitation for low energies, extensively used in this work. However, they have not addressed the following important difficulty: although rotational excitation and de-excitation is the dominant energy loss mechanism at low reduced electric fields (typically $E/N \lesssim 1$ Td), to date, the near-threshold magnitudes of these cross sections are not accessible experimentally and the available calculations are incompatible with the generally accepted effective momentum transfer cross section. This issue is carefully addressed and discussed in section 3.2.2 and a proposal of a solution to this problem constitutes one important contribution from this work. Finally, we have adopted cross sections for vibrational excitation and de-excitation largely based on the R-matrix calculations for resonant excitation from Laporta and co-workers [40], including also contributions from non-resonant collisions taken from [41].

The electron kinetics in CO plasmas has been recently studied in a series of papers from the Bari group [18, 19, 43–45] where CO discharges are analysed for non-equilibrium conditions. The theoretical investigation addresses the coupling between the electron and heavy-particle kinetics, including electron-molecule resonant processes and the whole vibrational *ladder-climbing* mechanism of the CO molecule. These authors adopt the momentum transfer cross section from [42], which can be used without the inclusion of the rotational excitation and de-excitation for the range of the reduced fields studied in [19] (30-60 Td). They also analyse the evolution of the EEDF in a microwave discharge and its post-discharge, highlighting the role of superelastic collisions with vibrational and electronic states in shaping the EEDF. The effect of superelastic collisions with vibrationally excited states is also discussed in this chapter (section 3.4). The dissociative electron attachment from vibrationally excited CO through formation of CO^- is calculated in [45]. These processes are important in shaping the EEDF for high-pressure plasmas with high vibrational excitation, when taking into account vibrational-vibrational (VV) collisions between two vibrationally excited molecules [44].

Studies of the electron kinetics in CO_2 discharges were recently carried out by Pietanza *et al* [46] and Grofulović *et al* [47]. The latter paper proposes a complete and consistent set of electron impact cross sections for CO_2, available in the IST-Lisbon database with LXCat. For relatively low reduced electric fields, $E/N \lesssim 70$ Td (see section 3.4.3), such as those encountered in many plasma applications, most of the energy absorbed by electrons in a pure CO_2 discharge is transmitted to the excitation of the vibrational levels of the CO_2 molecule. For this reason, vibrational kinetics can play an important role in the overall kinetics. For instance, it has been suggested that the excitation along the asymmetric stretching mode may have an important contribution in enhancing CO_2 dissociation [22]. The role of superelastic vibrational collisions in pure CO_2 discharges and afterglows is addressed in detail in [46].

In this chapter, the studies from [19, 46, 47] are extended towards mixtures of CO_2 and CO, by investigating the electron kinetics in CO_2-CO mixture, from pure CO_2 to pure CO, and by studying the influence of the various vibrational temperatures and the role of superelastic collisions with vibrationally excited states of both CO_2 and CO. In fact, when dissociation takes place in plasma discharge, other species, like O and, after chemical transition, O_2 may influence the EEDF, power balance and electron impact rate coefficients. However, due to the higher concentration of CO and the globally higher cross sections as compared with O and O_2, as a first step we study separetly the influence of CO in CO_2 plasmas. The cross section set for CO_2 is taken from [47] and CO is accounted for with the cross section set proposed in this work. The present results constitute an update of the seminal paper by Nighan [48], where the role of superelastic collisions with vibrationally excited states are pointed out for the first time, using as examples N_2, CO_2 and CO, as well as CO_2-CO and other mixtures.

The structure of this chapter is as follows. Section 3.2 describes in detail the construction

of the IST-Lisbon cross section set for CO. Specific attention is given to the modifications in relation to published data of the rotational and elastic cross sections. The comparison of swarm parameters, calculated from a two-term Boltzmann equation and measured, is presented and discussed in section 3.3. Section 3.4 is devoted to the description of the electron kinetics in CO-CO_2 mixtures with different concentrations of CO_2. Finally, the concluding remarks are summarized in section 3.5.

3.2 Description of the electron cross section set in CO

3.2.1 Overview

Figure 3.1 presents the proposed swarm-derived complete and consistent set of electron-neutral scattering cross sections for CO, to be included in the IST-Lisbon database with LXCat. The set contains elastic momentum transfer, excitation and deexcitation of 16 rotational states (including cross sections for all the transitions involving a single jump of the rotational quantum number, $J \rightleftharpoons J+1$) and of 10 vibrational states (including all the transitions between these vibrational levels, $v = 0-10 \rightleftharpoons w = 0-10$), excitation of 7 electronic states from the ground state, as well as the cross sections for dissociation, dissociative attachment and ionization. Tables 3.1 - 3.3 summarize the mechanisms included in the current cross section set.

Hake and Phelps [39] have obtained an effective momentum-transfer and inelastic cross sections from experimentally measured values of electron transport coefficients such as the drift velocity, the characteristic energy and the Townsend ionization coefficient. Using the same method, Land [38] revisited and improved the previously obtained cross section for effective momentum transfer, taking into account more recent experimental results. Land's results seem to be compatible with the newer measurements reported by Itikawa [37]. However, in the swarm analysis from [38, 39] the rotational transitions are taken into account as one of the inelastic processes. Thus, the swarm derived momentum-transfer cross section [38] cannot be simply compared with the data from [37], and a rigorous assessment of the compatibility between both cross sections is not easy to perform. In this work the elastic momentum transfer cross section was built in two steps, with the mid- and high-energy regions taken from [49, 50], as given in [37], with small adjustments, while the low-energy region was re-calculated from an effective cross section [38] in order to ensure consistency when rotational excitations are explicitly accounted for (see section 3.2.2). The rotational excitation and de-excitation cross sections are taken from [39], with a small number of modifications in the near-threshold region (also described in section 3.2.2). Vibrational excitation is based in [40, 41]. The electronic excitation cross sections are essentially the ones from [37, 38], based on the proposals of [50–55] with an extension up to electron energies of 1000 eV. Finally, the dissociation, dissociative attachment and ionization cross sections are the ones recommended and given in [37], obtained by Cosby [56], Rapp and Briglia [57] and Rapp [58], respectively. These cross sections, and the modifications introduced in the IST-Lisbon dataset with respect to the literature, are further discussed below.

3.2.2 Elastic and rotational excitation cross sections

A preliminary analysis of the electron transport parameters has shown that for low reduced electric fields ($10^{-4} - 10^{-1}$ Td) most of the electron energy losses are associated with rotational excitation. For dipole interactions these cross sections can be calculated from the Born approximation, as discussed by Hake and Phelps [39], who reported good usability of this approximation

No	Name	Heavy-species products	Threshold (eV)	Reference
1	Elastic	CO		[37](⋆)
2	Vibrational excitation	CO(X, $v = 1$)	0.266	[40], [41](⋆)
3	Vibrational excitation	CO(X, $v = 2$)	0.266	[40]
4	Vibrational excitation	CO(X, $v = 3$)	0.54	[40]
5	Vibrational excitation	CO(X, $v = 4$)	0.81	[40]
6	Vibrational excitation	CO(X, $v = 5$)	1.07	[40]
7	Vibrational excitation	CO(X, $v = 6$)	1.33	[40]
8	Vibrational excitation	CO(X, $v = 7$)	1.59	[40]
9	Vibrational excitation	CO(X, $v = 8$)	1.84	[40]
10	Vibrational excitation	CO(X, $v = 9$)	2.09	[40]
11	Vibrational excitation	CO(X, $v = 10$)	2.33	[40]
12	Electronic excitation	CO($a\ ^3\Pi$)	6.006	[51]
13	Electronic excitation	CO($a'\ ^3\Sigma^+$)	6.8	[52], [53](⋆)
14	Electronic excitation	CO($A\ ^1\Pi$)	8.024	[54]
15	Electronic excitation	CO($b\ ^3\Sigma^+$)	10.399	[51]
16	Electronic excitation	CO($B\ ^1\Sigma^+$)	10.777	[50]
17	Electronic excitation	CO($C\ ^1\Sigma^+$)	11.396	[55]
18	Electronic excitation	CO($E\ ^1\Pi$)	11.524	[55]
19	Ionization	$CO^+ + e$	14.01	[58]
20	Dissociative attachment	$C + O^-$		[57]
21	Dissociation	C + O	11.1	[56]

(⋆) this work (see text)

Table 3.1: Summary of the cross section set proposed in this work: elastic collisions, excitations of vibrational states from CO($X, v = 0$), excitation of electronic states, ionization, dissociative attachment and dissociation from the ground state CO.

No	Initial state	Final state	Threshold (eV)	Reference
22	CO(X, $v = 0$, $J = 0$)	CO(X, $v = 0$, $J = 1$)	$4.73 \cdot 10^{-4}$	[39](⋆)
23	CO(X, $v = 0$, $J = 1$)	CO(X, $v = 0$, $J = 2$)	$9.574 \cdot 10^{-4}$	[39](⋆)
24	CO(X, $v = 0$, $J = 2$)	CO(X, $v = 0$, $J = 3$)	$1.419 \cdot 10^{-3}$	[39](⋆)
25	CO(X, $v = 0$, $J = 3$)	CO(X, $v = 0$, $J = 4$)	$1.9 \cdot 10^{-3}$	[39](⋆)
26	CO(X, $v = 0$, $J = 4$)	CO(X, $v = 0$, $J = 5$)	$2.368 \cdot 10^{-3}$	[39](⋆)
27	CO(X, $v = 0$, $J = 5$)	CO(X, $v = 0$, $J = 6$)	$2.876 \cdot 10^{-3}$	[39]
28	CO(X, $v = 0$, $J = 6$)	CO(X, $v = 0$, $J = 7$)	$3.339 \cdot 10^{-3}$	[39]
29	CO(X, $v = 0$, $J = 7$)	CO(X, $v = 0$, $J = 8$)	$3.789 \cdot 10^{-3}$	[39]
30	CO(X, $v = 0$, $J = 8$)	CO(X, $v = 0$, $J = 9$)	$4.293 \cdot 10^{-3}$	[39]
31	CO(X, $v = 0$, $J = 9$)	CO(X, $v = 0$, $J = 10$)	$4.76 \cdot 10^{-3}$	[39]
32	CO(X, $v = 0$, $J = 10$)	CO(X, $v = 0$, $J = 11$)	$5.272 \cdot 10^{-3}$	[39]
33	CO(X, $v = 0$, $J = 11$)	CO(X, $v = 0$, $J = 12$)	$5.718 \cdot 10^{-3}$	[39]
34	CO(X, $v = 0$, $J = 12$)	CO(X, $v = 0$, $J = 13$)	$6.198 \cdot 10^{-3}$	[39]
35	CO(X, $v = 0$, $J = 13$)	CO(X, $v = 0$, $J = 14$)	$6.715 \cdot 10^{-3}$	[39]
36	CO(X, $v = 0$, $J = 14$)	CO(X, $v = 0$, $J = 15$)	$7.128 \cdot 10^{-3}$	[39]
37	CO(X, $v = 0$, $J = 15$)	CO(X, $v = 0$, $J = 16$)	$7.564 \cdot 10^{-3}$	[39]

(⋆) this work (see text) .

Table 3.2: Summary of the cross section set proposed in this work (cont.): rotational excitation

No	Initial state	Final state	Reference
38	CO(X, $v = 1$)	CO(X, $w = 2$)	[40]
⋮	⋮	⋮	⋮
47	CO(X, $v = 1$)	CO(X, $w = 10$)	[40]
48	CO(X, $v = 2$)	CO(X, $w = 3$)	[40]
⋮	⋮	⋮	⋮
83	CO(X, $v = 9$)	CO(X, $w = 10$)	[40]

Table 3.3: Summary of the cross section set proposed in this work (cont.): stepwise vibrational excitation

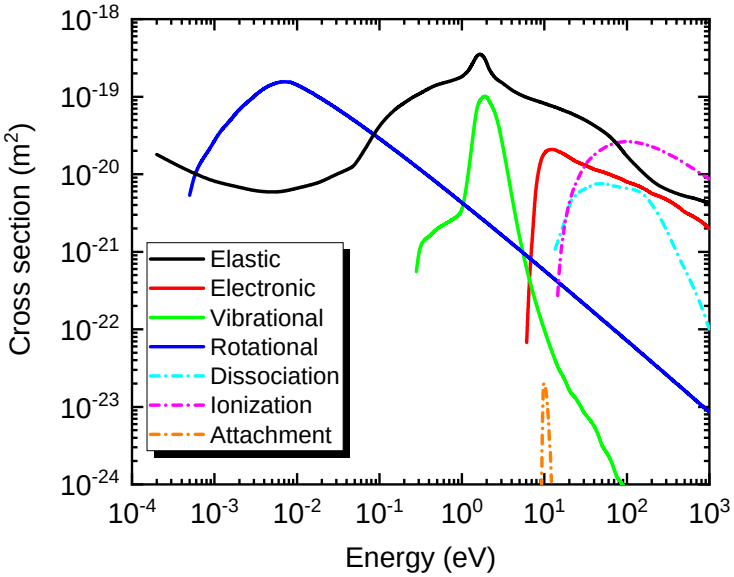

Figure 3.1: Summary of the IST-Lisbon set of electron-impact cross sections for CO, as a function of the electron kinetic energy. Here, for mere representation purposes, both the rotational and the vibrational cross sections are total cross sections, calculated as the sum of contributions from the individual levels, weighted by their populations for a Boltzmann distribution at T_g = 300 K.

for carbon monoxide. Therefore, the cross sections for rotational inelastic processes $J \rightarrow J+1$ are given by [39]

$$\sigma_{J,J+1}(\epsilon) = \frac{(J+1)R_y\sigma_r}{(2J+1)\epsilon} ln\frac{[\epsilon^{1/2} + (\epsilon - \epsilon_J)^{1/2}]}{[\epsilon^{1/2} - (\epsilon - \epsilon_J)^{1/2}]}, \tag{3.1}$$

where ϵ is the electron kinetic energy in eV, $\sigma_r = 8\pi\mu^2 a_0^2/3$, $\mu = 4.4 \cdot 10^{-2}$ is the electric dipole moment in units of ea_0, a_0 is the Bohr radius, J is the rotational quantum number of the initial state, R_y = 13.6 eV is the Rydberg constant in eV and $\epsilon_J = 2(J+1)B_0$ is the energy threshold, with $B_0 = 2.4 \cdot 10^{-4}$ eV the rotational constant for CO. The cross sections for the $J \rightarrow J-1$ de-excitation of the Jth rotational level are given by

$$\sigma_{J,J-1}(\epsilon) = \frac{JR_y\sigma_r}{(2J+1)\epsilon} ln\frac{[(\epsilon + \epsilon_{-J})^{1/2} + \epsilon^{1/2}]}{[(\epsilon + \epsilon_{-J})^{1/2} - \epsilon^{1/2}]}, \tag{3.2}$$

where $\epsilon_{-J} = 2JB_0$ is the energy gained by an electron in the collision. Note, that

$$g_{J+1}\sigma_{J,J+1}(\epsilon)\epsilon = g_J\sigma_{J,J+1}(\epsilon + \epsilon_J)(\epsilon + \epsilon_J), \tag{3.3}$$

where g_J and g_{g+1} are the degeneracies of rotational level J and J +1, respectively and, for the case of CO, can be calculated as

$$g_J = 2J(J+1), \tag{3.4}$$

$$g_{J+1} = 2(J+1)(J+2). \tag{3.5}$$

This approximation does not include the resonant structure of the rotational cross sections near 1.7 eV; however, the error introduced by omitting this structure is expected to be small, since the energy lost to rotational excitation in the resonance region is much smaller than that due to vibrational excitations [38].

The cross sections calculated from (3.1) and (3.2) are consistent with the studies of Crawford and Dalgarno [59], who have applied the close-coupling method to calculate the rotational cross sections for energies below 0.1 eV. Dickinson and Richards [60] have presented a model to calculate the rotational excitation of polar molecules by electrons; the difference with the Born approximation is noticeable only near the energy threshold, whereas in the mid and high energy ranges it corresponds well to the calculations from (3.1)-(3.2). (*cf.* figure 3.2(a)). Dyatko and co-workers studied numerically the vibrational and the electron energy distribution functions in CO decaying plasmas [61]. The rotational cross sections used in [61] are taken from [62] and include the resonance peak at 1.7 eV. Chandra [62] divided the scattering problem in two regions separated by the boundary point where a molecule-fixed frame of reference is transformed into a space-fixed reference frame. He obtained the momentum transfer cross section, as well as the total scattering cross section, the differential and the integral cross sections for electron-impact rotational transitions. His momentum transfer cross section disagrees in the intensity of the resonance peak with that obtained by Hake and Phelps [39] and Land [38], but the agreement is good in the remaining regions. Moreover, for electron energies in the range $0.1 - 0.2$ eV the rotational cross section from Chandra [62] is also in good agreement with the ones obtained by Dickinson [60], Crawford and Dalgarno [59] and the ones included in the current set (*cf.* figure 3.2(a)). We have also verified that the inclusion of the resonance peak in the rotational cross sections does not lead to any relevant changes in the calculated values of electron transport parameters, as predicted by Land [38].

In plasma modelling it is common practice to use swarm-derived *effective* momentum transfer cross sections, including total momentum transfer contributions from elastic collisions, as well as from the total excitation and ionization processes [39, 47, 63]. In this case, an elastic momentum transfer cross section can be approximately obtained from the corresponding effective cross section by *subtraction* of all the inelastic cross sections assumed isotropic. When solving the electron Boltzmann equation, the effective momentum transfer cross section should be used in the term of energy gain in the electric field operator, whereas the elastic momentum transfer cross section should be used in the elastic collision operator [35, 63, 64]. This procedure poses a stringent difficulty in the case of CO, as it is evident by inspection of figure 3.2(b), where the effective momentum transfer cross section proposed by Land [38] and the total rotational cross section calculated from (3.1)-(3.2) are depicted. The total rotational cross section is calculated as a sum of the individual inelastic and superelastic cross sections, weighted by the populations of the corresponding rotational levels, assuming a Boltzmann distribution at a gas temperature $T_g = 300$ K.

Because the momentum transfer cross section at low energies is dominated by inelastic transitions [65], the effective momentum transfer and the rotational cross sections from [38] and [39] are physically inconsistent. As shown in figure 3.2(b), the effective momentum transfer cross section is *lower* than the total rotational cross section in the region $10^{-3} - 10^{-1}$ eV. Hence, if an elastic cross section were to be obtained from that effective momentum transfer, it would yield negative values. Thus, while the effective momentum-transfer cross section inferred from the swarm analysis may be a useful construct, when inelastic processes dominate it is not clear how the different mechanisms should actually being taken into account when solving the electron Boltzmann equation. Another difficulty in using effective cross sections as input to Boltzmann solvers resides in the fact that the rotational and vibrational level populations depend on the

gas temperature (assuming equilibrium distributions among these levels, otherwise they would depend on the characteristic rotational and vibrational temperatures, T_{rot} and T_{vib}). This means that, for conditions corresponding to different values of T_g (and/or T_{rot} and T_{vib}), different elastic cross sections are obtained, which is unphysical. For these reasons, we recommend, whenever possible, to adopt elastic momentum transfer cross sections as input data to any Boltzmann solver, calculating the corresponding effective cross sections by *addition* of the inelastic and superelastic contributions.

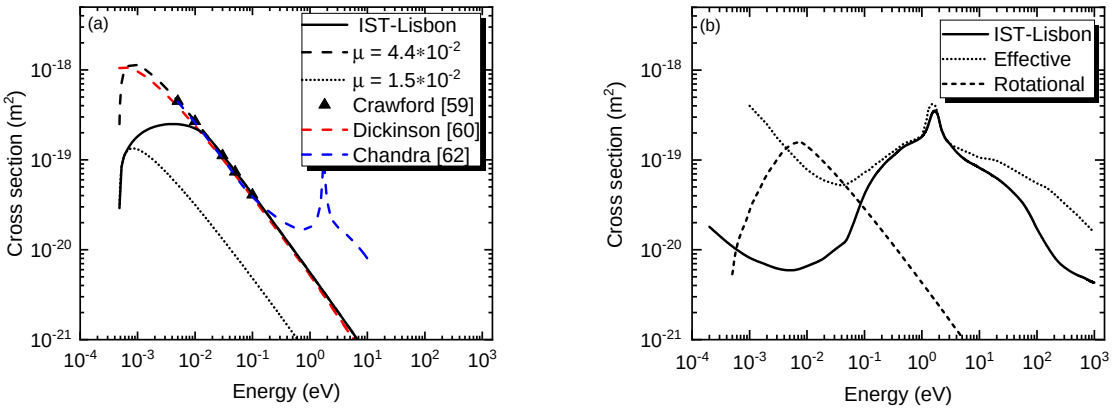

Figure 3.2: (a) 0→1 rotational cross section calculated from the Born approximation with $\mu = 4.4 \cdot 10^{-2}$ (– –) and $1.5 \cdot 10^{-2}$ (···), proposed in the calculations from [59] (▲), [60] (– –), [62] (– –), and used in this work (—); (b) Proposed elastic cross section (—) , effective momentum transfer cross section from [38] (···) and total rotational excitation cross section (– –) assuming that the populations of the rotational states follow a Boltzmann distribution with temperature T_{rot} = 300 K.

Figure 3.2.b presents the elastic momentum transfer cross section proposed in this work, assumed the same for all energy states, hence not embedding any temperature dependence. The subtraction of all inelastic processes from the effective momentum transfer cross section of [38] gives a good platform for start building the elastic momentum transfer cross section. For electron energies above 10^{-1} eV, the result of this procedure closely follows the elastic momentum transfer cross section given by Itikawa [37], with very small differences in the resonant part. The momentum-transfer cross section for the low-energy region was reported by Jain and Norcross [65]. Their theoretical work presents calculations of rotationally elastic, inelastic and total cross sections (including a thermal average over a Boltzmann distribution on the rotational states) down to 10^{-3} eV. The rotationally elastic cross section includes contributions from different energy levels, thus it depends on the gas temperature. Here, to obtain a "pure elastic" momentum transfer cross section in the low energy region, we have extrapolated the higher energy region of Itikawa's cross section [37] down to electron energies below 10^{-1} eV, where the effective/rotational cross section inconsistency just described emerges, while ensuring a good calculation of the swarm parameters of the plasma (see section 3.3). The resulting cross section does not include any contribution from rotational excitation and de-excitation processes and is significantly smaller than the effective cross section from [39].

The same criterion of validation with swarm data led to a modification in the near-threshold region of some rotational excitation cross sections, which had to be decreased in order to get an effective cross section closer to the one proposed in [38]. Figure 3.2(a) presents the changes

made to the rotational cross section for the excitation of level $J = 1$ from $J = 0$, as well as the comparison with the cross sections from [39] given by expressions (3.1) and those calculated by Dickinson and Richards [60], Crawford and Dalgarno [59] and by Chandra [62]. The near-threshold rotational cross section in our set is calculated using expression (3.1) with a decreased dipole moment ($\mu = 1 - 1.5 \cdot 10^{-2}$) while matching the theoretical estimations for electron energies above $\sim 10^{-2}$ eV, in agreement with calculations from (3.1) at $\mu = 4.4 \cdot 10^{-2}$, as of figure 3.2.a. Similar modifications were made in the excitation cross sections of the first 5 rotational transitions. For consistency, the superelastic cross sections for rotational de-excitations are obtained from the Klein-Rosseland relation [66].

3.2.3 Other inelastic cross sections

The IST-Lisbon cross section set accounts for the excitation and de-excitation of 10 vibrational levels. In a recent work, Laporta *et al.* [40] calculated state-to-state cross sections for the electron impact resonant vibrational excitations $v_i \rightarrow v_f$, where the initial and final quantum numbers vary between 0 and 81, $0 \leq v_i \leq v_f \leq 81$. Their calculations give more accurate and detailed vibrational excitation cross sections than those reported before [37, 38]. However, the near threshold region for the excitation of the first vibrational level described by Phelps [41] seems to include a significant contribution from non-resonant excitation. Figure 3.3 depicts the cross sections for resonant excitation of levels $v_f = 1 - 5$ from $v_i = 0$ from [40], together with the low-energy region of the $0 \rightarrow 1$ transition from [41]. For this latter process, we keep the low-energy cross section from [41] below ~ 1 eV, while the cross section from [40] is used for larger electron energies. For all the other transitions, corresponding to $v_i < v_f \leq 10$, Laporta's cross sections [40] are used without any modification. Superelastic collisions with vibrationally excited molecules are considered using the Klein-Rosseland relation. The energy gained by superelastic collisions is noticeable for low reduced electric fields, as discussed in section 3.3.

The cross sections for electron-impact excitation of the electronic states of CO are based on the works by Itikawa [37], Sawada *et al* [51] and Chung and Lin [53], accounting for the excitation of states $a\ ^3\Pi$, $a'\ ^3\Sigma^+$, $A\ ^1\Pi$, $b\ ^3\Sigma^+$, $B\ ^1\Sigma^+$, $C\ ^1\Sigma^+$ and $E\ ^1\Pi$. The same states have been considered in [38]. In the construction of the current set, preference was given to electronic excitation cross sections determined up to high electron energies and/or to experimentally measured data. In [51] the cross sections are determined up to 1000 eV, on the basis of electron impact spectra and the Born approximation. New experimental data to assess these cross sections was used in [37]. However, not all of the data from [37] are determined in the whole energy range from threshold up to 1000 eV. Thus, the cross sections for excitation of the $a\ ^3\Pi$ and $b\ ^3\Sigma^+$ levels were taken from [51], whereas $A\ ^1\Pi$, $B\ ^1\Sigma^+$, $C\ ^1\Sigma^+$ and $E\ ^1\Pi$ were taken from [50, 54, 55] as reported in [37]. In what concerns the $a'\ ^3\Sigma^+$ state, the high energy part above 15 eV is taken from [51], while in the near threshold region Sawada's cross section [51] is re-scaled to approach the values proposed by Zobel *et al.* [52]. This adjustment leads to a better agreement with available experimental data for the reduced Townsend coefficient (*cf.* figure 3.6) while not introducing changes for other swarm parameters. The difference between the cross section proposed by Sawada [51] and the one recommended by Itikawa [37] is between 10 to 35%, depending on the electron energy. By choosing one or the other set of electronic excitation cross sections the calculated characteristic energy and reduced mobility are modified by less than 5%.

The dissociation cross section measured by Cosby [56] is defined only up to 200 eV and was extended up to 1000 eV using linear extrapolation in log-log space. The dissociative attachment and the total ionization cross sections are the ones recommended in [37], as obtained by Rapp and Briglia [57] and by Rapp [58], respectively. Notice that the dissociative attachment cross

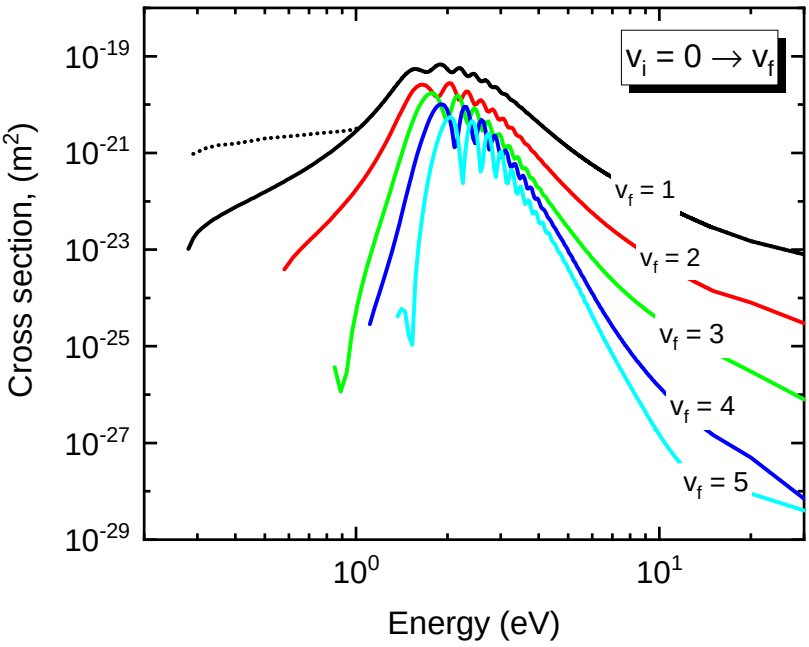

Figure 3.3: Vibrational excitation cross section for the first 5 transitions $v_i = 0 \rightarrow v_f = 1-5$ [40]. The dotted line represents the near threshold region of the 0→1 cross section proposed by Phelps [41] (included in the IST-Lisbon set).

section is defined only up to 13 eV and was not extended here, due to its small value and very negative slope (*cf.* figure 3.1), being considered as zero outside the range where it is defined in [37]. The contribution from this process in the calculation of the electron swarm parameters is expected to be small.

3.3 Validation

In this section, the proposed set of electron impact cross sections for CO is validated from the comparison between calculated and measured values of electron swarm parameters, namely the reduced mobility, μN, the characteristic energy, $u_k = D_T/\mu$, where D_T is the transverse diffusion coefficient, and the reduced Townsend ionization coefficient, α/N. The calculations were performed using LoKI-B, a numerical code solving the two-term approximation of the electron Boltzmann equation developed in spherical harmonics [35, 36], while the measurements are taken from the Dutton [67] and the LAPLACE [68] databases of the LXCat open access website.

Figure 3.4 presents measured and calculated values of the reduced mobility for two different values of the gas temperature, T_g = 300 K and T_g = 77 K. For comparison, two different cross section sets were used: the IST-Lisbon set proposed in this work, which includes the elastic momentum transfer cross section described in section 3.2.2; and a set labelled "effective", where this elastic momentum transfer cross section is replaced by the effective momentum transfer cross section from Phelps' database [42]. In the latter set, the elastic momentum transfer cross section derived by subtracting all the inelastic cross sections from the effective can become

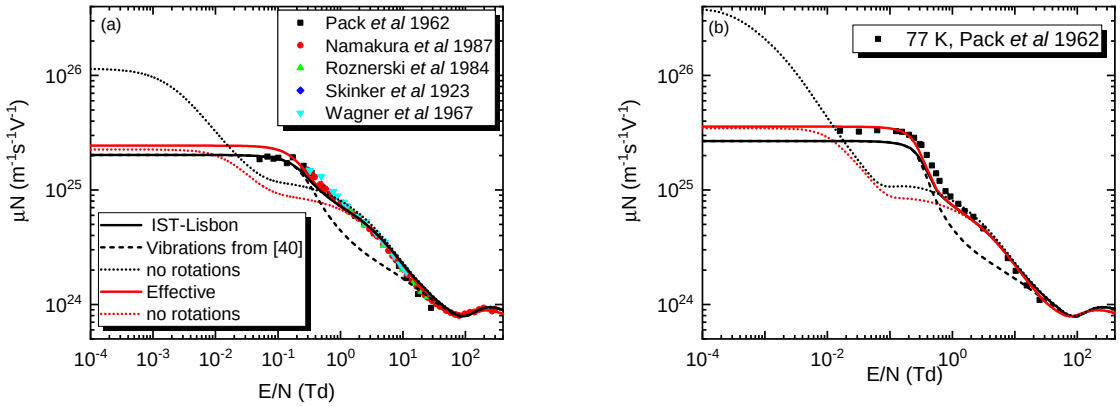

Figure 3.4: Calculated and measured reduced electron mobility in CO as a function of E/N for T_{gas} = 300 K (a) and T_{gas} = 77 K (b); the symbols are experimental data from ■ [69], ● [70], ▲ [71], ♦ [72], ▼ [73]; the solid curves are calculations performed with the current cross section set; dashed lines replace the cross section for the excitation of the first vibrational level with that proposed in [40] (without the contribution from non-resonant excitation); dotted curves neglect the rotational excitation/deexcitation processes; black/red curves consider the elastic momentum transfer cross section from the current set or replace it with the effective momentum transfer cross section from [42].

negative, as discussed in section 3.2.2; when this happens, the elastic cross section was simply set to zero. The calculations are performed by including and excluding the rotational excitation and de-excitation cross sections. We have also tested the cross section proposed in [40] for the excitation of the first vibrational level, where the contribution from non-resonant excitation is not considered (see section 3.2.3). The remaining processes, described in the previous section, are included similarly in both sets.

All the calculations carried out including rotational excitation and de-excitation cross sections are in reasonable agreement with the experimental data over the full range of E/N values considered. As can be seen in figure 3.4, both the IST-Lisbon and the "effective" cross section sets consistently reproduce the reduced mobility in the range of mid and high values of E/N, within 1% of the measurements. The predictions at 300 K in the region $E/N < 10^{-1}$ Td differ from the measurements at most by 1% and 20%, respectively for the IST-Lisbon and the "effective" sets. At 77 K and low E/N, the calculations made with the IST-Lisbon set deviate from the measurements less than 20%. The influence of choosing either sets is visible only for low reduced electric fields, where in general the IST-Lisbon data set describes better the measured values, despite some deviations at T_g = 77 K and E/N around 10^{-1} Td.

The importance of the near-threshold region of the cross section for the excitation of the first vibrational level, mentioned in the previous section, can also be asserted by analysing the results in figure 3.4. As can be clearly seen, neglecting the contribution from non-resonant excitation leads to much worse results for reduced electric fields in the range between 0.5 and 10 Td, at both T_{gas} = 300 K and 77 K, the relative error with respect to measurements increasing up to 50%.

In contrast with the importance of superelastic collisions from rotationally excited states, the calculation of swarm parameters in carbon monoxide is not influenced by superelastic collisions with vibrationally excited molecules in the range of gas temperatures studied. However,

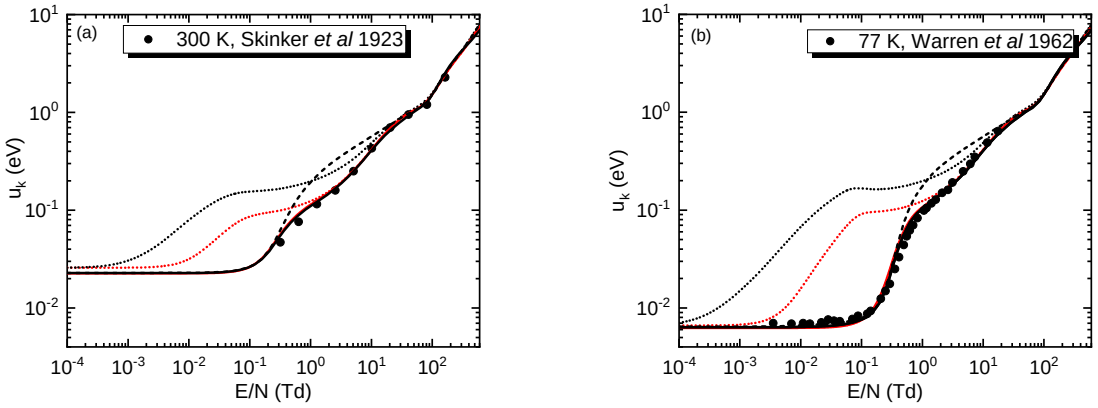

Figure 3.5: Calculated and measured characteristic energy in CO as a function of E/N, for: (a) T_{gas} = 300 K with experimental results from [72] and (b) T_{gas} = 77 K with experimental results from [74]. The curves are as in fig. 3.4.

superelastic processes with vibrationally excited states can affect the EEDFs for higher degrees of vibrational excitation, as pointed out in [19] and further discussed in the next section.

Figure 3.5 shows calculated and measured values of the characteristic energy for the same two values of the gas temperature, using the same cross section sets as before. The measurements are taken from the Dutton [67] and the LAPLACE [68] databases. The calculations performed with the IST-Lisbon set are in excellent agreement with the experimental data, within 1% of the measured values for both temperatures, whereas the "effective" set predicts measured values within 1% of the measurements for 300 K and 10% for 77 K. As it was noticed before, the non-resonant contribution to the excitation of the first vibrational level affects noticeably the calculations for reduced electric fields between 0.5 and 10 Td. Furthermore, the importance of the rotational excitation and de-excitation mechanisms for $E/N < 10$ Td is immediately evident from the figure.

Figure 3.6 compares the calculated and measured values of the reduced Townsend ionization coefficient using the same two datasets as before, and also replacing our cross section for the excitation of the $a'\ ^3\Sigma^+$ state with the one proposed by Sawada *et al* [51]. As it is clear from the figure, the IST-Lisbon dataset, which adjusts the electronic excitation cross section of Sawada's, leads to a much better agreement between measured and calculated values of α/N for $E/N < 200$ Td. In the range of reduced electric fields between 100 and 300 Td neither the contribution of the rotational mechanisms nor the contribution of the non-resonant part of the first vibrational excitation play a significant role.

As referred to in section 3.2.2, the validity of the two-term approximation to solve the electron Boltzmann equation is questionable when the magnitude of the inelastic collision cross sections exceeds that of the elastic momentum transfer collision cross section [78, 79], as is the case here for electron energies below ~ 0.1 eV. A prior observation relates to the very notion of a *consistent* cross section set *(cf* section 3.1), often misunderstood. The current set is a consistent swarm-derived cross section set, that, *when used in a two-term Boltzmann solver*, leads to good agreement between the calculated and measured electron transport parameters. In this sense, the set is to be used in Boltzmann solvers written under the same approximations adopted in the swarm analysis defining the cross sections. Nevertheless, the question of whether the two-term approximation is actually valid and, accordingly, whether or not these cross sections can be used

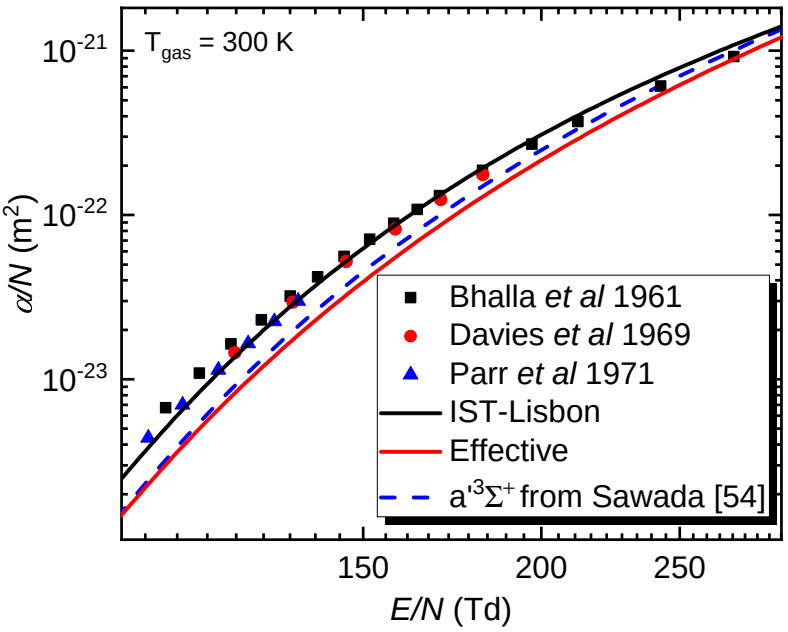

Figure 3.6: Calculated and measured reduced ionization coefficient in CO, as a function of E/N. The symbols represent experimental data from: ■ [75]; • [76]; and ▲ [77]. The lines are calculations obtained with the IST-Lisbon (—), IST-Lisbon with $a'\ ^3\Sigma^+$ cross section from Sawada [51] (– –) and the "effective" [42](—) data sets.

in multi-term or Monte Carlo simulations, remains.

A final answer regarding the validity of the two-term approximation can only be given by a thorough comparison of calculations made adopting different formulations, which goes beyond the scope of the present work. In any case, we expect the two-term approximation to be valid in the range of E/N under study, with a possible deviation in a narrow region around ~1 Td. First, it is well known that the two-term approximation is often valid, even when the inelastic scattering is not negligible, yet isotropic, leading to the definition of an effective momentum transfer cross section that may include significant inelastic contributions [78]; in this respect, note that our construction of an elastic momentum transfer cross section started precisely from an effective cross section (section 3.2.2). Second, the validity of the two-term approximation is questionable here for electron energies below 0.1 eV only. Moreover, our calculations show that for reduced electric fields of 0.1 Td, 1 Td and 10 Td, the electron kinetic temperatures are, respectively, 0.03 eV, 0.09 eV and 0.31 eV (*cf* as well figure 3.5); thus, a possible difficulty of the two-term approximation due to the low elastic momentum transfer cross section should be confined to values of E/N below ~1 Td, where the electron kinetic temperature becomes comparable with the electron kinetic energies where a very low elastic momentum transfer cross section is observed. However, for very low E/N <0.1 Td the EEDF approaches an isotropic Maxwellian distribution at the gas (and rotational) temperature, as can be inferred from inspection of figure 3.5, which confirms the validity of the two-term approximation, even in this range of E/N. Finally, the former conclusions are reinforced by the analysis of figure 3.7, where the ratio of the anisotropic component of the distribution function,

f_1, to the isotropic component, f_0, is represented. Evidently, whenever $f_1/f_0 \ll 1$ the two-term approximation should be valid. Figure 3.7 confirms that this condition is always verified for E/N below 0.1 Td, where the unfavourable ratio between inelastic and elastic cross sections for electron energies below 0.1 eV is more significant. Quite interestingly, this figure also confirms that the anisotropy is more important at 1 Td than at 10 Td, in agreement with the prior analysis and suggesting the validity of the two-term approximation in the E/N range considered in this paper, albeit with a possible deviation around 1 Td.

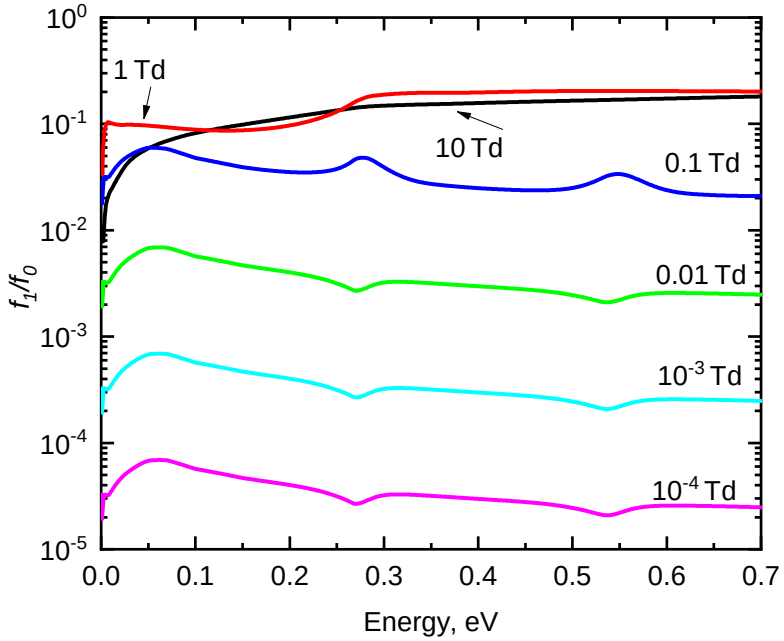

Figure 3.7: The ratio of the anisotropic (f_1) and isotropic (f_0) components of the electron velocity distribution function, as a function of the electron energy, for different values of E/N.

3.4 Electron kinetics in CO_2 - CO mixtures

This section presents a study of the electron kinetics in CO_2-CO mixtures, extending and updating the research made in [19, 27, 46, 47] in pure gases and the pioneering work by Nighan [48]. The discussion is divided into three sub-sections, describing the modifications on the EEDF due to the mixture composition and the degree of vibrational excitation, as well as their impact on the electron impact rate coefficients and on the electron power transfer. Along this section, T_{12} represents the common vibrational temperature of the CO_2 symmetric stretching and bending modes [32, 33], T_3 the vibrational temperature of the CO_2 asymmetric stretching mode and T_{CO} the vibrational temperature of CO. All vibrational levels that are taken into account are assumed to follow a Boltzmann at the corresponding vibrational temperatures. Moreover, the value of the gas temperature, T_g, is always considered equal to 300 K.

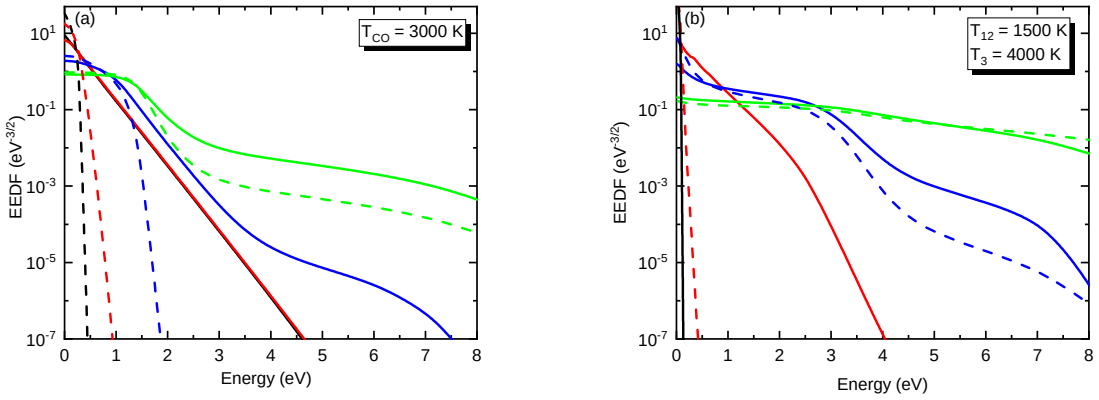

Figure 3.8: Electron Energy Distribution Functions in pure CO (a) and pure CO_2 (b), for E/N = 0.01 (—), 1 (—), 10 (—) and 50 Td (—), accounting (—) and neglecting (– –) superelastic collisions from vibrationally excited states, for T_{CO} = 3000 K (a) and T_{12} = 1500 K and T_3 = 4000 K (b).

3.4.1 Electron energy distribution functions

The influence of superelastic collisions with vibrationally excited states on the electron kinetics can be inferred by inspection of figures 3.8(a) and (b), depicting the EEDFs $f(u)$ in pure CO and CO_2, respectively, normalized in the usual way as $\int_0^\infty f(u)\sqrt{u}du$ = 1 [35], for reduced electric fields in the range 0.01-50 Td and vibrational temperatures T_{12} = 1500 K, T_3 = 4000 K and T_{CO} = 3000 K, which are typical values found in different discharges [13, 32, 33, 80, 81]. As it can be seen, superelastic collisions with vibrationally excited states can strongly modify the EEDF, especially at low values of E/N. For pure CO, the high energy tail of the EEDF is significantly more populated due to the effect of superelastic collisions. The situation is more complex in CO_2, where for the higher values of E/N the detailed shape of the different cross sections leads to an over or an underpopulation of the EEDF in different energy regions when superelastic collisions are taken into account. The form of the different EEDFs in the pure gases is similar to the ones presented in [19, 46] and confirms that superelastic collisions with vibrationally excited states cannot be neglected for an accurate calculation of electron impact rate coefficients, under discharge conditions for reduced fields $E/N \lesssim 100$ Td.

Figure 3.9 shows the influence of the different vibrational temperatures on the EEDFs, for three values of the reduced electric field, in pure CO (a), pure CO_2 (b) and in the CO_2-CO mixture (c). Once more, the importance of vibrational excitation in enhancing the tail of the EEDF due to superelastic collisions is evident from the figure. At the lower values of E/N the EEDFs in a 50%CO_2-50%CO mixture are closer to the ones in pure CO, as a result of the larger inelastic cross sections in CO for electron energies between $\sim 1-3$ eV [which translate into dominant losses to CO for $E/N \sim 10-200$ Td, see figure 3.11(b)]. In addition, for moderate and high electric fields the tail of the EEDF is more populated in pure CO_2 than in CO so that, for the same value of E/N, the presence of CO will result in smaller electron impact rate coefficients for processes with moderate and high energy thresholds [excitation of electronically excited states, dissociation and ionization, *cf.* figures 3.10(c) and (d)].

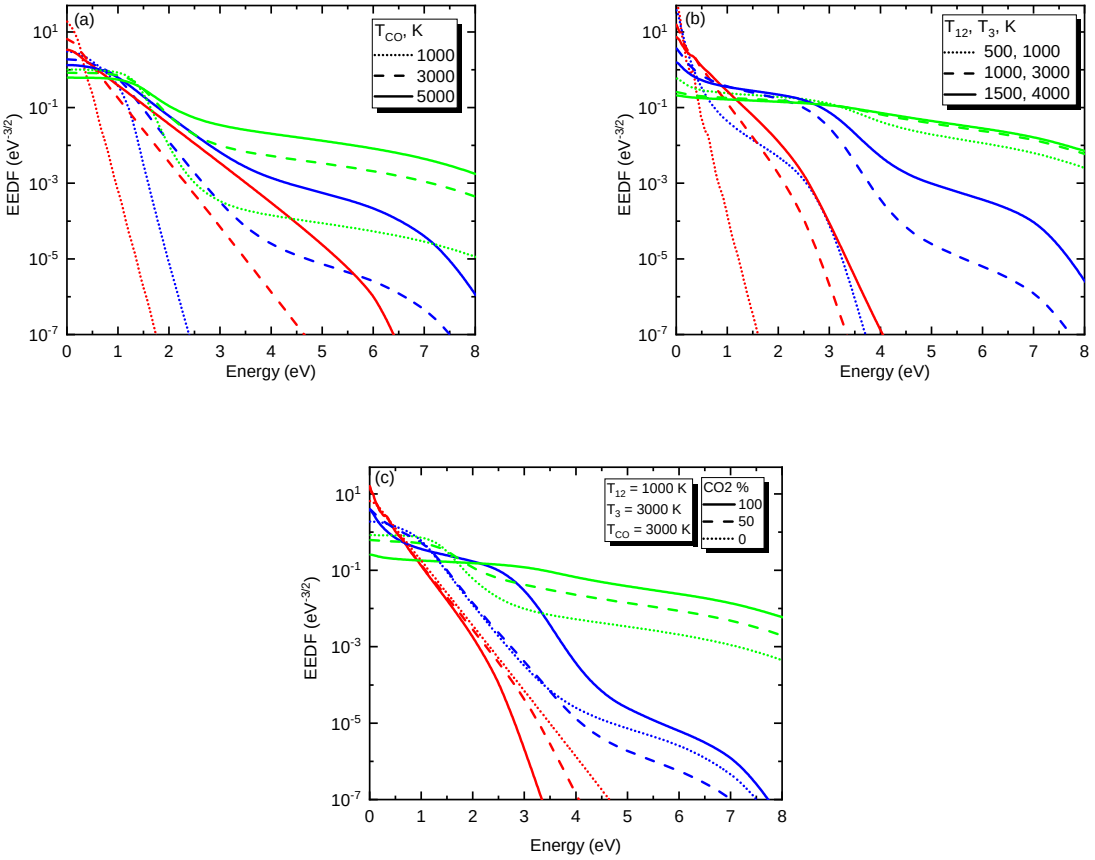

Figure 3.9: Electron Energy Distribution Functions for E/N = 1 (—), 10 (—) and 50 Td (—): for different values of the vibrational temperatures in pure CO (a) in pure CO_2 (b) and in a CO_2-CO mixture (c).

3.4.2 Electron impact rate coefficients

The rate coefficients for the excitation of the first asymmetric stretching level and the first bending level of CO_2 are presented in figures 3.10(a) and (b), as a function of the reduced electric field, for different mixture compositions, from pure to 10% CO_2, and for vibrational temperatures in the ranges 500 K - 1500 K and 1000 K - 4000 K for T_{12} and T_3, respectively. The rate coefficient for the excitation of the first asymmetric stretching level of CO_2 is a measure of the input of energy into this vibrational mode, which may be of importance in the plasma reforming of CO_2 [22]. For the bending rate coefficient in figure 3.10(b) the curves for temperatures 1000, 3000, 3000 K for T_{12}, T_3 and T_{CO}, respectively, closely follow the ones for 1500, 4000, 5000 K and were not included to simplify the figure. For reduced fields above $\sim 100 - 200$ Td, neither the vibrational temperatures nor the mixture composition modify this excitation rate coefficient, as a result of the low energy threshold of the corresponding cross section, and a high enough populated EEDF. For lower values of E/N, higher vibrational temperatures and/or addition of CO lead to an increase in the excitation rate coefficient, in agreement with the dependences of the EEDFs shown in figure 3.9(c). The excitation rate coefficient of the first bending mode exhibits a somewhat similar behaviour, albeit a more complex dependence for low values of E/N and low vibrational temperatures.

Figures 3.10(c) and (d) present the CO_2 dissociative attachment and direct dissociation rate coefficients as a function of the reduced electric field for pure CO_2 and in mixtures containing 50% and 90% of CO, for three different combinations of the vibrational temperatures as in figures 3.10(a)-(b). Following the analysis of the EEDFs in the previous sub-section, figures 3.10(c) and (d) corroborate the importance of vibrational excitation for $E/N \lesssim 100$ Td. For example, at E/N = 10 Td and in pure CO_2, an increase in T_{12} from 500 K to 1500 K leads to an increase in the dissociative attachment rate coefficient of ~ 7 orders of magnitude. The composition of the plasma plays an important role as well. For low values of E/N, below ~ 10 Td, the addition of CO leads to an increase in the dissociative attachment rate coefficient, whereas the opposite behaviour occurs for higher values of E/N. The CO_2 dissociation rate coefficient presented in figure 3.10(d) has a very similar behaviour as the dissociative attachment one. Moreover, for $E/N \gtrsim 30$ Td the former mechanism dominates over the latter.

One important question is to understand how the CO_2 dissociation and the total ionization rate coefficients are modified in the presence of CO. Therefore, figures 3.10(e) and (f) depict these rate coefficients as a function of the CO_2 content in the mixture. The rate coefficients for dissociation of CO_2 and for ionization of CO, CO_2 and total ionization are shown for three values of the reduced electric field. The total ionization rate coefficient decreases with the concentration of CO in the mixture, as the ionization rate for CO is lower than for CO_2 for all of the conditions, due to its higher energy threshold. The dissociation rate coefficients are shown for three values of E/N and the same combinations of the vibrational temperatures as in the previous figures. The dissocaition rate coefficient for the reduced field 10 Td and low vibrational temperatures is 8-10 orders of magnitude lower than the dissocaition rate coefficient for the same reduced field and vibrational temperatures (T_{12}, T_3, T_{CO}) in K (1000, 3000, 3000) and thus is not depicted. As anticipated in the discussion of figure 3.9, for the higher values of E/N the presence of CO induces a decrease of these electron impact rate coefficients, as a consequence of the decrease in the high-energy tail of the EEDF. For the lower value of the reduced electric field considered, E/N = 10 Td, the behaviour of the dissociation rate coefficient is not monotonous, exhibiting a sharp decrease upon addition of CO in pure CO_2 and a subsequent slow raise after passing through a minimum. The role of vibrational excitation can be verified one last time, being particularly important in CO and for the lower values of E/N.

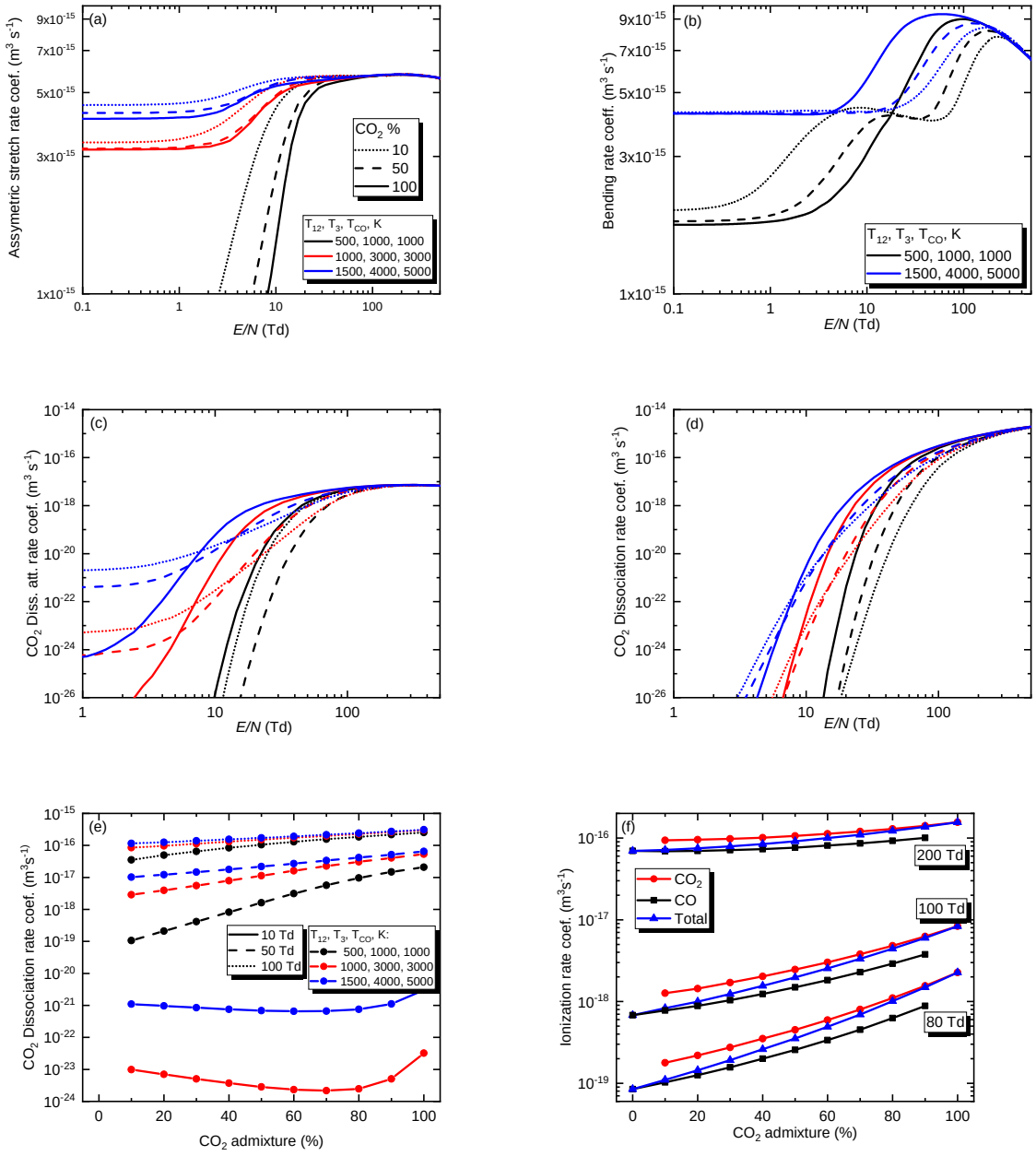

Figure 3.10: Electron impact rate coefficients for excitation of the first level of CO_2 asymmetric stretching mode (a) and excitation of the first level of the CO_2 bending mode (b), CO_2 dissociative attachment (c) and CO_2 dissociation (d) as a function of E/N for three different combinations of values of vibrational temperatures (T_{12}, T_3, T_{CO}) in K [(—) (500, 1000, 1000); (—) (1000, 3000, 3000); (—) (1500, 4000, 5000)], and the following CO_2-CO mixture compositions: 100% CO_2 (—), 50% CO_2 (– –) and 10% CO_2 (···). Dissociation (e) electron impact rate coefficients as a function of the CO_2 percentage in CO_2-CO mixture, for the same combination of values of vibrational temperatures as before, and the following E/N values in Td: 10 (—), 50 (– –), 100 (···). Ionization (f) electron impact rate coefficients of CO (—), CO_2 (—) and combined ionization rate coefficient in the mixture (—) as a function of the CO_2 percentage in the CO_2-CO mixture and vibrational temperatures T_{12} = 1000 K, T_3 = 3000 K, T_{CO} = 3000 K and the following E/N values in Td: [80, 100, 200].

3.4.3 Power balance

The power gained by the electrons from the applied electric field can be transferred to the gases through different collisional channels, namely elastic collisions, excitation of rotational, vibrational and electronic states, ionization, attachment and dissociation. On the other hand, electrons can gain energy in superelastic collisions with excited states and, for very low values of the reduced electric field, also in elastic collisions with the background gases [64]. In what follows, the curves for the power transferred in rotational and vibrational collisions correspond to the *net* power, *i.e.*, to the difference between the power lost in inelastic collisions, P_{inel}, and the power gained in superelastic collisions, P_{sup}. Therefore, a negative value simply corresponds to conditions where $P_{sup} > P_{inel}$ hence corresponding to a net power gain.

Fig 3.11(a) shows the absolute values of the power per electron at unit gas density, dissipated in different inelastic and superelestic channels of CO_2 and CO as a function of E/N, for pure CO and for a 50%CO-50%CO_2 mixture, for vibrational temperatures T_{CO} = T_{12} = T_3 = 300 K. In pure CO, the power lost in rotational excitation and de-excitation is by far the dominant loss mechanism for reduced fields below 1 Td. However, when CO_2 is added into the mixture, its vibrational excitation and de-excitation becomes dominant in this region.

Figures 3.11(b)-(d) report the fractional power transferred to the different collisional channels, defined as the ratio between the net power transferred from the electrons into each channel and the power gained by the electrons from the applied electric field, P_E, as a function of E/N and for different mixtures from pure CO to pure CO_2. Superelastic collisions are the dominant process of electron energy gain for reduced fields lower than 10 Td, being larger than P_E. Thus, the fractional power for some processes can be higher than 1 in this region. Figure 3.11(b) depicts the general picture of the power balance for CO_2-CO mixtures with vibrational temperatures T_{12} = 500 K, T_3 = T_{CO} = 1000 K. For reduced electric fields above 100 Td, the excitation of the electronic states and the ionization processes are the main electron energy loss channels. Addition of CO_2 leads to a shift of the onset of the excitation of electronic states to lower values of E/N, as a consequence of the enhancement of the high-energy tail of the EEDF in CO_2 as compared with CO (*cf.* figure 3.9(c)). For E/N approximately in the range 2-70 Td, vibrational excitation consumes an extremely large amount of the electron energy gained from the field, above 95%, CO and CO_2 contributing more for this consumption at the higher and lower values of E/N in this range, respectively. For a 50%CO_2-50%CO mixture and $E/N \in [30, 70]$ Td, most of the electron energy is transferred into vibrational excitation of CO, showing that the presence of CO hinders the vibrational pumping of CO_2 by electron impact. These results are in very good qualitative agreement with the calculations from [48].

The detailed analysis of the power transferred into the excitation/de-excitation of the asymmetric stretching and bending modes of CO_2, relevant for plasma reforming of CO_2 [22], is presented in figures 3.11(c) and (d). Figure 3.11(c) shows the evolution of the power transfer into these modes as well as to the total vibrational excitation, for T_{12} = 1000 K and T_3 = T_{CO} = 3000 K. It can be confirmed that preferential excitation of the asymmetric stretching mode takes place for moderate reduced electric fields, $\sim 5 - 50$ Td. Figure 3.11.d) further shows the influence of the CO_2 vibration temperatures in the case of pure CO_2, revealing that the ideal working point for channeling the electron energy into the asymmetric stretching mode is strongly dependent on the degree of vibrational excitation. For completeness, the power transfer to the dissociation by direct electron impact is also shown, calculated with the cross section from [82] according to the recommendation from [47], exhibiting a maximum at around 100 Td.

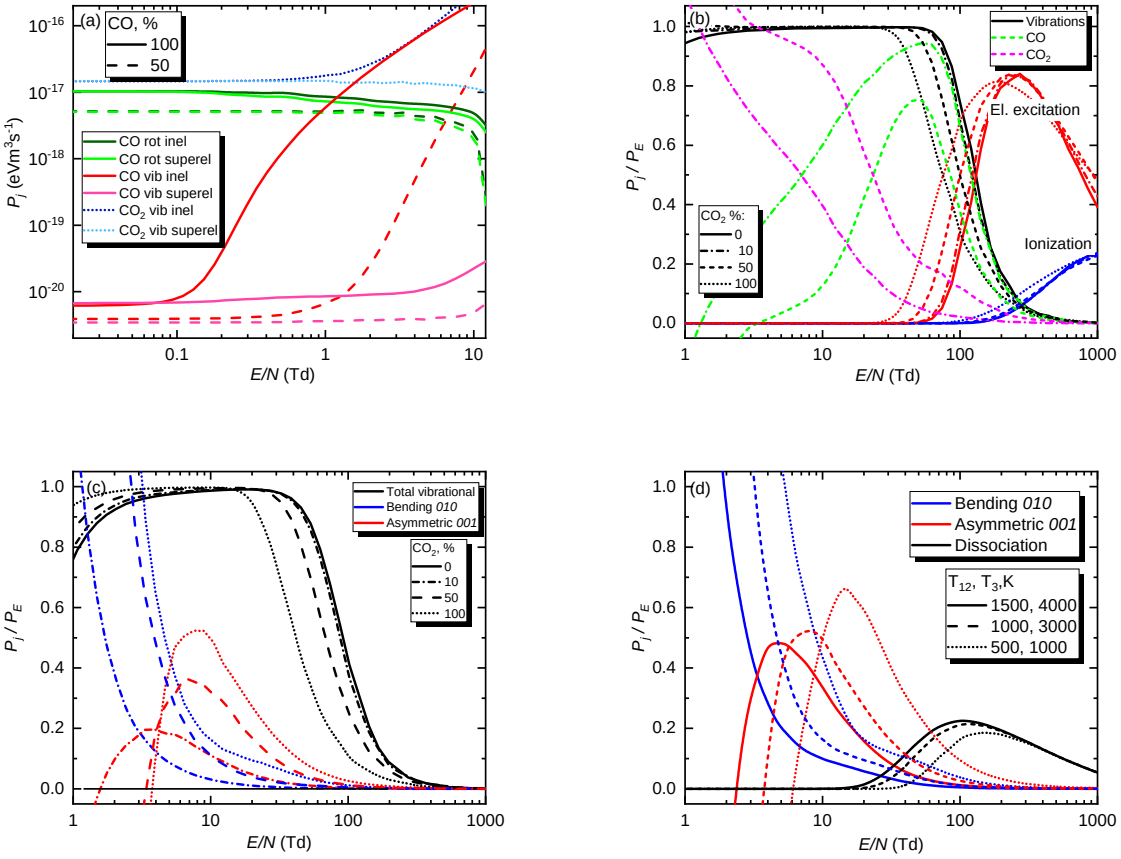

Figure 3.11: (a) Absolute power per electron of unit gas density, transferred to rotational excitation/de-excitation of CO and vibrational excitation/de-excitation of CO and CO_2, for T_{CO} = T_{12} = T_3 = T_g = 300 K, in pure CO (—) and 50%CO_2-50%CO (– –). (b) Relative (to the power absorbed by the electric field, P_E) net power transfered to different mechanisms, for T_{12} = 500 K and T_3 = T_{CO} = 1000 K and the following CO_2-CO mixtures: 0% CO_2 - 100% CO (—), 10% CO_2 - 90% CO (–·–), 50% CO_2 - 50% CO (– –), 100% CO_2 - 0% CO (···). (c) Relative (to the power absorbed by the electric field, P_E) net power transfered to the total excitation of vibrational levels in CO and CO_2 (—), as well as in the excitation of the first bending (—) and first asymmetric stretching (—) levels of CO_2, for T_{12} = 1000 K and T_3 = T_{CO} = 3000 K and the same mixture composition as in (b). (d) Relative (to the power absorbed by the electric field, P_E) net power transfer in the excitation of the first bending (—) and first asymmetric stretching (—) levels of CO_2 and in dissociation by direct electron impact (—) in pure CO_2, for the following values of (T_{12}, T_3) in K: (···) (500, 1000), (– –) (1000, 3000), (—) (1500, 4000).

3.5 Conclusions

In this chapter an original complete and consistent set of electron impact cross sections for CO is proposed. The set is to be made publicly available for download at the IST-Lisbon database with LXCat. It comprises an elastic momentum transfer cross section, cross sections for 16 $J \rightleftharpoons J+1$ rotational excitation and de-excitation transitions of $CO(X, v = 0)$, for the full matrix $v = 0-10 \rightleftharpoons w = 0-10$ of vibrational excitation and de-excitation processes of $CO(X)$, the excitation of the $CO(a\ ^3\Pi,\ a'\ ^3\Sigma^+,\ A\ ^1\Pi,\ b\ ^3\Sigma^+,\ B\ ^1\Sigma^+,\ C\ ^1\Sigma^+,\ E\ ^1\Pi)$ electronically excited states, dissociative attachment, dissociation and ionization. The current set corrects a serious inconsistency found in most sets available in the literature, related to the high value of the rotational excitation/de-excitation cross sections at low electron energies, surpassing the effective momentum transfer cross-section. It is shown that, for reduced electric fields below ~ 3 Td, an accurate calculation of the EEDF requires an appropriate treatment of rotational inelastic and superelastic collisions. The inclusion of the contribution of non-resonant excitation to the excitation of the first vibrational level leads to a significant improvement between calculated and measured swarm parameters, for reduced electric fields between 0.5 and 10 Td. The proposed set of cross sections is complete and calculated swarm parameters are in very good agreement with the experimental data over the full range of reduced electric fields considered.

The electron kinetics in CO_2-CO mixtures, relevant for plasma reforming applications, is investigated in detail. Superelastic collisions with vibrationally excited states of both CO and CO_2 induce strong modifications in the EEDF and should be included in the modelling of CO_2 and CO plasmas, as the electron impact rate coefficients exhibit a marked dependence with the vibrational temperatures of CO and of the different vibrational modes of CO_2. In addition, the presence of moderate amounts of CO in the mixture, such as those resulting from CO_2 dissociation in the plasma, has a noticeable influence in the EEDF, electron impact rate coefficients and electron power transfer channels. In particular, the presence of CO in discharges operating at moderate reduced electric fields in the range ~ 30 – 100 Td shifts the input of electron energy from vibrational excitation of CO_2 into vibrational excitation of CO and may affect the overall performance of plasma processes aiming at CO_2 reforming, enhanced by the ladder-climbing mechanism along the asymmetric stretching mode as proposed in [22].

Bibliography

[1] G. A. Landis and D. L. Linne, "Mars rocket vehicle using in situ propellants," *J. Spacecraft Rockets*, vol. 38, no. 5, pp. 730–735, 2001. [Online]. Available: http://arc.aiaa.org/doi/pdf/10.2514/2.3739

[2] P. Connes, J. Connes, L. Kaplan, and W. S. Benedict, "Carbon monoxide in the Venus atmosphere," *Astrophys. J.*, vol. 152, 1968.

[3] R. T. Clancy, D. O. Muhleman, and B. M. Jakosky, "Variability of carbon monoxide in the Mars atmosphere," *Icarus*, vol. 55, no. 2, pp. 282–301, 1983.

[4] L. Campbell, M. Allan, and M. J. Brunger, "Electron impact vibrational excitation of carbon monoxide in the upper atmospheres of Mars and Venus," *J. Geophys. Res.-Space*, vol. 116, no. 9, pp. 1–8, 2011.

[5] L. Campbell and M. J. Brunger, "Electron impact excitation of carbon monoxide in comet Hale-Bopp L03101," *Geophys. Res. Lett.*, vol. 36, no. 3, pp. 2–6, 2009.

[6] L. Campbell, M. Allan, and M. J. Brunger, "Electron cooling by carbon monoxide in the atmospheres of Mars and Venus," *PMC Physics B*, vol. 1, pp. 1–10, 2008.

[7] C. Park, J. T. Howe, R. L. Jaffe, and G. V. Candler, "Review of chemical-kinetic problems of future NASA missions. II - Mars entries," *J Thermophys Heat Tr.*, vol. 8, no. 1, pp. 9–23, 1994. [Online]. Available: http://arc.aiaa.org/doi/10.2514/3.496

[8] S. A. Haider, J. Kim, A. F. Nagy, C. N. Keller, M. I. Verigin, K. I. Gringauz, N. M. Shutte, K. Szego, and P. Kiraly, "Calculated ionization rates, ion densities, and airglow emission rates due to precipitating electrons in the nightside ionosphere of Mars," *J. Geophys. Res.*, vol. 97, no. A7, pp. 10 637–10 641, 1992. [Online]. Available: http://dx.doi.org/10.1029/92JA00317%5CnUsers/wang/GoogleDrive/Papers/haider1992.pdf

[9] D. Crider, P. Cloutier, C. Law, P. Walker, Y. Chen, M. Acuña, J. Connerney, D. Mitchell, R. Lin, K. Anderson, C. Carlson, J. McFadden, H. Rème, C. Mazelle, C. D'Uston, J. Sauvaud, D. Vignes, D. Brain, and N. Ness, "Evidence of electron impact ionization in the magnetic pileup boundary of Mars," *Geophys. Res. Lett.*, vol. 27, no. 1, pp. 45–48, 2000.

[10] R. L. Ash, D. Wu, and R. A. Outlaw, "A study of glow-discharge and permeation techniques for extraterrestrial oxygen beneficiation," *Adv. Space Res.*, vol. 14, no. 6, pp. 259–263, 1994.

[11] V. Guerra, T. Silva, P. Ogloblina, M. Grofulović, L. Terraz, M. Silva, C. D. Pintassilgo, L. L. Alves, and O. Guaitella, "The case for in situ resource utilisation for oxygen production on Mars by non-equilibrium plasmas," *Plasma Sources Sci. Technol.*, vol. 26, no. 11, 2017.

[12] V. Guerra, T. Silva, and O. Guaitella, "Living on mars: how to produce oxygen and fuel to get home," *Europhysics News*, vol. 49, no. 3, pp. 15–18, 2018.

[13] I. V. Adamovich, S. Saupe, M. J. Grassi, O. Schulz, S. Macheret, and J. W. Rich, "Vibrationally stimulated ionization of carbon monoxide in optical pumping experiments," *Chemical Physics*, vol. 173, no. 3, pp. 491–504, 1993.

[14] J. W. Rich, "Kinetic modeling of the high-power carbon monoxide laser," *J. Appl. Phys.*, vol. 42, no. 7, pp. 2719–2730, 1971.

[15] A. Frassoldati, T. Faravelli, and E. Ranzi, "The ignition, combustion and flame structure of carbon monoxide/hydrogen mixtures. Note 1: Detailed kinetic modeling of syngas combustion also in presence of nitrogen compounds," *Int. J. Hydrog. Energy*, vol. 32, pp. 3471–3485, 2007.

[16] S. M. Walton, X. He, B. T. Zigler, and M. S. Wooldridge, "An experimental investigation of the ignition properties of hydrogen and carbon monoxide mixtures for syngas turbine applications," *Proc. Combust. Inst.*, vol. 31, pp. 3147–3154, 2007.

[17] G. Chen, T. Silva, V. Georgieva, T. Godfroid, N. Britun, R. Snyders, and M. P. Delplancke-Ogletree, "Simultaneous dissociation of CO_2 and H_2O to syngas in a surface-wave microwave discharge," *Int. J. Hydrog. Energy*, vol. 40, no. 9, pp. 3789–3796, 2015. [Online]. Available: http://dx.doi.org/10.1016/j.ijhydene.2015.01.084

[18] L. D. Pietanza, G. Colonna, and M. Capitelli, "Electron energy and vibrational distribution functions of carbon monoxide in nanosecond atmospheric discharges and microsecond afterglows," *J. Plasma Phys.*, vol. 83, no. 06, p. 725830603, 2017. [Online]. Available: https://www.cambridge.org/core/product/identifier/S0022377817000952/type/journal_article

[19] L. D. Pietanza, G. Colonna, and M. Capitelli, "Non-equilibrium plasma kinetics of reacting CO: an improved state to state approach," *Plasma Sources Sci. Technol*, vol. 26, no. 12, 2017.

[20] G. Colonna, M. Capitelli, S. Debenedictis, C. Gorse, and F. Paniccia, "Electron energy distribution functions in CO_2 laser mixture: the effects of second kind collisions from metastable electronic states," *Contrib. Plasm. Phys.*, vol. 31, no. 6, pp. 575–579, 1991.

[21] E. Plonjes, P. Palm, J. William Rich, I. V. Adamovich, and W. Urban, "Electron-mediated vibration-electronic (V-E) energy transfer in optically pumped plasmas," *Chemical Physics*, vol. 279, no. 1, pp. 43–54, 2002.

[22] A. Fridman, *Plasma Chemistry*, 2008. [Online]. Available: http://books.google.com/books?hl=en&lr=&id=ZzmtGEHCC9MC&oi=fnd&pg=PR39&dq=Plasma+chemistry&ots=YhbAAcm08f&sig=iHC2mizqtafrUBFdPIMf50p6bvA

[23] R. Aerts, T. Martens, and A. Bogaerts, "Influence of vibrational states on CO_2 splitting by dielectric barrier discharges," *The Journal of Physical Chemistry C*, vol. 116, no. 44, pp. 23 257–23 273, 2012. [Online]. Available: http://pubs.acs.org/doi/abs/10.1021/jp307525t

[24] T. Kozák and A. Bogaerts, "Splitting of CO_2 by vibrational excitation in non-equilibrium plasmas: a reaction kinetics model," *Plasma Sources Science and Technology*, vol. 23, p. 045004, 2014. [Online]. Available: http://stacks.iop.org/0963-0252/23/i=4/a=045004?key=crossref.ae2245ca0b3f38b3e8652fc96aea2549

[25] T. Kozák and A. Bogaerts, "Evaluation of the energy efficiency of CO_2 conversion in microwave discharges using a reaction kinetics model," *Plasma Sources Sci. Technol.*, vol. 24, no. 1, p. 015024, 2014. [Online]. Available: http://stacks.iop.org/0963-0252/24/i=1/a=015024?key=crossref.6ddb8a33aa4ce58fca197f080841e769

[26] G. van Rooij, D. van den Bekerom, N. den Harder, T. Minea, G. Berden, W. Bongers, R. Engeln, M. Graswinckel, E. Zoethout, and M. van de Sanden, "Taming microwave plasma to beat thermodynamics in CO_2 dissociation," *Faraday discuss.*, vol. 183, pp. 233–248, 2015. [Online]. Available: http://pubs.rsc.org/en/Content/ArticleHTML/2015/FD/C5FD00045A

[27] A. Janeco, N. R. Pinhão, and V. Guerra, "Electron kinetics in $He/CH_4/CO_2$ mixtures used for methane conversion," *J. Phys. Chem. C*, vol. 119, no. 1, pp. 109–120, 2015.

[28] A. Bogaerts, T. Kozák, K. van Laer, and R. Snoeckx, "Plasma-based conversion of CO_2: current status and future challenges," *Faraday Discuss.*, pp. 217–232, 2015. [Online]. Available: http://xlink.rsc.org/?DOI=C5FD00053J

[29] S. Heijkers, R. Snoeckx, T. Kozák, T. Silva, T. Godfroid, N. Britun, R. Snyders, and A. Bogaerts, "CO_2 conversion in a microwave plasma reactor in the presence of N_2: Elucidating the role of vibrational levels," *J. Phys. Chem. C*, vol. 119, no. 23, pp. 12 815–12 828, 2015.

[30] A. Berthelot and A. Bogaerts, "Modeling of plasma-based CO_2 conversion: lumping of the vibrational levels," *Plasma Sources Sci. Technol.*, vol. 25, no. 4, p. 045022, 2016. [Online]. Available: http://stacks.iop.org/0963-0252/25/i=4/a=045022?key=crossref.c20e4eb36e1a507bb594fd0b8e5e98c4

[31] S. Ponduri, M. M. Becker, S. Welzel, M. C. Van De Sanden, D. Loffhagen, and R. Engeln, "Fluid modelling of CO_2 dissociation in a dielectric barrier discharge," *Journal of Applied Physics*, vol. 119, no. 9, 2016. [Online]. Available: http://dx.doi.org/10.1063/1.4941530

[32] T. Silva, M. Grofulović, B. Klarenaar, A. Morillo-Candas, O. Guaitella, R. Engeln, C. Pintassilgo, and V. Guerra, "Kinetic study of low-temperature CO_2 plasmas under non-equilibrium conditions. I. Relaxation of vibrational energy," *Plasma Sources Sci. Technol.*, 2017.

[33] M. Grofulović, T. Silva, B. Klarenaar, A. Morillo Candas, O. Guaitella, R. Engeln, C. Pintassilgo, and V. Guerra, "Kinetic study of CO_2 plasmas under non- equilibrium conditions . II . Input of vibrational energy," *Plasma Sources Sci. Technol*, vol. 27, p. 115009, 2018.

[34] L. Alves, "The IST-LISBON database on LXCat," *J. Phys.: Conf. Ser.*, vol. 565, p. 012007, 2014.

[35] A. Tejero-del Caz, V. Guerra, D. Goncalves, M. L. da Silva, L. Marques, N. Pinhão, C. D. Pintassilgo, and L. L. Alves, "The LisbOn KInetics Boltzmann solver," *Plasma Sources Sci. Technol.*, vol. 28, p. 043001, 2019.

[36] A. Tejero, "The LisbOn KInetics Boltzmann solver https://github.com/IST-Lisbon/LoKI," 2019.

[37] Y. Itikawa, "Cross sections for electron collisions with carbon monoxide," *J. Phys. Chem. Ref. Data*, vol. 44, no. 1, 2015.

[38] J. E. Land, "Electron scattering cross sections for momentum transfer and inelastic excitation in carbon monoxide," *J. Appl. Phys.*, vol. 49, no. 12, pp. 5716–5721, 1978.

[39] R. D. Hake and A. V. Phelps, "Momentum-transfer and inelastic-collision cross sections for electrons in O_2, CO, and CO_2," *Phys. Rev.*, vol. 158, no. 1, pp. 70–84, 1967.

[40] V. Laporta, C. M. Cassidy, J. Tennyson, and R. Celiberto, "Electron-impact resonant vibration excitation cross sections and rate coefficients for carbon monoxide," *Plasma Sources Sci. Technol.*, vol. 21, no. 4, p. 045005, 2012. [Online]. Available: http://stacks.iop.org/0963-0252/21/i=4/a=045005?key=crossref.1096e4f9706e81d1eba90fc8ead5131e

[41] A. V. Phelps, "Rotational and vibrational excitation of molecules by low-energy electrons," *Rev. Mod. Phys.*, vol. 40, no. 2, pp. 399–410, 1968.

[42]

[43] M. Capitelli, G. Colonna, G. D'Ammando, V. Laporta, and A. Laricchiuta, "Nonequilibrium dissociation mechanisms in low temperature nitrogen and carbon monoxide plasmas," *Chem. Phys.*, vol. 438, pp. 31–36, 2014. [Online]. Available: http://dx.doi.org/10.1016/j.chemphys.2014.04.003

[44] L. D. Pietanza, G. Colonna, and M. Capitelli, "Dissociative electron attachment from vibrationally excited molecules in nanosecond repetitively pulsed CO discharges and afterglows," *Front. Chem.*, vol. 7, no. 163, 2019.

[45] V. Laporta, J. Tennyson, and R. Celiberto, "Carbon monoxide dissociative attachment and resonant dissociation by electron-impact," *Plasma Sources Sci. Technol*, vol. 25, no. 1, p. 01LT04, 2016. [Online]. Available: http://stacks.iop.org/0963-0252/25/i=1/a=01LT04?key=crossref.7e470eb962746e8fa4ed3920787de173

[46] L. D. Pietanza, G. Colonna, G. D'Ammando, A. Laricchiuta, and M. Capitelli, "Electron energy distribution functions and fractional power transfer in "cold" and excited CO_2 discharge and post discharge conditions," *Phys. Plasmas*, vol. 23, p. 013515, 2016. [Online]. Available: http://dx.doi.org/10.1063/1.4940782

[47] M. Grofulović, L. L. Alves, and V. Guerra, "Electron-neutral scattering cross sections for CO_2: a complete and consistent set and an assessment of dissociation," *J. Phys. D: Appl. Phys.*, vol. 49, p. 395207, 2016.

[48] W. L. Nighan, "Electron energy distributions and collision rates in electrically excited N_2, CO, and CO_2," *Phys. Rev. A*, vol. 2, no. 5, pp. 1989–2000, 1970.

[49] M. Allan, "Electron collisions with CO: Elastic and vibrational excitation cross sections," *Phys. Rev. A*, vol. 81, no. 4, 2010.

[50] I. Kanik, S. Trajmar, and J. C. Nickel, "Total electron scattering and electronic state excitations cross sections for O_2, CO, and CH_4," *J. Geophys. Res.*, vol. 98, no. E4, pp. 7447–7460, 1993.

[51] T. Sawada, D. L. Sellin, and A. E. S. Green, "Electron impact excitation cross sections and energy degradation in CO," *J. Geophys. Res.*, vol. 77, no. 25, pp. 4819–28, 1972.

[52] J. Zobel, U. Mayer, and H. Ehrhardt, "Absolute differential cross sections for electron-impact excitation of CO near threshold: I. The valence states of CO," *J. Phys. B: At. Mol. Opt. Phys.*, vol. 29, pp. 813–838, 1996.

[53] S. Chung and C. C. Lin, "Electron excitation of electronic states of the CO molecule," *Phys. Rev. A*, vol. 9, no. 5, pp. 1954–1964, 1974.

[54] H. Kato, H. Kawahara, M. Hoshino, H. Tanaka, M. J. Brunger, and Y.-K. Kim, "Cross sections for electron impact excitation of the vibrationally resolved A 1Pi electronic state of carbon monoxide." *J. Chem. Phys.*, vol. 126, no. 6, p. 064307, 2007.

[55] H. Kawanhara, H. Kato, M. Hoshino, H. Tanaka, and M. J. Brunger, "Excitation of the $C^1\Sigma^+ + c^3\Pi$ and $E^1\Pi$ electronic states of carbon monoxide by electron impact," *Phys. Rev. A*, vol. 77, no. 1, p. 012713, 2008. [Online]. Available: https://link.aps.org/doi/10.1103/PhysRevA.77.012713

[56] P. C. Cosby, "Electron-impact dissociation of carbon monoxide," *J. Chem. Phys.*, vol. 98, no. 10, pp. 7804–7818, 1993. [Online]. Available: https://doi.org/10.1063/1.464588

[57] D. Rapp and D. D. Briglia, "Total cross sections for ionization and attachment in gases by electron impact. II. Negative-ion formation," *J. Chem. Phys.*, vol. 43, no. 5, pp. 1480–1489, 1965. [Online]. Available: http://aip.scitation.org/doi/10.1063/1.1696957

[58] D. Rapp and P. Englander-Golden, "Total Cross Sections for Ionization and Attachment in Gases by Electron Impact. I. Positive Ionization," *J. Chem. Phys.*, vol. 43, no. 5, pp. 1464–1479, 1965. [Online]. Available: http://aip.scitation.org/doi/10.1063/1.1696957

[59] O. Crawford and A. Dalgarno, "The scattering of thermal electrons by carbon monoxide," *J. Phys. B: At. Mol. Opt. Phys.Phy*, vol. 4, no. 4, pp. 494–502, 1971.

[60] A. Dickinson and D. Richards, "The rotational excitation of polar molecules by electrons," *J. Phys. B: Atom. Molec. Phys.*, vol. 8, no. 17, pp. 2846–2857, 1975.

[61] N. Dyatko, I. Kochetov, A. Kurnosov, and A. Napartovich, "Electron Energy Distribution Function in decaying plasma of He-CO mixture," *Plasma Phys. Rep.*, vol. 21, no. 2, pp. 180–186, 1995.

[62] N. Chandra, "Low-energy electron scattering from CO. II. Ab initio study using the frame-transformation theory," *Phys. Rev. A*, vol. 16, no. 1, pp. 80–100, 1977.

[63] L. L. Alves, P. Coche, M. A. Ridenti, and V. Guerra, "Electron scattering cross sections for the modelling of oxygen-containing plasmas," *European Physical Journal D*, vol. 70, no. 6, pp. 1–9, 2016.

[64] M. A. Ridenti, L. L. Alves, V. Guerra, and J. Amorim, "The role of rotational mechanisms in electron swarm parameters at low reduced electric field in N_2 , O_2 and H_2," *Plasma Sources Sci. Technol.*, vol. 24, no. 3, p. 035002, 2015. [Online]. Available: http://stacks.iop.org/0963-0252/24/i=3/a=035002?key=crossref.5746b8fc769aded53dc968976c00e48b

[65] A. Jain and D. W. Norcross, "Slow-electron collisions with CO molecules in an exact-exchange plus parameter-free polarization model," *Phys. Rev. A*, vol. 45, no. 3, pp. 1644–1656, 1992.

[66] J. Loureiro and J. Amorim, *Kinetics and spectroscopy of low temperature plasmas*, 2016. [Online]. Available: http://link.springer.com/10.1007/978-3-319-09253-9

[67] J. Dutton, "Survey of electron swarm data, Dutton database www.lxcat.net/Dutton," *J. Phys. Chem. Ref. Data*, vol. 4, no. 577, 1975, retrieved on July 23, 2019.

[68] "LAPLACE database www.lxcat.net/LAPLACE," retrieved on July 23, 2019.

[69] J. L. Pack, R. E. Voshall, and A. V. Phelps, "Drift velocities of slow electrons in krypton, xenon, deuterium, carbon monoxide, carbon dioxide, water vapor, nitrous oxide, and ammonia," *Phys. Rev.*, vol. 127, no. 6, pp. 2084–2089, 1962.

[70] Y. Nakamura, "Drift velocity and longitudinal diffusion coefficient of electrons in pure ethene," *J. Phys. D: Appl. Phys.*, vol. 20, pp. 933–938, 1987. [Online]. Available: http://stacks.iop.org/0022-3727/44/i=31/a=315201?key=crossref.d8d7a57126a7072fd617ab42fe2f59d1

[71] W. Roznerski and K. Leja, "Electron drift velocity in hydrogen, nitrogen, oxygen, carbon monoxide, carbon dioxide and air at moderate E/N," *J. Phys. D: Appl. Phys.*, vol. 17, pp. 279–285, 1984.

[72] M. F. Skinker and J. V. White, "LXIX. The motion of electrons in carbon monoxide , nitrous oxide , and nitric oxide," *Philos. Mag. Ser. 6*, vol. 46, no. 274, pp. 630–637, 1923.

[73] E. B. Wagner, F. J. Davis, and G. S. Hurst, "Time-of-flight investigations of electron transport in some atomic and molecular gases," *J. Chem. Phys.*, vol. 47, no. 9, pp. 3138–3147, 1967.

[74] R. W. Warren and J. H. J. Parker, "Ratio of the diffusion coefficient to the mobility coefficient for electrons in He, Ar, N_2, H_2, D_2, CO, and CO_2 at low temperatures and low E/p," *Phys. Rev.*, vol. 128, no. 6, pp. 2661–2671, 1962.

[75] M. Bhalla and J. Craggs, "Measurement of ionization and attachment coefficients in carbon monoxide in uniform fields," *Proc. Phys. Soc.*, vol. 78, pp. 438–447, 1961.

[76] G. H. L. Davies and A. W. Williams, "In Contributed papers of the Ninth International Conference on Phenomena in Ionized Gases (IX ICPIG), Bucharest, Romania," 1969, p. 46.

[77] J. E. Parr and J. L. Moruzzi, "Tenth International Conference on Phenomena in Ionized Gases (X ICPIG) 1971: Oxford, England, September 13-18th," 1971, p. 8.

[78] L. C. Pitchford and A. V. Phelpst, "Comparative calculations of electron-swarm properties in N_2 at moderate E/N values," *Phys. Rev. A*, vol. 25, no. 1, pp. 540–554, 1982.

[79] A. V. Phelps and L. C. Pitchford, "Anisotropic scattering of electrons by N_2 and its effect on electron transport," *Phys. Rev. A*, vol. 31, no. 5, pp. 2932–2949, 1985.

[80] T. Silva, N. Britun, T. Godfroid, and R. Snyders, "Optical characterization of a microwave pulsed discharge used for dissociation of CO2," *Plasma Sources Sci. Technol.*, vol. 23, no. 2, 2014.

[81] B. Klarenaar, R. Engeln, D. van den Bekerom, M. van De Sanden, A. Morillo Candas, and O. Guaitella, "Time evolution of vibrational temperatures in a CO_2 glow discharge measured with infrared absorption spectroscopy," *Plasma Sources Sci. Technol.*, vol. 26, no. 11, p. 115008, 2017. [Online]. Available: http://dx.doi.org/10.1088/1361-6595/aa902e

[82] L. S. Polak and D. I. Y. Slovetsky, "Electron impact induced electronic excitation and molecular dissociation," *Int. J. Radiat. Phys. Chem.*, vol. 8, pp. 257–282, 1976.

Chapter 4

In situ oxygen and propellant production on Mars

It has been advocated that Mars has excellent conditions for oxygen and fuel production directly from atmospheric CO_2 using non-equilibrium plasmas. The Martian conditions would be favorable for vibrational excitation and/or enhanced dissociation by electron impact, two important pathways for CO_2 plasma dissociation. Herein we confirm these theoretical predictions by measuring, for the first time, the vibrational temperatures of CO_2 and the CO concentrations in reproduced with high precision Martian conditions. *In situ* Fourier transform infrared spectroscopy (FTIR) measurements are performed in experiments conducted in DC glow discharge operating at pressures $p = 0.5 - 5$ Torr, discharge currents $I = 20 - 50$ mA, initial background gas temperatures of 220 K and 300 K, both in pure CO_2 and in the synthetic Martian atmosphere 96%CO_2-2%Ar-2%N_2. To analyse and interpret the experimental results, we develop a detailed self-consistent kinetic model for pure CO_2 plasmas, describing the coupled electron and heavy-particle kinetics. The simulation results are in very good agreement with the experimental data. It is shown that the low-temperature conditions may enhance the degree of vibrational non-equilibrium and that the Martian atmospheric composition has a positive effect on CO_2 decomposition. Accordingly, the present investigation confirms the potential of plasma technologies for ISRU on Mars. [1]

[1]The preleminary results were published as *Plasma reforming for oxygen production on Mars*, Polina Ogloblina, Vasco Guerra, Ana-Sofia Morillo-Candas and Olivier Guaitella, 2019 Proceedings of 8th European Conference for Aeronautics and Space Science(EUCASS), 715.

4.1 Introduction

Mars exploration draws ever more attention nowadays, with new plans from space agencies and private companies announced frequently [1]. Current missions to the surface of the red planet focus on robotic landers and rovers, but proposals for the first human missions and settlements will certainly follow soon. Future missions will require the ability to collect resources *in situ* and transform them into breathable air, water, propellants or food. Mars has resources that can be used for a sustainable settlement, such as carbon dioxide, which is the most abundant (95.9%) component of its atmosphere, with smaller percentages of Ar, N_2 and other gases (*sf.* table 1.1). The local production of oxygen on Mars directly from atmospheric CO_2 may help solving some of these challenges, such as manufacturing fuels to get back to Earth, and creating a breathable environment for a future outpost.

Even though CO_2 reforming is a widely discussed topic and a vast research is devoted to it in terms of reduction of greenhouse emission, production of solar fuels and chemical materials on Earth, very few studies are available regarding the use of plasmas in Martian conditions. The suggestion to use plasmas for ISRU on Mars dates back to the 1990s in a series of papers by Outlaw and co-workers [2–4], with a very recent follow-up by Premathilake et al. [5]. Alternative ideas have been proposed by Gruwenwald [6]. Some works related to plasmas on Mars do not focus on ISRU and address, *e.g.*, the characterisation of electrical discharges in $CO_2/Ar/N_2$ mixtures [7, 8], the study of vibrational-energy transfers in spacecraft entry conditions [9], or the calculation of cross sections [10] and transport coefficients [11] for the dominant heavy-particles in the Martian atmosphere.

In the chapter 2, we have put forward a strong case for oxygen and propellant production on Mars directly from the atmosphere using low-temperature plasmas, by showing that the red planet has nearly ideal conditions for CO_2 dissociation by plasmas [12, 13]. In particular, it was advocated that: i) the pressure on Mars (~ 4.5 Torr) is very suitable for plasma operation; ii) the cold Martian atmosphere may enhance VV up-pumping and hinder VT deactivation, thus leading to a higher degree of non-equilibrium, which favours dissociation via the indirect route that takes advantage of vibrational excitation; iii) Ar and N_2 may shift the electron energy to higher energies and help pumping the CO_2 asymmetric stretching mode, respectively, contributing as well to enhance dissociation and increase its efficiency. The simulations in chapter 2 show very promising results, but no experimental confirmation of these predictions was attempted to date.

In this chapter we undertake a joint experimental and theoretical investigation to assess the validity of the ideas advanced by Guerra et al. [12, 13]. To this purpose, experiments are carried out in plasmas created in simple and reproducible DC glow discharge, in pure CO_2 and in a synthetic Martian atmosphere of 96% of CO_2 with 2% of Ar and 2% of N_2, for pressures in range 0.5-6 Torr, discharge currents from 20 to 50 mA, both with the background gas at room temperature (300 K) and typical Mars average temperatures (220 K). The CO_2 and CO vibrational temperatures, the conversion factor, and the gas temperature are measured in these conditions using *in situ* FTIR spectroscopy, while the reduced electric field is determined from the voltage drop between the two tungsten probes at the floating potential. The bases of the experimental set-up are similar to the ones used in former fundamental studies on CO_2 reforming on Earth [14–16]. The low-temperature Martian conditions are recreated here by immersing the plasma reactor in a bath of dry ice and ethanol. To the best of our knowledge, these measurements constitute the first experimental characterisation of plasmas created in a realistic Martian environment and address, at the same time, the vibrational non-equilibrium and the CO_2 conversion in these plasmas. Preliminary results were presented in [17].

To complement the experimental study, a detailed self-consistent kinetic model is developed

to analyse and interpret the experimental data obtained in pure CO_2. The model describes the electron kinetics, by solving the electron Boltzmann equation for a $CO_2/CO/O_2/O$ mixture [18] using the two-term Boltzmann solver LoKI-B [19], coupled with the heavy-particle kinetics, described by a set of rate balance equations for the creation and destruction of the most important neutral and charged heavy-particles in the plasma, namely $CO_2(\nu_1\nu_2^{l_2}\nu_3)$, $CO(X\ ^1\Sigma^+, a\ ^3\Pi_r)$, $O_2(X\ ^3\Sigma_g^-, a\ ^1\Delta_g, b\ ^1\Sigma_g^+)$, $O(^3P, ^1D_g)$, O_3, CO_2^+, CO^+, O_2^+, O^+, and O^-, following the formulation from Guerra and Loureiro [20], implemented in the LoKI simulation tool as described in [21, 22]. Here, $CO_2(\nu_1\nu_2^{l_2}\nu_3)$ accounts for 72 individual CO_2 vibrational levels (see section 4.3). This description constitutes a major improvement regarding our previous models for CO_2 plasmas, where only the coupling between the electron kinetics and the $CO_2(\nu_1\nu_2^{l_2}\nu_3)$ vibrational levels was taken into account [23–26], where no vibrational excited states of CO_2 were included [27], or where vibrational states of CO_2 are included with very reduced set of chemical reactions [28].

The structure of this chapter is as follows. Section 4.2 briefly describes the experimental setup and the diagnostics used. Section 4.3 details the formulation of the model and describes the input data. The experimental and modelling results are presented and discussed in section 4.4. Finally, section 4.4 summarises our main findings.

4.2 Experiment

The experimental setup and diagnostics used are very similar as described in [14–16]. In addition, a new system had to be devised and included in the setup to reproduce the Martian low-temperature conditions, as further described below.

The plasma reactor under study is a cylindrically shaped Pyrex tube, with a 2 cm inner diameter and a length of 23 cm. The electrodes are positioned 17 cm apart, opposite to the gas in- and outlet. The reactor is connected in series with a 40 kΩ resistor to a DC power supply. The electric field in the reactor is measured with two tungsten pins radially pointing inside the positive column of the plasma. The positive column of the discharge is considered homogeneous and, therefore, the measurement of E field with two pins gives a reasonable value of the average field in the whole bulk of the plasma. The discharge current is varied between 10 and 50 mA. The pressure is varied between 0.5 and 5 Torr, using a scroll pump (Edwards XDS-5), and a pressure gauge (Pfeiffer CMR263) with feedback to an automated pressure regulating valve (Pfeiffer EVR116) and controller (Pfeiffer RVC300).

The experiments are conduced both in pure CO_2 and in synthetic Martian atmosphere corresponding to a mixture of 96% CO_2 with 2% of Ar and 2% of N_2 (all Air Liquide Alphagaz 1). The gas flows are controlled using a mass flow controller (Bronkhorst F-201CV). A total gas flow of 7.4 sccm has been used in our previous work comparing experiment with models [23, 25, 27, 29] and as well was employed as the reference condition in the present experiment. However, to insure a good precision of the concentration of the small admixtures of Ar nad N_2 necessary to reproduce Martian mixture, for the corresponding additional measurements a larger total gas flow of 19.25 sccm is used, composed of 0.39 sccm of nitrogen and 0.39 sccm of argon and the remainder of CO_2.

The reactor is positioned in the sample compartment of an FTIR spectrometer (Bruker V70) as presented in figure 4.1. The chosen configuration ensures that IR absorption measurements (line-of sight-integrated) are taken only through the positive column of the glow discharge. The contribution of the IR emission from the plasma is subtracted to the transmission spectra. The detected IR spectra contain several lines of CO and CO_2 vibrational transitions and are fitted according the procedure described by Klarenaar et al. [15, 30]. It is assumed that the

rotational and vibrational temperatures are uniform along the length of the positive column. As an outcome of the fitting procedure, the vibrational temperatures of CO_2 and CO, the rotational temperature of CO and CO_2 (assumed to be representative of the gas temperature), and the dissociation fraction

$$\alpha = \frac{[CO]}{[CO] + [CO_2]} \ ,$$

where [CO] and [CO_2] represent the gas phase concentrations of CO and CO_2 molecules, respectively, are obtained from the acquired spectra.

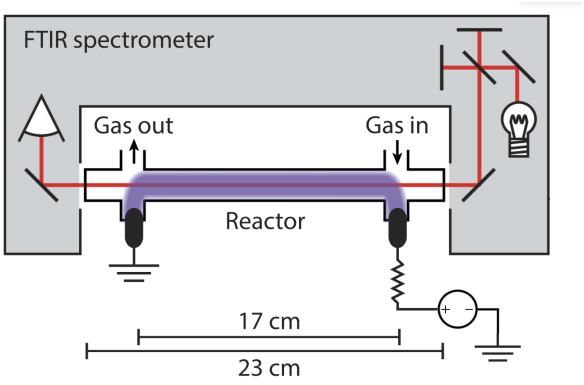

Figure 4.1: Schematic representation of the discharge reactor placed in the sample compartment of the FTIR spectrometer.

To mimic Mars-like temperature conditions, the reactor was immersed into a mixture of dry ice and ethanol (see photo of the setup and the discharge when the plasma is OFF and ON in figure 4.2). Both, the mixture temperature and the gas temperature inside the reactor were controlled with a temperature dependent platinum thin film chip resistor (Vishay PTS 0603). The nominal resistance temperature specifications from the manufacturer (given down to 215 K) was cross checked by calibrating it with a chiller (Huber 230) down to 243 K. The temperature of the gas before experiencing the plasma was further controlled by the FTIR measurements and was approximately 220–230 K. Both techniques agree within a 5% error for "plasma off" gas temperature measurements. As the temperature probe sensor is a an intrusive diagnostics, it was not used for the "plasma on" measurements and only the results obtained from the FTIR absorption spectra were considered. For the Earth temperature conditions, the same operating conditions were tested without surrounding the reactor by the dry ice and ethanol bath.

4.3 Model

A self-consistent kinetic model was developed to interpret the experimental results and describe the detailed kinetics of the major species in plasmas created in DC CO_2 discharges. It couples the electron, vibrational, chemical and ion kinetics, and builds on previous models for CO_2-containing plasmas, already tested and validated in discharges and afterglows and for various operating conditions [23–27, 29]. The model takes as input the parameters controlled in a real experiment, in particular the discharge current, I, pressure, p, gas flow, Φ, and tube radius, R. Additionally, in the present simulations the gas temperature, T_g, is also given as an input parameter, since its value is available from experiment and our purpose is not to focus on the gas heating mechanisms but rather on the plasma chemistry in the system. Note that the gas

Figure 4.2: Discharge reactor immersed into a mixture of dry ice and ethanol and positioned in the sample compartment of the FTIR when the plasma is OFF (left) and ON (right).

thermal balance equation can be incorporated in the present formulation, as it was already done in [26].

The EEDF is obtained from the solution of the homogeneous and stationary electron Boltzmann equation in a $CO_2/CO/O_2/O$ mixture, solved in the usual two-term expansion in Legendre polynomials. The calculations are done with the LisbOn KInetics Boltzmann solver LoKI-B [21, 22], an in-house code developed in object-oriented programming under MATLAB® and distributed in open source. The electron impact cross sections for the different gases have been previously validated and are described in [24] for CO_2, [18] for CO, and in [31] for O_2 and O, and can be obtained from IST-Lisbon database at the open-access web-platform LXCat [32]. These cross sections have been mostly based on [33–35] for CO_2, [36–41] for CO, [42, 43] for O_2 and [44] for O. The EEDF is calculated taken into account elastic and inelastic collisions of electrons with the parent gases, whose concentrations are self-consistently calculated (see below), as well as stepwise and superelastic collisions with vibrationally excited CO_2 molecules and electronically excited metastables $O_2(a, b)$ molecules.

The electron Boltzmann equation is coupled to a system of rate balance equations describing the creation and loss of neutral and charged heavy-species, using the approach from Guerra and Loureiro [20, 45]. The resulting global model was with the LoKI simulation tool [21, 22]. The species considered in the model include: 72 vibrationally excited CO_2 levels, represented as $CO_2(\nu_1\nu_2^{l_2}\nu_3)$, where $\nu_1 \leq 2$, $\nu_2 \leq 5$ and $\nu_3 \leq 5$ denote the vibrational quanta in the symmetric stretching, bending, and asymmetric stretching vibrational modes, respectively, and l_2

defines the projection of the angular momentum of bending vibrations onto the axis of the molecule [23]; ground-state and electronically excited CO and O_2 molecules, $CO(X\ ^1\Sigma^+, a\ ^3\Pi_r)$, $O_2(X\ ^3\Sigma_g^-, a\ ^1\Delta_g, b\ ^1\Sigma_g^+)$; ground-state and electronically excited oxygen atoms, $O(^3P, ^1D_g)$; ground-state ozone, O_3; and positive and negative ions, CO_2^+, CO^+, O_2^+, O^+, and O^-. The loss probability of O atoms at the wall, γ_O, is considered with the expression proposed in [16], deduced from the experimental determination of O-atom loss frequencies. The details on the complex plasma chemistry taken into account can be found in previous publications dealing with the CO_2 vibrational kinetics [23, 24], the kinetic mechanisms in O_2 plasmas [46], and the plasma chemistry in vibrationally cold CO_2 [27].

Note that no chemistry was included in [23, 24], a reduced chemistry set with only five reactions was coupled with the vibrational kinetics in [28], while no vibrational kinetics was included in [27]. The current model thus constitutes a significant upgrade of our prior models, by describing the coupled electron, vibrational and chemical kinetics. Moreover, Silva et al. [23], Grofulović et al. [24] only consider vibrational energy transfers in CO_2-CO_2 collisions and vibrational deactivation at the wall, as they focused on the so-called 'single-pulse' experiment, where CO_2 dissociation was very low. However, in a steady-state situation, significant amounts of CO, O_2 and O are present in the plasma (*cf.* section 4.4). Therefore, we have additionally included vibrational-to-translation (VT) energy exchanges in CO_2-O:

$$\begin{aligned} CO_2(00^0\nu_3) + O &\rightarrow CO_2(02^2(\nu_3 - 1)) + O \\ CO_2(00^0\nu_3) + O &\rightarrow CO_2(03^3(\nu_3 - 1)) + O\ , \end{aligned}$$

as they can affect significantly the vibrational distribution functions even for relatively small amounts of atomic oxygen [29]. The corresponding rate coefficients are given by López-Puertas et al. [47] for $\nu_3 = 1$ and scaled with a harmonic oscillator scaling (linear with ν_3) was assumed for $\nu_3 > 1$.

Some of the most important reactions considered in the model are listed in Table 4.1 alongside with corresponding references. This is by no means an exhaustive list and its main purpose is to guide the discussion in section 4.4. The reader should refer to our publications [23, 24, 27, 46] for a complete kinetic scheme. The rate coefficients for the heavy-particle reactions involving the metastable state $CO(a\ ^3\Pi_r)$ are taken from [48], to which is added reaction R4 from [49].

The self-consistent sustaining reduced electric field, E/N, is obtained as an eigenvalue to the problem, from the requirement that, under steady-state conditions, the total rate of production of electrons in ionisation events must compensate exactly their total loss rate due to ambipolar diffusion and electron-ion recombination, while respecting quasi-neutrality [20, 45]. A generic flowchart of the algorithm used to couple the electron, neutral, and ion kinetics, is presented in Guerra et al. [51] and an additional scheme is available at the LoKI website [22].

4.4 Results and Discussion

This section presents and analyses the experimental and simulation results in continuous DC discharges at pressures $p = 0.5 - 5$ Torr, discharge currents $I = \{20, 50\}$ mA, addressing: *i)* the differences induced by Earth and Mars atmospheric temperature conditions in the plasma chemistry in pure CO_2 (section 4.4.1); *ii)* the influence of the ambient temperature on the vibrational kinetics of CO_2 (section 4.4.2); *iii)* the effect of the Mars atmospheric minor constituents N_2 and Ar in CO_2 decomposition (section 4.4.3). The total gas flow is $\Phi = 7.4$ sccm for i) and ii) and $\Phi = 19.25$ sccm for iii).

Table 4.1: List of some important reactions mentioned in the text.

R1a	$CO(a) + O_2(X) \rightarrow CO(X) + O(^3P) + O(^3P)$	[48]
R1b	$CO(a) + O_2(X) \rightarrow CO(X) + O_2(X)$	[48]
R2	$CO(a) + CO(X) \rightarrow CO(X) + CO(X)$	[48]
R3a	$CO(a) + CO_2 \rightarrow CO(X) + CO_2$	[48]
R3b	$CO(a) + CO_2(00^00) \rightarrow CO(X) + CO(X) + O(^3P)$	[48]
R4	$CO(a) + O(^3P) \rightarrow CO(X) + O(^3P)$	[49]
R5	$e + CO_2(00^00) \rightarrow e + CO(X) + O(^1D)$	[50]
R6a	$e + CO_2(01^10) \rightarrow e + CO(X) + O(^1D)$	[50]
R6b	$e + CO_2(02^20) \rightarrow e + CO(X) + O(^1D)$	[50]
R6c	$e + CO_2(10^00 + 02^00) \rightarrow e + CO(X) + O(^1D)$	[50]
R7	$O^- + CO(X) \rightarrow e + CO_2(00^00)$	[27]
R8	$e + CO(X) \rightleftharpoons e + CO(a)$	[18]
R9	$CO(a) + O_2(X) \rightarrow CO_2(00^00) + O(^3P)$	[48]
R10	$e + CO_2(00^00) \rightarrow CO(X) + O^-$	[50]
R11	$O_2(b) + O(^3P) \rightarrow O_2(X) + O(^3P)$	[46]
R12	$O_2(a) + \text{wall} \rightarrow O_2(X)$	[46]
R13	$O_2(b) + \text{wall} \rightarrow O_2(X)$	[46]
R14	$O(^3P) + \text{wall} \rightarrow 0.5O_2(X)$	[16]
R15	$e + O_2(X) \rightleftharpoons e + O_2(a)$	[46]
R16	$e + O_2(X) \rightleftharpoons e + O_2(b)$	[46]
R17	$e + O_2(X) \rightarrow e + O(^3P) + O(^3P)$	[46]
R18	$e + O_2(X) \rightarrow e + O(^3P) + O(^1D)$	[46]
R19	$O(^1D) + O_2(X) \rightarrow O(^3P) + O_2(b)$	[46]

4.4.1 CO_2 plasma chemistry at Mars and Earth temperature conditions

In this section we investigate the influence of the ambient temperature on the plasma chemistry in pure CO_2 plasmas, while keeping the pressure around the Martian atmospheric pressure. For this purpose, we compare the results obtained when the plasma is ignited at Martian (~ 220 K) or Earthly (~ 300 K) ambient temperatures, in order to find out up to which extent the results obtained on Earth at low pressure can be assumed to be valid on Mars.

Figure 4.3 shows the measured and calculated the values of the reduced electric field, E/N, as a function of the he gas density (N) - tube radius (R) product for currents I = 20 mA and 50 mA. The E/N values are deduced from two independent measurements: on the one hand from the electric field evaluation performed by measuring the floating potential of two tungsten pins inserted in the positive column, and on the other hand from the measurement of the gas temperature from which the gas density is deduced via the ideal gas law. A true statistical study of reproducibility on these two measurements has not been carried out and the error bars shown are only an upper value estimate based on the accumulative errors of these two measurements. The corresponding values of the gas temperature, T_g, obtained from the FTIR measurements of the rotational distribution of CO_2 (*cf.* section 4.2), are given in Table 4.2. The gas heating, induced by plasma, remains very similar for both - Mars and Earth conditions and, therefore, the gas temperature for all conditions is shifted by an offset of ~70 - 80 K. The experimental results suggest that Martian conditions may lead to slightly lower values of the reduced field than on

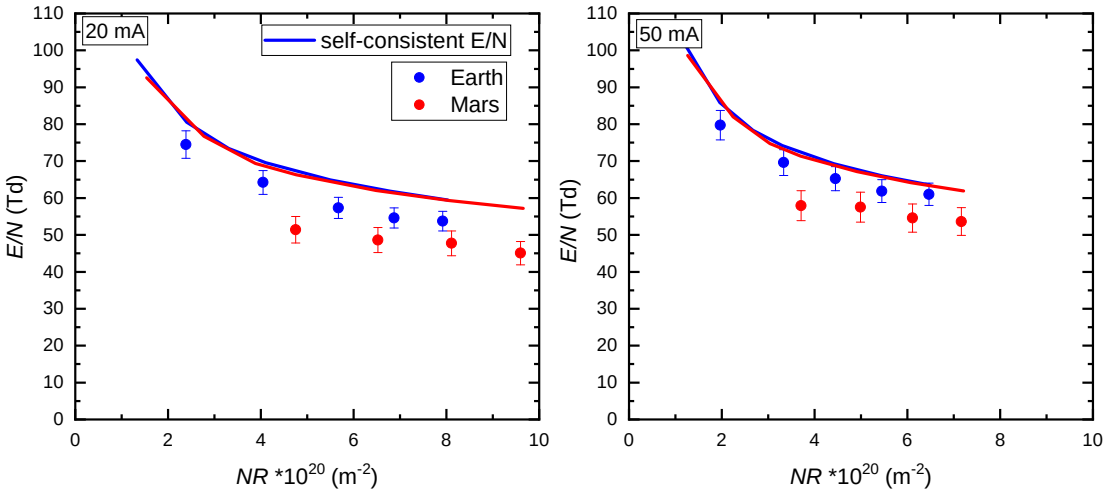

Figure 4.3: Reduced electric field, E/N, as a function of NR product, when a pure CO_2 discharge is ignited in Mars and Earth background temperatures at currents I = 20 mA (left panel) and I = 50 mA (right panel): experiment (•), self-consistent calculation (—).

Table 4.2: Measured gas temperature (K) deduced from rotational temperature of CO and CO_2 in pure CO_2 plasmas

	20 mA		50 mA	
p (Torr)	Mars	Earth	Mars	Earth
0.5	309	390	380	430
1	348	405	425	490
1.5	378	463	485	555
2	406	477	520	580
3	444	511	580	651
4	476	562	632	709
5	503	610	674	747

Earth. However, the observed differences lay within the experimental errors and no noticeable variation is found in the self-consistent calculations, so that this potential minor effect requires further verification. Increasing the discharge current induces a small raise in the value of E/N, a behavior that is captured in the simulations and is partially due to the easier ionization of CO_2 as compared with CO [18] and to the increase of the dissociation of CO_2 with the discharge current (see Figure 4.4). Overall, the self-consistent calculations of reduced electric field are in very satisfactory agreement with experiment and the results show that the model can be used as a predictive tool when no experimental data for E/N are available. Nevertheless, the small differences in magnitude between model predictions and measurements suggest that some details of the charged particle kinetics may be missing in the model. To avoid an error propagation in the analysis, the experimental values of E/N are given as input to the simulations shown in the remainder of the chapter.

The measured and calculated CO_2 dissociation fractions, $\alpha = [CO]/([CO] + [CO_2])$, are represented in Figure 4.4. The calculations are performed both considering and neglecting the

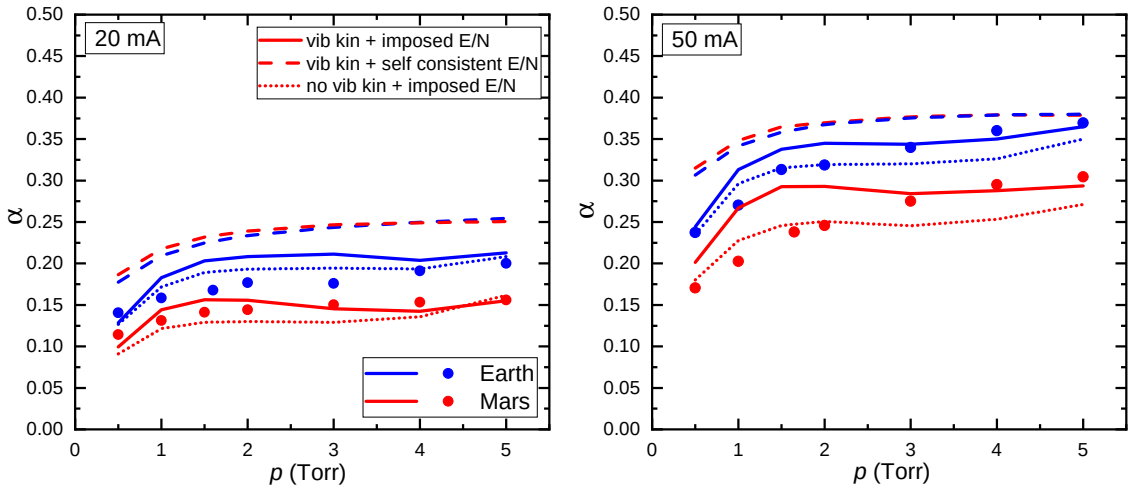

Figure 4.4: CO_2 dissociation fraction when a pure CO_2 discharge is ignited in Mars and Earth background temperatures at currents I = 20 mA (left panel) and I = 50 mA (right panel): experiment (•), model calculations by including (—) and excluding (···) the vibrational kinetics.

vibrational kinetics in the model. There is a quite good agreement between the model predictions and the experimental data. The inclusion of the vibrational kinetics increases the calculated dissociation fraction, as a consequence of the modifications of the EEDF due to superelastic collisions with vibrationally excited CO [18, 52] and, mostly, to the contribution to dissociation of the vibrational states of CO_2. Dissociation fractions in the range 10-30% are observed for Martian temperature conditions, which is already an interesting result regarding the use of plasma technologies for ISRU on Mars, specially taking into account that the present reactor was designed for fundamental studies and is far from any system that would be used in a prototype.

According to the simulations, ground-state $CO(X\ ^1\Sigma^+)$ molecules are essentially created by dissociation by electron impact on $CO_2(\nu_1\nu_2^{l_2}\nu_3)$ molecules, mainly on the (00^00), (01^10), (02^20) and the Fermi $(10^00 + 02^00)$ states (see reactions R5 and R6 in Table 4.1), and by the quenching of the $CO(a\ ^3\Pi_r)$ state. The latter mechanism has to be looked at with caution, as the excitation of $CO(a\ ^3\Pi_r)$ from ground-state $CO(X\ ^1\Sigma^+)$ is also one of the main processes of destruction of $CO(X\ ^1\Sigma^+)$, so that reactions involving only $CO(X)$ and $CO(a)$ do not constitute true creation/destruction mechanisms of CO molecules, but rather redistribute its population between the two electronic levels. An additional destruction mechanism of $CO(X\ ^1\Sigma^+)$ worth mentioning is the transport by the gas flow. Figure 4.5 quantifies the contribution of the different creation and destruction mechanisms of $CO(X\ ^1\Sigma^+)$ molecules for p = 5 Torr and I = 50 mA. Reactions R1 and R6 in the figure correspond to the total contributions identified in Table 4.1, R1 = R1a+R1b, R6 = R6a+R6b+R6c. The differences between the results obtained by including and neglecting the vibrational kinetics are largely due the the associated difference in the meaning of "$CO_2(00^00)$" in Table 4.1: in the former case it corresponds to a single individual level carrying only a fraction of the total CO_2 electronic ground-state, while in the latter case it corresponds to the total population of the electronic ground-state (*cf.* as well Figure 4.12 and respective discussion). Nevertheless, an increase in the dissociation fraction is observed in the simulations when the vibrational kinetics is taken into account. A couple of contributions could

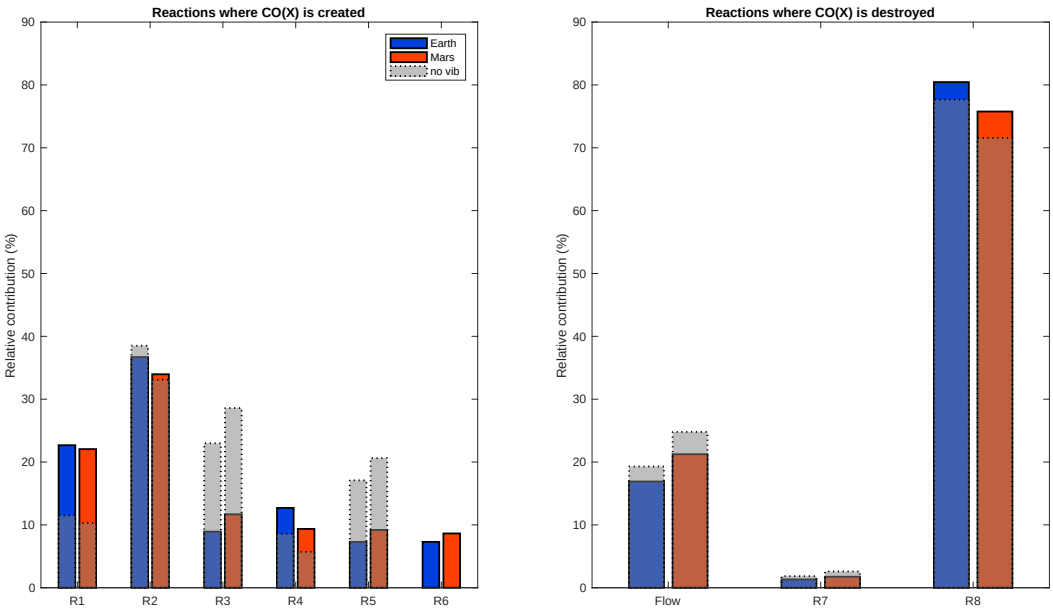

Figure 4.5: Relative contribution (in %) of the main mechanisms of creation and destruction of CO($X\ ^1\Sigma^+$) when a pure CO_2 discharge at $p = 5$ Torr and $I = 50$ mA is ignited in Mars and Earth background temperatures, including (colored bars) and neglecting (grey bars) the vibrational kinetics.The reactions are identified in Table 4.1.

explain the higher alpha calculated when the vibrations are included: either a small influence of the lower energy required to dissociate a pre-excited vibrational level, or the modification of the EEDF obtained when vibrations are included which results in higher population of the electrons above 7 eV, or both.

Figures 4.6-4.8 show, respectively, the calculated concentrations of the dominant neutral species, electronically-excited states and O_3, and the charged particles. The densities represented in Figure 4.6 are the total densities of the parent species, *i.e.*, the sum of the populations of all the electronically metastable states; note that for CO_2, CO and O, more than 99.9% of the total population is in the ground electronic state, while for O_2 up to ~ 20% of the population can be in the $O_2(a\ ^1\Delta_g, b\ ^1\Sigma_g^+)$ excited states. Experimental data for CO_2 and CO are also plotted in Figure 4.6.

Most species represented in Figures 4.6-4.8 follow the trend expected by a production dictated by electron-impact dominant mechanisms [27], with a decrease with pressure and an increase with current, as an outcome of the lower reduced electric field (and corresponding lower electron impact rate coefficients) and higher electron density, respectively. A noticeable and important exception to this trend is CO, whose relative concentration remains nearly constant for pressures above ~ 1.5 Torr, although it is mainly produced by electron impact. The increasing behavior of O_2 is partially due to the shift from O to O_2 as the pressure increases and the associated reduction in the total number of particles. The shift in the relative concentrations of O and O_2 with pressure is mainly a consequence of the increase of the recombination probability of O atoms at the wall with pressure [16], as surface recombination is the main destruction mechanism of O atoms for the present conditions. The O atom densities for the Earth background temperature are in a good agreement with the values obtained in [16]. It is also worth noting that O_2^+ is always the dominant ionic species, due to the efficient charge transfer processes from

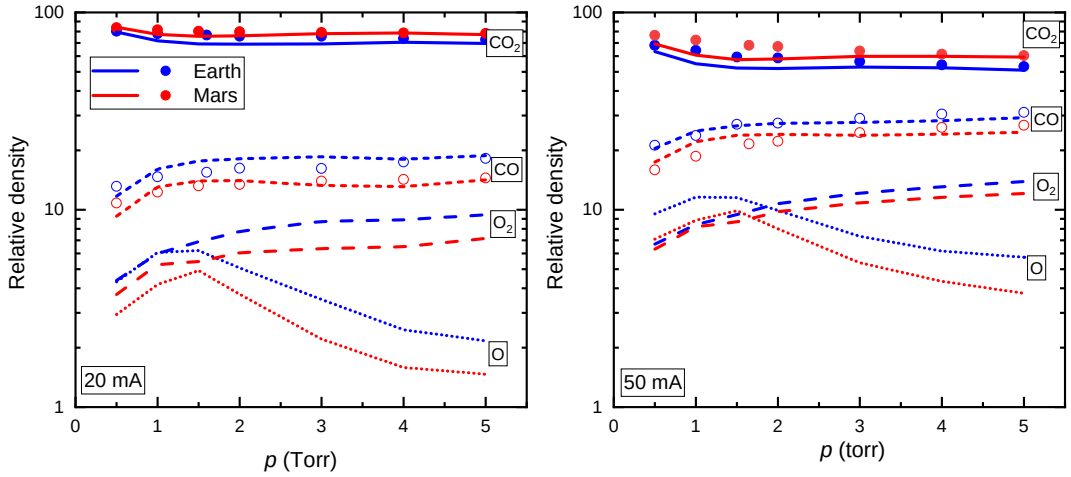

Figure 4.6: Relative density of the dominant species when a pure CO_2 discharge is ignited in Mars and Earth background temperatures at currents I = 20 mA (left panel) and I = 50 mA (right panel). The symbols correspond to experimental data for CO_2 (•) and CO (◦).

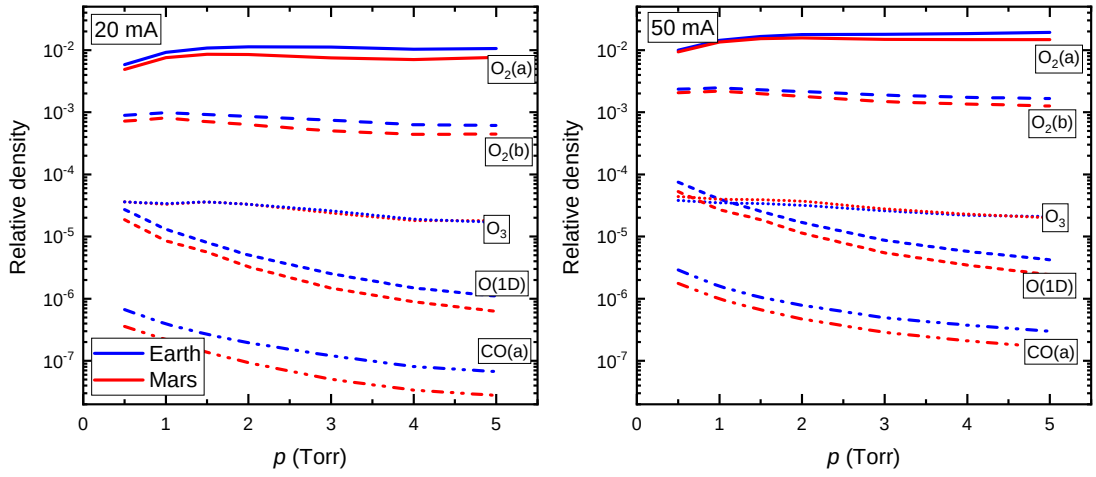

Figure 4.7: Relative density of various electronically excited states and of ozone, when a pure CO_2 discharge is ignited in Mars and Earth background temperatures at currents I = 20 mA (left panel) and I = 50 mA (right panel).

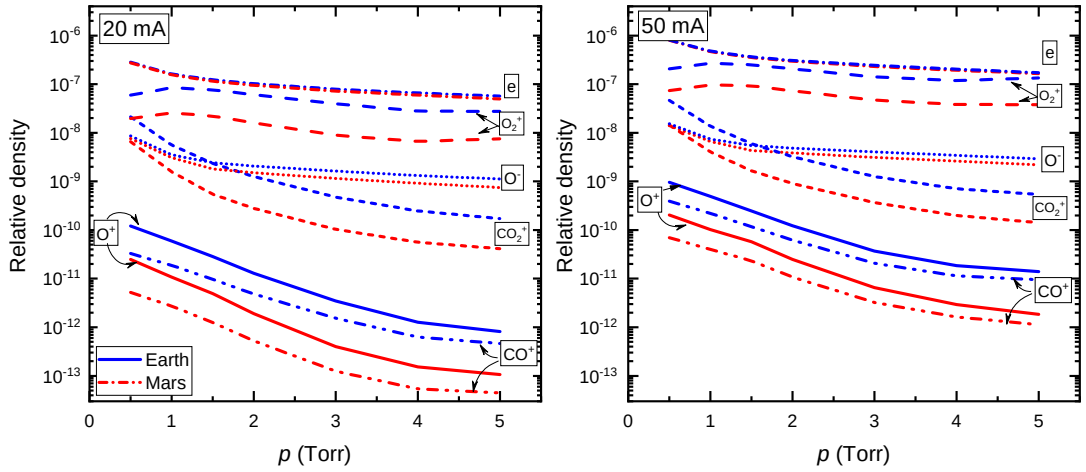

Figure 4.8: Relative density of various charged particles, when a pure CO_2 discharge is ignited in Mars and Earth background temperatures at currents I = 20 mA (left panel) and I = 50 mA (right panel).

CO_2^+ and O^+ to O_2^+, namely,

$$\begin{aligned} CO_2^+ + O &\rightarrow CO + O_2^+ \ , \\ O^+ + CO_2 &\rightarrow CO + O_2^+ \ , \\ CO_2^+ + O_2 &\rightarrow CO_2 + O_2^+ \ . \end{aligned}$$

Further insight into the complex coupled kinetics taking place in the plasma is given by inspection of figures 4.9 and 4.10. Figure 4.9 displays the relative contribution of the dominant creation and destruction mechanisms of O_2, for the same conditions as in Figure 4.5, p = 5 Torr and I = 50 mA. Most of the mechanisms include the excitation from $O_2(X\ ^3\Sigma_g^-)$ to $O_2(a\ ^1\Delta_g)$ or $O_2(b\ ^1\Sigma_g^+)$, or the de-excitation from these excited metastable states back to ground-state. Therefore, they essentially redistribute the population among the three O_2 electronic states. Exceptions are the mechanisms of wall recombination of O atoms (R14), dissociation of O_2 (R17,R18) and dissociation due to the quenching of $CO(a\ ^3\Pi_r)$ (R1a), which, therefore, play a significant role in the kinetics.

Figure 4.10 depicts the relative contribution of the dominant destruction mechanisms of the $CO(a\ ^3\Pi_r)$ electronically excited state. $CO(a\ ^3\Pi_r)$ is predominantly quenched to $CO(X\ ^1\Sigma^+)$ in collisions with O_2, CO, CO_2 and O, in mechanisms that do not lead to a destruction of a CO molecule. Similarly, it is created by direct electron impact on $CO(X\ ^1\Sigma^+)$ (R8). An effective destruction mechanism of CO molecules is reaction (R9), a back reaction mechanism involving $CO(a\ ^3\Pi_r)$ and O_2 giving back CO_2, recently evinced by Morillo-Candas [53, 54]. It contributes about 1% to the destruction of the $CO(a\ ^3\Pi_r)$ state, but its actual importance should not be underestimated, as it brings an exit path from the CO manifold.

It is worth noting the prevalence of processes involving electronically excited states, $O_2(a\ ^1\Delta_g)$, $O_2(b\ ^1\Sigma_g^+)$, $O(^1D_g)$ and $CO(a\ ^3\Pi_r)$, in the overall kinetics. This remark is particularly striking for the cases of $O(^1D_g)$ and $CO(a\ ^3\Pi_r)$, whose relative densities are rather low, as it can be seen in Figure 4.7. Nonetheless, the results reveal a strong coupling between the kinetics of all these electronically excited states and the parent atoms and molecules. Similar conclusions have been drawn for oxygen plasmas in [46]. A more detailed analysis of the plasma chemistry in

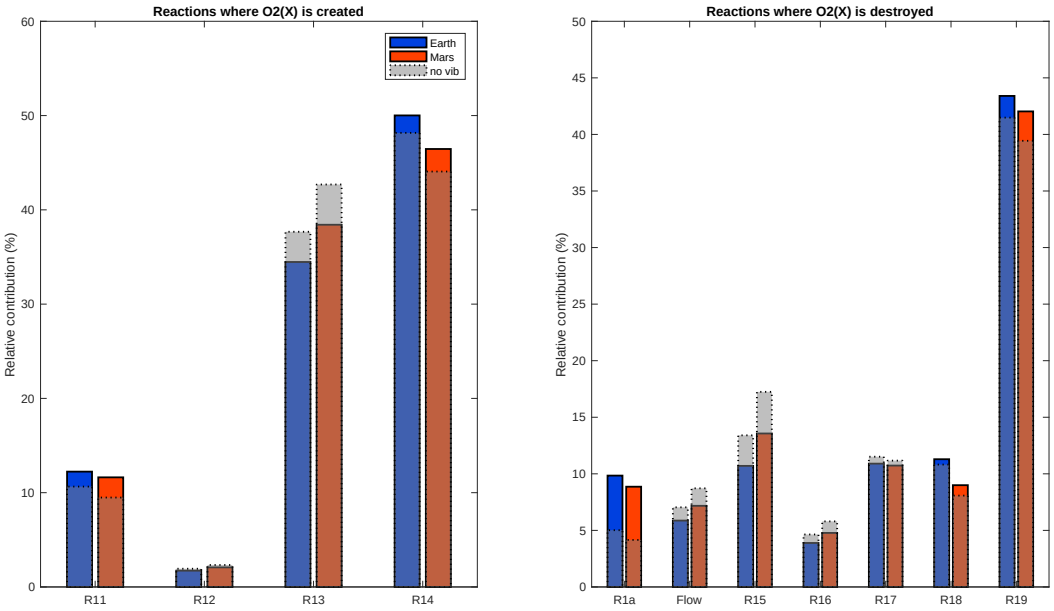

Figure 4.9: Relative contribution (in %) of the main mechanisms of creation and destruction of $O_2(X\ ^3\Sigma_g^-)$ when a pure CO_2 discharge is ignited at $p = 5$ Torr and $I = 50$ mA in Mars and Earth background temperatures, including (colored bars) and neglecting (grey bars) the vibrational kinetics. The reactions are identified in Table 4.1.

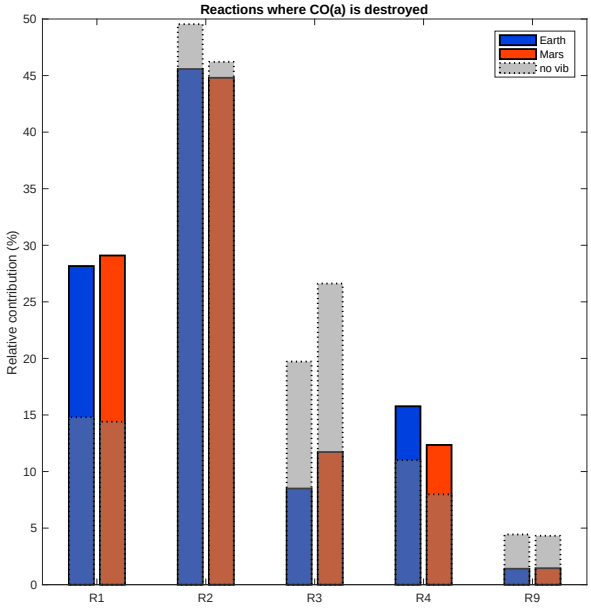

Figure 4.10: Relative contribution (in %) of the main mechanisms of destruction of $CO(a\ ^3\Pi_r)$ when a pure CO_2 discharge is ignited at $p = 5$ Torr and $I = 50$ mA in Mars and Earth background temperatures, including (colored bars) and neglecting (grey bars) the vibrational kinetics. The reactions are identified in Table 4.1.

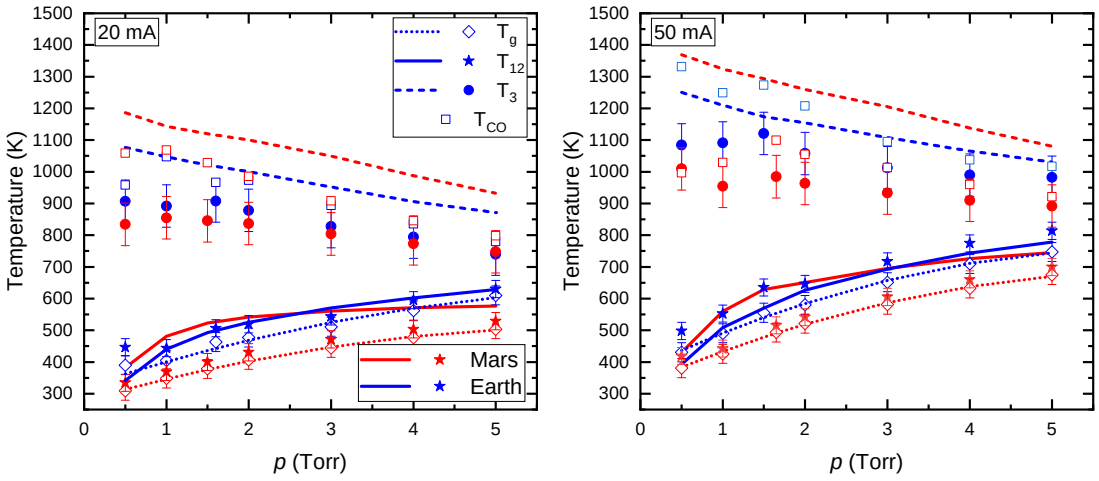

Figure 4.11: Experimental value of the gas temperature T_g ($\cdot \diamond \cdot$), together with the measured (symbols) and calculated (lines) vibrational temperatures of the asymmetric stretching mode T_3 ($\bullet$, – –) and the common temperature of the bending and symmetric modes T_{12} ($\star$, —) and CO vibrational temperature T_{CO} (*square*), when a pure CO_2 discharge is ignited in Mars and Earth background temperatures at currents I = 20 mA (left panel) and I = 50 mA (right panel).

CO_2-containing discharges will be presented in future publications.

4.4.2 CO_2 vibrational kinetics at Mars and Earth temperature conditions

One argument advanced in chapter 2 and in [12, 13] in favor of ISRU on Mars by plasmas was the increased degree of vibrational non-equilibrium that would be promoted by the ambient conditions on the red planet. In appropriate discharge configurations, such as radio-frequency, microwave or gliding arc discharges, it might be possible to benefit from the energy stored in the vibrational levels to enhance the energy efficiency of CO_2 dissociation [55]. In the DC glow discharges under study, CO_2 dissociation proceeds mainly by direct electron impact, with a small to negligible contribution from purely vibrational mechanisms [28, 54]. Nevertheless, it is very instructive to verify the validity of the conjecture in chapter 2, to guide the development of plasmas sources designed for ISRU on Mars, as well as to further analyze the results in Figure 4.4.

Figure 4.11 represents the measured gas temperature, T_g, the vibrational temperature of the asymmetric stretching mode, T_3, the common temperature of the bending and symmetric stretching modes, T_{12} and vibrational temperature of CO, T_{CO}, together with the model predictions for CO_2 "vibrational temperatures." The CO vibrational temperature is taken into account as an input parameter for the EEDF calculation, but CO vibrations are not accounted for in the chemistry module and, thus, are not calculated in the model. It is worth emphasizing that the current state-to-state model provides the populations of the individual vibrational levels of the CO_2 molecules. Therefore, the "vibrational temperatures" correspond to the fitting of the individual populations to Treanor and Boltzmann distributions, respectively for the asymmetric

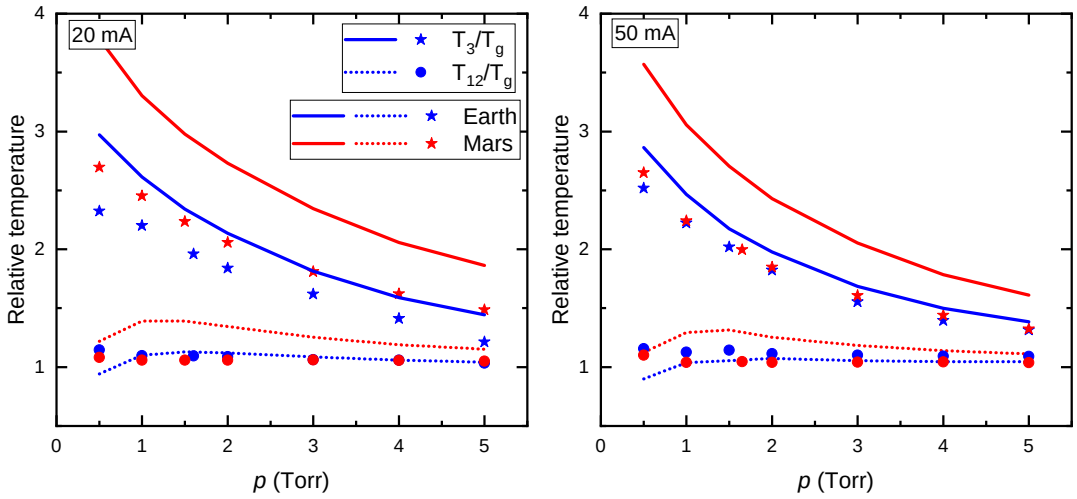

Figure 4.12: Measured (symbols) and calculated (lines) ratios T_3/T_g (—,⋆) and T_{12}/T_g (···, •) when a pure CO_2 discharge is ignited in Mars and Earth background temperatures at currents I = 20 mA (left panel) and I = 50 mA (right panel).

stretching mode and for both the symmetric stretching and bending modes. Moreover, the fact that the bending and symmetric stretching modes can be described by a common "temperature" in these conditions is not an imposition of the model but rather an outcome of the simulations, as also pointed out in [24]. Additional details on the fitting of the individual populations to the corresponding distributions are given in [23, 24], where some vibrational distribution functions are presented. The simulations describe satisfactorily the trend and magnitude of the observed T_{12} and T_3, whose values do not change significantly from a discharge ignited in Martian or Earthly ambient temperatures. The model predicts slightly larger vibrational temperature of the asymmetric stretching mode on Mars than on Earth, that is not confirmed experimentally. This discrepancy is likely due to the simplified vibrational kinetics considered here concerning energy transfers between CO_2 and the dissociation products, O, O_2 and CO, that only accounts for very few VT collisions of vibrationally excited CO_2 with O atoms and disregards collisions with O_2 and CO (see section 4.3 and chapter 5). In any case, the main effects seem to be already captured with the present model. The variations of T_3 with pressure and current are similar to the ones reported and carefully discussed by Morillo-Candas [53] for Earth conditions. They further confirm the interest of the Martian pressure range to benefit from vibrational non-equilibrium to decompose CO_2.

One interesting phenomenon revealed by Figure 4.11 is a small increase of the degree of vibrational non-equilibrium when passing from Earth to Mars, as predicted theoretically in [12]. This effect is more clearly exhibited in Figure 4.12, which shows the ratios T_3/T_g and T_{12}/T_g, characterizing the degree of non-equilibrium in the plasma [12, 13]. It can be verified that the common temperature of the bending and symmetric stretching modes remains always nearly in equilibrium with the gas temperature. On the contrary, the asymmetric stretching mode, of major interest for vibrationally-driven dissociation [55], is clearly out of equilibrium, with a bigger departure from equilibrium in Martian conditions than on Earth, but only for the lower current, I = 20 mA. In this case, the ratio T_3/T_g is always 25 – 30% higher on Mars than

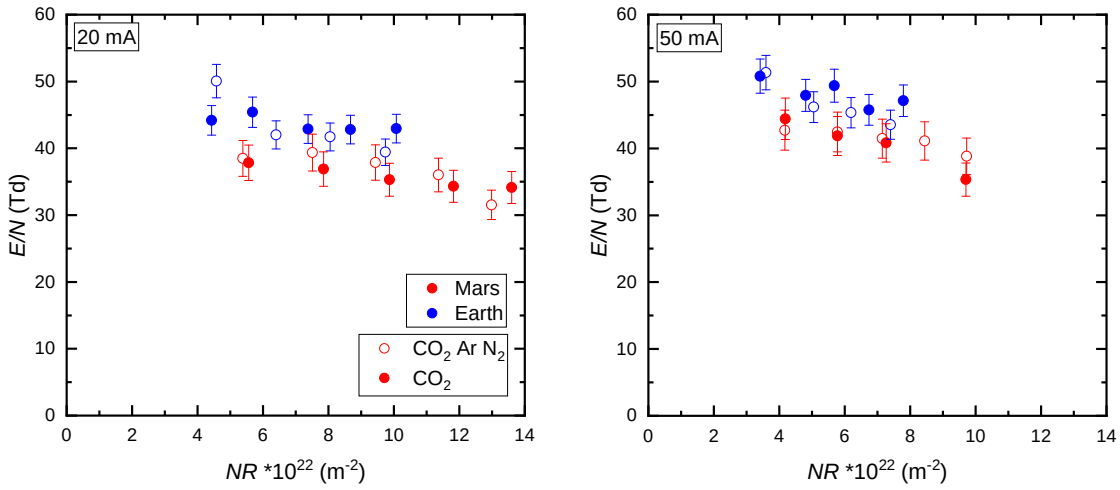

Figure 4.13: Reduced electric field, E/N, as a function of NR product, measured when pure CO_2 (•) and 96%CO_2-2%Ar-2%N_2 (∘) discharges are ignited in Mars and Earth background temperatures at currents I = 20 mA (left panel) and I = 50 mA (right panel).

on Earth. This behavior is the outcome of the enhanced up-pumping along the asymmetric stretching mode as the temperature decreases,

$$CO_2(00^0\nu_3) + CO_2(00^0\nu_3') \rightleftharpoons CO_2(00^0(\nu_3+1)) + CO_2(00^0(\nu_3'-1)) \ ,$$

since in the present temperature domain this VV interaction is dominated by long-range attractive forces [56], and of the decrease of the deactivation in VT mechanisms, dominated by short range repulsive forces. A somewhat similar effect is predicted from the model for I = 50 mA but is not confirmed experimentally. As noted above, these differences might stem from the simplified vibrational kinetics included in the model.

It is now possible to get further insight into the results of Figure 4.4, evincing a larger CO production when the vibrational kinetics is taken into account in the calculations. The effect is mainly attributed to the contribution of electron impact dissociation from vibrationally excited levels, process R6 in Table 4.1. Figure 4.11 allows a quantification of the population of the levels that contribute the most to this mechanism, by converting back the vibrational temperatures to the species concentrations. As an example, for Earthly conditions at 5 Torr and 50 mA, the relative populations of levels (00^00), (01^10), (02^20) and $(10^00 + 02^00)$ are, respectively, 0.439, 0.255, 0.074 and 0.075.

4.4.3 Synthetic Martian atmosphere

This section addresses the experimental investigation of the influence of the minor constituents of the Martian atmosphere, Ar and N_2, on the plasma properties and CO_2 decomposition. Experiments are carried-out in pure CO_2 and in 96%CO_2-2%Ar-2%N_2 plasmas, with a gas flow Φ = 19.25 sccm, ignited both in Mars and Earth background gas temperatures. It has been speculated that the presence of traces of Ar and N_2 could be beneficial for the production of oxygen and carbon monoxide by enhancing CO_2 plasma dissociation [12, 13], but no experimental evidence has been presented to date.

The measured values of the reduced electric field are shown in Figure 4.13, the temperatures T_g, T_{12} and T_3 in Figure 4.14, the temperature ratios T_3/T_g, T_{12}/T_g and T_3/T_{12} in Figure 4.15,

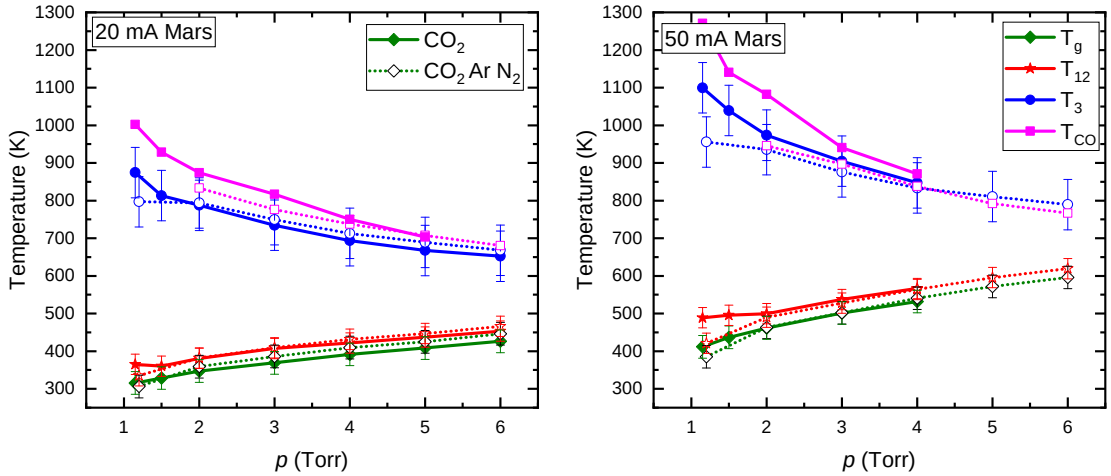

Figure 4.14: Experimental values of the gas temperature T_g (◆, ◇), the vibrational temperature of the asymmetric stretching mode T_3 (●, ○) and the common vibrational temperature of the bending and symmetric modes T_{12} (⋆, ☆) and CO vibrational temperature T_{CO} (■,□), when pure CO_2 (—, closed symbols) and 96%CO_2-2%Ar-2%N_2 (···, open symbols) discharges are ignited in Mars background temperature at currents I = 20 mA (left panel) and I = 50 mA (right panel).

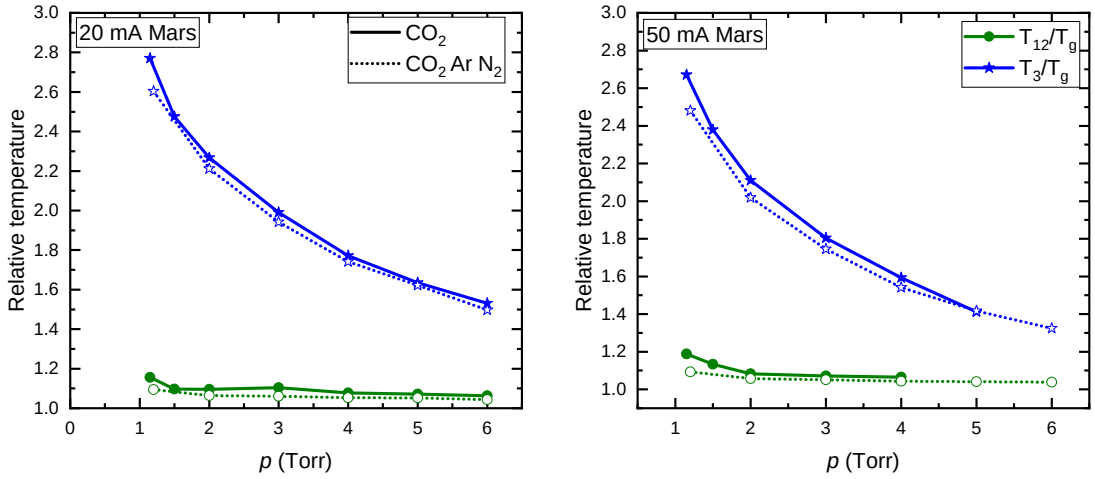

Figure 4.15: Experimental values of the ratios T_3/T_g (⋆, ☆) and T_{12}/T_g (●, ○), when pure CO_2 (—, closed symbols) and 96%CO_2-2%Ar-2%N_2 (···, open symbols) discharges are ignited in Mars background temperature at currents I = 20 mA (left panel) and I = 50 mA (right panel).

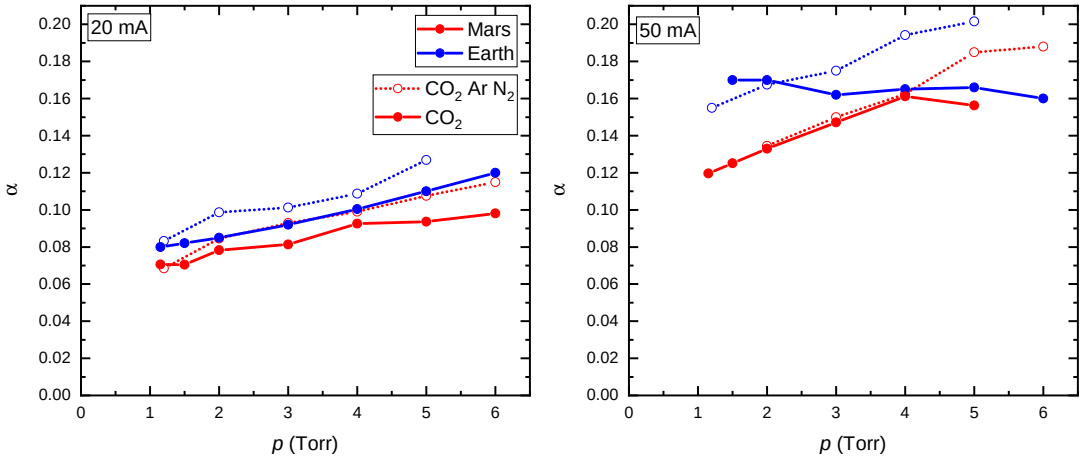

Figure 4.16: Experimental CO_2 dissociation fraction when pure CO_2 (-•-) and 96%CO_2-2%Ar-2%N_2 (· ∘ ·) discharges are ignited in Mars and Earth background temperatures at currents I = 20 mA (left panel) and I = 50 mA (right panel)

and the dissociation fraction α in Figure 4.16. Figures 4.13-4.15 indicate that the presence of Ar and N_2 in the Martian atmosphere has a negligible effect on the reduced field and on the vibrational temperatures, maintaining a significant degree of non-equilibrium. Even though, a small but consistent positive influence on the production of CO from CO_2 is visible in Figure 4.16, despite some fluctuation of the results and the outlier data on Earth at $p \leq 2$ Torr and I = 50 mA. It is worth noting, that the decomposition here is lower, than what is reported in figure 4.4. This is due to the lower residence times of the gas in the plasma, which decrease ~3 times as the flow increases.

The reasons for a favorable effect of traces of N_2 and Ar in CO_2 decomposition are most likely due to the modifications induced by Ar and N_2 in the EEDF. Figure 4.17 shows the EEDFs calculated for the experimental conditions of reduced field, E/N, common vibrational temperature of the symmetric stretching and bending modes, T_{12}, vibrational temperatures of the asymmetric stretching mode, T_3, and of CO, T_{CO}, for a discharge ignited at Mars background temperature, current I = 50 mA and pressures p = 3 Torr and p = 5 Torr, in pure CO_2 and in a synthetic Martian atmosphere 96%CO_2-2%Ar-2%N_2. The vibrational temperature of N_2 was assumed to be the same as T_{CO}. To separate the effects of Ar and N_2, additional calculations are shown for the mixtures 96%CO_2-4%Ar and 96%CO_2-4%N_2, for the same conditions as in the CO_2-Ar-N_2 mixture. Figure 4.17 shows that both Ar and N_2 addition enhance the tail of the EEDF in the region of energies around 7 eV, the energy threshold for dissociaiton [50, 57] and, accordingly, lead to an increase in the electron impact dissociation rate coefficient. The effect is due to the differences in the cross sections between the different gases, as well as to a small increase in the values of E/N when passing from pure CO_2 to CO_2-Ar-N_2 (from 41.9 Td to 42.5 Td at 3 Torr, and from 35.3 Td to 41.1 Td at 5 Torr). The presence of Ar is expected to shift the EEDF to higher energies [58], but the effect does not seem to be relevant at the low Ar concentrations involved.

Another possibility for a positive influence of N_2 would be the transfer of vibrational energy from nitrogen to the asymmetric stretching mode of CO_2 and the enhancement of dissociation via the purely vibrational mechanism [55]. Notwithstanding, the measured vibrational temperatures are not significantly affected and, in addition, the purely vibrational mechanism does not seem

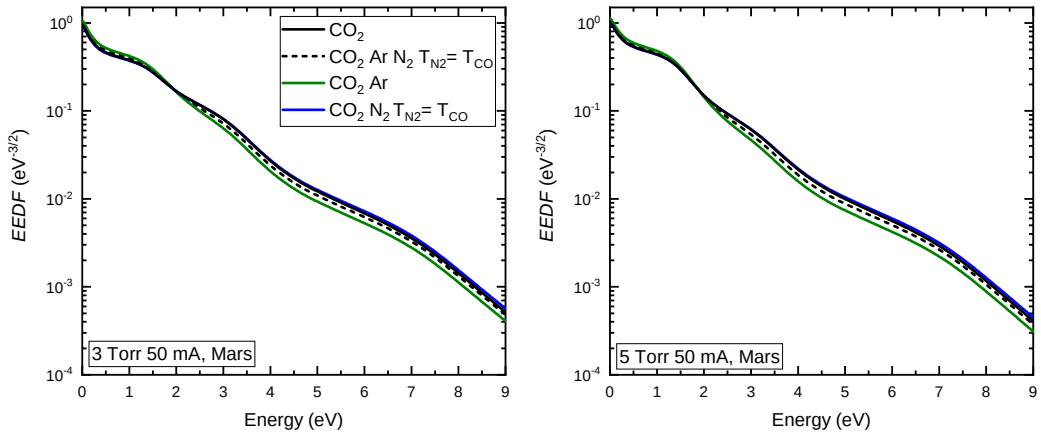

Figure 4.17: Electron Energy Distribution Functions calculated for the experimental values of E/N, T_{12}, T_3 and T_{CO} at p = 3 Torr (left panel) and p = 5 Torr (right panel), I = 50 mA, and Mars background temperature, for pure CO_2 (—) and 96%CO_2-2%Ar-2%N_2 (– –). Additional curves for 96%CO_2-4%Ar (—); 96%CO_2-4%N_2 (—) are calculated for the same conditions as in the CO_2-Ar-N_2 mixture.

to play a significant role in the present conditions. Note, however, that the measured vibrational "temperatures" are only representative of the populations of the lower vibrational levels and do not bring any information regarding the populations of the higher ones, which may deviate from equilibrium Boltzmann distributions and be modified by the presence of N_2. A positive effect of N_2 addition was also observed in experiments by [29, 59], reinforcing the suggestion from Figure 4.17 that the answer to why the CO yield is higher in synthetic Martian atmosphere than in pure CO_2 plasmas may lay in the CO_2-N_2 kinetics. Further research is necessary to elucidate the origin of this effect.

4.5 Conclusions

This chapter presents an experimental and modeling investigation on the potential of low-temperature plasmas for *in situ* resource utilization (ISRU) on Mars. The research focus on the decomposition of CO_2, which is freely abundant in the Martian atmosphere and creates the building blocks for the local production of oxygen and fuels.

DC glow discharges operating at pressures in the range 0.5-5 Torr are ignited in pure CO_2 and in a synthetic Martian atmosphere composed of 96%CO_2-2%Ar-2%N_2, discharge currents I = 20 – 50 mA, with the background gas either at Martian (~ 220 K) or Earthly (~ 300 K) temperatures. The CO_2 and CO vibrational temperatures and the CO and CO_2 concentrations are measured, providing an experimental characterization of plasmas created in conditions realistically mimicking the atmosphere of Mars.

In the system under study, CO_2 is essentially decomposed by direct electron impact, both on molecules in the vibrational ground-state (00^00) and in vibrational excited states. The contribution of the latter sates comes mainly from the lower-laying levels (01^10), (02^20) and ($10^00 + 02^00$), with several other levels having contributions of a few percent. Dissociation fractions up to 30% are observed, a very encouraging result considering that the present setup is designed for fundamental studies and is far from suited for the development a prototype.

The plasma chemistry is significantly influenced by electronically excited states, such as $O_2(a\ ^1\Delta_g)$, $O_2(b\ ^1\Sigma_g^+)$, $O(^1D_g)$ and $CO(a\ ^3\Pi)$. Therefore, a full control and optimization of the plasma requires a detailed understanding of the strongly coupled kinetics of these states.

The results confirm that Martian conditions of temperature and pressure can pump the asymmetric stretching vibration mode and achieve a stronger non-equilibrium than on Earth, believed to have a positive influence in dissociation [55], by up to a factor of ~ 30%. However, for the current discharge configuration, dissociation is driven by electron impact and the conversion factor at low temperature is slightly lower than at room temperature.

The new experimental data corroborate the conjecture of a positive effect of the Martian atmospheric composition on dissociation advanced in chapter 2. This behavior is most likely related to modifications in the electron kinetics induced by the presence of nitrogen and argon and the associated enhanced dissociation by electron impact.

Despite the beneficial effects of the low ambient temperature and of the presence of Ar and N_2 in the Martian atmosphere, their impact on CO_2 decomposition is relatively small. Indeed, the results obtained for Mars and Earth background temperatures, as well as for pure CO_2 and for the synthetic Martian atmosphere, are rather similar in what concerns the identification of the main creation/destruction mechanisms and all the trends observed. Thus, knowledge on the energy-transfer pathways acquired on Earth can, to a very considerable extent, be transposed to Mars.

The present results establish experimental evidence of the feasibility of oxygen and propellant production by plasma decomposition of CO_2 from the Martian atmosphere and suggest the possible development of more sophisticated setups that can take fully advantage of non-equilibrium and/or promote dissociation by electron impact. Future research should concentrate on the design and optimization of robust and efficient plasma sources and on the procedure to separate O_2 from the other dissociation products. Recent proposals for product separation include the use of silver membranes by Premathilake et al. [5] and a new electrochemical membrane reactor presented in [60, 61].

Finally, it is worth noticing that emerging plasma technologies for CO_2 reforming on Earth are already expected to be competitive with solid oxide electrolysis (SOEC) [62–64], the technology proposed in NASA's MOXIE program. Therefore, a plasma-electrochemical process will most certainly be a viable alternative to SOEC for oxygen production on Mars. In fact, the efficiency of SOEC is likely to decrease as compared to that on Earth, because extra energy is necessary to compress the gas up to 1 atm, pre-heat it up to 1100 K and cool down the exhaust stream [65, 66]. Furthermore, sophisticated thermal insulation systems are mandatory. In turn, the efficiency of plasma dissociation of CO_2 on Mars is likely to increase as compared to that on Earth, due to the beneficial effects demonstrated in this chapter and the absence of vacuum pumps. A conservative estimation can be made as follows. Consider a thermodynamic value of ~ 50% energy efficiency for gas phase dissociation, as reached recently by den Harder et al. [63], marginally amplified by the interaction with catalytic walls and membrane to about 55%. At 300 W it corresponds to the production of 35g of O_2 per hour, at an energy cost of 10 eV/molecule. A decrease in performance of about 50%, to account for unexpected difficulties and the uncertainties of development of a new technology, brings these numbers to approximately 20 g of O_2 per hour, at an energy cost of 18 eV per molecule and 31% energy efficiency. These rather prudent values outperform the most optimistic predictions of MOXIE by 100% and bring further evidence in favor of the plausibility and significance of plasma ISRU on Mars as a complementary technology to SOEC.

Bibliography

[1] NASA, "Chronology of Mars Exploration," 2020. [Online]. Available: https://nssdc.gsfc.nasa.gov/planetary/chronology_mars.html

[2] R. A. Outlaw, "O_2 and CO_2 glow-discharge-assisted oxygen transport through Ag," *J. Appl. Phys.*, vol. 68, pp. 1002–1004, 1990.

[3] R. L. Ash, D. Wu, and R. A. Outlaw, "A study of glow-discharge and permeation techniques for extraterrestrial oxygen beneficiation," *Adv. Space Res.*, vol. 14, pp. (6)259–(6)263, 1994.

[4] D. Wu, R. A. Outlaw, and R. L. Ash, "Extraction of oxygen from CO_2 using glow-discharge and permeation techniques," *J. Vac. Sci. Technol. A*, vol. 14, pp. 408–414, 1996.

[5] D. Premathilake, R. A. Outlaw, R. A. Quinlan, and C. E. Byvik, "Oxygen generation by carbon dioxide glow discharge and separation by permeation through ultrathin silver membranes," *Earth and Space Science*, 2019.

[6] J. Gruwenwald, "A proposal for a plasma technology based hybrid life support system for future Mars habitats," *J. Space Technol.*, vol. 4, pp. 1–6, 2014.

[7] H. L. K. Manning, I. L. ten Kate, S. J. Battel, and P. R. Mahaff, "Electric discharge in the martian atmosphere, Paschen curves and implications for future missions," *Adv. Space Res.*, vol. 46, pp. 13 340–1340, 2010.

[8] G. Garcia-Cosio, H. Martinez, M. Calixto-Rodriguez, and A. Gomez, "DC discharge experiment in an $Ar/N_2/CO_2$ ternary mixture: A laboratory simulation of the martian ionosphere's plasma environment," *JQSRT*, vol. 112, pp. 2787–2793, 2011.

[9] J. Annaloro and A. Bultel, "Vibrational and electronic collisional-radiative model in CO_2-N_2-Ar mixtures for mars entry problems," *Phys. Plasmas*, vol. 26, p. 103505, 2019.

[10] A. Laricchiuta, D. Bruno, M. Capitelli, C. Catalfamo, R. Celiberto, G. Colonna, P. Diomede, D. Giordano, C. Gorse, S. Longo, D. Pagano, and F. Pirani, "High temperature Mars atmosphere. Part I: transport cross sections," *Eur. Phys. J. D*, vol. 54, pp. 607–612, 2009.

[11] C. Catalfamo, D. Bruno, G. Colonna, A. Laricchiuta, and M. Capitelli, "High temperature Mars atmosphere. Part II: transport properties," *Eur. Phys. J. D*, vol. 54, pp. 613–621, 2009.

[12] V. Guerra, T. Silva, P. Ogloblina, M. Grofulović, L. Terraz, M. Lino da Silva, C. D. Pintassilgo, L. L. Alves, and O. Guaitella, "The case for in situ resource utilisation for oxygen production on Mars by non- equilibrium plasmas," *Plasma Sources Sci. Technol.*, vol. 26, p. 11LT01, 2017.

[13] V. Guerra, T. Silva, and O. Guaitella, "Living on Mars: how to produce oxygen and fuel to get home," *EPN*, vol. 49/2, pp. 15–18, 2018.

[14] B. L. M. Klarenaar, R. Engeln, M. A. Damen, M. C. M. van de Sanden, A. S. Morillo-Candas, P. Auvray, and O. Guaitella, "Measuring vibrational excitation of CO_2 in a pulsed glow discharge," in *Proceedings of the ISPC23 (International Symposium on Plasma Chemistry)*, Montréal, Canada, 2017.

[15] B. L. M. Klarenaar, R. Engeln, D. C. M. van den Bekerom, M. C. M. van de Sanden, A. S. Morillo-Candas, and O. Guaitella, "Time evolution of vibrational temperatures in a CO_2 glow discharge measured with infrared absorption spectroscopy," *Plasma Sources Sci. Technol.*, vol. 26, p. 115008, 2017.

[16] A. S. Morillo-Candas, C. Drag, J. P. Booth, T. C. Dias, V. Guerra, and O. Guaitella, "Oxygen atom kinetics in CO_2 plasmas ignited in a DC glow discharge," *Plasma Sources Sci. Technol.*, vol. 28, p. 075010, 2019.

[17] P. Ogloblina, V. Guerra, A. S. Morillo-Candas, and O. Guaitella, "Plasma reforming for oxygen production on mars," in *8^{th} European Conference for Aeronautics and aero-Space Sciences (EUCASS)*, 2019.

[18] P. Ogloblina, A. Tejero-del-Caz, V. Guerra, and L. L. Alves, "Electron impact cross sections for carbon monoxide and their importance in the electron kinetics of CO_2–CO mixtures," *Plasma Sources Sci. Technol.*, vol. 29, p. 015002, 2020.

[19] A. Tejero-del-Caz, V. Guerra, D. Gonçalves, M. Lino da Silva, L. Marques, N. Pinhão, C. D. Pintassilgo, and L. L. Alves, "The LisbOn KInetics Boltzmann solver," *Plasma Sources Sci. Technol.*, vol. 28, p. 043001, 2019.

[20] V. Guerra and J. Loureiro, "Kinetic model of a low pressure microwave discharge in O_2-N_2 including the effects of O^- ions on the characteristics for plasma maintenance," *Plasma Sources Sci. Technol.*, vol. 6, pp. 373–385, 1999.

[21] A. Tejero-del-Caz, L. L. Alves, V. Guerra, D. Gonçalves, M. Lino da Silva, N. Pinhão, L. Marques, and C. D. Pintassilgo, "The LisbOn KInetics tool suit," in *71st Annual Gaseous Electronics Conference*, Portland, OR, 2018, p. GT1.071.

[22] (2019) The LisbOn KInetics - LoKI. [Online]. Available: https://nprime.tecnico.ulisboa.pt/loki/tools.html;https://github.com/IST-Lisbon/LoKI

[23] T. Silva, M. Grofulović, B. L. M. Klarenaar, O. Guaitella, R. Engeln, C. D. Pintassilgo, and V. Guerra, "Kinetic study of CO_2 plasmas under non-equilibrium conditions. I. Relaxation of vibrational energy," *Plasma Sources Sci. Technol.*, vol. 27, p. 015019, 2018.

[24] M. Grofulović, T. Silva, B. L. M. Klarenaar, A. S. Morillo-Candas, O. Guaitella, R. Engeln, C. D. Pintassilgo, and V. Guerra, "Kinetic study of CO_2 plasmas under non-equilibrium conditions. II. Input of vibrational energy," *Plasma Sources Sci. Technol.*, vol. 27, p. 015009, 2018.

[25] T. Silva, M. Grofulović, L. Terraz, C. D. Pintassilgo, and V. Guerra, "Modelling the input and relaxation of vibrational energy in CO_2 plasmas," *J. Phys. D: Appl. Phys.*, vol. 51, p. 464001, 2018.

[26] ——, "Dynamics of gas heating in the afterglow of pulsed CO_2 and CO_2-N_2 glow discharges at low pressure," *Plasma Chem. Plasma Process.*, 2020.

[27] A. F. Silva, A. S. Morillo-Candas, A. Tejero-del-Caz, L. L. Alves, O. Guaitella, and V. Guerra, "A reaction mechanism for vibrationally cold CO_2 plasmas," *Plasma Sources Sci. Technol.*, p. (In preparation), 2020.

[28] A. S. Morillo-Candas, T. Silva, B. L. M. Klarenaar, M. Grofulović, V. Guerra, and O. Guaitella, "Electron impact dissociation of CO_2," *Plasma Sources Sci. Technol.*, vol. 29, p. 01LT01, 2020.

[29] L. Terraz, T. Silva, A. Morillo-Candas, O. Guaitella, A. Tejero-del-Caz, L. L. Alves, and V. Guerra, "Influence of N_2 on the CO_2 vibrational distribution function and dissociation yield in non-equilibrium plasmas," *J. Phys. D: Appl. Phys.*, vol. 53, p. 094002, 2020.

[30] B. L. M. Klarenaar, A. S. Morillo-Candas, M. Grofulović, M. C. M. van de Sanden, R. Engeln, and O. Guaitella, "Excitation and relaxation of the asymmetric stretch mode of CO_2 in a pulsed glowdischarge," *Plasma Sources Sci. Technol.*, vol. 28, p. 035011, 2019.

[31] L. L. Alves, P. Coche, M. A. Ridenti, and V. Guerra, "Electron scattering cross sections for the modelling of oxygen-containing plasmas," *Eur. Phys. J. D*, vol. 70, p. 124, 2016.

[32] (2010) Plasma data exchange project. [Online]. Available: www.lxcat.net

[33] J. . Lowke, A. V. Phelps, and B. W. Irwin, "Predicted electron transport coefficients and operating characteristics of CO_2-N_2-He laser mixtures," *J. Appl. Phys.*, vol. 44, p. 4664, 1973.

[34] R. Celiberto, V. Laporta, A. Laricchiuta, J. Tennyson, and J. M. Wadehra, "Molecular physics of elementary processes relevant to hypersonics: Electron-molecule collisions," *Open Plasma Phys. J.*, vol. 7 (suppl 1:M2), pp. 33–47, 2014.

[35] R. Celiberto, I. Armenise, M. Cacciatore, M. Capitelli, F. Esposito, P. Gamallo, R. K. Janev, A. Laganà, V. Laporta, A. Laricchiuta, A. Lombardi, M. Rutigliano, R. Sayós, J. Tennyson, and J. M. Wadehra, "Atomic and molecular data for spacecraft re-entry plasmas," *Plasma Sources Sci. Technol.*, vol. 25, p. 033004, 2016.

[36] Y. Itikawa, "Cross sections for electron collisions with carbon monoxide," *J. Phys. Chem. Ref. Data*, vol. 44, p. 013105, 2015.

[37] V. Laporta, C. M. Cassidy, J. Tennyson, and R. Celiberto, "Electron-impact resonant vibration excitation cross sections and rate coefficients for carbon monoxi," *Plasma Sources Sci. Technol.*, vol. 21, p. 045005, 2012.

[38] T. Sawada, D. L. Sellin, and A. E. S. Green, "Electron impact excitation cross sections and energy degradation in CO," *J. Geophys. Res.*, vol. 77, no. 25, pp. 4819–28, 1972.

[39] D. Rapp and D. D. Briglia, "Total cross sections for ionization and attachment in gases by electron impact. II. Negative-ion formation," *J. Chem. Phys.*, vol. 43, no. 5, pp. 1480–1489, 1965. [Online]. Available: http://aip.scitation.org/doi/10.1063/1.1696957

[40] D. Rapp and P. Englander-Golden, "Total cross sections for ionization and attachment in gases by electron impact. I. Positive ionization," *J. Chem. Phys.*, vol. 43, pp. 1464–1479, 1965.

[41] P. C. Cosby, "Electron-impact dissociation of carbon monoxide," *J. Chem. Phys.*, vol. 98, no. 10, pp. 7804–7818, 1993. [Online]. Available: https://doi.org/10.1063/1.464588

[42] A. V. Phelps, "Tabulations of collision cross sections and calculated transport and reaction coefficients for electron collisions with O_2," JILA Information Center Report, Tech. Rep. 28, 1985, university of Colorado, Boulder, Colorado, USA.

[43] S. A. Lawton and A. V. Phelps, "Excitation of the $b^1\Sigma_g^+$ state of O_2 by low energy electrons," *J. Chem. Phys.*, vol. 69, p. 1055, 1978.

[44] R. R. Laher and F. R. Gilmore, "Updated excitation and ionization cross sections for electron impact on atomic oxygen," *J. Phys. Chem. Ref. Data*, vol. 19, p. 277, 1990.

[45] V. Guerra and J. Loureiro, "Electron and heavy particle kinetics in a low pressure nitrogen glow discharge," *Plasma Sources Sci. Technol.*, vol. 6, pp. 361–372, 1997.

[46] A. Annušová, D. Marinov, J. P. Booth, N. Sirse, M. Lino da Silva, B. Lopez, and V. Guerra, "Kinetics of highly vibrationally excited O_2(X) molecules in inductively-coupled oxygen plasmas," *Plasma Sources Sci. Technol.*, vol. 27, p. 045006, 2018.

[47] M. López-Puertas, R. Rodrigo, J. J. López-Moreno, and F. W. Taylor, "A non-LTE radiative transfer model for infrared bands in the middle atmosphere. II. CO_2 (2.7 and 4.3 μm) and water vapour (6.3 μm) bands and $N_2(1)$ and $O_2(1)$ vibrational levels," *J. Atmospheric Terr. Phys.*, vol. 48, pp. 749–746, 1986.

[48] A. Cenian, A. Chernukho, V. Borodin, and G. Śliwiński, "Modeling of plasma-chemical reactions in gas mixture of CO_2 lasers I. Gas decomposition in pure CO_2 glow discharge," *Contrib. Plasma Phys.*, vol. 34, pp. 25–37, 1994.

[49] K. Shofield, "Critically evaluated rate constants for gaseous reactions of several electronically excited species," *J. Phys. Chem. Ref. Data*, vol. 8, pp. 723–798, 1979.

[50] M. Grofulović, L. L. Alves, and V. Guerra, "Electron-neutral scattering cross sections for CO_2: a complete and consistent set and an assessment of dissociation," *J. Phys. D: Appl. Phys.*, vol. 49, p. 395207, 2016.

[51] V. Guerra, E. Tatarova, F. M. Dias, and C. M. Ferreira, "On the self-consistent modeling of a traveling wave sustained nitrogen discharge," *J. Appl. Phys.*, vol. 91, pp. 2648–2661, 2002.

[52] L. D. Pietanza, G. Colonna, and M. Capitelli, "Self-consistent electron energy distribution functions, vibrational distributions, electronic excited state kinetics in reacting microwave CO_2 plasma: An advanced model," *Phys. Plasmas*, vol. 27, p. 023513, 2020.

[53] A. S. Morillo-Candas, "Investigation of fundamental mechanisms of CO_2 plasmas," PhD thesis, Ecole Polytechnique - Université Paris-Saclay, 2019.

[54] A. S. Morillo-Candas, V. Guerra, and O. Guaitella, "Time evolution of the dissociation fraction in RF CO_2 plasmas: impact and nature of back reaction mechanisms," *J. Phys. Chem. C*, p. (submitted), 2020.

[55] A. Fridman, *Plasma Chemistry.* Cambridge University Press, 2008.

[56] R. T. Pack, "Analytic estimation of almost resonant molecular energy transfer due to multipolar potentials. VV processes involving CO_2," *J. Chem. Phys.*, vol. 72, pp. 6140–6152, 1980.

[57] L. S. Polak and D. I. Slovetsky, "Electron impact induced electronic excitation and molecular dissociation," *Int. J. Radiat. Phys. Chem.*, vol. 8, pp. 257–282, 1976.

[58] A. Janeco, N. R. Pinhão, and V. Guerra, "Electron kinetics in $He/CH_4/CO_2$ mixtures used for methane conversion," *J. Phys. Chem. C*, vol. 119, pp. 109–120, 2015.

[59] M. Grofulović, B. L. M. Klarenaar, O. Guaitella, V. Guerra, and R. Engeln, "A rotational Raman study under non-thermal conditions in pulsed CO_2-N_2 and CO_2-O_2 glow discharges," *Plasma Sources Sci. Technol.*, vol. 28, p. 045014, 2019.

[60] A. P. H. Goede, "CO_2 neutral fuels," *EPJ Web Conf.*, vol. 189, p. 00010, 2018.

[61] A. Pandiyan, D. Neagu, V. Kyriakou, R. Sharma, V. Middelkoop, S. Weber, A. Goede, S. Welzel, and M. Tsampas, "Electrochemical membrane reactor for oxygen separation after CO_2 plasmolysis," in *14th International Conference on Catalysis in Membrane Reactors (ICCMR-14)*, 2019.

[62] G. J. van Rooij, D. C. M. van den Bekerom, N. den Harder, T. Minea, G. Berden, W. A. Bongers, R. Engeln, M. F. Graswinckel, E. Zoethout, and M. C. M. van de Sanden, "Taming microwave plasma to beat thermodynamics in CO_2 dissociation," *Faraday discussions*, vol. 183, pp. 233–248, 2015. [Online]. Available: http://pubs.rsc.org/en/Content/ArticleHTML/2015/FD/C5FD00045A

[63] N. den Harder, D. C. M. van den Bekerom, R. S. Al, M. F. Graswinckel, J. M. Palomares, F. J. J. Peeters, S. Ponduri, T. Minea, W. A. Bongers, M. C. M. van de Sanden, and G. J. van Rooij, "Homogeneous CO_2 conversion by microwave plasma: Wave propagation and diagnostics," *Plasma Process. Polym.*, vol. 14, p. e1600120, 2017.

[64] A. Boagerts and E. C. Neyts, "Plasma technology: An emerging technologyfor energy storage," *ACS Energy Lett.*, vol. 3, pp. 1013–1027, 2018.

[65] M. H. Hecht, D. R. Rapp, and J. A. Hoffman, "The Mars Oxygen ISRU experiment (MOXIE)," in *International Workshop on Instrumentation for Planetary Missions*, Greenbelt, MD, 2014, p. 1134.

[66] M. H. Hecht and J. A. Hoffman, "The mars oxygen ISRU experiment (MOXIE) on the mars 2020 rover," in *3rd International Workshop on Instrumentation for Planetary Missions*, Pasadena, CA, 2016, p. 4130.

Chapter 5

Influence of carbon monoxide on CO_2 plasma

Herein a joint experimental and modelling work is carried out to study the influence of the mixture composition in CO_2/CO DC glow discharges operating at pressures around the Torr and currents of a few 10s of mA. The mixing ratio is varied between 0 and 67% of CO in the initial mixture, with a total gas flow of 7.4 sccm. *In situ* Fourier transform infrared spectroscopy is used to establish new benchmark measurements of the gas temperature and of the CO_2 and CO concentrations and vibrational temperatures. A self-consistent model, coupling the electron, vibrational, chemical and ion kinetics, and previously validated in pure CO_2 plasmas, is used to simulate and interpret the experimental data. The calculations are in very good agreement with the measured data. The correctness of the model predictions, not only in pure CO_2 but also in CO_2/CO mixtures, in a wide range of discharge parameters and mixture compositions, further validates the proposed kinetic scheme. The simulations reveal the major role of atomic oxygen, particularly through CO_2-O vibration-translation (VT) energy exchanges, in controlling the vibrational kinetics of CO_2. The importance of wall deactivation and recombination processes and of the kinetics of electronically excited metastable states is also pointed out.

5.1 Introduction

Carbon dioxide dissociation is studied in a wide range of applications, from syngas production [1, 2] to oxygen extraction on Mars [3–6]. In recent years the emission of carbon dioxide has proven to be one of the main causes of global warming, which increased interest in CO_2 conversion. CO_2 can be artificially dissociated in 3 different main ways, according to thermal, catalytic, and plasma-based processes [7–9]. Major research efforts in carbon dioxide plasma chemistry have been reviewed by Fridman [7], who discusses the possibility of using non-thermal plasmas for CO_2 utilisation and argues that non-equilibrium plasmas are one of the best ways to reach high CO_2 conversion with high energy efficiency. Different types of discharges were used to demonstrate this claim, although CO_2 conversion and energy efficiency depend on the discharge type and operating conditions [9, 10].

The products of dissociation of CO_2 are interesting for a variety of reasons. As discussed in the introduction to this thesis, carbon monoxide can be used as one of the ingredients of syngas (CO + H_2) production, of interest as fuel for an hopper-vehicle on Mars [12] and as a key ingredient in the production of solar fuels. Oxygen is no less important, as it can be extracted and used also as a combustive fuel or as part of the breathing gas [3–6]. As CO_2 dissociates, the products of dissociation, CO, O, and later on O_2, C and their excited states, influence the discharge operation and the pathways for further dissociation, directly through reactions such as

$$CO_2(v) + O \rightarrow CO + O_2 \ , \tag{5.1}$$

or indirectly by shifting the EEDF and absorbing most of the electron energy as in the case of CO_2/CO plasmas [13]. Reaction (5.1) is claimed to be an important driver for efficient CO_2 dissociation [7, 14, 15]. On the other hand, recombination of the oxygen atoms with CO molecules leads to a decrease in the conversion degree,

$$CO + O + M \rightarrow CO_2 + M. \tag{5.2}$$

Besides, very recent works [16, 17] show that in some conditions the main back reaction mechanism involves the excited state CO(a) and O_2 molecules, through reaction

$$CO(a) + O_2 \rightarrow CO_2 + O. \tag{5.3}$$

Finally, VT processes with dissociation products such as O and O_2 may have higher contributions than with other species [18] and will decrease the CO_2 vibrational temperature, contributing negatively to dissociation through the vibrational channels.

Although methods to promote high dissociation degrees and high energy efficiencies in CO_2 plasmas are being actively pursued, many fundamental aspects of the plasma and its components are still understudied. Moreover, to pursue the main theme of the thesis and follow the idea of oxygen extraction for *in situ* utilization on Mars, understanding the importance of the leftover species is of immense value.

The influence of the O atom density in CO_2 DC glow discharges was studied by Morillo-Candas [17, 19]. It was shown that the concentration of oxygen atoms effectively changes the CO_2 vibrational temperatures, while no significant changes in CO_2 conversion are observed. Additionally, the influence of CO on the CO_2 electron kinetics is well described in chapter 3, but the plasma chemistry of the CO_2-CO mixture was not taken into account and still lacks investigation.

The purpose of this chapter is to study the plasma chemistry and CO_2 dissociation in CO_2/CO gas mixtures. To address this question, we have chosen to use as plasma source a DC glow discharge and study its positive column, which is uniform, well-known, reproducible,

and accessible to a variety of diagnostics. Therefore, it forms a perfect system for validating kinetic models, understanding the influence of the mixture composition in the overall discharge behaviour and optimise the actual discharges to be used in future applications.

We report a thorough experimental characterization of the CO_2/CO plasma, by measuring the vibrational temperatures of CO_2 and CO as well as their densities in the discharge, for different pressures $p = 1 - 5$ Torr, currents $I = 10 - 50$ mA and for CO concentrations in the initial mixture composition varying from 0 to 67%. The experimental studies are complemented by a self-consitent model describing the input and transfer of energy in CO_2/CO plasmas. More specifically, the model includes the electron kinetics, based on the results from chapter 3, here coupled with the heavy-particle kinetics accounting for the creation and loss of the most important neutral and charged heavy-particles in the plasma, as presented in chapter 4.

The structure of this chapter is as follows. Section 5.2 describes the experimental setup and the diagnostics used. Section 5.3 details the formulation of the model and describes the input data. A comparison of the results obtained from the model with the experimentally measured values is made and discussed in section 5.4. Finally, the concluding remarks are given in section 5.5.

5.2 Experimental setup

The substance of the experimental setup was presented in the previous chapter and here only essential or different details of the setup are mentioned.

In situ FTIR spectroscopy is used in order to detect and accurately determine the vibrational temperatures in the plasma, the gas temperature and the concentration of CO and CO_2. The plasma reactor under study is a cylindrically shaped Pyrex tube, with a 2 cm inner diameter and a length of 23 cm. The electrodes are positioned 17 cm apart, opposite to the gas in- and outlet. The reactor is connected in series with a 40 kΩ resistor to a DC power supply. The incoming gas consists of a mixture of CO_2 and CO, where the total gas flow is controlled at 7.4 sccm using a mass flow controller (Bronkhorst F-201CV). The pressure was varied between 1 and 5 torr and controlled using a scroll pump (Edwards XDS-5), and a pressure gauge (Pfeiffer CMR263) with feedback to an automated pressure regulating valve (Pfeiffer EVR116)and controller (Pfeiffer RVC300). The discharge current was varied between 10 and 50 mA. The experiments were conducted in two mixture compositions: 10% and 50% of CO in the initial flow. Additionally, a CO-concentration variation study was also performed at fixed pressure 2 torr and current 40 mA.

The reactor is positioned in the sample compartment of an FTIR spectrometer (Bruker V70). The absorption spectrum is corrected and the emission spectrum is subtracted, as described in [20]. The detected IR spectrum contains several lines of CO and CO_2 vibrational transitions and was fitted according to the procedure described in [19, 20]. It is assumed that the rotational and vibrational temperatures are uniform along the length of the reactor and reach a steady state on relatively short distances from the entrance of the reactor. The temperature of the gas on the entrance of the reactor is assumed to be 300 K. The reduced electric field in the reactor is measured with two metal pins radially pointing inside the positive column of the reactor. All measurements were taken at the axial centre of the positive column of the glow discharge.

5.3 Model

The simulations in chapter 4 reproduce very well the experiments for pure CO_2, hence the self-consistent model including electron kinetics, vibrational kinetics and heavy-species chemistry is used here to describe the CO_2/CO DC plasmas under study. The model formulation follows the LoKI (LisbOn KInetics) approach [21], by coupling the electron Boltzmann equation with a system of rate balance equations describing the creation and loss of 72 individual vibration levels of CO_2 electronic ground state, electronically excited and ground state of the CO and O_2 molecules, ground state and electronically excited oxygen atoms O, ozone, several positive ions and the negative ion O^-.

The present simulations are performed for DC glow discharges as described before ensuring that the time-dependent rate balance equations for the heavy-particles evolve to a steady state. The model predictions are compared with the experimental results obtained for the corresponding current, pressure and initial gas composition. The initial gas mixture consists of CO_2 at room temperature and CO at the experimentally obtained vibrational temperature, T_{CO}. The latter value is given as input to the Boltzmann solver LoKI-B [21] to account for superelastic collisions with vibrationally excited $CO(X)$ molecules. Recombination of oxygen atoms on the wall is taken from [19] and the corresponding recombination probability is assumed equal to the recombination probability of oxygen in pure CO_2 plasma. The influence of γ_O on the results is addressed in section 5.4.3, where other assumptions are tested and discussed.

More detailed information about the flowchart of the model and the chemistry scheme can be found in [22, 23], in chapter 4 and in the Appendix A.

5.4 Results and discussion

This section compares the experimental measurements with the corresponding self-consistent simulations. The evolution of the reduced electric field, densities of the main species and vibrational temperatures as a function of pressure and current for 10 and 50% of CO in the initial mixture, are presented in section 5.4.1. The effect of the initial CO concentration is discussed in section 5.4.2. The influence of wall deactivation and CO_2-O VT processes are discussed in section 5.4.3.

5.4.1 Influence of the current and pressure on CO_2/CO plasmas

Here, the influence of the pressure and current on the chemistry is investigated in two different mixture compositions. The compositions under study are 90/10% and 50/50% of CO_2/CO according to the experimental conditions.

The axial electric field was measured from the voltage drop along the positive column of the glow discharge, between the two tungsten probes. The gas density in the discharge tube was calculated from the pressure and the measured gas temperature using the ideal gas law. Figure 5.1 presents the experimentally measured and the calculated self-consistent reduced electric field, E/N, as a function of the NR product. The experimental results show that for the lower CO concentration in the initial mixture the reduced field increases with the current. This effect was observed before for pure CO_2 plasmas (see chapter 4). However, when the initial CO concentration is significantly increased to 50%, CO becomes the dominant species in the plasma (see figure 5.2) and the opposite effect is observed, *i.e.* for given pressure the reduced electric field decreases with the current. In both cases, for a fixed current the reduced electric field decreases with the pressure, as an outcome of the increase in the electron-neutral collision

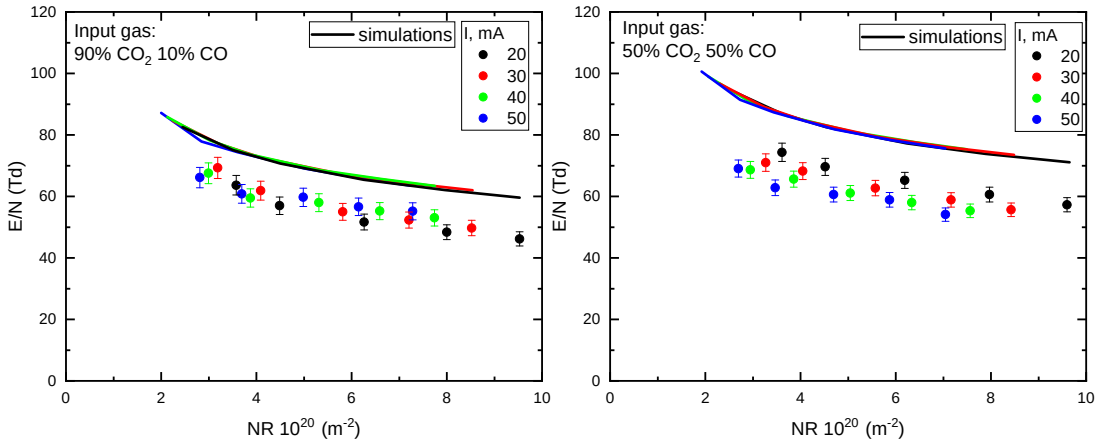

Figure 5.1: Reduced electric field as a function of NR for currents I = 20-50 mA and CO_2/CO initial mixtures 90/10% (left) and 50/50% (right). The symbols correspond to the experimental data, the lines to the self-consistent calculations.

frequency (so that approximately the same ionization rate can be kept with a lower electron impact ionization rate coefficient) and the smaller charge losses by diffusion.

The self-consistent calculations predict very well the trend of E/N with the pressure, but somewhat overestimate the magnitude of the reduced electric field. This discrepancy in the magnitude may come from the approximations considered in the calculation of the reduced mobility and diffusion coefficients of the ionized species. In particular, the ion diffusion and mobility coefficients are considered for a certain single species diffusing in the parent gas, and no correction is made for diffusion in the mixture. Moreover, zero-field values of these quantities are used and no dependence of the mobility and diffusion coefficient with E/N is taken into account. In the CO_2/CO plasmas under investigation, O_2^+ is the main positively charged species (see figure 5.5). The diffusion coefficients of oxygen ions is taken from [24], where it is measured for diffusion in the corresponding ambient gas at zero-field. Corrected reduced mobility and diffusion coefficients according to the actual field in the plasma and the correct gas mixture may reduce the calculated reduced electric field. Another possibility relates with the diffusion scheme considered. Here classical ambipolar diffusion was assumed. However, the effective diffusion scheme proposed in [25] may be considered instead, which is likely to reduce as well the self-consistently calculated values of E/N, albeit only for the lower values of the pressure.

As CO is not only produced in the plasma but is also a part of the incoming gas mixture, it is not appropriate here to compare the dissociation parameter $\alpha = \frac{[CO]}{[CO]+[CO_2]}$ as it was done in the previous chapter. Therefore, the measured and calculated relative densities of CO and CO_2 are directly represented in figure 5.2, together with the calculated densities of oxygen atoms and oxygen molecules. Here, for both mixtures, the calculated and experimental results are in quite good agreement, with maximum relative error of 15%. Overall, we can conclude that our model and the corresponding kinetic scheme, previously validated for pure CO_2 plasmas, describes very well the CO_2/CO chemistry. This further validation, in a wider range of operating parameters brought by the different mixture compositions, reinforces the correctness of the present description.

As the discharge type and conditions are similar to the ones in chapter 4, most of the reactions mentioned in table 4.1 are the main contributors to the destruction and creation of

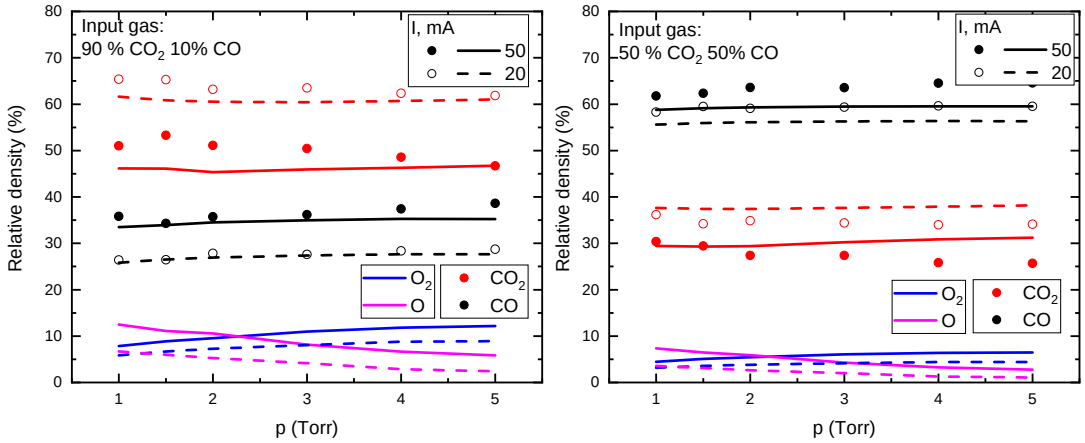

Figure 5.2: Calculated (lines) and measured (points) relative densities of the main species in the discharge, for currents $I = 20$ (– –,∘) and 50 (—,•) mA and CO_2/CO initial mixtures 90/10% (left) and 50/50% (right).

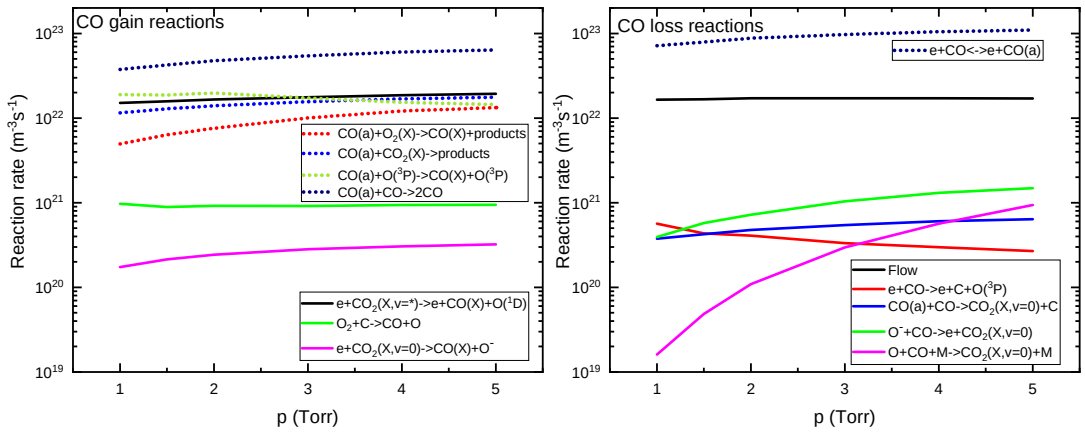

Figure 5.3: Creation and destruction rates of CO(X) molecules as a function of pressure, for a current $I = 40$ mA and a CO_2/CO initial mixture 50/50%. The reactions that contribute to the creation and loss of CO(X) from/to the excited state CO(a) are indicated with dotted lines (···). Additionally, the (- -) line corresponds to the reaction CO(a)+O_2 → CO_2+ O, that does not destroy CO(X), but removes molecules from the CO manifold.

species in CO_2/CO plasmas as well. Figure 5.3 shows the CO(X) creation and destruction rates as a function of the pressure for I= 40 mA and 50/50% CO_2/CO initial mixture composition. Two types of reactions are indicated. The first type depicted with full lines represents reactions in which ground state CO(X) molecules are created or destroyed from/to other species, *i.e.* CO_2, O, O_2. The dotted lines represent reactions of CO(X) transformation to/from the excited state CO(a), *i.e.*, they correspond to a redistribution between the ground and the excited state. The main creation process for the CO(X) molecule is the electron impact dissociation of CO_2(X,v∗), which is calculated as the sum of the individual dissociation rates from each vibrationally excited level. The main destruction mechanism is the convective transport due to the gas flow, overcoming recombination with negative O ions and three-body recombination. As expected, the latter mechanism gains importance as the pressure grows.

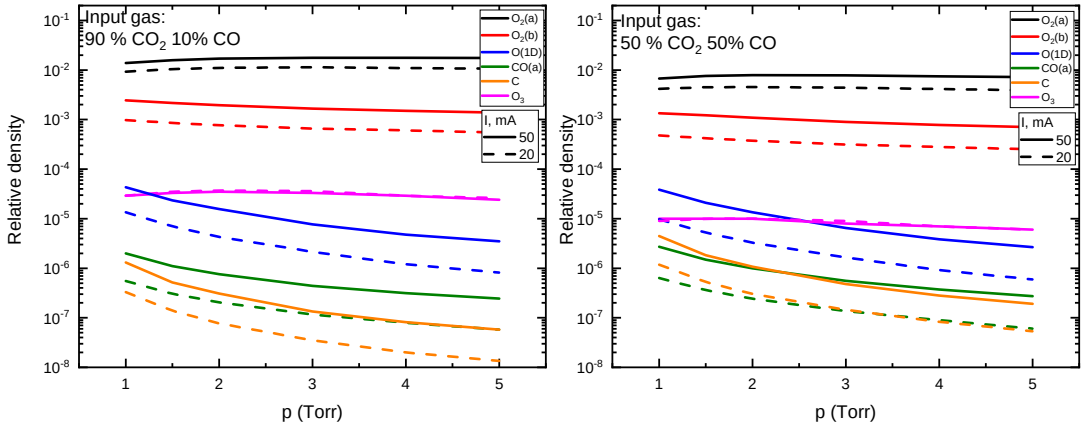

Figure 5.4: Relative density of excited species and carbon atom and ozone as a function of pressure, for currents I = 20 (– –) and 50 (—) mA and CO_2/CO initial mixtures 90/10% (left) and 50/50% (right).

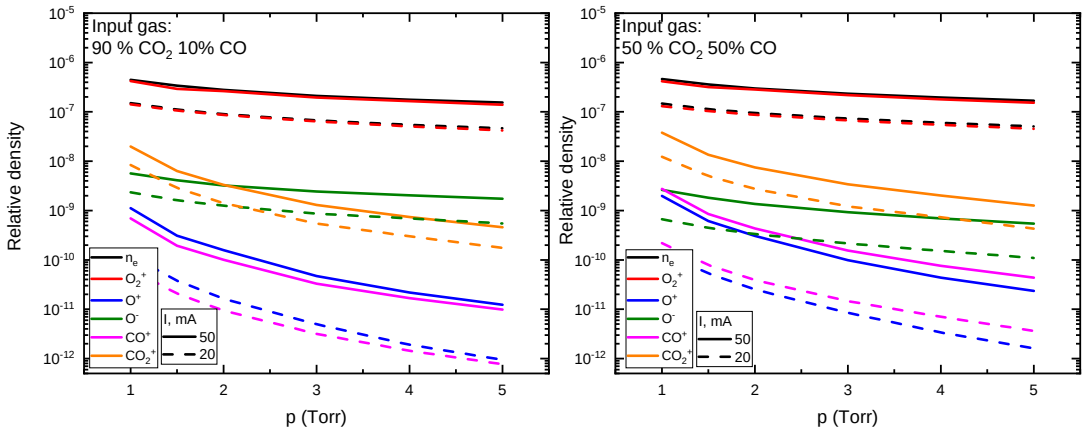

Figure 5.5: Relative densities of various charged particles as a function of pressure, for currents I = 20 (– –) and 50 (—) mA and CO_2/CO mixtures 90/10% (left) and 50/50% (right) in the initial gas input.

Figures 5.4 and 5.5 represent the densities of the excited and ionized species, as well as species that are present in small amounts in the plasma, such as O_3 and C. Both charged and neutral species exhibit a behaviour similar to the one observed in pure CO_2 plasmas in chapter 4. It is worth noting that the kinetics of the metastable states $CO(a)$ and $O(^1D)$ are strongly coupled to those of ground-state $CO(X)$ molecules and $O(^3P)$ atoms (see figure 5.3 and 4.6), despite the relatively low concentration of these metastable excited states. In the present conditions O_2^+ is always the dominant positive ion, as a result of many charge transfer reactions from other positive ions to O_2^+. It is also worth noting that the degree of electronegativity, $[O^-]/n_e$, is always relatively small, below ~ 2%.

It is not unusual to have a complete dissociation in CO_2 thermal plasmas with the formation of C and subsequent coking of the reactor [9]. In CO_2/CO plasmas, where the relative C/O ratio is higher than in pure CO_2, this can be a major concern. However, in the low-temperature conditions under consideration, carbon deposition was not observed experimentally and modelling predictions show a maximum concentration of free carbon atoms of ~ 10^{-6} and ~ 10^{-5} in the 90/10% and 50/50% of CO_2/CO mixtures, respectively.

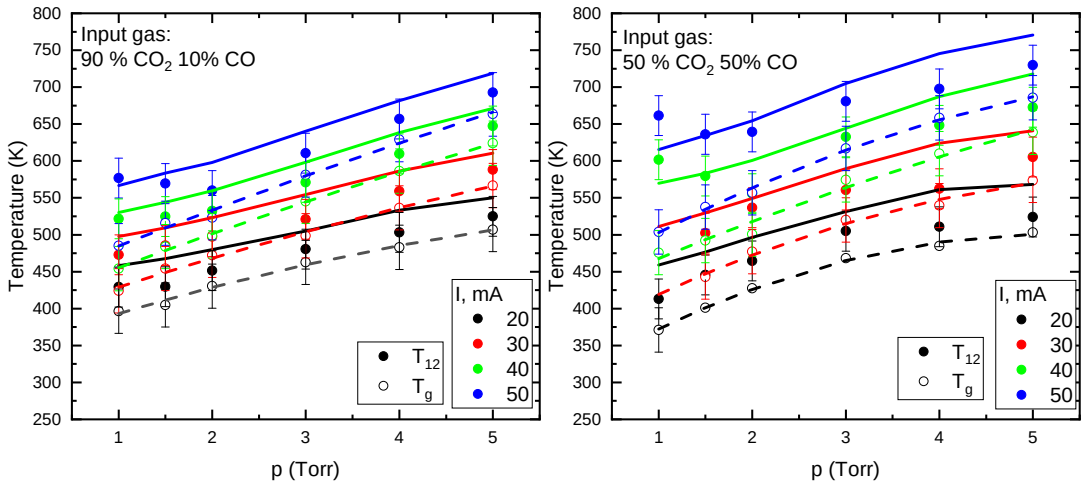

Figure 5.6: Experimental values of the gas temperature, T_g, together with the measured (symbols) and calculated (lines) vibrational temperatures of the bending and symmetric stretching mode, T_{12}, when a discharge is ignited in 90/10% (left) and 50/50 % (right) CO_2/CO mixtures.

Figure 5.6 and 5.7 represent the measurements and the model predictions for the common vibrational temperature of the bending and symmetric vibrational modes of CO_2 [11, 20], T_{12}, asymmetric stretching mode, T_3, and the measured values of the gas temperature, T_g, and of the vibrational temperature of CO, T_{CO}, in the studied 90/10% and 50/50% CO_2-CO mixtures, for currents I = 20 - 50 mA and pressures p = 1 - 5 torr. The error bars are based on the fitting accuracy of the IR spectra and vary between 30 and 67 K [20]. From the analysis of figure 5.6 it can be pointed out that the joint bending and symmetric temperature, T_{12}, is nearly thermalized with T_g for the range of pressures investigated. The vibrational temperatures T_3 and T_{CO} decrease with pressure, approaching the values of T_{12} and T_g at the higher pressures considered. All the temperatures increase as the current increases, reflecting the enhanced input of vibrational energy by electron impact associated with the increase in the electron density. The calculated temperatures describe the experimental results within ~ 8 and 23% error for T_{12}

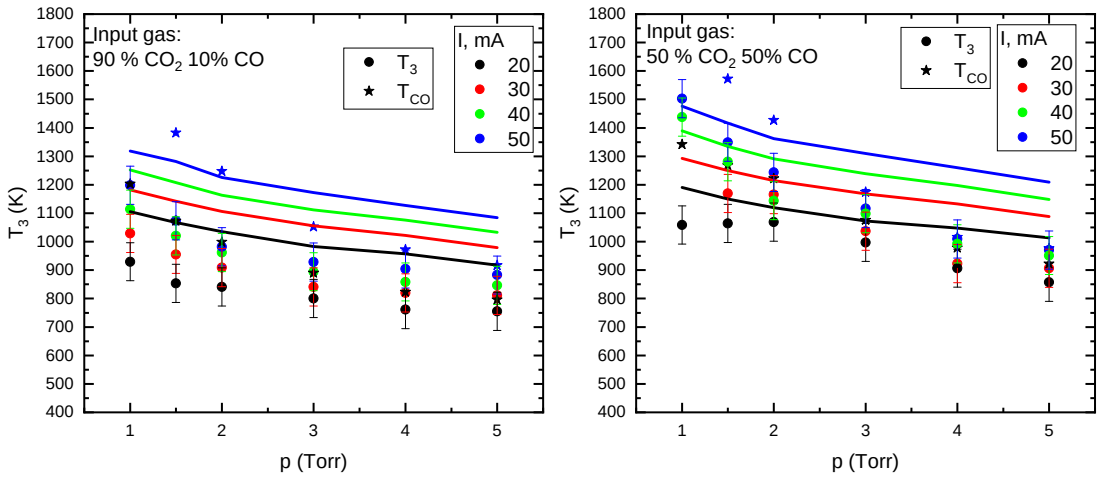

Figure 5.7: Measured (symbols) and calculated (lines) vibrational temperatures of the asymmetric stretching modeof CO_2, T_3, and CO vibrational temperature, T_{CO}, when a discharge is ignited in 90/10% (left) and 50/50% (right) CO_2/CO mixtures.

and T_3, respectively. Further insight into the vibrational kinetics is given in section 5.4.3

5.4.2 Influence of the CO concentration

In this section, we discuss the importance of the CO initial concentration in the mixture where the discharge is ignited. The experiments were conducted for pressure p = 2 Torr and current I = 40 mA, while the initial CO concentration was varied between 10 and 67%.

Different initial CO_2/CO mixing ratios can be represented as the initial CO fraction in the mixture, given by the input factor

$$\alpha_i = \frac{[CO^*]}{[CO^*] + [CO_2^*]} \ ,$$

where [CO*] and [CO_2^*] are the initial concentrations. The figures in this subsection use the *input* factor α_i as x-axis.

Figure 5.8 depicts the dependency of the "conversion factor" in the plasma, $\alpha = \frac{[CO]}{[CO]+[CO_2]}$, as a function of the input CO fraction in the mixture, α_i, for the pressure p = 2 Torr and current I = 40 mA, where the symbols are experimental measurements and the solid line are calculated results from the model. The dotted line is a schematic representation of the baseline for α, which indicates the amount of CO injected into the system. From the difference between the dotted line and the open symbols we can conclude that the precision of the gas-flow system (flowmeters and pressure gauges) is quite good, within a maximum error of about 7%, obtained at the higher concentrations of CO. The red symbols present results for the same working conditions, obtained from the set of measurements presented in section 5.4.1, and confirm a good reproducibility of the results.

After switching the plasma on the amount of CO in the system increases due to CO_2 dissociation. For low concentrations of CO_2, α for plasma ON approaches the plasma OFF values, since, on the one hand, fewer CO_2 molecules are available to participate in dissociation and increase the CO concentration and, on the other hand, back reactions with CO forming back

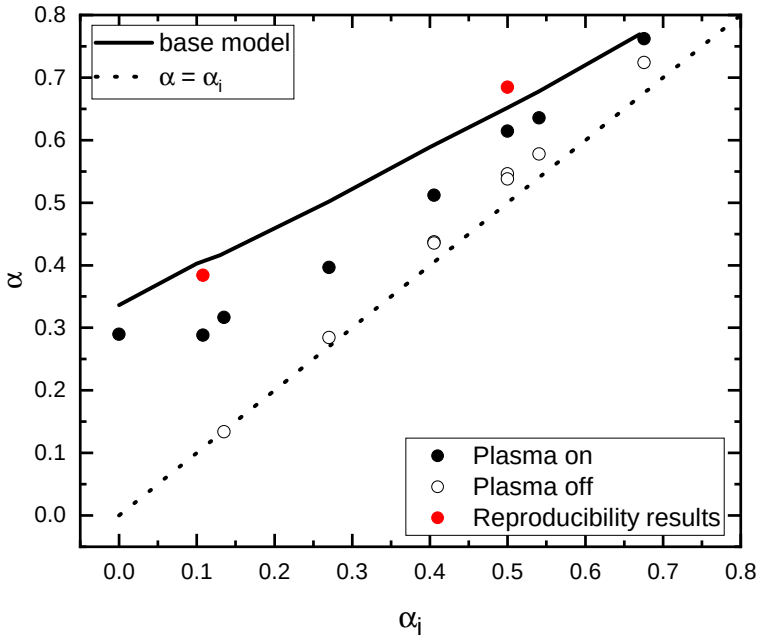

Figure 5.8: Variation of the conversion parameter α at pressure 2 torr and current 40 mA (closed symbols) and 0 mA (open symbols), as a function of the input ratio α_i or CO % (see text) in the gas mixture.

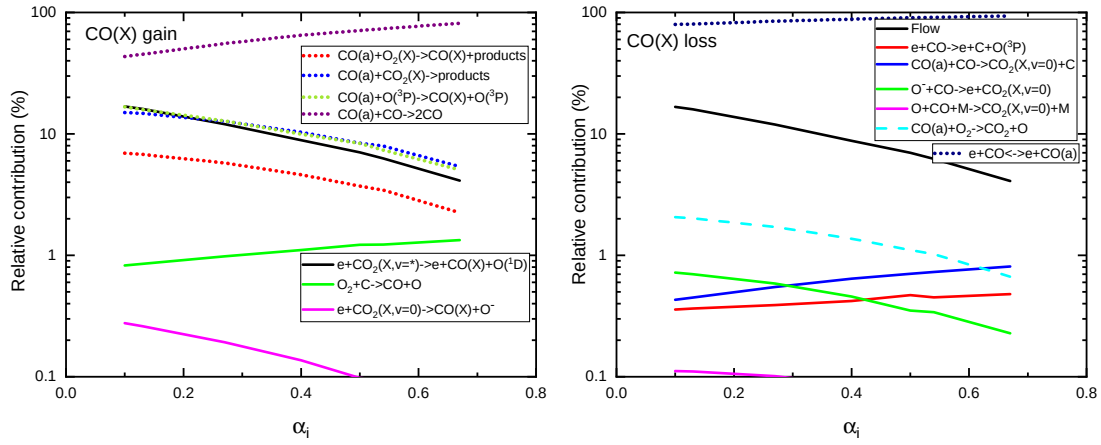

Figure 5.9: Relative contribution of the main mechanisms of creation and destruction of CO(X) as a function of the input ratio α_i, for pressure p = 2 Torr and current = 40 mA. The reactions that contribute to the creation and loss of CO(X) from/to the excited state CO(a) are indicated with dotted lines (···). Additionally, the (- -) line correspond to the reaction CO(a)+O_2 → CO_2+ O, that does not destroy CO(X), but removes molecules from the CO manifold.

CO_2 are enhanced. These conclusions can be verified by inspection of figure 5.9, showing the dominant creation and loss mechanisms of CO(X). It can be seen that as the input α_i (or CO concentration) increases, the processes involving the formation of CO(X) from the other species become less important, with contributions smaller than 20% of produced CO, while reaction

$$CO(a) + CO(X) \rightarrow 2CO(X) \tag{5.4}$$

becomes largely dominant. However, this reaction simply redistributes the population of the CO(X) and CO(a) states and does not constitute a true creation mechanism. In turn, the losses of CO molecules in the back reaction

$$CO(a) + CO \rightarrow CO_2 + C \tag{5.5}$$

gain importance as α_i increases. A similar back reaction, but involving O_2 molecules,

$$CO(a) + O_2 \rightarrow CO_2 + O \ , \tag{5.6}$$

has also an important role, as proposed by A.S. Morillo-Candas [16, 17]. Indeed, figure 5.9 confirms that reaction 5.6 overcomes any other recombination process for almost all initial mixture concentrations. Note that the increase in importance of these two back reactions as true CO loss mechanisms is higher than it can be thought at first sight, as can be verified by inspection of the *full curves* in figure 5.9. The prevalence of the excited state chemistry is remarkable, taking into account the small relative density of these states.

5.4.3 Importance of the oxygen atoms and wall reactions on vibrational temperatures of CO_2

Step-by-step "ladder climbing" vibrational excitation is believed to be only the first stage of the efficient dissociation of CO_2 by non-equilibrium plasmas [7]. A subsequent and crucial stage is that the oxygen atom released after a first dissociation process reacts with another CO_2 molecule, producing a second CO molecule (see eq. 5.1) and lowering the net energy required for dissociation [7, 15, 26, 27]. In this section, we explore how oxygen atoms influence the non-equilibrium vibrational kinetics and the corresponding characteristic vibrational temperatures in CO_2/CO plasmas.

Figure 5.10 depicts the relative contribution of the main creation and destruction mechanimsm of O(^3P) atoms, as a function of the initial fraction of CO in the mixture, α_i, for p = 2 Torr and I = 40 mA. Following the same notation as for the CO rates shown in figures 5.3 and 5.9, the dotted lines in figure 5.10 indicate the rates of reactions that redistribute the population between the two electronic levels of atomic oxygen, O(^3P) and O(^1D), but do not directly contribute to the global creation or destruction of the oxygen atoms.

Similarly to the case of CO, the atomic oxygen chemistry is mainly defined by the kinetics of electronically excited states, namely O(^1D) and CO(a). Apart from dissociation of the ground and excited states of O_2 by electron impact, the main source of oxygen atoms are reactions between CO(a) and O_2 or CO_2 molecules,

$$CO(a) + O_2(X) \rightarrow CO(X) + 2O(^3P) \tag{5.7}$$

$$CO(a) + O_2(X) \rightarrow CO_2(00^00) + O(^3P) \tag{5.8}$$

$$CO(a) + CO_2(00^00) \rightarrow 2CO(X) + O(^3P) \tag{5.9}$$

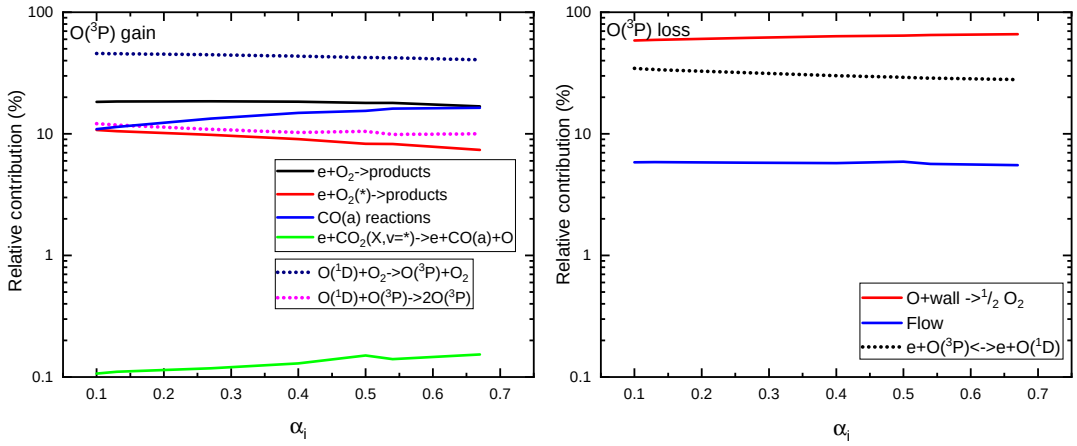

Figure 5.10: Relative contribution of the main mechanisms of creation and destruction of $O(^3P)$ as a function of the initial CO fraction in the mixture α_i, for pressure p = 2 Torr and current = 40 mA. The reactions that contribute to the creation and loss of $O(^3P)$ from/to the excited state $O(^1D)$ are indicated with dotted lines (···).

At the higher initial CO fraction α_i considered, these mechanisms can have the same contribution as electron impact dissociation. The main loss mechanism for oxygen atoms is recombination on the wall, which remains dominant as the mixture changes, accounting for ~ 60 – 70% of the total O-atom destruction.

Figure 5.11 compares the gas temperature, the vibrational temperatures T_{12} and T_3 and the ratio T_3/T_g, for the pressure p = 2 Torr and current I = 40 mA, as a function of the initial CO fraction in the mixture, and for different assumptions made in the model. The symbols represent the experimentally measured values and the solid lines correspond to the calculations made with our base formulation ("base model"). It can be noted that at high initial fractions α_i, the measured vibrational temperature T_3 increases with α_i, while T_g and T_{12} remain nearly constant, albeit a small deviation between T_g and T_{12} can be seen at the higher CO contents in the initial mixture. The behaviour of T_3 and T_{12} is well captured by the model, which suggests that vibrational energy exchanges in CO_2-CO collisions are not very significant in defining the vibrational temperatures of CO_2 at the present conditions, as these processes are not included in the model. The observed trends are thus justified by the predominance of CO_2-O collisions (see below) and by the dilution of CO_2 in the mixture. The ratio of temperatures T_3/T_g is a good measure of the non-equilibrium degree in the plasma. Figure 5.11 reveals that a high non-equilibrium is achieved at higher CO concentrations. This is another indicator that by changing the ratio [O]/[CO], we can control vibrational temperature in our system.

The fact that higher concentrations of CO_2 in the initial mixture lead to a decrease in T_3 and to a lower degree of non-equilibrium is mainly due to the higher concentration of oxygen in the plasma and to the effect of CO_2-O VT reactions in this case. These mechanisms are well described by López-Puertas [18], and several authors [17, 28] noted their importance in the CO_2 vibrational kinetics. The dashed-dotted lines in figure 5.11 correspond to the vibrational temperatures obtained when CO_2-O VT processes are not included in the model. Both, T_3 and T_{12} are significantly overestimated in this case, for the whole range of input α_i. And as presented in figure 5.11, the removal of CO_2-O VT mechanisms from the model brings an increase of non-equilibrium by a factor of about 1.5 to 2, depending on the initial concentration of CO in the mixture. However, in the present conditions, these changes bring no modification to the

dissociation degree - α.

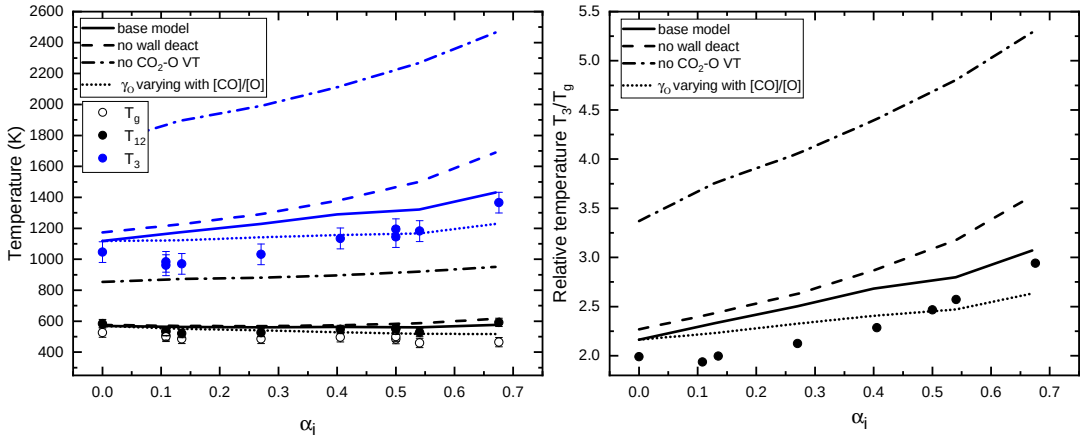

Figure 5.11: Experimental value of the gas temperature, together with measured (symbols) and calculated (lines) vibrational temperatures of the joint symmetric stretching and bending mode T_{12} and the asymmetric stretching mode T_3 (left), and the ratio of T_3/T_g (right) of CO_2, as a function of the input CO fraction α_i, for pressure p = 2 Torr and current I = 40 mA. The different curves correspond to modelling results for the base model (—), chemistry without CO_2-O VT processes (-·-), without vibrational quenching on the wall (- -) and with a varying γ_O (···).

The importance of CO_2-O VT exchanges calls for a verification of the accuracy of the calculation of the atomic oxygen concentration, which depends on the value of the wall recombination probability, γ_O, since wall recombination is the main O-atom destruction mechanism (*cf.* figure 5.10). In our base calculations, γ_O, was assumed to remain constant for the different mixture compositions, equal to the probability measured in pure CO_2 in [19] and dependent on gas temperature, that can be reasonably approximated as:

$$\gamma_O = 1.8 \cdot 10^{-3} exp(-948/T_g). \tag{5.10}$$

However, further work by Morillo-Candas [17] shows a dependence of the wall loss probability on the mixture composition in CO_2/O_2 plasma. The loss probability in CO_2/O_2 plasmas was measured in pulsed plasmas for p = 2 Torr and I = 40 mA during the ON phase. On figure 5.12 we show the results obtained in [17], represented as a function of [O]/[CO]. To evaluate the possible influence of changes in γ_O with the CO content, we fitted the values from [17] as a function of [O]/[CO], as shown in figure 5.12, and used the extrapolated values of the loss probability for CO_2/CO plasmas according to the calculated [O]/[CO] ratios. These changes in γ_O bring no significant modifications to the conversion factor α and lead to an increase in the O-atom concentrations by factors of approximately 1.3 - 2.5, from the lower to the higher concentrations of CO, respectively. The vibrational temperatures obtained with this varying γ_O are shown as dotted lines in figure 5.11. As it can be verified, the vibrational temperatures decrease to some extent, since a lower γ_O corresponds to a higher O-atom concentration and higher deactivation in CO_2-O VT collisions. Therefore, it can be concluded that accurate experimental data for γ_O is needed for further studies on CO_2-CO mixtures.

Another phenomenon that can affect the vibrational kinetics of CO_2 in the present conditions is the quenching of vibrationally excited CO_2(X,v) molecules on the wall [28]. The dashed curves

in figure 5.11 show simulation results when the deactivation of vibrationally excited CO_2 is not included in the model. As expected, they reveal an increase of the vibrational temperature and degree of non-equilibrium, but not as significant as the removal of VT CO_2-O processes. The role of wall deactivation will become progressively more important as the pressure decreases [28].

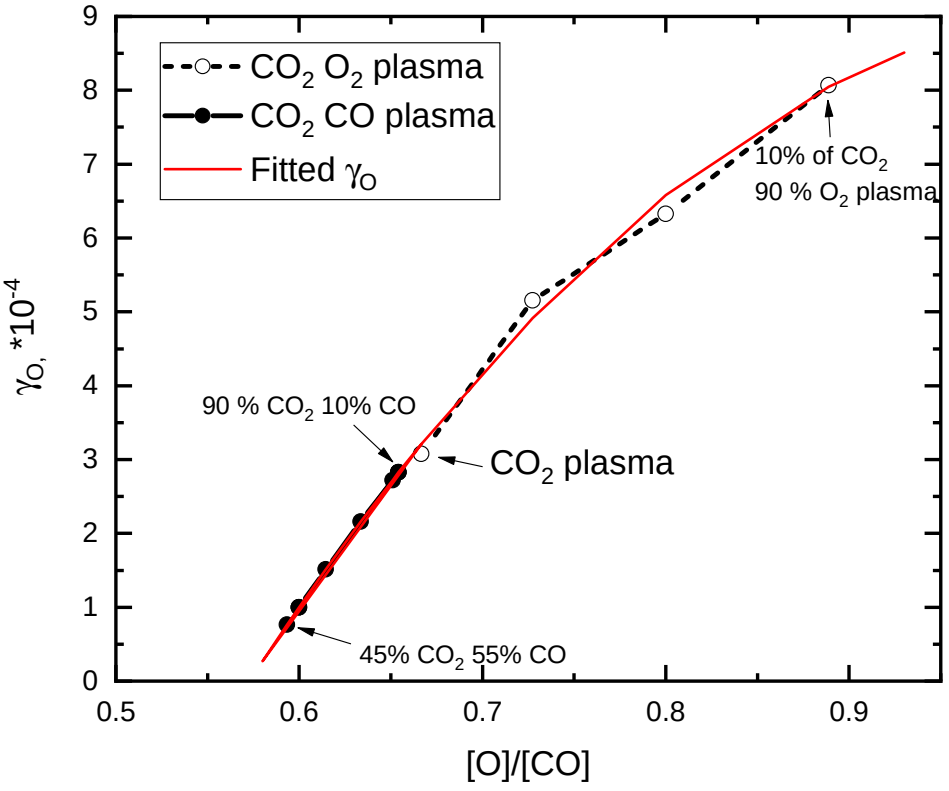

Figure 5.12: Fitted variation of the wall recombination probability for atomic oxygen, γ_O, as a function of the [O]/[CO] ratio in CO_2/O_2 plasmas [17], measured at $p = 2$ Torr and $I = 40$ mA, and extrapolated for CO_2/CO plasmas.

The importance of deactivation of vibrationally excited carbon dioxide in VT CO_2-O collisions raises the question of the effectiveness of dissociation through process (5.1), a reaction that has been invoked as promoting an efficient dissociation of CO_2 by a vibrational mechanism [7, 27]. For instance, the calculations in [27] for a microwave discharge predict that up to 10% of the vibrational energy is used for dissociation according to (5.1). Although a full state-to-state model is not used here, the influence of VT CO_2-O collisions in vibrational dissociation can be estimated as follows. Let us consider the 50%-50% CO_2/CO case at 2 torr and 40 mA and assume a Treanor distribution along the asymmetric stretching mode characterized by the vibrational temperature T_3 obtained in our simulations. Using the rate coefficient reported in [27], the rate of dissociation according to (5.1) is about $2.7{\cdot}10^{11}$ $m^{-3}s^{-1}$. This corresponds only to a very small fraction of the CO creation rate (*cf.* figure 5.3 for typical values). However, if the same estimation is made neglecting CO_2-O VT exchanges, the dissociation rate from (5.1) is evaluated as $3.0{\cdot}10^{20}m^{-3}s^{-1}$, 9 orders of magnitude higher, about 1% of the electron impact

dissociation rate. Therefore, despite the particular case studied here, where vibrational excitation is not very efficient, it seems clear that CO_2-O VT collisions have necessarily to be taken into account to have a correct prediction of the vibrational distribution functions and of the dissociation rate by a purely vibrational mechanism.

5.5 Conclusions

In this chapter the model presented in chapter 4 is one more time successfully validated for low pressure DC glow discharges, now in a CO_2/CO plasmas. The investigation is focused on the influence of CO and oxygen on CO_2 plasma discharge and is also an extension of the work presented in chapter 3, where the electron kinetics in this mixture was studied in detail.

The experimental study is performed in a DC glow discharge operating at pressures p = 1 – 5 Torr and currents I = 20 – 50 mA, at room temperature. The initial CO concentration in the mixture is varied between 10 and 67%. The concentrations and vibrational temperatures of CO_2 and CO are measured using *in situ* FTIR diagnostics, and are compared against the results of the self-consistent model described in detail in the previous chapter, that couples the electron and heavy-particle kinetics in the plasma.

It is confirmed that our model, already validated in pure CO_2 plasmas, describes very well different mixture compositions in a wide range of the operating parameters. This additional validation gives confidence on the accurateness of the present approach. Indeed, the calculations predict very well both the trend and magnitude of the relative densities and vibrational temperatures of CO_2 and CO, while overestimating the reduced electric field, within a maximum error of ~ 30%.

For the conditions under investigation, dissociation in the CO_2/CO plasma is mainly driven by the electron kinetics. In turn, the chemistry is significantly dependent on the kinetics of electronically excited states. Hence, a proper control of the plasma operating conditions, with low CO recombination rates and hence high CO yields, can only be achieved after a deep understanding of the excited states kinetics.

It is shown that by changing the [O]/[CO] ratio in the mixture we can effectively influence the degree of vibrational non-equilibrium in the system. Furthermore, oxygen atoms are shown to have a tremendous influence on the characteristic vibrational temperatures, through CO_2-O VT quenching reactions. However, since it is claimed that O atoms can also significantly contribute to dissociation in plasmas exhibiting high vibrational non-equilibrium, the oxygen kinetics, including the surface kinetics, needs further experimental and theoretical studies. Deactivation of vibrationally excited states on the walls is shown to have a meaningful influence on the vibrational characteristic temperatures, albeit smaller than that of CO_2-O VT processes.

Both wall deactivation of vibrational quanta and the O atom surface kinetics have to be taken into account when choosing the discharge type and building a prototype for oxygen extraction on Mars. As the prototype should include a membrane for oxygen separation which, by extracting oxygen, will act as a wall, the understanding of both surface processes is crucial for an adequate design of the reactor.

Bibliography

[1] A. Janeco, N. R. Pinhão, and V. Guerra, "Electron kinetics in $He/CH_4/CO_2$ mixtures used for methane conversion," *J. Phys. Chem. C*, vol. 119, no. 1, pp. 109–120, 2015.

[2] G. Chen, T. Silva, V. Georgieva, T. Godfroid, N. Britun, R. Snyders, and M. P. Delplancke-Ogletree, "Simultaneous dissociation of CO_2 and H_2O to syngas in a surface-wave microwave discharge," *Int. J. Hydrog. Energy*, vol. 40, no. 9, pp. 3789–3796, 2015.

[3] V. Guerra, T. Silva, P. Ogloblina, M. Grofulović, L. Terraz, M. da Silva, C. Pintassilgo, L. Alves, and O. Guaitella, "The case for in situ resource utilisation for oxygen production on Mars by non- equilibrium plasmas," *Plasma Sources Sci. Technol.*, vol. 26, 2017.

[4] V. Guerra, T. Silva, P. Ogloblina, M. Grofulović, L. Terraz, M. L. D. Silva, C. D. Pintassilgo, L. L. Alves, and O. Guaitella, "Reply to Comment on 'The case for in situ resource utilisation for oxygen production on Mars by non-equilibrium plasmas'," *Plasma Sources Science and Technology*, vol. 27, no. 2, pp. 15–17, 2018.

[5] V. Guerra, T. Silva, and O. Guaitella, "Living on mars: how to produce oxygen and fuel to get home," *Europhys. News*, vol. 49, no. 3, pp. 15–18, 2018.

[6] R. A. Outlaw, "O_2 and CO_2 glow-discharge-assisted oxygen transport through Ag," *Journal of Applied Physics*, vol. 68, no. 3, pp. 1002–1004, 1990.

[7] A. Fridman, *Plasma Chemistry*. 2008.

[8] M. Aresta, *Carbon Dioxide Recovery and Utilization*. 2003.

[9] R. Snoeckx and A. Bogaerts, "Plasma technology-a novel solution for CO2 conversion?," *Chemical Society Reviews*, vol. 46, no. 19, pp. 5805–5863, 2017.

[10] N. Britun, T. Silva, G. Chen, T. Godfroid, J. Van Der Mullen, and R. Snyders, "Plasma-assisted CO_2 conversion: Optimizing performance via microwave power modulation," *Journal of Physics D: Applied Physics*, vol. 51, no. 14, 2018.

[11] M. Grofulović, T. Silva, B. Klarenaar, A. Morillo Candas, O. Guaitella, R. Engeln, C. Pintassilgo, and V. Guerra, "Kinetic study of CO_2 plasmas under non-equilibrium conditions. II.Input of vibrational energy," *Plasma Sources Sci. Technol*, vol. 27, p. 115009, 2018.

[12] G. A. Landis and D. L. Linne, "Mars rocket vehicle using in situ propellants," *J. Spacecraft Rockets*, vol. 38, no. 5, pp. 730–735, 2001.

[13] P. Ogloblina, A. Tejero-Del-Caz, V. Guerra, and L. L. Alves, "Electron impact cross sections for carbon monoxide and their importance in the electron kinetics of CO2-CO mixtures," *Plasma Sources Science and Technology*, vol. 29, no. 1, 2020.

[14] V. D. Rusanov, "The physics of a chemically active plasma with nonequilibrium vibrational excitation of molecules," *Soviet Physics Uspekhi*, vol. 24, no. 6, p. 447, 1981.

[15] A. Goede and R. Van De Sanden, "CO_2-neutral fuels," *Europhysics News*, vol. 47, no. 3, pp. 22–25, 2016.

[16] A.-S. Morillo-Candas, V. Guerra, and O. Guaitella, "Time evolution of the dissociation fraction in RF CO_2 plasmas: impact and nature of back reaction mechanisms," *Submitted to Plasma Sources Sci. Technol.*

[17] A.-S. Morillo-Candas, *Investigation of fundamental mechanisms of CO_2 plasmas.* PhD thesis, 2019.

[18] M. López-Puertas, R. Rodrigo, A. Molina, and F. W. Taylor, "A non-LTE radiative transfer model for infrared bands in the middle atmosphere. I. Theoretical basis and application to CO_2 15 μm bands," *Journal of Atmospheric and Terrestrial Physics*, vol. 48, no. 8, pp. 729–748, 1986.

[19] A. Morillo-Candas, C. Drag, J.-P. Booth, T. Dias, V. Guerra, and O. Guaitella, "Oxygen atom kinetics in CO_2 plasmas ignited in a DC glow discharge," *Plasma Sources Sci. Technol*, vol. 28, no. 7, p. 075010, 2019.

[20] B. Klarenaar, R. Engeln, D. van den Bekerom, M. van De Sanden, A. Morillo Candas, and O. Guaitella, "Time evolution of vibrational temperatures in a CO_2 glow discharge measured with infrared absorption spectroscopy," *Plasma Sources Sci. Technol.*, vol. 26, no. 11, p. 115008, 2017.

[21] A. Tejero-del Caz, V. Guerra, D. Goncalves, M. L. da Silva, L. Marques, N. Pinhão, C. D. Pintassilgo, and L. L. Alves, "The LisbOn KInetics Boltzmann solver," *Plasma Sources Sci. Technol.*, vol. 28, p. 043001, 2019.

[22] V. Guerra and J. Loureiro, "Electron and heavy particle kinetics in a low-pressure nitrogen glow discharge," *Plasma Sources Science and Technology*, vol. 6, no. 3, pp. 361–372, 1997.

[23] V. Guerra and J. Loureiro, "Kinetic model of a low-pressure microwave discharge in O_2-N_2 including the effects of O^- ions on the characteristics for plasma maintenance," *Plasma Sources Science and Technology*, vol. 8, no. 1, pp. 110–124, 1999.

[24] E. A. Mason and E. W. McDaniel, *The Mobility and Diffusion of Ions in Gases.* 1973.

[25] P. Coche, V. Guerra, and L. L. Alves, "Microwave air plasmas in capillaries at low pressure I. Self-consistent modeling," *Journal of Physics D: Applied Physics*, vol. 49, no. 23, p. 235207, 2016.

[26] T. Kozák and A. Bogaerts, "Splitting of CO_2 by vibrational excitation in non-equilibrium plasmas: a reaction kinetics model," *Plasma Sources Sci. Technol*, vol. 23, no. 4, p. 045004, 2014.

[27] T. Kozák and A. Bogaerts, *Evaluation of the energy efficiency of CO2 conversion in microwave discharges using a reaction kinetics model*, vol. 24. 2015.

[28] L. Terraz, T. Silva, A. Morillo-Candas, O. Guaitella, A. Tejero-del Caz, L. L. Alves, and V. Guerra, "Influence of N_2 on the CO_2 vibrational distribution function and dissociation yield in non-equilibrium plasmas," *Journal of Physics D: Applied Physics*, vol. 53, no. 9, 2019.

Chapter 6

Conclusions

The objective of this thesis was to investigate the possibility of using non-equilibrium plasmas for *in situ* oxygen production on Mars. The idea is to take advantage of the atmosphere of Mars, which consists of ~ 96% of carbon dioxide, using it as the raw material for *In Situ* Resource Utilization. Atmospheric CO_2 could be decomposed into carbon monoxide and oxygen, that could be used to make propellants and, in the case of oxygen, to create a breathable environment. The existing technology of solid oxide electrolysis is a promising candidate, but has a list of setbacks comparing to non-equilibrium plasmas for CO_2 dissociation and oxygen production.

The studies carried out are of a fundamental nature and aim at unveiling various details of the complex plasma kinetics in Martian conditions and to assess the feasibility of using plasmas for the local production of oxygen. In order to reach these goals, the positive column of DC glow discharges was investigated. This system was chosen due to its simple geometry, straightforward determination of the electric field, homogeneity of the positive column and reproducibility of the results, that make it accessible to a variety of diagnostics.

Fourier transform infrared spectroscopy (FTIR) was used to determine densities of CO_2 and CO, as well as their vibrational temperatures. The experiments, conducted at LPP (Laboratoire de Physique des Plasmas, École Polytechnique, France), were performed in pure CO_2 plasmas, in mixtures with Ar and N_2 (trace gases found in small amount in Mars' atmosphere), and in CO_2-CO mixtures. The measurements were performed at room temperature and also by decreasing the ambient gas temperature to ~ 220-230 K, in order to reproduce temperature conditions on Mars. The pressure regime was kept around of Mars ambience, in the range 0.5-5 Torr.

The experimental study was complemented with simulations from a 0D detailed self-consistent kinetic model developed in the N-PRiME team within IPFN (Instituto de Plasmas e Fusão Nuclear, Instituto Superior Técnico, Universidade de Lisboa, Portugal). The model describes the electron kinetics, by solving the electron Boltzmann equation using the two-term Boltzmann solver LoKI-B, coupled with the heavy-particle kinetics and accounting for 72 individual CO_2 vibrational levels. The model was further developed in the framework of this thesis, by including the effects of CO in the electron kinetics and by coupling to the system of equations the rate balance equations of the most important neutral and charged heavy-particles besides vibrationally excited CO_2.

Dissociation of CO_2 is a complex topic by itself, further complicated when aiming at oxygen production in Mars' ambient. Some of the main questions are answered in this thesis, for example: what is the importance of CO on the EEDF and CO_2 vibrational temperatures? what is the impact of the gas temperature on the non-equilibrium of the plasma and dissociation? But other challenges, like finding the optimal discharge type, configuration and operating conditions, and how to separate the products of dissociation are left for future investigations.

The main findings can be summarized as follows.

- Preliminary simulations of DC pulsed discharges ignited in Earth's and Mars' temperature conditions, taking into account only the electron and vibrational kinetics, have shown an advantage for Martian atmospheric conditions. In particular, a more efficient up-pumping of vibrational quanta into the asymmetric stretching mode and a higher degree of non-equilibrium in the plasma was obtained with typical conditions on Mars than on Earth.

- The electron kinetics is one of the main building blocks that has to be studied and understood to achieve a correct description of the plasma. A new complete and consistent electron impact cross section set for CO was presented. The current set corrects a serious inconsistency found in most sets available in the literature, related to the high value of the rotational excitation/de-excitation cross sections at low electron energies, surpassing the effective momentum transfer cross-section. The proposed set of cross sections includes all the main collisional processes and provides swarm calculations in very good agreement with the experimental data over the full range of reduced electric fields considered, 10^{-4} – 10^{3} Td.

- The Martian atmosphere was successfully reproduced in laboratory conditions. The results confirm that Martian conditions of temperature and pressure can up-pump the asymmetric stretching vibration mode and achieve a stronger non-equilibrium than on Earth. Dissociation fractions up to 30% were observed. The influence of the trace gases argon and nitrogen in CO_2 dissociation was found to be small.

- It was also shown that the products of dissociation can influence the discharge. By changing the [O]/[CO] ratio in the mixture we can effectively influence the degree of vibrational non-equilibrium in the system. Furthermore, oxygen atoms are shown to have a tremendous influence on the characteristic vibrational temperatures of CO_2, through CO_2-O vibrational-translation (VT) quenching reactions.

- In all the conditions studied dissociation mainly takes place through electron impact collision with ground-state and low-laying vibrational levels of CO_2. In turn, the chemistry is significantly dependent on the kinetics of electronically excited states, such as $O_2(a^1\Delta_g)$, $O_2(b^1\Sigma_g^+)$, $O(^1D)$ and $CO(a^3\Pi)$. Therefore, a full control and optimization of the plasma requires a detailed understanding of the strongly coupled kinetics of these states.

The results obtained in this thesis encourage pursuing the idea of using non-equilibrium plasmas for ISRU and CO_2 dissociation on Mars. Indeed, even though the glow discharge is not the most energetically and conversion efficient, the achieved dissociation degree of ~ 30% is quite high. That is a very promising result, considering that the present setup is designed for fundamental studies and is still far from suited for the development of a prototype.

Despite the exciting results, many challenges remain. Some of the tasks for future research are: to determine what are the optimal discharge type, configuration and operating conditions for oxygen production on Mars; to expand the knowledge about the coupling between the excited states kinetics and its influence on the overall chemistry; to gain a deeper understanding of the role of the gas temperature and temperature gradients; to solve the question of the separation of the products of dissociation. The latter task is probably one of the most urgent tasks to dwell on, since it can be seen as a showstopper and the competing technology already has a solution. However, work is in progress in this direction and the solution may even come with a bonus: the coupling between catalysis and a membrane could enhance dissociation and at the same time transfer oxygen out of the zone of discharge.

Clearly, oxygen production on Mars using non-equilibrium plasmas should involve collaboration between physicists, chemists and engineers for the production of an efficient prototype. This is a thrilling endeavour that, hopefully, this thesis contributes to start paving.

Appendix A

Appendix - Input files

The appendix is written in such a way so that it can be directly used as input files in LoKI code to run a simple case of CO_2 plasma.

A.1 CO_2 reactions

Flow

```
CO2(X) ->CO2(X) + CO2(X,v=00001) | flowCO2 |7.4|
```

Electron-impact

```
e + CO2(X,v=*) -> e + CO(X) + O(1D) | eedf | |
e + CO2(X,v=*) -> e + CO(a) + O(3P) | eedf | |
e + CO2(X,v=*) -> e + e + CO2(+,X) | eedf | |
```

e-ion and e-attachment

```
e + CO2(+,X) -> CO(X) + O(3P) | powerGasElecTemp | 2.7e-14, -0.75, 0 |
e + CO2(X,v=00001) -> CO(X) + O(-,gnd) | eedf | |
```

Neutral-Neutral

```
CO(a) + O2(X) -> CO(X) + 2O(3P)| constantRateCoeff | 5e-11*1e-6 |
CO(a) + O2(X) -> CO(X) + O2(X)| constantRateCoeff | 5e-11*1e-6 |
CO(a) + O2(X) -> CO2(X,v=00001) + O(3P)| constantRateCoeff | 3e-11*1e-6 |
CO(a) + CO(X) -> CO2(X,v=00001) + C(X) |constantRateCoeff | 1.4e-12*1e-6 |
CO(a) + CO(X) -> CO(X) + CO(X)| constantRateCoeff | 1.4e-10*1e-6 |
CO(a) + CO2(X) -> CO(X) + CO2(X)| constantRateCoeff | 1.5e-11*1e-6 |
CO(a) + CO2(X,v=00001) -> 2CO(X) + O(3P) |constantRateCoeff | 1.5e-11*1e-6 |
CO(a) + O(3P) -> CO(X) + O(3P)| constantRateCoeff | 1.9e-10*1e-6 |
O(3P) + CO(X) + CO2(X) -> CO2(X,v=00001) + CO2(X) | arrheniusGasTemp | 2*8.2e-46, -1510 |
O(3P) + CO(X) + CO(X) -> CO2(X,v=00001) + CO(X) | arrheniusGasTemp | 8.2e-46, -1510 |
O(3P) + CO(X) + O2(X) -> CO2(X,v=00001) + O2(X) | arrheniusGasTemp | 8.2e-46, -1510 |
O2(X) + C(X) -> CO(X) + O(3P) | constantRateCoeff | 3e-17 |
```

Ion-Neutral & Ion-Ion

```
CO(+,X) + O2(X) -> O2(+,X) + CO(X) |constantRateCoeff | 5e-16 |
O(+,gnd) + CO2(X,v=00001) -> O2(+,X) + CO(X) | constantRateCoeff | 8.1e-16 |
O(+,gnd) + CO2(X,v=00001) -> CO2(+,X) + O(3P) | constantRateCoeff | 4.5e-10*1e-6 |
CO2(+,X) + O2(X) -> O2(+,X) + CO2(X,v=00001) | constantRateCoeff | 5.3e-17 |
CO2(+,X) + O(3P) -> O2(+,X) + CO(X) | constantRateCoeff | 1.64e-16 |
CO2(+,X) + O(3P) -> O(+,gnd) + CO2(X,v=00001) | constantRateCoeff | 9.62e-17 |
CO(+,X) + CO2(X,v=00001) -> CO2(+,X) + CO(X) | constantRateCoeff| 1e-15 |
CO2(+,X) + wall -> CO2(X,v=00001) | classicalAmbipolarDiff | true |
CO(+,X) + wall -> CO(X) | classicalAmbipolarDiff | true |
```

Negative ions

```
O(-,gnd) + CO(X) -> CO2(X,v=00001) + e | powerGasTemp | 5.8e-15,-0.39 |
```

A.2 O_2 and O reactions

Flow

```
2O2(X)->O2(X) | flowO2 |7.4|
2O(3P)->O(3P) | flowO |7.4|
```

Electron-impact

```
e + O2(X) <-> e + O2(a1Dg) | eedf | |
e + O2(X) <-> e + O2(b1Sg+) | eedf | |
e + O2(a1Dg) <-> e + O2(b1Sg+) | eedf | |
e + O(3P) <-> e + O(1D) | eedf | |
e + O2(X) -> e + 2O(3P) | eedf | | 0.9
e + O2(X) -> e + O(3P) + O(1D) | eedf | | 1.3
e + O2(a1Dg) -> e + 2O(3P) | eedf | |
e + O2(a1Dg) -> e + O(3P) + O(1D) | eedf | |
e + O2(b1Sg+) -> e + 2O(3P) | eedf | |
e + O2(b1Sg+) -> e + O(3P) + O(1D) | eedf | |
e + O3(X) -> e + O(3P) + O2(X) | eedf | | 5.0 e + O2(X) -> 2e + O2(+,X) | eedf | |
e + O2(a1Dg) -> 2e + O2(+,X) | eedf | |
e + O(3P) -> 2e + O(+,gnd) | eedf | |
e + O(-,gnd) -> 2e + O(3P) | eedf | | e + O2(X) -> 2e + O(3P) + O(+,gnd) | eedf | |
e + O2(a1Dg) -> 2e + O(3P) + O(+,gnd) | eedf | | e + O2(X) -> O(-,gnd) + O(3P) | eedf | |
e + O2(a1Dg) -> O(-,gnd) + O(3P) | eedf | |  e + O2(+,X) -> 2O(3P) | powerElectronTemp | 2e-13*300*(11604.51)^-1, -1 | 7
e + O2(+,X) -> O(3P) + O(1D) | powerElectronTemp | 1.95e-13*300^0.7*11604.51^-0.7, -0.7 | 5
```

Heavy species collisions

```
O2(a1Dg) + O(3P) -> O2(X) + O(3P) | constantRateCoeff | 7e-23 | 0.98
O2(b1Sg+) + O(3P) -> O2(X) + O(3P) | constantRateCoeff | 4e-20 | 1.63
O2(b1Sg+) + O(3P) -> O2(a1Dg) + O(3P) | constantRateCoeff | 4e-20 | 0.65
O(3P) + O(1D) -> O(3P) + O(3P) | constantRateCoeff | 8e-18 | 1.96
O(1D) + O2(X) -> O(3P) + O2(a1Dg) | constantRateCoeff | 1e-18 | 0.98
O2(b1Sg+) + O3(X) -> 2O2(X) + O(3P) | constantRateCoeff | 1.50E-17 | 2.67
O(1D) + O3(X) -> 2O2(X) | constantRateCoeff | 1.20E-16 | -2.14
O(1D) + O3(X) -> O2(X) + 2O(3P) | constantRateCoeff | 1.20E-16 | 2.98
O3(exc) + O(3P) -> O3(X) + O(3P) | constantRateCoeff | 2.00E-19 |
O3(exc) + O2(X) -> O3(X) + O2(X) | constantRateCoeff | 3.00E-21 |
2O(3P) + O2(X) -> O3(X) + O(3P) | arrheniusGasTemp | 2.10E-46, 345 | -1.04
O2(a1Dg) + O3(X) -> 2O2(X) + O(3P) | arrheniusGasTemp | 5.20E-17, -2840 | 2.02
O(3P) + O3(X) -> 2O2(X) | arrheniusGasTemp | 0.5*1.8e-17, -2300 | -4.08
O(3P) + O3(X) -> O2(a1Dg) + O2(X) | arrheniusGasTemp | 0.33*1.8e-17, -2300 | -5.06
O(3P) + O3(X) -> O2(b1Sg+) + O2(X) | arrheniusGasTemp | 0.17*1.8e-17, -2300 | -5.71
O(1D) + O2(X) -> O(3P) + O2(b1Sg+) | arrheniusGasTemp | 2.56E-17, 67 | 0.33
O2(a1Dg) + O3(exc) -> 2O2(X) + O(3P) | arrheniusGasTemp | 5*5.2e-17, -1287 |
O(3P) + O3(exc) -> 2O2(X) | arrheniusGasTemp | 8.00E-18, -507 |
O(3P) + O2(X) + O2(X) -> O3(X) + O2(X) | arrheniusGasTemp | 0.33*6.40E-47, 663 | -1.04
O(3P) + O2(X) + O2(X) -> O3(exc) + O2(X) | arrheniusGasTemp | 0.67*6.4E-47, 663 |
O(1D) + O2(X) -> O(3P) + O2(X) | arrheniusGasTemp | 7.00E-18, 67 | 1.96
2O2(a1Dg) -> O2(b1Sg+) + O2(X) | modifiedArrheniusGasTemp | 1.81e-24*300^-3.8, 3.8, 700 | 0.33
2O(3P) + O2(X) -> O2(X) + O2(X) | modifiedArrheniusGasTemp | 0.5*3.81e-42, -1, -170 | -5.12
2O(3P) + O2(X) -> O2(X) + O2(a1Dg) | modifiedArrheniusGasTemp | 0.33*3.81e-42, -1, -170 | -6.1
2O(3P) + O2(X) -> O2(X) + O2(b1Sg+) | modifiedArrheniusGasTemp | 0.17*3.81e-42, -1, -170 | -6.75
O(3P) + O2(X) + O3(X) -> 2O3(X) | expGasTemp | 1.66e-46, 300 | -1.04
3O(3P) -> O2(X) + O(3P) | powerGasTemp | 3.60E-44, -0.63 | -5.12
O2(a1Dg) + O2(X) -> O2(X) + O2(X) | powerGasTemp | 2.20E-24*300^-0.8, 0.8 | 0.98
O(-,gnd) + O2(a1Dg) -> O3(X) + e | constantRateCoeff | 0.75*1.9e-16 |
O(-,gnd) + O(3P) -> O2(X) + e | constantRateCoeff | 1.30E-15 |
O(-,gnd) + O2(X) -> O3(X) + e | constantRateCoeff | 1.00E-18 |
O(-,gnd) + O2(b1Sg+) -> O(3P) + O2(X) + e | constantRateCoeff | 6.90E-16 |
O(+,gnd) + O(-,gnd) -> 2O(3P) | constantRateCoeff | 2.8e-13 |
O(+,gnd) + O3(X) -> O2(+,X) + O2(X) | constantRateCoeff | 1.00e-16 |
O(+,gnd) + O2(X) -> O2(+,X) + O(3P) | powerGasTemp | 2e-17*300^0.5, -0.5 |
O(+,gnd) + O2(a1Dg) -> O2(+,X) + O(3P) | powerGasTemp | 2e-17*300^0.5, -0.5 |
O2(+,X) + O(-,gnd) -> O2(X) + O(3P) | powerGasTemp | 9.6e-14*300^0.5, -0.5 |
```

Ion transport

```
O2(+,X) + wall -> O2(X) | classicalAmbipolarDiff | true |
O(+,gnd) + wall -> O(3P) | classicalAmbipolarDiff | true |
```

Neutral transport

```
O2(a1Dg) + wall -> O2(X) | gasOnGasDiffOxygen | 5e-5 | 0.98*(1-0.5)
O2(b1Sg+) + wall -> O2(X) | gasOnGasDiffOxygen | 2e-2 | 1.63*(1-0.5)
O(3P) + wall -> 0.5O2(X) | gasOnGasDiffOxygen | 3.9870800000000001e-04 |
O(1D) + wall -> O(3P) | gasOnGasDiffOxygen | 1 | 1.96*(1-0.5)
O3(exc) + wall -> O3(X) | gasOnGasDiffOxygen | 0.01 |
```

A.3 CO reactions

A.3.1 Flow

```
CO(X)+ CO(X) -> CO(X) | flowCO |7.4|
```

A.3.2 Electron-impact

```
e + CO(X) -> C(X) + O(-,gnd) | eedf | |
e + CO(X) <-> e + CO(a) | eedf | |
e + CO(X) -> e + C(X) + O(3P) | eedf | |
e + CO(X) -> e + e + CO(+,X) | eedf | |
```

A.4 CO_2 vib wall deactivation reactions

```
CO2(X,v=00011) + wall -> CO2(X,v=00001) | wallReaction | 2.300e-02 |
CO2(X,v=00021) + wall -> CO2(X,v=00001) | wallReaction | 2.300e-02 |
CO2(X,v=00031) + wall -> CO2(X,v=00001) | wallReaction | 2.300e-02 |
CO2(X,v=00041) + wall -> CO2(X,v=00001) | wallReaction | 2.300e-02 |
CO2(X,v=00051) + wall -> CO2(X,v=00001) | wallReaction | 2.300e-02 |
```

A.5 CO_2-O VT reactions

```
CO2(X,v=00011) + O(3P) <-> CO2(X,v=02201) + O(3P) | powerGasTemp | 2e-13*1e-6*300^-0.5, 0.5 |
CO2(X,v=00011) + O(3P) <-> CO2(X,v=03301) + O(3P) | powerGasTemp | 2e-13*1e-6*300^-0.5, 0.5 |
CO2(X,v=00011) + O(3P) <-> CO2(X,v=04401) + O(3P) | powerGasTemp | 2e-13*1e-6*300^-0.5, 0.5 |
CO2(X,v=00021) + O(3P) <-> CO2(X,v=02201) + O(3P) | powerGasTemp | 2*2e-13*1e-6*300^-0.5, 0.5 |
CO2(X,v=00021) + O(3P) <-> CO2(X,v=03301) + O(3P) | powerGasTemp | 2*2e-13*1e-6*300^-0.5, 0.5 |
CO2(X,v=00021) + O(3P) <-> CO2(X,v=04401) + O(3P) | powerGasTemp | 2*2e-13*1e-6*300^-0.5, 0.5 |
CO2(X,v=00031) + O(3P) <-> CO2(X,v=02201) + O(3P) | powerGasTemp | 3*2e-13*1e-6*300^-0.5, 0.5 |
CO2(X,v=00031) + O(3P) <-> CO2(X,v=03301) + O(3P) | powerGasTemp | 3*2e-13*1e-6*300^-0.5, 0.5 |
CO2(X,v=00031) + O(3P) <-> CO2(X,v=04401) + O(3P) | powerGasTemp | 3*2e-13*1e-6*300^-0.5, 0.5 |
CO2(X,v=00041) + O(3P) <-> CO2(X,v=02201) + O(3P) | powerGasTemp | 4*2e-13*1e-6*300^-0.5, 0.5 |
CO2(X,v=00041) + O(3P) <-> CO2(X,v=03301) + O(3P) | powerGasTemp | 4*2e-13*1e-6*300^-0.5, 0.5 |
CO2(X,v=00041) + O(3P) <-> CO2(X,v=04401) + O(3P) | powerGasTemp | 4*2e-13*1e-6*300^-0.5, 0.5 |
CO2(X,v=00051) + O(3P) <-> CO2(X,v=02201) + O(3P) | powerGasTemp | 5*2e-13*1e-6*300^-0.5, 0.5 |
CO2(X,v=00051) + O(3P) <-> CO2(X,v=03301) + O(3P) | powerGasTemp | 5*2e-13*1e-6*300^-0.5, 0.5 |
CO2(X,v=00051) + O(3P) <-> CO2(X,v=04401) + O(3P) | powerGasTemp | 5*2e-13*1e-6*300^-0.5, 0.5 |
CO2(X,v=01101) + O(3P) <-> CO2(X,v=00001) + O(3P) | powerGasTemp | 1.8e-12*1e-6*300^-0.5, 0.5 |
CO2(X,v=02201) + O(3P) <-> CO2(X,v=01101) + O(3P) | powerGasTemp | 2*3e-12*1e-6*300^-0.5, 0.5 |
CO2(X,v=03301) + O(3P) <-> CO2(X,v=02201) + O(3P) | powerGasTemp | 3*3e-12*1e-6*300^-0.5, 0.5 |
CO2(X,v=04401) + O(3P) <-> CO2(X,v=03301) + O(3P) | powerGasTemp | 4*3e-12*1e-6*300^-0.5, 0.5 |
CO2(X,v=05501) + O(3P) <-> CO2(X,v=04401) + O(3P) | powerGasTemp | 5*3e-12*1e-6*300^-0.5, 0.5 |
```

A.6 CO_2-O_2 VT reactions

```
CO2(X,v=00011) + O2(X) <-> CO2(X,v=02201) + O2(X) | CO2vibO2quench | 2.3e-15*1e-6, 1.54e-10*1e-6, -76.75 |
CO2(X,v=00011) + O2(X) <-> CO2(X,v=03301) + O2(X) | CO2vibO2quench | 2.3e-15*1e-6, 1.54e-10*1e-6, -76.75 |
CO2(X,v=00011) + O2(X) <-> CO2(X,v=04401) + O2(X) | CO2vibO2quench | 2.3e-15*1e-6, 1.54e-10*1e-6, -76.75 |
CO2(X,v=00021) + O2(X) <-> CO2(X,v=02201) + O2(X) | CO2vibO2quench | 2*2.3e-15*1e-6, 2*1.54e-10*1e-6, -76.75 |
CO2(X,v=00021) + O2(X) <-> CO2(X,v=03301) + O2(X) | CO2vibO2quench | 2*2.3e-15*1e-6, 2*1.54e-10*1e-6, -76.75 |
CO2(X,v=00021) + O2(X) <-> CO2(X,v=04401) + O2(X) | CO2vibO2quench | 2*2.3e-15*1e-6, 2*1.54e-10*1e-6, -76.75 |
CO2(X,v=00031) + O2(X) <-> CO2(X,v=02201) + O2(X) | CO2vibO2quench | 3*2.3e-15*1e-6, 3*1.54e-10*1e-6, -76.75 |
CO2(X,v=00031) + O2(X) <-> CO2(X,v=03301) + O2(X) | CO2vibO2quench | 3*2.3e-15*1e-6, 3*1.54e-10*1e-6, -76.75 |
CO2(X,v=00031) + O2(X) <-> CO2(X,v=04401) + O2(X) | CO2vibO2quench | 3*2.3e-15*1e-6, 3*1.54e-10*1e-6, -76.75 |
CO2(X,v=00041) + O2(X) <-> CO2(X,v=02201) + O2(X) | CO2vibO2quench | 4*2.3e-15*1e-6, 4*1.54e-10*1e-6, -76.75 |
CO2(X,v=00041) + O2(X) <-> CO2(X,v=03301) + O2(X) | CO2vibO2quench | 4*2.3e-15*1e-6, 4*1.54e-10*1e-6, -76.75 |
CO2(X,v=00041) + O2(X) <-> CO2(X,v=04401) + O2(X) | CO2vibO2quench | 4*2.3e-15*1e-6, 4*1.54e-10*1e-6, -76.75 |
CO2(X,v=00051) + O2(X) <-> CO2(X,v=02201) + O2(X) | CO2vibO2quench | 5*2.3e-15*1e-6, 5*1.54e-10*1e-6, -76.75 |
CO2(X,v=00051) + O2(X) <-> CO2(X,v=03301) + O2(X) | CO2vibO2quench | 5*2.3e-15*1e-6, 5*1.54e-10*1e-6, -76.75 |
CO2(X,v=00051) + O2(X) <-> CO2(X,v=04401) + O2(X) | CO2vibO2quench | 5*2.3e-15*1e-6, 5*1.54e-10*1e-6, -76.75 |
```

A.7 CO_2-CO_2 VT reactions

```
CO2(X,v=00011) + CO2(X) <-> CO2(X,v=01101) + CO2(X) | CO2vib | 1, 53.90000000000037, -407.0000000000065, 824.000000000028 |
CO2(X,v=00011) + CO2(X) <-> CO2(X,v=10002) + CO2(X) | CO2vib | 1, 54.600000000001955, -404.0000000000368, 1096.0000000001728 |
CO2(X,v=00011) + CO2(X) <-> CO2(X,v=11102) + CO2(X) | CO2vib | 1, 43.60000000000014, -252.00000000000264, 685.0000000000123 |
CO2(X,v=00021) + CO2(X) <-> CO2(X,v=01111) + CO2(X) | CO2vib | 1, 54.57940883718311, -406.0093215184438, 828.6783523567856 |
CO2(X,v=00021) + CO2(X) <-> CO2(X,v=10012) + CO2(X) | CO2vib | 1, 55.28721873004317, -403.53358308898373, 1098.1431824908393 |
CO2(X,v=00021) + CO2(X) <-> CO2(X,v=11112) + CO2(X) | CO2vib | 1, 44.29909661389566, -252.6265183163722, 682.8860297200965 |
CO2(X,v=00031) + CO2(X) <-> CO2(X,v=01121) + CO2(X) | CO2vib | 1, 54.97122460895508, -405.02374294261324, 833.3284647148541 |
CO2(X,v=00031) + CO2(X) <-> CO2(X,v=10022) + CO2(X) | CO2vib | 1, 55.686671449507216, -403.0628227319206, 1100.3031844411862 |
CO2(X,v=00031) + CO2(X) <-> CO2(X,v=11122) + CO2(X) | CO2vib | 1, 44.71020891912093, -253.24368091861558, 680.7859518144106 |
CO2(X,v=00041) + CO2(X) <-> CO2(X,v=01131) + CO2(X) | CO2vib | 1, 55.24534590652499, -404.04325379314577, 837.9502872346928 |
CO2(X,v=00041) + CO2(X) <-> CO2(X,v=10032) + CO2(X) | CO2vib | 1, 55.96825614010337, -402.58769856955917, 1102.4799105437019 |
CO2(X,v=00041) + CO2(X) <-> CO2(X,v=11132) + CO2(X) | CO2vib | 1, 45.00324649033911, -253.8515870172153, 678.6999033618913 |
CO2(X,v=00051) + CO2(X) <-> CO2(X,v=01141) + CO2(X) | CO2vib | 1, 55.4550167783832, -403.06784318424695, 842.5437681725144 |
CO2(X,v=00051) + CO2(X) <-> CO2(X,v=10042) + CO2(X) | CO2vib | 1, 56.18521620621876, -402.108189228433, 1104.6732608434706 |
CO2(X,v=00051) + CO2(X) <-> CO2(X,v=11142) + CO2(X) | CO2vib | 1, 45.23146413647302, -254.45033998632073, 676.6280569662545 |
```

```
CO2(X,v=01101) + CO2(X) <-> CO2(X,v=00001) + CO2(X) | CO2vib | 1, 38.3, -177, 451 |
CO2(X,v=01111) + CO2(X) <-> CO2(X,v=00011) + CO2(X) | CO2vib | 1, 38.3, -177, 451 |
CO2(X,v=01111) + CO2(X) <-> CO2(X,v=02201) + CO2(X) | CO2vib | 1, 53.90000000000037, -407.0000000000065, 824.000000000028 |
CO2(X,v=01111) + CO2(X) <-> CO2(X,v=11102) + CO2(X) | CO2vib | 1, 54.600000000001955, -404.0000000000368, 1096.0000000001728 |
CO2(X,v=01111) + CO2(X) <-> CO2(X,v=12202) + CO2(X) | CO2vib | 1, 43.60000000000014, -252.00000000000264, 685.0000000000123 |
CO2(X,v=01111) + CO2(X) <-> CO2(X,v=20003) + CO2(X) | CO2vib | 1, 43.60000000000014, -252.00000000000264, 685.0000000000123 |
CO2(X,v=01121) + CO2(X) <-> CO2(X,v=00021) + CO2(X) | CO2vib | 1, 38.3, -177, 451 |
CO2(X,v=01121) + CO2(X) <-> CO2(X,v=02211) + CO2(X) | CO2vib | 1, 54.57940883718311, -406.0093215184438, 828.6783523567856 |
CO2(X,v=01121) + CO2(X) <-> CO2(X,v=11112) + CO2(X) | CO2vib | 1, 55.28721873004317, -403.53358308898373, 1098.1431824908393 |
CO2(X,v=01121) + CO2(X) <-> CO2(X,v=12212) + CO2(X) | CO2vib | 1, 44.29909661389566, -252.6265183163722, 682.8860297200965 |
CO2(X,v=01121) + CO2(X) <-> CO2(X,v=20013) + CO2(X) | CO2vib | 1, 44.29909661389566, -252.6265183163722, 682.8860297200965 |
CO2(X,v=01131) + CO2(X) <-> CO2(X,v=00031) + CO2(X) | CO2vib | 1, 38.3, -177, 451 |
CO2(X,v=01131) + CO2(X) <-> CO2(X,v=02221) + CO2(X) | CO2vib | 1, 54.97122460895508, -405.02374294261324, 833.3284647148541 |
CO2(X,v=01131) + CO2(X) <-> CO2(X,v=11122) + CO2(X) | CO2vib | 1, 55.686671449507216, -403.0628227319206, 1100.3031844411862 |
CO2(X,v=01131) + CO2(X) <-> CO2(X,v=12222) + CO2(X) | CO2vib | 1, 44.71020891912093, -253.24368091861558, 680.7859518144106 |
CO2(X,v=01131) + CO2(X) <-> CO2(X,v=20023) + CO2(X) | CO2vib | 1, 44.71020891912093, -253.24368091861558, 680.7859518144106 |
CO2(X,v=01141) + CO2(X) <-> CO2(X,v=00041) + CO2(X) | CO2vib | 1, 38.3, -177, 451 |
CO2(X,v=01141) + CO2(X) <-> CO2(X,v=02231) + CO2(X) | CO2vib | 1, 55.24534590652499, -404.04325379314577, 837.9502872346928 |
CO2(X,v=01141) + CO2(X) <-> CO2(X,v=11132) + CO2(X) | CO2vib | 1, 55.96825614010337, -402.58769856955917, 1102.4799105437019 |
CO2(X,v=01141) + CO2(X) <-> CO2(X,v=12232) + CO2(X) | CO2vib | 1, 45.00324649033911, -253.8515870172153, 678.6999033618913 |
CO2(X,v=01141) + CO2(X) <-> CO2(X,v=20033) + CO2(X) | CO2vib | 1, 45.00324649033911, -253.8515870172153, 678.6999033618913 |
CO2(X,v=01151) + CO2(X) <-> CO2(X,v=00051) + CO2(X) | CO2vib | 1, 38.3, -177, 451 |
CO2(X,v=01151) + CO2(X) <-> CO2(X,v=02241) + CO2(X) | CO2vib | 1, 55.4550167783832, -403.06784318424695, 842.5437681725144 |
CO2(X,v=01151) + CO2(X) <-> CO2(X,v=11142) + CO2(X) | CO2vib | 1, 56.18521620621876, -402.108189228433, 1104.6732608434706 |
CO2(X,v=01151) + CO2(X) <-> CO2(X,v=12242) + CO2(X) | CO2vib | 1, 45.23146413647302, -254.45033998632073, 676.6280569662545 |
CO2(X,v=01151) + CO2(X) <-> CO2(X,v=20043) + CO2(X) | CO2vib | 1, 45.23146413647302, -254.45033998632073, 676.6280569662545 |
CO2(X,v=02201) + CO2(X) <-> CO2(X,v=01101) + CO2(X) | CO2vib | 1, 39., -177, 451 |
CO2(X,v=02211) + CO2(X) <-> CO2(X,v=01111) + CO2(X) | CO2vib | 1, 39., -177, 451 |
CO2(X,v=02211) + CO2(X) <-> CO2(X,v=03301) + CO2(X) | CO2vib | 1, 53.90000000000037, -407.0000000000065, 824.000000000028 |
CO2(X,v=02211) + CO2(X) <-> CO2(X,v=12202) + CO2(X) | CO2vib | 1, 54.600000000001955, -404.0000000000368, 1096.0000000001728 |
CO2(X,v=02211) + CO2(X) <-> CO2(X,v=13302) + CO2(X) | CO2vib | 1, 43.60000000000014, -252.00000000000264, 685.0000000000123 |
CO2(X,v=02211) + CO2(X) <-> CO2(X,v=20003) + CO2(X) | CO2vib | 1, 54.600000000001955, -404.0000000000368, 1096.0000000001728 |
CO2(X,v=02211) + CO2(X) <-> CO2(X,v=21103) + CO2(X) | CO2vib | 1, 43.60000000000014, -252.00000000000264, 685.0000000000123 |
CO2(X,v=02221) + CO2(X) <-> CO2(X,v=01121) + CO2(X) | CO2vib | 1, 39., -177, 451 |
CO2(X,v=02221) + CO2(X) <-> CO2(X,v=03311) + CO2(X) | CO2vib | 1, 54.57940883718311, -406.0093215184438, 828.6783523567856 |
CO2(X,v=02221) + CO2(X) <-> CO2(X,v=12212) + CO2(X) | CO2vib | 1, 55.28721873004317, -403.53358308898373, 1098.1431824908393 |
CO2(X,v=02221) + CO2(X) <-> CO2(X,v=13312) + CO2(X) | CO2vib | 1, 44.29909661389566, -252.6265183163722, 682.8860297200965 |
CO2(X,v=02221) + CO2(X) <-> CO2(X,v=20013) + CO2(X) | CO2vib | 1, 55.28721873004317, -403.53358308898373, 1098.1431824908393 |
CO2(X,v=02221) + CO2(X) <-> CO2(X,v=21113) + CO2(X) | CO2vib | 1, 44.29909661389566, -252.6265183163722, 682.8860297200965 |
CO2(X,v=02231) + CO2(X) <-> CO2(X,v=01131) + CO2(X) | CO2vib | 1, 39., -177, 451 |
CO2(X,v=02231) + CO2(X) <-> CO2(X,v=03321) + CO2(X) | CO2vib | 1, 54.97122460895508, -405.02374294261324, 833.3284647148541 |
CO2(X,v=02231) + CO2(X) <-> CO2(X,v=12222) + CO2(X) | CO2vib | 1, 55.686671449507216, -403.0628227319206, 1100.3031844411862 |
CO2(X,v=02231) + CO2(X) <-> CO2(X,v=13322) + CO2(X) | CO2vib | 1, 44.71020891912093, -253.24368091861558, 680.7859518144106 |
CO2(X,v=02231) + CO2(X) <-> CO2(X,v=20023) + CO2(X) | CO2vib | 1, 55.686671449507216, -403.0628227319206, 1100.3031844411862 |
CO2(X,v=02231) + CO2(X) <-> CO2(X,v=21123) + CO2(X) | CO2vib | 1, 44.71020891912093, -253.24368091861558, 680.7859518144106 |
CO2(X,v=02241) + CO2(X) <-> CO2(X,v=01141) + CO2(X) | CO2vib | 1, 39., -177, 451 |
CO2(X,v=02241) + CO2(X) <-> CO2(X,v=03331) + CO2(X) | CO2vib | 1, 55.24534590652499, -404.04325379314577, 837.9502872346928 |
CO2(X,v=02241) + CO2(X) <-> CO2(X,v=12232) + CO2(X) | CO2vib | 1, 55.96825614010337, -402.58769856955917, 1102.4799105437019 |
CO2(X,v=02241) + CO2(X) <-> CO2(X,v=13332) + CO2(X) | CO2vib | 1, 45.00324649033911, -253.8515870172153, 678.6999033618913 |
CO2(X,v=02241) + CO2(X) <-> CO2(X,v=20033) + CO2(X) | CO2vib | 1, 55.96825614010337, -402.58769856955917, 1102.4799105437019 |
CO2(X,v=02241) + CO2(X) <-> CO2(X,v=21133) + CO2(X) | CO2vib | 1, 45.00324649033911, -253.8515870172153, 678.6999033618913 |
CO2(X,v=02251) + CO2(X) <-> CO2(X,v=01151) + CO2(X) | CO2vib | 1, 39., -177, 451 |
CO2(X,v=02251) + CO2(X) <-> CO2(X,v=03341) + CO2(X) | CO2vib | 1, 55.4550167783832, -403.06784318424695, 842.5437681725144 |
CO2(X,v=02251) + CO2(X) <-> CO2(X,v=12242) + CO2(X) | CO2vib | 1, 56.18521620621876, -402.108189228433, 1104.6732608434706 |
CO2(X,v=02251) + CO2(X) <-> CO2(X,v=13342) + CO2(X) | CO2vib | 1, 45.23146413647302, -254.45033998632073, 676.6280569662545 |
CO2(X,v=02251) + CO2(X) <-> CO2(X,v=20043) + CO2(X) | CO2vib | 1, 56.18521620621876, -402.108189228433, 1104.6732608434706 |
CO2(X,v=02251) + CO2(X) <-> CO2(X,v=21143) + CO2(X) | CO2vib | 1, 45.23146413647302, -254.45033998632073, 676.6280569662545 |
CO2(X,v=03301) + CO2(X) <-> CO2(X,v=02201) + CO2(X) | CO2vib | 1, 39.4, -177, 451 |
CO2(X,v=03301) + CO2(X) <-> CO2(X,v=10002) + CO2(X) | CO2vib | 1, 31.5, -171, 264 |
CO2(X,v=03311) + CO2(X) <-> CO2(X,v=02211) + CO2(X) | CO2vib | 1, 39.4, -177, 451 |
CO2(X,v=03311) + CO2(X) <-> CO2(X,v=04401) + CO2(X) | CO2vib | 1, 53.90000000000037, -407.0000000000065, 824.000000000028 |
CO2(X,v=03311) + CO2(X) <-> CO2(X,v=10012) + CO2(X) | CO2vib | 1, 31.5, -171, 264 |
CO2(X,v=03311) + CO2(X) <-> CO2(X,v=13302) + CO2(X) | CO2vib | 1, 54.600000000001955, -404.0000000000368, 1096.0000000001728 |
CO2(X,v=03311) + CO2(X) <-> CO2(X,v=21103) + CO2(X) | CO2vib | 1, 54.600000000001955, -404.0000000000368, 1096.0000000001728 |
CO2(X,v=03321) + CO2(X) <-> CO2(X,v=02221) + CO2(X) | CO2vib | 1, 39.4, -177, 451 |
CO2(X,v=03321) + CO2(X) <-> CO2(X,v=04411) + CO2(X) | CO2vib | 1, 54.57940883718311, -406.0093215184438, 828.6783523567856 |
CO2(X,v=03321) + CO2(X) <-> CO2(X,v=10022) + CO2(X) | CO2vib | 1, 31.5, -171, 264 |
CO2(X,v=03321) + CO2(X) <-> CO2(X,v=13312) + CO2(X) | CO2vib | 1, 55.28721873004317, -403.53358308898373, 1098.1431824908393 |
CO2(X,v=03321) + CO2(X) <-> CO2(X,v=21113) + CO2(X) | CO2vib | 1, 55.28721873004317, -403.53358308898373, 1098.1431824908393 |
CO2(X,v=03331) + CO2(X) <-> CO2(X,v=02231) + CO2(X) | CO2vib | 1, 39.4, -177, 451 |
CO2(X,v=03331) + CO2(X) <-> CO2(X,v=04421) + CO2(X) | CO2vib | 1, 54.97122460895508, -405.02374294261324, 833.3284647148541 |
CO2(X,v=03331) + CO2(X) <-> CO2(X,v=10032) + CO2(X) | CO2vib | 1, 31.5, -171, 264 |
CO2(X,v=03331) + CO2(X) <-> CO2(X,v=13322) + CO2(X) | CO2vib | 1, 55.686671449507216, -403.0628227319206, 1100.3031844411862 |
CO2(X,v=03331) + CO2(X) <-> CO2(X,v=21123) + CO2(X) | CO2vib | 1, 55.686671449507216, -403.0628227319206, 1100.3031844411862 |
CO2(X,v=03341) + CO2(X) <-> CO2(X,v=02241) + CO2(X) | CO2vib | 1, 39.4, -177, 451 |
CO2(X,v=03341) + CO2(X) <-> CO2(X,v=04431) + CO2(X) | CO2vib | 1, 55.24534590652499, -404.04325379314577, 837.9502872346928 |
CO2(X,v=03341) + CO2(X) <-> CO2(X,v=10042) + CO2(X) | CO2vib | 1, 31.5, -171, 264 |
CO2(X,v=03341) + CO2(X) <-> CO2(X,v=13332) + CO2(X) | CO2vib | 1, 55.96825614010337, -402.58769856955917, 1102.4799105437019 |
CO2(X,v=03341) + CO2(X) <-> CO2(X,v=21133) + CO2(X) | CO2vib | 1, 55.96825614010337, -402.58769856955917, 1102.4799105437019 |
CO2(X,v=03351) + CO2(X) <-> CO2(X,v=02251) + CO2(X) | CO2vib | 1, 39.4, -177, 451 |
CO2(X,v=03351) + CO2(X) <-> CO2(X,v=04441) + CO2(X) | CO2vib | 1, 55.4550167783832, -403.06784318424695, 842.5437681725144 |
CO2(X,v=03351) + CO2(X) <-> CO2(X,v=10052) + CO2(X) | CO2vib | 1, 31.5, -171, 264 |
CO2(X,v=03351) + CO2(X) <-> CO2(X,v=13342) + CO2(X) | CO2vib | 1, 56.18521620621876, -402.108189228433, 1104.6732608434706 |
CO2(X,v=03351) + CO2(X) <-> CO2(X,v=21143) + CO2(X) | CO2vib | 1, 56.18521620621876, -402.108189228433, 1104.6732608434706 |
CO2(X,v=04401) + CO2(X) <-> CO2(X,v=03301) + CO2(X) | CO2vib | 1, 39.7, -177, 451 |
CO2(X,v=04401) + CO2(X) <-> CO2(X,v=11102) + CO2(X) | CO2vib | 1, 30.1, -171, 264 |
CO2(X,v=04411) + CO2(X) <-> CO2(X,v=03311) + CO2(X) | CO2vib | 1, 39.7, -177, 451 |
CO2(X,v=04411) + CO2(X) <-> CO2(X,v=05501) + CO2(X) | CO2vib | 1, 53.90000000000037, -407.0000000000065, 824.000000000028 |
CO2(X,v=04411) + CO2(X) <-> CO2(X,v=11112) + CO2(X) | CO2vib | 1, 30.1, -171, 264 |
CO2(X,v=04421) + CO2(X) <-> CO2(X,v=03321) + CO2(X) | CO2vib | 1, 39.7, -177, 451 |
CO2(X,v=04421) + CO2(X) <-> CO2(X,v=05511) + CO2(X) | CO2vib | 1, 54.57940883718311, -406.0093215184438, 828.6783523567856 |
CO2(X,v=04421) + CO2(X) <-> CO2(X,v=11122) + CO2(X) | CO2vib | 1, 30.1, -171, 264 |
CO2(X,v=04431) + CO2(X) <-> CO2(X,v=03331) + CO2(X) | CO2vib | 1, 39.7, -177, 451 |
CO2(X,v=04431) + CO2(X) <-> CO2(X,v=05521) + CO2(X) | CO2vib | 1, 54.97122460895508, -405.02374294261324, 833.3284647148541 |
```

```
CO2(X,v=04431) + CO2(X) <-> CO2(X,v=11132) + CO2(X) | CO2vib | 1, 30.1, -171, 264 |
CO2(X,v=04441) + CO2(X) <-> CO2(X,v=03341) + CO2(X) | CO2vib | 1, 39.7, -177, 451 |
CO2(X,v=04441) + CO2(X) <-> CO2(X,v=05531) + CO2(X) | CO2vib | 1, 55.24534590652499, -404.04325379314577, 837.9502872346928 |
CO2(X,v=04441) + CO2(X) <-> CO2(X,v=11142) + CO2(X) | CO2vib | 1, 30.1, -171, 264 |
CO2(X,v=04451) + CO2(X) <-> CO2(X,v=03351) + CO2(X) | CO2vib | 1, 39.7, -177, 451 |
CO2(X,v=04451) + CO2(X) <-> CO2(X,v=05541) + CO2(X) | CO2vib | 1, 55.4550167783832, -403.06784318424695, 842.5437681725144 |
CO2(X,v=04451) + CO2(X) <-> CO2(X,v=11152) + CO2(X) | CO2vib | 1, 30.1, -171, 264 |
CO2(X,v=05501) + CO2(X) <-> CO2(X,v=04401) + CO2(X) | CO2vib | 1, 39.9, -177, 451 |
CO2(X,v=05511) + CO2(X) <-> CO2(X,v=04411) + CO2(X) | CO2vib | 1, 39.9, -177, 451 |
CO2(X,v=05521) + CO2(X) <-> CO2(X,v=04421) + CO2(X) | CO2vib | 1, 39.9, -177, 451 |
CO2(X,v=05531) + CO2(X) <-> CO2(X,v=04431) + CO2(X) | CO2vib | 1, 39.9, -177, 451 |
CO2(X,v=05541) + CO2(X) <-> CO2(X,v=04441) + CO2(X) | CO2vib | 1, 39.9, -177, 451 |
CO2(X,v=05551) + CO2(X) <-> CO2(X,v=04451) + CO2(X) | CO2vib | 1, 39.9, -177, 451 |
CO2(X,v=10002) + CO2(X) <-> CO2(X,v=00001) + CO2(X) | CO2vib | 1, 34.1, -137, 0 |
CO2(X,v=10002) + CO2(X) <-> CO2(X,v=01101) + CO2(X) | CO2vib | 1, 39.3, -177, 451 |
CO2(X,v=10002) + CO2(X) <-> CO2(X,v=02201) + CO2(X) | CO2vib | 1, 36.5, -88.9, 226 |
CO2(X,v=10012) + CO2(X) <-> CO2(X,v=00011) + CO2(X) | CO2vib | 1, 34.1, -137, 0 |
CO2(X,v=10012) + CO2(X) <-> CO2(X,v=01111) + CO2(X) | CO2vib | 1, 39.3, -177, 451 |
CO2(X,v=10012) + CO2(X) <-> CO2(X,v=02211) + CO2(X) | CO2vib | 1, 36.5, -88.9, 226 |
CO2(X,v=10022) + CO2(X) <-> CO2(X,v=00021) + CO2(X) | CO2vib | 1, 34.1, -137, 0 |
CO2(X,v=10022) + CO2(X) <-> CO2(X,v=01121) + CO2(X) | CO2vib | 1, 39.3, -177, 451 |
CO2(X,v=10022) + CO2(X) <-> CO2(X,v=02221) + CO2(X) | CO2vib | 1, 36.5, -88.9, 226 |
CO2(X,v=10032) + CO2(X) <-> CO2(X,v=00031) + CO2(X) | CO2vib | 1, 34.1, -137, 0 |
CO2(X,v=10032) + CO2(X) <-> CO2(X,v=01131) + CO2(X) | CO2vib | 1, 39.3, -177, 451 |
CO2(X,v=10032) + CO2(X) <-> CO2(X,v=02231) + CO2(X) | CO2vib | 1, 36.5, -88.9, 226 |
CO2(X,v=10042) + CO2(X) <-> CO2(X,v=00041) + CO2(X) | CO2vib | 1, 34.1, -137, 0 |
CO2(X,v=10042) + CO2(X) <-> CO2(X,v=01141) + CO2(X) | CO2vib | 1, 39.3, -177, 451 |
CO2(X,v=10042) + CO2(X) <-> CO2(X,v=02241) + CO2(X) | CO2vib | 1, 36.5, -88.9, 226 |
CO2(X,v=10052) + CO2(X) <-> CO2(X,v=00051) + CO2(X) | CO2vib | 1, 34.1, -137, 0 |
CO2(X,v=10052) + CO2(X) <-> CO2(X,v=01151) + CO2(X) | CO2vib | 1, 39.3, -177, 451 |
CO2(X,v=10052) + CO2(X) <-> CO2(X,v=02251) + CO2(X) | CO2vib | 1, 36.5, -88.9, 226 |
CO2(X,v=11102) + CO2(X) <-> CO2(X,v=01101) + CO2(X) | CO2vib | 1, 34.1, -137, 0 |
CO2(X,v=11102) + CO2(X) <-> CO2(X,v=02201) + CO2(X) | CO2vib | 1, 39.4, -177, 451 |
CO2(X,v=11102) + CO2(X) <-> CO2(X,v=03301) + CO2(X) | CO2vib | 1, 37.2, -89.3, 227 |
CO2(X,v=11102) + CO2(X) <-> CO2(X,v=10002) + CO2(X) | CO2vib | 1, 39.7, -177, 451 |
CO2(X,v=11112) + CO2(X) <-> CO2(X,v=01111) + CO2(X) | CO2vib | 1, 34.1, -137, 0 |
CO2(X,v=11112) + CO2(X) <-> CO2(X,v=02211) + CO2(X) | CO2vib | 1, 39.4, -177, 451 |
CO2(X,v=11112) + CO2(X) <-> CO2(X,v=03311) + CO2(X) | CO2vib | 1, 37.2, -89.3, 227 |
CO2(X,v=11112) + CO2(X) <-> CO2(X,v=10012) + CO2(X) | CO2vib | 1, 39.7, -177, 451 |
CO2(X,v=11122) + CO2(X) <-> CO2(X,v=01121) + CO2(X) | CO2vib | 1, 34.1, -137, 0 |
CO2(X,v=11122) + CO2(X) <-> CO2(X,v=02221) + CO2(X) | CO2vib | 1, 39.4, -177, 451 |
CO2(X,v=11122) + CO2(X) <-> CO2(X,v=03321) + CO2(X) | CO2vib | 1, 37.2, -89.3, 227 |
CO2(X,v=11122) + CO2(X) <-> CO2(X,v=10022) + CO2(X) | CO2vib | 1, 39.7, -177, 451 |
CO2(X,v=11132) + CO2(X) <-> CO2(X,v=01131) + CO2(X) | CO2vib | 1, 34.1, -137, 0 |
CO2(X,v=11132) + CO2(X) <-> CO2(X,v=02231) + CO2(X) | CO2vib | 1, 39.4, -177, 451 |
CO2(X,v=11132) + CO2(X) <-> CO2(X,v=03331) + CO2(X) | CO2vib | 1, 37.2, -89.3, 227 |
CO2(X,v=11132) + CO2(X) <-> CO2(X,v=10032) + CO2(X) | CO2vib | 1, 39.7, -177, 451 |
CO2(X,v=11142) + CO2(X) <-> CO2(X,v=01141) + CO2(X) | CO2vib | 1, 34.1, -137, 0 |
CO2(X,v=11142) + CO2(X) <-> CO2(X,v=02241) + CO2(X) | CO2vib | 1, 39.4, -177, 451 |
CO2(X,v=11142) + CO2(X) <-> CO2(X,v=03341) + CO2(X) | CO2vib | 1, 37.2, -89.3, 227 |
CO2(X,v=11142) + CO2(X) <-> CO2(X,v=10042) + CO2(X) | CO2vib | 1, 39.7, -177, 451 |
CO2(X,v=11152) + CO2(X) <-> CO2(X,v=01151) + CO2(X) | CO2vib | 1, 34.1, -137, 0 |
CO2(X,v=11152) + CO2(X) <-> CO2(X,v=02251) + CO2(X) | CO2vib | 1, 39.4, -177, 451 |
CO2(X,v=11152) + CO2(X) <-> CO2(X,v=03351) + CO2(X) | CO2vib | 1, 37.2, -89.3, 227 |
CO2(X,v=11152) + CO2(X) <-> CO2(X,v=10052) + CO2(X) | CO2vib | 1, 39.7, -177, 451 |
CO2(X,v=12202) + CO2(X) <-> CO2(X,v=03301) + CO2(X) | CO2vib | 1, 39.7, -177, 451 |
CO2(X,v=12202) + CO2(X) <-> CO2(X,v=04401) + CO2(X) | CO2vib | 1, 37.8, -90.4, 230 |
CO2(X,v=12202) + CO2(X) <-> CO2(X,v=11102) + CO2(X) | CO2vib | 1, 40.1, -177, 451 |
CO2(X,v=12202) + CO2(X) <-> CO2(X,v=20003) + CO2(X) | CO2vib | 1, 38.1, -90.4, 230 |
CO2(X,v=12212) + CO2(X) <-> CO2(X,v=03311) + CO2(X) | CO2vib | 1, 39.7, -177, 451 |
CO2(X,v=12212) + CO2(X) <-> CO2(X,v=04411) + CO2(X) | CO2vib | 1, 37.8, -90.4, 230 |
CO2(X,v=12212) + CO2(X) <-> CO2(X,v=11112) + CO2(X) | CO2vib | 1, 40.1, -177, 451 |
CO2(X,v=12212) + CO2(X) <-> CO2(X,v=20013) + CO2(X) | CO2vib | 1, 38.1, -90.4, 230 |
CO2(X,v=12222) + CO2(X) <-> CO2(X,v=03321) + CO2(X) | CO2vib | 1, 39.7, -177, 451 |
CO2(X,v=12222) + CO2(X) <-> CO2(X,v=04421) + CO2(X) | CO2vib | 1, 37.8, -90.4, 230 |
CO2(X,v=12222) + CO2(X) <-> CO2(X,v=11122) + CO2(X) | CO2vib | 1, 40.1, -177, 451 |
CO2(X,v=12222) + CO2(X) <-> CO2(X,v=20023) + CO2(X) | CO2vib | 1, 38.1, -90.4, 230 |
CO2(X,v=12232) + CO2(X) <-> CO2(X,v=03331) + CO2(X) | CO2vib | 1, 39.7, -177, 451 |
CO2(X,v=12232) + CO2(X) <-> CO2(X,v=04431) + CO2(X) | CO2vib | 1, 37.8, -90.4, 230 |
CO2(X,v=12232) + CO2(X) <-> CO2(X,v=11132) + CO2(X) | CO2vib | 1, 40.1, -177, 451 |
CO2(X,v=12232) + CO2(X) <-> CO2(X,v=20033) + CO2(X) | CO2vib | 1, 38.1, -90.4, 230 |
CO2(X,v=12242) + CO2(X) <-> CO2(X,v=03341) + CO2(X) | CO2vib | 1, 39.7, -177, 451 |
CO2(X,v=12242) + CO2(X) <-> CO2(X,v=04441) + CO2(X) | CO2vib | 1, 37.8, -90.4, 230 |
CO2(X,v=12242) + CO2(X) <-> CO2(X,v=11142) + CO2(X) | CO2vib | 1, 40.1, -177, 451 |
CO2(X,v=12242) + CO2(X) <-> CO2(X,v=20043) + CO2(X) | CO2vib | 1, 38.1, -90.4, 230 |
CO2(X,v=12252) + CO2(X) <-> CO2(X,v=03351) + CO2(X) | CO2vib | 1, 39.7, -177, 451 |
CO2(X,v=12252) + CO2(X) <-> CO2(X,v=04451) + CO2(X) | CO2vib | 1, 37.8, -90.4, 230 |
CO2(X,v=12252) + CO2(X) <-> CO2(X,v=11152) + CO2(X) | CO2vib | 1, 40.1, -177, 451 |
CO2(X,v=12252) + CO2(X) <-> CO2(X,v=20053) + CO2(X) | CO2vib | 1, 38.1, -90.4, 230 |
CO2(X,v=13302) + CO2(X) <-> CO2(X,v=03301) + CO2(X) | CO2vib | 1, 34.1, -137, 0 |
CO2(X,v=13302) + CO2(X) <-> CO2(X,v=04401) + CO2(X) | CO2vib | 1, 39.9, -177, 451 |
CO2(X,v=13302) + CO2(X) <-> CO2(X,v=05501) + CO2(X) | CO2vib | 1, 38., -88.9, 226 |
CO2(X,v=13302) + CO2(X) <-> CO2(X,v=12202) + CO2(X) | CO2vib | 1, 40.4, -177, 451 |
CO2(X,v=13312) + CO2(X) <-> CO2(X,v=03311) + CO2(X) | CO2vib | 1, 34.1, -137, 0 |
CO2(X,v=13312) + CO2(X) <-> CO2(X,v=04411) + CO2(X) | CO2vib | 1, 39.9, -177, 451 |
CO2(X,v=13312) + CO2(X) <-> CO2(X,v=05511) + CO2(X) | CO2vib | 1, 38., -88.9, 226 |
CO2(X,v=13312) + CO2(X) <-> CO2(X,v=12212) + CO2(X) | CO2vib | 1, 40.4, -177, 451 |
CO2(X,v=13322) + CO2(X) <-> CO2(X,v=03321) + CO2(X) | CO2vib | 1, 34.1, -137, 0 |
CO2(X,v=13322) + CO2(X) <-> CO2(X,v=04421) + CO2(X) | CO2vib | 1, 39.9, -177, 451 |
CO2(X,v=13322) + CO2(X) <-> CO2(X,v=05521) + CO2(X) | CO2vib | 1, 38., -88.9, 226 |
CO2(X,v=13322) + CO2(X) <-> CO2(X,v=12222) + CO2(X) | CO2vib | 1, 40.4, -177, 451 |
CO2(X,v=13332) + CO2(X) <-> CO2(X,v=03331) + CO2(X) | CO2vib | 1, 34.1, -137, 0 |
CO2(X,v=13332) + CO2(X) <-> CO2(X,v=04431) + CO2(X) | CO2vib | 1, 39.9, -177, 451 |
CO2(X,v=13332) + CO2(X) <-> CO2(X,v=05531) + CO2(X) | CO2vib | 1, 38., -88.9, 226 |
```

```
CO2(X,v=13332) + CO2(X) <-> CO2(X,v=12232) + CO2(X) | CO2vib | 1, 40.4, -177, 451 |
CO2(X,v=13342) + CO2(X) <-> CO2(X,v=03341) + CO2(X) | CO2vib | 1, 34.1, -137, 0 |
CO2(X,v=13342) + CO2(X) <-> CO2(X,v=04441) + CO2(X) | CO2vib | 1, 39.9, -177, 451 |
CO2(X,v=13342) + CO2(X) <-> CO2(X,v=05541) + CO2(X) | CO2vib | 1, 38., -88.9, 226 |
CO2(X,v=13342) + CO2(X) <-> CO2(X,v=12242) + CO2(X) | CO2vib | 1, 40.4, -177, 451 |
CO2(X,v=13352) + CO2(X) <-> CO2(X,v=03351) + CO2(X) | CO2vib | 1, 34.1, -137, 0 |
CO2(X,v=13352) + CO2(X) <-> CO2(X,v=04451) + CO2(X) | CO2vib | 1, 39.9, -177, 451 |
CO2(X,v=13352) + CO2(X) <-> CO2(X,v=05551) + CO2(X) | CO2vib | 1, 38., -88.9, 226 |
CO2(X,v=13352) + CO2(X) <-> CO2(X,v=12252) + CO2(X) | CO2vib | 1, 40.4, -177, 451 |
CO2(X,v=20003) + CO2(X) <-> CO2(X,v=00011) + CO2(X) | CO2vib | 1, 30., -108, 165 |
CO2(X,v=20003) + CO2(X) <-> CO2(X,v=02201) + CO2(X) | CO2vib | 1, 39.2, -271, 438 |
CO2(X,v=20003) + CO2(X) <-> CO2(X,v=03301) + CO2(X) | CO2vib | 1, 30.2, -171, 264 |
CO2(X,v=20003) + CO2(X) <-> CO2(X,v=10002) + CO2(X) | CO2vib | 1, 43.7, -272, 437 |
CO2(X,v=20003) + CO2(X) <-> CO2(X,v=11102) + CO2(X) | CO2vib | 1, 40.1, -177, 451 |
CO2(X,v=20013) + CO2(X) <-> CO2(X,v=00021) + CO2(X) | CO2vib | 1, 30., -108, 165 |
CO2(X,v=20013) + CO2(X) <-> CO2(X,v=02211) + CO2(X) | CO2vib | 1, 39.2, -271, 438 |
CO2(X,v=20013) + CO2(X) <-> CO2(X,v=03311) + CO2(X) | CO2vib | 1, 30.2, -171, 264 |
CO2(X,v=20013) + CO2(X) <-> CO2(X,v=10012) + CO2(X) | CO2vib | 1, 43.7, -272, 437 |
CO2(X,v=20013) + CO2(X) <-> CO2(X,v=11112) + CO2(X) | CO2vib | 1, 40.1, -177, 451 |
CO2(X,v=20023) + CO2(X) <-> CO2(X,v=00031) + CO2(X) | CO2vib | 1, 30., -108, 165 |
CO2(X,v=20023) + CO2(X) <-> CO2(X,v=02221) + CO2(X) | CO2vib | 1, 39.2, -271, 438 |
CO2(X,v=20023) + CO2(X) <-> CO2(X,v=03321) + CO2(X) | CO2vib | 1, 30.2, -171, 264 |
CO2(X,v=20023) + CO2(X) <-> CO2(X,v=10022) + CO2(X) | CO2vib | 1, 43.7, -272, 437 |
CO2(X,v=20023) + CO2(X) <-> CO2(X,v=11122) + CO2(X) | CO2vib | 1, 40.1, -177, 451 |
CO2(X,v=20033) + CO2(X) <-> CO2(X,v=00041) + CO2(X) | CO2vib | 1, 30., -108, 165 |
CO2(X,v=20033) + CO2(X) <-> CO2(X,v=02231) + CO2(X) | CO2vib | 1, 39.2, -271, 438 |
CO2(X,v=20033) + CO2(X) <-> CO2(X,v=03331) + CO2(X) | CO2vib | 1, 30.2, -171, 264 |
CO2(X,v=20033) + CO2(X) <-> CO2(X,v=10032) + CO2(X) | CO2vib | 1, 43.7, -272, 437 |
CO2(X,v=20033) + CO2(X) <-> CO2(X,v=11132) + CO2(X) | CO2vib | 1, 40.1, -177, 451 |
CO2(X,v=20043) + CO2(X) <-> CO2(X,v=00051) + CO2(X) | CO2vib | 1, 30., -108, 165 |
CO2(X,v=20043) + CO2(X) <-> CO2(X,v=02241) + CO2(X) | CO2vib | 1, 39.2, -271, 438 |
CO2(X,v=20043) + CO2(X) <-> CO2(X,v=03341) + CO2(X) | CO2vib | 1, 30.2, -171, 264 |
CO2(X,v=20043) + CO2(X) <-> CO2(X,v=10042) + CO2(X) | CO2vib | 1, 43.7, -272, 437 |
CO2(X,v=20043) + CO2(X) <-> CO2(X,v=11142) + CO2(X) | CO2vib | 1, 40.1, -177, 451 |
CO2(X,v=20053) + CO2(X) <-> CO2(X,v=02251) + CO2(X) | CO2vib | 1, 39.2, -271, 438 |
CO2(X,v=20053) + CO2(X) <-> CO2(X,v=03351) + CO2(X) | CO2vib | 1, 30.2, -171, 264 |
CO2(X,v=20053) + CO2(X) <-> CO2(X,v=10052) + CO2(X) | CO2vib | 1, 43.7, -272, 437 |
CO2(X,v=20053) + CO2(X) <-> CO2(X,v=11152) + CO2(X) | CO2vib | 1, 40.1, -177, 451 |
CO2(X,v=21103) + CO2(X) <-> CO2(X,v=11102) + CO2(X) | CO2vib | 1, 35.2, -137, 0 |
CO2(X,v=21103) + CO2(X) <-> CO2(X,v=12202) + CO2(X) | CO2vib | 1, 40.4, -177, 451 |
CO2(X,v=21103) + CO2(X) <-> CO2(X,v=13302) + CO2(X) | CO2vib | 1, 38.4, -88.9, 226 |
CO2(X,v=21103) + CO2(X) <-> CO2(X,v=20003) + CO2(X) | CO2vib | 1, 40.5, -177, 451 |
CO2(X,v=21113) + CO2(X) <-> CO2(X,v=11112) + CO2(X) | CO2vib | 1, 35.2, -137, 0 |
CO2(X,v=21113) + CO2(X) <-> CO2(X,v=12212) + CO2(X) | CO2vib | 1, 40.4, -177, 451 |
CO2(X,v=21113) + CO2(X) <-> CO2(X,v=13312) + CO2(X) | CO2vib | 1, 38.4, -88.9, 226 |
CO2(X,v=21113) + CO2(X) <-> CO2(X,v=20013) + CO2(X) | CO2vib | 1, 40.5, -177, 451 |
CO2(X,v=21123) + CO2(X) <-> CO2(X,v=11122) + CO2(X) | CO2vib | 1, 35.2, -137, 0 |
CO2(X,v=21123) + CO2(X) <-> CO2(X,v=12222) + CO2(X) | CO2vib | 1, 40.4, -177, 451 |
CO2(X,v=21123) + CO2(X) <-> CO2(X,v=13322) + CO2(X) | CO2vib | 1, 38.4, -88.9, 226 |
CO2(X,v=21123) + CO2(X) <-> CO2(X,v=20023) + CO2(X) | CO2vib | 1, 40.5, -177, 451 |
CO2(X,v=21133) + CO2(X) <-> CO2(X,v=11132) + CO2(X) | CO2vib | 1, 35.2, -137, 0 |
CO2(X,v=21133) + CO2(X) <-> CO2(X,v=12232) + CO2(X) | CO2vib | 1, 40.4, -177, 451 |
CO2(X,v=21133) + CO2(X) <-> CO2(X,v=13332) + CO2(X) | CO2vib | 1, 38.4, -88.9, 226 |
CO2(X,v=21133) + CO2(X) <-> CO2(X,v=20033) + CO2(X) | CO2vib | 1, 40.5, -177, 451 |
CO2(X,v=21143) + CO2(X) <-> CO2(X,v=11142) + CO2(X) | CO2vib | 1, 35.2, -137, 0 |
CO2(X,v=21143) + CO2(X) <-> CO2(X,v=12242) + CO2(X) | CO2vib | 1, 40.4, -177, 451 |
CO2(X,v=21143) + CO2(X) <-> CO2(X,v=13342) + CO2(X) | CO2vib | 1, 38.4, -88.9, 226 |
CO2(X,v=21143) + CO2(X) <-> CO2(X,v=20043) + CO2(X) | CO2vib | 1, 40.5, -177, 451 |
CO2(X,v=21153) + CO2(X) <-> CO2(X,v=11152) + CO2(X) | CO2vib | 1, 35.2, -137, 0 |
CO2(X,v=21153) + CO2(X) <-> CO2(X,v=12252) + CO2(X) | CO2vib | 1, 40.4, -177, 451 |
CO2(X,v=21153) + CO2(X) <-> CO2(X,v=13352) + CO2(X) | CO2vib | 1, 38.4, -88.9, 226 |
CO2(X,v=21153) + CO2(X) <-> CO2(X,v=20053) + CO2(X) | CO2vib | 1, 40.5, -177, 451 |
```

A.8 CO_2-CO_2 VV reactions

```
CO2(X,v=00011) + CO2(X,v=00001) <-> CO2(X,v=02201) + CO2(X,v=01101) | CO2vib | 1, 43.999999999999794, -241.99999999999625, 632.9999999999832 |
CO2(X,v=00011) + CO2(X,v=00001) <-> CO2(X,v=10002) + CO2(X,v=01101) | CO2vib | 1, 43.999999999999794, -241.99999999999625, 632.9999999999832 |
CO2(X,v=00011) + CO2(X,v=00011) <-> CO2(X,v=00001) + CO2(X,v=00021) | CO2vib | 1, 29.822599999999984, 22.100000000000335, -40.30000000000138 |
CO2(X,v=00011) + CO2(X,v=00021) <-> CO2(X,v=00001) + CO2(X,v=00031) | CO2vib | 1, 30.541279933945304, 21.37052885579892, -53.022341944275425 |
CO2(X,v=00011) + CO2(X,v=00031) <-> CO2(X,v=00001) + CO2(X,v=00041) | CO2vib | 1, 30.99839830344565, 20.112365406493918, -65.13565770383947 |
CO2(X,v=00011) + CO2(X,v=00041) <-> CO2(X,v=00001) + CO2(X,v=00051) | CO2vib | 1, 31.356604201915104, 18.402884815929248, -76.05434741755224 |
CO2(X,v=00021) + CO2(X,v=00001) <-> CO2(X,v=01111) + CO2(X,v=02201) | CO2vib | 1, 44.67991931452609, -240.81317055199702, 636.9551263082907 |
CO2(X,v=00021) + CO2(X,v=00001) <-> CO2(X,v=01111) + CO2(X,v=10002) | CO2vib | 1, 44.67991931452609, -240.81317055199702, 636.9551263082907 |
CO2(X,v=00021) + CO2(X,v=00001) <-> CO2(X,v=02211) + CO2(X,v=01101) | CO2vib | 1, 44.686043579991015, -241.44996240563094, 634.8405832082474 |
CO2(X,v=00021) + CO2(X,v=00001) <-> CO2(X,v=10012) + CO2(X,v=01101) | CO2vib | 1, 44.686043579991015, -241.44996240563094, 634.8405832082474 |
CO2(X,v=00021) + CO2(X,v=00021) <-> CO2(X,v=00011) + CO2(X,v=00031) | CO2vib | 1, 29.822599999999984, 22.100000000000335, -40.30000000000138 |
CO2(X,v=00031) + CO2(X,v=00001) <-> CO2(X,v=01121) + CO2(X,v=02201) | CO2vib | 1, 45.07176928487963, -239.6232508852019, 640.8613215274014 |
CO2(X,v=00031) + CO2(X,v=00001) <-> CO2(X,v=01121) + CO2(X,v=10002) | CO2vib | 1, 45.07176928487963, -239.6232508852019, 640.8613215274014 |
CO2(X,v=00031) + CO2(X,v=00001) <-> CO2(X,v=02221) + CO2(X,v=01101) | CO2vib | 1, 45.084142206783284, -240.89304265445733, 636.690846150963 |
CO2(X,v=00031) + CO2(X,v=00001) <-> CO2(X,v=10022) + CO2(X,v=01101) | CO2vib | 1, 45.084142206783284, -240.89304265445733, 636.690846150963 |
CO2(X,v=00031) + CO2(X,v=00031) <-> CO2(X,v=00021) + CO2(X,v=00041) | CO2vib | 1, 29.822599999999984, 22.100000000000335, -40.30000000000138 |
CO2(X,v=00041) + CO2(X,v=00001) <-> CO2(X,v=01131) + CO2(X,v=02201) | CO2vib | 1, 45.34544893197955, -238.4306145879866, 644.7212813811431 |
CO2(X,v=00041) + CO2(X,v=00001) <-> CO2(X,v=01131) + CO2(X,v=10002) | CO2vib | 1, 45.34544893197955, -238.4306145879866, 644.7212813811431 |
CO2(X,v=00041) + CO2(X,v=00001) <-> CO2(X,v=02231) + CO2(X,v=01101) | CO2vib | 1, 45.36418751862963, -240.32919632862897, 638.5508175264691 |
CO2(X,v=00041) + CO2(X,v=00001) <-> CO2(X,v=10032) + CO2(X,v=01101) | CO2vib | 1, 45.36418751862963, -240.32919632862897, 638.5508175264691 |
CO2(X,v=00041) + CO2(X,v=00011) <-> CO2(X,v=00031) + CO2(X,v=00021) | CO2vib | 1, 29.82259, 22.1, -40.3 |
CO2(X,v=00041) + CO2(X,v=00041) <-> CO2(X,v=00031) + CO2(X,v=00051) | CO2vib | 1, 29.822599999999984, 22.100000000000335, -40.30000000000138 |
CO2(X,v=00051) + CO2(X,v=00001) <-> CO2(X,v=01141) + CO2(X,v=02201) | CO2vib | 1, 45.55420918730157, -237.23578312018964, 648.5383282768058 |
CO2(X,v=00051) + CO2(X,v=00001) <-> CO2(X,v=01141) + CO2(X,v=10002) | CO2vib | 1, 45.55420918730157, -237.23578312018964, 648.5383282768058 |
CO2(X,v=00051) + CO2(X,v=00001) <-> CO2(X,v=02241) + CO2(X,v=01101) | CO2vib | 1, 45.57941662414474, -239.7583856832574, 640.4205652276081 |
CO2(X,v=00051) + CO2(X,v=00001) <-> CO2(X,v=10042) + CO2(X,v=01101) | CO2vib | 1, 45.57941662414474, -239.7583856832574, 640.4205652276081 |
```

```
CO2(X,v=00051) + CO2(X,v=00011) <-> CO2(X,v=00041) + CO2(X,v=00021) | CO2vib | 1, 29.82259, 22.1, -40.3 |
CO2(X,v=00051) + CO2(X,v=00021) <-> CO2(X,v=00041) + CO2(X,v=00031) | CO2vib | 1, 29.82259, 22.1, -40.3 |
CO2(X,v=01111) + CO2(X,v=00001) <-> CO2(X,v=00011) + CO2(X,v=01101) | CO2vib | 1, 34.1, -87.7, 230 |
CO2(X,v=01111) + CO2(X,v=01101) <-> CO2(X,v=00011) + CO2(X,v=02201) | CO2vib | 1, 34.8, -88., 233 |
CO2(X,v=01111) + CO2(X,v=01101) <-> CO2(X,v=00011) + CO2(X,v=10002) | CO2vib | 1, 34.8, -88., 233 |
CO2(X,v=01111) + CO2(X,v=02201) <-> CO2(X,v=00011) + CO2(X,v=03301) | CO2vib | 1, 35.2, -88., 233 |
CO2(X,v=01111) + CO2(X,v=02201) <-> CO2(X,v=00011) + CO2(X,v=11102) | CO2vib | 1, 35.2, -88., 233 |
CO2(X,v=01111) + CO2(X,v=03301) <-> CO2(X,v=00011) + CO2(X,v=04401) | CO2vib | 1, 35.2, -88., 233 |
CO2(X,v=01111) + CO2(X,v=10002) <-> CO2(X,v=00011) + CO2(X,v=11102) | CO2vib | 1, 35.5, -88., 233 |
CO2(X,v=01111) + CO2(X,v=11102) <-> CO2(X,v=00011) + CO2(X,v=12202) | CO2vib | 1, 35.9, -88., 233 |
CO2(X,v=01111) + CO2(X,v=11102) <-> CO2(X,v=00011) + CO2(X,v=20003) | CO2vib | 1, 35.9, -88., 233 |
CO2(X,v=01121) + CO2(X,v=00011) <-> CO2(X,v=00021) + CO2(X,v=01111) | CO2vib | 1, 34.1, -87.7, 230 |
CO2(X,v=01121) + CO2(X,v=01111) <-> CO2(X,v=00021) + CO2(X,v=02211) | CO2vib | 1, 34.8, -88., 233 |
CO2(X,v=01121) + CO2(X,v=01111) <-> CO2(X,v=00021) + CO2(X,v=10012) | CO2vib | 1, 34.8, -88., 233 |
CO2(X,v=01121) + CO2(X,v=02211) <-> CO2(X,v=00021) + CO2(X,v=03311) | CO2vib | 1, 35.2, -88., 233 |
CO2(X,v=01121) + CO2(X,v=02211) <-> CO2(X,v=00021) + CO2(X,v=11112) | CO2vib | 1, 35.2, -88., 233 |
CO2(X,v=01121) + CO2(X,v=03311) <-> CO2(X,v=00021) + CO2(X,v=04411) | CO2vib | 1, 35.2, -88., 233 |
CO2(X,v=01121) + CO2(X,v=10012) <-> CO2(X,v=00021) + CO2(X,v=11112) | CO2vib | 1, 35.5, -88., 233 |
CO2(X,v=01121) + CO2(X,v=11112) <-> CO2(X,v=00021) + CO2(X,v=12212) | CO2vib | 1, 35.9, -88., 233 |
CO2(X,v=01121) + CO2(X,v=11112) <-> CO2(X,v=00021) + CO2(X,v=20013) | CO2vib | 1, 35.9, -88., 233 |
CO2(X,v=01131) + CO2(X,v=00021) <-> CO2(X,v=00031) + CO2(X,v=01121) | CO2vib | 1, 34.1, -87.7, 230 |
CO2(X,v=01131) + CO2(X,v=01121) <-> CO2(X,v=00031) + CO2(X,v=02221) | CO2vib | 1, 34.8, -88., 233 |
CO2(X,v=01131) + CO2(X,v=01121) <-> CO2(X,v=00031) + CO2(X,v=10022) | CO2vib | 1, 34.8, -88., 233 |
CO2(X,v=01131) + CO2(X,v=02221) <-> CO2(X,v=00031) + CO2(X,v=03321) | CO2vib | 1, 35.2, -88., 233 |
CO2(X,v=01131) + CO2(X,v=02221) <-> CO2(X,v=00031) + CO2(X,v=11122) | CO2vib | 1, 35.2, -88., 233 |
CO2(X,v=01131) + CO2(X,v=03321) <-> CO2(X,v=00031) + CO2(X,v=04421) | CO2vib | 1, 35.2, -88., 233 |
CO2(X,v=01131) + CO2(X,v=10022) <-> CO2(X,v=00031) + CO2(X,v=11122) | CO2vib | 1, 35.5, -88., 233 |
CO2(X,v=01131) + CO2(X,v=11122) <-> CO2(X,v=00031) + CO2(X,v=12222) | CO2vib | 1, 35.9, -88., 233 |
CO2(X,v=01131) + CO2(X,v=11122) <-> CO2(X,v=00031) + CO2(X,v=20023) | CO2vib | 1, 35.9, -88., 233 |
CO2(X,v=01141) + CO2(X,v=00031) <-> CO2(X,v=00041) + CO2(X,v=01131) | CO2vib | 1, 34.1, -87.7, 230 |
CO2(X,v=01141) + CO2(X,v=01131) <-> CO2(X,v=00041) + CO2(X,v=02231) | CO2vib | 1, 34.8, -88., 233 |
CO2(X,v=01141) + CO2(X,v=01131) <-> CO2(X,v=00041) + CO2(X,v=10032) | CO2vib | 1, 34.8, -88., 233 |
CO2(X,v=01141) + CO2(X,v=02231) <-> CO2(X,v=00041) + CO2(X,v=03331) | CO2vib | 1, 35.2, -88., 233 |
CO2(X,v=01141) + CO2(X,v=02231) <-> CO2(X,v=00041) + CO2(X,v=11132) | CO2vib | 1, 35.2, -88., 233 |
CO2(X,v=01141) + CO2(X,v=03331) <-> CO2(X,v=00041) + CO2(X,v=04431) | CO2vib | 1, 35.2, -88., 233 |
CO2(X,v=01141) + CO2(X,v=10032) <-> CO2(X,v=00041) + CO2(X,v=11132) | CO2vib | 1, 35.5, -88., 233 |
CO2(X,v=01141) + CO2(X,v=11132) <-> CO2(X,v=00041) + CO2(X,v=12232) | CO2vib | 1, 35.9, -88., 233 |
CO2(X,v=01141) + CO2(X,v=11132) <-> CO2(X,v=00041) + CO2(X,v=20033) | CO2vib | 1, 35.9, -88., 233 |
CO2(X,v=01151) + CO2(X,v=00041) <-> CO2(X,v=00051) + CO2(X,v=01141) | CO2vib | 1, 34.1, -87.7, 230 |
CO2(X,v=01151) + CO2(X,v=01141) <-> CO2(X,v=00051) + CO2(X,v=02241) | CO2vib | 1, 34.8, -88., 233 |
CO2(X,v=01151) + CO2(X,v=01141) <-> CO2(X,v=00051) + CO2(X,v=10042) | CO2vib | 1, 34.8, -88., 233 |
CO2(X,v=01151) + CO2(X,v=02241) <-> CO2(X,v=00051) + CO2(X,v=03341) | CO2vib | 1, 35.2, -88., 233 |
CO2(X,v=01151) + CO2(X,v=02241) <-> CO2(X,v=00051) + CO2(X,v=11142) | CO2vib | 1, 35.2, -88., 233 |
CO2(X,v=01151) + CO2(X,v=03341) <-> CO2(X,v=00051) + CO2(X,v=04441) | CO2vib | 1, 35.2, -88., 233 |
CO2(X,v=01151) + CO2(X,v=10042) <-> CO2(X,v=00051) + CO2(X,v=11142) | CO2vib | 1, 35.5, -88., 233 |
CO2(X,v=01151) + CO2(X,v=11142) <-> CO2(X,v=00051) + CO2(X,v=12242) | CO2vib | 1, 35.9, -88., 233 |
CO2(X,v=01151) + CO2(X,v=11142) <-> CO2(X,v=00051) + CO2(X,v=20043) | CO2vib | 1, 35.9, -88., 233 |
CO2(X,v=02201) + CO2(X,v=00001) <-> CO2(X,v=01101) + CO2(X,v=01101) | CO2vib | 1, 34.8, -88., 233 |
CO2(X,v=02211) + CO2(X,v=00011) <-> CO2(X,v=01111) + CO2(X,v=01111) | CO2vib | 1, 34.8, -88., 233 |
CO2(X,v=02221) + CO2(X,v=00021) <-> CO2(X,v=01121) + CO2(X,v=01121) | CO2vib | 1, 34.8, -88., 233 |
CO2(X,v=02231) + CO2(X,v=00031) <-> CO2(X,v=01131) + CO2(X,v=01131) | CO2vib | 1, 34.8, -88., 233 |
CO2(X,v=02241) + CO2(X,v=00041) <-> CO2(X,v=01141) + CO2(X,v=01141) | CO2vib | 1, 34.8, -88., 233 |
CO2(X,v=02251) + CO2(X,v=00051) <-> CO2(X,v=01151) + CO2(X,v=01151) | CO2vib | 1, 34.8, -88., 233 |
CO2(X,v=03301) + CO2(X,v=00001) <-> CO2(X,v=02201) + CO2(X,v=01101) | CO2vib | 1, 35.9, -88., 233 |
CO2(X,v=03301) + CO2(X,v=01101) <-> CO2(X,v=02201) + CO2(X,v=02201) | CO2vib | 1, 35.9, -88., 233 |
CO2(X,v=03301) + CO2(X,v=01101) <-> CO2(X,v=02201) + CO2(X,v=10002) | CO2vib | 1, 35.9, -88., 233 |
CO2(X,v=03311) + CO2(X,v=00011) <-> CO2(X,v=02211) + CO2(X,v=01111) | CO2vib | 1, 35.9, -88., 233 |
CO2(X,v=03311) + CO2(X,v=01111) <-> CO2(X,v=02211) + CO2(X,v=02211) | CO2vib | 1, 35.9, -88., 233 |
CO2(X,v=03311) + CO2(X,v=01111) <-> CO2(X,v=02211) + CO2(X,v=10012) | CO2vib | 1, 35.9, -88., 233 |
CO2(X,v=03321) + CO2(X,v=00021) <-> CO2(X,v=02221) + CO2(X,v=01121) | CO2vib | 1, 35.9, -88., 233 |
CO2(X,v=03321) + CO2(X,v=01121) <-> CO2(X,v=02221) + CO2(X,v=02221) | CO2vib | 1, 35.9, -88., 233 |
CO2(X,v=03321) + CO2(X,v=01121) <-> CO2(X,v=02221) + CO2(X,v=10022) | CO2vib | 1, 35.9, -88., 233 |
CO2(X,v=03331) + CO2(X,v=00031) <-> CO2(X,v=02231) + CO2(X,v=01131) | CO2vib | 1, 35.9, -88., 233 |
CO2(X,v=03331) + CO2(X,v=01131) <-> CO2(X,v=02231) + CO2(X,v=02231) | CO2vib | 1, 35.9, -88., 233 |
CO2(X,v=03331) + CO2(X,v=01131) <-> CO2(X,v=02231) + CO2(X,v=10032) | CO2vib | 1, 35.9, -88., 233 |
CO2(X,v=03341) + CO2(X,v=00041) <-> CO2(X,v=02241) + CO2(X,v=01141) | CO2vib | 1, 35.9, -88., 233 |
CO2(X,v=03341) + CO2(X,v=01141) <-> CO2(X,v=02241) + CO2(X,v=02241) | CO2vib | 1, 35.9, -88., 233 |
CO2(X,v=03341) + CO2(X,v=01141) <-> CO2(X,v=02241) + CO2(X,v=10042) | CO2vib | 1, 35.9, -88., 233 |
CO2(X,v=03351) + CO2(X,v=00051) <-> CO2(X,v=02251) + CO2(X,v=01151) | CO2vib | 1, 35.9, -88., 233 |
CO2(X,v=03351) + CO2(X,v=01151) <-> CO2(X,v=02251) + CO2(X,v=02251) | CO2vib | 1, 35.9, -88., 233 |
CO2(X,v=03351) + CO2(X,v=01151) <-> CO2(X,v=02251) + CO2(X,v=10052) | CO2vib | 1, 35.9, -88., 233 |
CO2(X,v=04401) + CO2(X,v=00001) <-> CO2(X,v=03301) + CO2(X,v=01101) | CO2vib | 1, 35.5, -88., 233 |
CO2(X,v=04401) + CO2(X,v=01101) <-> CO2(X,v=03301) + CO2(X,v=02201) | CO2vib | 1, 36.2, -88., 233 |
CO2(X,v=04401) + CO2(X,v=01101) <-> CO2(X,v=03301) + CO2(X,v=10002) | CO2vib | 1, 36.2, -88., 233 |
CO2(X,v=04401) + CO2(X,v=02201) <-> CO2(X,v=03301) + CO2(X,v=03301) | CO2vib | 1, 36.6, -88., 233 |
CO2(X,v=04401) + CO2(X,v=02201) <-> CO2(X,v=03301) + CO2(X,v=11102) | CO2vib | 1, 36.6, -88., 233 |
CO2(X,v=04401) + CO2(X,v=10002) <-> CO2(X,v=03301) + CO2(X,v=11102) | CO2vib | 1, 36.9, -88., 234 |
CO2(X,v=04411) + CO2(X,v=00011) <-> CO2(X,v=03311) + CO2(X,v=01111) | CO2vib | 1, 35.5, -88., 233 |
CO2(X,v=04411) + CO2(X,v=01111) <-> CO2(X,v=03311) + CO2(X,v=02211) | CO2vib | 1, 36.2, -88., 233 |
CO2(X,v=04411) + CO2(X,v=01111) <-> CO2(X,v=03311) + CO2(X,v=10012) | CO2vib | 1, 36.2, -88., 233 |
CO2(X,v=04411) + CO2(X,v=02211) <-> CO2(X,v=03311) + CO2(X,v=03311) | CO2vib | 1, 36.6, -88., 233 |
CO2(X,v=04411) + CO2(X,v=02211) <-> CO2(X,v=03311) + CO2(X,v=11112) | CO2vib | 1, 36.6, -88., 233 |
CO2(X,v=04411) + CO2(X,v=10012) <-> CO2(X,v=03311) + CO2(X,v=11112) | CO2vib | 1, 36.9, -88., 234 |
CO2(X,v=04421) + CO2(X,v=00021) <-> CO2(X,v=03321) + CO2(X,v=01121) | CO2vib | 1, 35.5, -88., 233 |
CO2(X,v=04421) + CO2(X,v=01121) <-> CO2(X,v=03321) + CO2(X,v=02221) | CO2vib | 1, 36.2, -88., 233 |
CO2(X,v=04421) + CO2(X,v=01121) <-> CO2(X,v=03321) + CO2(X,v=10022) | CO2vib | 1, 36.2, -88., 233 |
CO2(X,v=04421) + CO2(X,v=02221) <-> CO2(X,v=03321) + CO2(X,v=03321) | CO2vib | 1, 36.6, -88., 233 |
CO2(X,v=04421) + CO2(X,v=02221) <-> CO2(X,v=03321) + CO2(X,v=11122) | CO2vib | 1, 36.6, -88., 233 |
CO2(X,v=04421) + CO2(X,v=10022) <-> CO2(X,v=03321) + CO2(X,v=11122) | CO2vib | 1, 36.9, -88., 234 |
CO2(X,v=04431) + CO2(X,v=00031) <-> CO2(X,v=03331) + CO2(X,v=01131) | CO2vib | 1, 35.5, -88., 233 |
CO2(X,v=04431) + CO2(X,v=01131) <-> CO2(X,v=03331) + CO2(X,v=02231) | CO2vib | 1, 36.2, -88., 233 |
CO2(X,v=04431) + CO2(X,v=01131) <-> CO2(X,v=03331) + CO2(X,v=10032) | CO2vib | 1, 36.2, -88., 233 |
CO2(X,v=04431) + CO2(X,v=02231) <-> CO2(X,v=03331) + CO2(X,v=03331) | CO2vib | 1, 36.6, -88., 233 |
CO2(X,v=04431) + CO2(X,v=02231) <-> CO2(X,v=03331) + CO2(X,v=11132) | CO2vib | 1, 36.6, -88., 233 |
```

```
CO2(X,v=04431) + CO2(X,v=10032) <-> CO2(X,v=03331) + CO2(X,v=11132) | CO2vib | 1, 36.9, -88., 234 |
CO2(X,v=04441) + CO2(X,v=00041) <-> CO2(X,v=03341) + CO2(X,v=01141) | CO2vib | 1, 35.5, -88., 233 |
CO2(X,v=04441) + CO2(X,v=01141) <-> CO2(X,v=03341) + CO2(X,v=02241) | CO2vib | 1, 36.2, -88., 233 |
CO2(X,v=04441) + CO2(X,v=01141) <-> CO2(X,v=03341) + CO2(X,v=10042) | CO2vib | 1, 36.2, -88., 233 |
CO2(X,v=04441) + CO2(X,v=02241) <-> CO2(X,v=03341) + CO2(X,v=03341) | CO2vib | 1, 36.6, -88., 233 |
CO2(X,v=04441) + CO2(X,v=02241) <-> CO2(X,v=03341) + CO2(X,v=11142) | CO2vib | 1, 36.6, -88., 233 |
CO2(X,v=04441) + CO2(X,v=10042) <-> CO2(X,v=03341) + CO2(X,v=11142) | CO2vib | 1, 36.9, -88., 234 |
CO2(X,v=04451) + CO2(X,v=00051) <-> CO2(X,v=03351) + CO2(X,v=01151) | CO2vib | 1, 35.5, -88., 233 |
CO2(X,v=04451) + CO2(X,v=01151) <-> CO2(X,v=03351) + CO2(X,v=02251) | CO2vib | 1, 36.2, -88., 233 |
CO2(X,v=04451) + CO2(X,v=01151) <-> CO2(X,v=03351) + CO2(X,v=10052) | CO2vib | 1, 36.2, -88., 233 |
CO2(X,v=04451) + CO2(X,v=02251) <-> CO2(X,v=03351) + CO2(X,v=03351) | CO2vib | 1, 36.6, -88., 233 |
CO2(X,v=04451) + CO2(X,v=02251) <-> CO2(X,v=03351) + CO2(X,v=11152) | CO2vib | 1, 36.6, -88., 233 |
CO2(X,v=04451) + CO2(X,v=10052) <-> CO2(X,v=03351) + CO2(X,v=11152) | CO2vib | 1, 36.9, -88., 234 |
CO2(X,v=05501) + CO2(X,v=00001) <-> CO2(X,v=04401) + CO2(X,v=01101) | CO2vib | 1, 35.7, -88., 233 |
CO2(X,v=05501) + CO2(X,v=01101) <-> CO2(X,v=04401) + CO2(X,v=02201) | CO2vib | 1, 36.4, -88., 233 |
CO2(X,v=05501) + CO2(X,v=01101) <-> CO2(X,v=04401) + CO2(X,v=10002) | CO2vib | 1, 36.4, -88., 233 |
CO2(X,v=05501) + CO2(X,v=02201) <-> CO2(X,v=04401) + CO2(X,v=03301) | CO2vib | 1, 36.9, -88., 233 |
CO2(X,v=05501) + CO2(X,v=02201) <-> CO2(X,v=04401) + CO2(X,v=11102) | CO2vib | 1, 36.3, -88., 233 |
CO2(X,v=05501) + CO2(X,v=10002) <-> CO2(X,v=04401) + CO2(X,v=11102) | CO2vib | 1, 37.1, -88., 233 |
CO2(X,v=05511) + CO2(X,v=00011) <-> CO2(X,v=04411) + CO2(X,v=01111) | CO2vib | 1, 35.7, -88., 233 |
CO2(X,v=05511) + CO2(X,v=01111) <-> CO2(X,v=04411) + CO2(X,v=02211) | CO2vib | 1, 36.4, -88., 233 |
CO2(X,v=05511) + CO2(X,v=01111) <-> CO2(X,v=04411) + CO2(X,v=10012) | CO2vib | 1, 36.4, -88., 233 |
CO2(X,v=05511) + CO2(X,v=02211) <-> CO2(X,v=04411) + CO2(X,v=03311) | CO2vib | 1, 36.9, -88., 233 |
CO2(X,v=05511) + CO2(X,v=02211) <-> CO2(X,v=04411) + CO2(X,v=11112) | CO2vib | 1, 36.3, -88., 233 |
CO2(X,v=05511) + CO2(X,v=10012) <-> CO2(X,v=04411) + CO2(X,v=11112) | CO2vib | 1, 37.1, -88., 233 |
CO2(X,v=05521) + CO2(X,v=00021) <-> CO2(X,v=04421) + CO2(X,v=01121) | CO2vib | 1, 35.7, -88., 233 |
CO2(X,v=05521) + CO2(X,v=01121) <-> CO2(X,v=04421) + CO2(X,v=02221) | CO2vib | 1, 36.4, -88., 233 |
CO2(X,v=05521) + CO2(X,v=01121) <-> CO2(X,v=04421) + CO2(X,v=10022) | CO2vib | 1, 36.4, -88., 233 |
CO2(X,v=05521) + CO2(X,v=02221) <-> CO2(X,v=04421) + CO2(X,v=03321) | CO2vib | 1, 36.9, -88., 233 |
CO2(X,v=05521) + CO2(X,v=02221) <-> CO2(X,v=04421) + CO2(X,v=11122) | CO2vib | 1, 36.3, -88., 233 |
CO2(X,v=05521) + CO2(X,v=10022) <-> CO2(X,v=04421) + CO2(X,v=11122) | CO2vib | 1, 37.1, -88., 233 |
CO2(X,v=05531) + CO2(X,v=00031) <-> CO2(X,v=04431) + CO2(X,v=01131) | CO2vib | 1, 35.7, -88., 233 |
CO2(X,v=05531) + CO2(X,v=01131) <-> CO2(X,v=04431) + CO2(X,v=02231) | CO2vib | 1, 36.4, -88., 233 |
CO2(X,v=05531) + CO2(X,v=01131) <-> CO2(X,v=04431) + CO2(X,v=10032) | CO2vib | 1, 36.4, -88., 233 |
CO2(X,v=05531) + CO2(X,v=02231) <-> CO2(X,v=04431) + CO2(X,v=03331) | CO2vib | 1, 36.9, -88., 233 |
CO2(X,v=05531) + CO2(X,v=02231) <-> CO2(X,v=04431) + CO2(X,v=11132) | CO2vib | 1, 36.3, -88., 233 |
CO2(X,v=05531) + CO2(X,v=10032) <-> CO2(X,v=04431) + CO2(X,v=11132) | CO2vib | 1, 37.1, -88., 233 |
CO2(X,v=05541) + CO2(X,v=00041) <-> CO2(X,v=04441) + CO2(X,v=01141) | CO2vib | 1, 35.7, -88., 233 |
CO2(X,v=05541) + CO2(X,v=01141) <-> CO2(X,v=04441) + CO2(X,v=02241) | CO2vib | 1, 36.4, -88., 233 |
CO2(X,v=05541) + CO2(X,v=01141) <-> CO2(X,v=04441) + CO2(X,v=10042) | CO2vib | 1, 36.4, -88., 233 |
CO2(X,v=05541) + CO2(X,v=02241) <-> CO2(X,v=04441) + CO2(X,v=03341) | CO2vib | 1, 36.9, -88., 233 |
CO2(X,v=05541) + CO2(X,v=02241) <-> CO2(X,v=04441) + CO2(X,v=11142) | CO2vib | 1, 36.3, -88., 233 |
CO2(X,v=05541) + CO2(X,v=10042) <-> CO2(X,v=04441) + CO2(X,v=11142) | CO2vib | 1, 37.1, -88., 233 |
CO2(X,v=05551) + CO2(X,v=00051) <-> CO2(X,v=04451) + CO2(X,v=01151) | CO2vib | 1, 35.7, -88., 233 |
CO2(X,v=05551) + CO2(X,v=01151) <-> CO2(X,v=04451) + CO2(X,v=02251) | CO2vib | 1, 36.4, -88., 233 |
CO2(X,v=05551) + CO2(X,v=01151) <-> CO2(X,v=04451) + CO2(X,v=10052) | CO2vib | 1, 36.4, -88., 233 |
CO2(X,v=05551) + CO2(X,v=02251) <-> CO2(X,v=04451) + CO2(X,v=03351) | CO2vib | 1, 36.9, -88., 233 |
CO2(X,v=05551) + CO2(X,v=02251) <-> CO2(X,v=04451) + CO2(X,v=11152) | CO2vib | 1, 36.3, -88., 233 |
CO2(X,v=05551) + CO2(X,v=10052) <-> CO2(X,v=04451) + CO2(X,v=11152) | CO2vib | 1, 37.1, -88., 233 |
CO2(X,v=10002) + CO2(X,v=00001) <-> CO2(X,v=01101) + CO2(X,v=01101) | CO2vib | 1, 34.8, -88., 233 |
CO2(X,v=10002) + CO2(X,v=01101) <-> CO2(X,v=01101) + CO2(X,v=02201) | CO2vib | 1, 35.5, -88., 233 |
CO2(X,v=10012) + CO2(X,v=00011) <-> CO2(X,v=01111) + CO2(X,v=01111) | CO2vib | 1, 34.8, -88., 233 |
CO2(X,v=10012) + CO2(X,v=01111) <-> CO2(X,v=01111) + CO2(X,v=02211) | CO2vib | 1, 35.5, -88., 233 |
CO2(X,v=10022) + CO2(X,v=00021) <-> CO2(X,v=01121) + CO2(X,v=01121) | CO2vib | 1, 34.8, -88., 233 |
CO2(X,v=10022) + CO2(X,v=01121) <-> CO2(X,v=01121) + CO2(X,v=02221) | CO2vib | 1, 35.5, -88., 233 |
CO2(X,v=10032) + CO2(X,v=00031) <-> CO2(X,v=01131) + CO2(X,v=01131) | CO2vib | 1, 34.8, -88., 233 |
CO2(X,v=10032) + CO2(X,v=01131) <-> CO2(X,v=01131) + CO2(X,v=02231) | CO2vib | 1, 35.5, -88., 233 |
CO2(X,v=10042) + CO2(X,v=00041) <-> CO2(X,v=01141) + CO2(X,v=01141) | CO2vib | 1, 34.8, -88., 233 |
CO2(X,v=10042) + CO2(X,v=01141) <-> CO2(X,v=01141) + CO2(X,v=02241) | CO2vib | 1, 35.5, -88., 233 |
CO2(X,v=10052) + CO2(X,v=00051) <-> CO2(X,v=01151) + CO2(X,v=01151) | CO2vib | 1, 34.8, -88., 233 |
CO2(X,v=10052) + CO2(X,v=01151) <-> CO2(X,v=01151) + CO2(X,v=02251) | CO2vib | 1, 35.5, -88., 233 |
CO2(X,v=11102) + CO2(X,v=00001) <-> CO2(X,v=02201) + CO2(X,v=01101) | CO2vib | 1, 35.2, -88., 233 |
CO2(X,v=11102) + CO2(X,v=00001) <-> CO2(X,v=10002) + CO2(X,v=01101) | CO2vib | 1, 35.7, -88.2, 233 |
CO2(X,v=11102) + CO2(X,v=01101) <-> CO2(X,v=02201) + CO2(X,v=02201) | CO2vib | 1, 35.9, -88., 233 |
CO2(X,v=11102) + CO2(X,v=01101) <-> CO2(X,v=10002) + CO2(X,v=02201) | CO2vib | 1, 36.2, -88., 233 |
CO2(X,v=11102) + CO2(X,v=01101) <-> CO2(X,v=10002) + CO2(X,v=10002) | CO2vib | 1, 35.7, -88., 233 |
CO2(X,v=11102) + CO2(X,v=02201) <-> CO2(X,v=02201) + CO2(X,v=03301) | CO2vib | 1, 36.3, -88., 233 |
CO2(X,v=11102) + CO2(X,v=02201) <-> CO2(X,v=10002) + CO2(X,v=11102) | CO2vib | 1, 36.6, -88., 233 |
CO2(X,v=11102) + CO2(X,v=10002) <-> CO2(X,v=02201) + CO2(X,v=11102) | CO2vib | 1, 36.3, -88., 233 |
CO2(X,v=11102) + CO2(X,v=10002) <-> CO2(X,v=10002) + CO2(X,v=03301) | CO2vib | 1, 36.6, -88., 233 |
CO2(X,v=11112) + CO2(X,v=00011) <-> CO2(X,v=02211) + CO2(X,v=01111) | CO2vib | 1, 35.2, -88., 233 |
CO2(X,v=11112) + CO2(X,v=00011) <-> CO2(X,v=10012) + CO2(X,v=01111) | CO2vib | 1, 35.7, -88.2, 233 |
CO2(X,v=11112) + CO2(X,v=01111) <-> CO2(X,v=02211) + CO2(X,v=02211) | CO2vib | 1, 35.9, -88., 233 |
CO2(X,v=11112) + CO2(X,v=01111) <-> CO2(X,v=10012) + CO2(X,v=02211) | CO2vib | 1, 36.2, -88., 233 |
CO2(X,v=11112) + CO2(X,v=01111) <-> CO2(X,v=10012) + CO2(X,v=10012) | CO2vib | 1, 35.7, -88., 233 |
CO2(X,v=11112) + CO2(X,v=02211) <-> CO2(X,v=02211) + CO2(X,v=03311) | CO2vib | 1, 36.3, -88., 233 |
CO2(X,v=11112) + CO2(X,v=02211) <-> CO2(X,v=10012) + CO2(X,v=11112) | CO2vib | 1, 36.6, -88., 233 |
CO2(X,v=11112) + CO2(X,v=10012) <-> CO2(X,v=02211) + CO2(X,v=11112) | CO2vib | 1, 36.3, -88., 233 |
CO2(X,v=11112) + CO2(X,v=10012) <-> CO2(X,v=10012) + CO2(X,v=03311) | CO2vib | 1, 36.6, -88., 233 |
CO2(X,v=11122) + CO2(X,v=00021) <-> CO2(X,v=02221) + CO2(X,v=01121) | CO2vib | 1, 35.2, -88., 233 |
CO2(X,v=11122) + CO2(X,v=00021) <-> CO2(X,v=10022) + CO2(X,v=01121) | CO2vib | 1, 35.7, -88.2, 233 |
CO2(X,v=11122) + CO2(X,v=01121) <-> CO2(X,v=02221) + CO2(X,v=02221) | CO2vib | 1, 35.9, -88., 233 |
CO2(X,v=11122) + CO2(X,v=01121) <-> CO2(X,v=10022) + CO2(X,v=02221) | CO2vib | 1, 36.2, -88., 233 |
CO2(X,v=11122) + CO2(X,v=01121) <-> CO2(X,v=10022) + CO2(X,v=10022) | CO2vib | 1, 35.7, -88., 233 |
CO2(X,v=11122) + CO2(X,v=02221) <-> CO2(X,v=02221) + CO2(X,v=03321) | CO2vib | 1, 36.3, -88., 233 |
CO2(X,v=11122) + CO2(X,v=02221) <-> CO2(X,v=10022) + CO2(X,v=11122) | CO2vib | 1, 36.6, -88., 233 |
CO2(X,v=11122) + CO2(X,v=10022) <-> CO2(X,v=02221) + CO2(X,v=11122) | CO2vib | 1, 36.3, -88., 233 |
CO2(X,v=11122) + CO2(X,v=10022) <-> CO2(X,v=10022) + CO2(X,v=03321) | CO2vib | 1, 36.6, -88., 233 |
CO2(X,v=11132) + CO2(X,v=00031) <-> CO2(X,v=02231) + CO2(X,v=01131) | CO2vib | 1, 35.2, -88., 233 |
CO2(X,v=11132) + CO2(X,v=00031) <-> CO2(X,v=10032) + CO2(X,v=01131) | CO2vib | 1, 35.7, -88.2, 233 |
CO2(X,v=11132) + CO2(X,v=01131) <-> CO2(X,v=02231) + CO2(X,v=02231) | CO2vib | 1, 35.9, -88., 233 |
CO2(X,v=11132) + CO2(X,v=01131) <-> CO2(X,v=10032) + CO2(X,v=02231) | CO2vib | 1, 36.2, -88., 233 |
CO2(X,v=11132) + CO2(X,v=01131) <-> CO2(X,v=10032) + CO2(X,v=10032) | CO2vib | 1, 35.7, -88., 233 |
CO2(X,v=11132) + CO2(X,v=02231) <-> CO2(X,v=02231) + CO2(X,v=03331) | CO2vib | 1, 36.3, -88., 233 |
```

```
CO2(X,v=11132) + CO2(X,v=02231) <-> CO2(X,v=10032) + CO2(X,v=11132) | CO2vib | 1, 36.6, -88., 233 |
CO2(X,v=11132) + CO2(X,v=10032) <-> CO2(X,v=02231) + CO2(X,v=11132) | CO2vib | 1, 36.3, -88., 233 |
CO2(X,v=11132) + CO2(X,v=10032) <-> CO2(X,v=10032) + CO2(X,v=03331) | CO2vib | 1, 36.6, -88., 233 |
CO2(X,v=11142) + CO2(X,v=00041) <-> CO2(X,v=02241) + CO2(X,v=01141) | CO2vib | 1, 35.2, -88., 233 |
CO2(X,v=11142) + CO2(X,v=00041) <-> CO2(X,v=10042) + CO2(X,v=01141) | CO2vib | 1, 35.7, -88.2, 233 |
CO2(X,v=11142) + CO2(X,v=01141) <-> CO2(X,v=02241) + CO2(X,v=02241) | CO2vib | 1, 35.9, -88., 233 |
CO2(X,v=11142) + CO2(X,v=01141) <-> CO2(X,v=10042) + CO2(X,v=02241) | CO2vib | 1, 36.2, -88., 233 |
CO2(X,v=11142) + CO2(X,v=01141) <-> CO2(X,v=10042) + CO2(X,v=10042) | CO2vib | 1, 35.7, -88., 233 |
CO2(X,v=11142) + CO2(X,v=02241) <-> CO2(X,v=02241) + CO2(X,v=03341) | CO2vib | 1, 36.3, -88., 233 |
CO2(X,v=11142) + CO2(X,v=02241) <-> CO2(X,v=10042) + CO2(X,v=11142) | CO2vib | 1, 36.6, -88., 233 |
CO2(X,v=11142) + CO2(X,v=10042) <-> CO2(X,v=02241) + CO2(X,v=11142) | CO2vib | 1, 36.3, -88., 233 |
CO2(X,v=11142) + CO2(X,v=10042) <-> CO2(X,v=10042) + CO2(X,v=03341) | CO2vib | 1, 36.6, -88., 233 |
CO2(X,v=11152) + CO2(X,v=00051) <-> CO2(X,v=02251) + CO2(X,v=01151) | CO2vib | 1, 35.2, -88., 233 |
CO2(X,v=11152) + CO2(X,v=00051) <-> CO2(X,v=10052) + CO2(X,v=01151) | CO2vib | 1, 35.7, -88.2, 233 |
CO2(X,v=11152) + CO2(X,v=01151) <-> CO2(X,v=02251) + CO2(X,v=02251) | CO2vib | 1, 35.9, -88., 233 |
CO2(X,v=11152) + CO2(X,v=01151) <-> CO2(X,v=10052) + CO2(X,v=02251) | CO2vib | 1, 36.2, -88., 233 |
CO2(X,v=11152) + CO2(X,v=01151) <-> CO2(X,v=10052) + CO2(X,v=10052) | CO2vib | 1, 35.7, -88., 233 |
CO2(X,v=11152) + CO2(X,v=02251) <-> CO2(X,v=02251) + CO2(X,v=03351) | CO2vib | 1, 36.3, -88., 233 |
CO2(X,v=11152) + CO2(X,v=02251) <-> CO2(X,v=10052) + CO2(X,v=11152) | CO2vib | 1, 36.6, -88., 233 |
CO2(X,v=11152) + CO2(X,v=10052) <-> CO2(X,v=02251) + CO2(X,v=11152) | CO2vib | 1, 36.3, -88., 233 |
CO2(X,v=11152) + CO2(X,v=10052) <-> CO2(X,v=10052) + CO2(X,v=03351) | CO2vib | 1, 36.6, -88., 233 |
CO2(X,v=12202) + CO2(X,v=00001) <-> CO2(X,v=02201) + CO2(X,v=10002) | CO2vib | 1, 33.8, -88., 233 |
CO2(X,v=12202) + CO2(X,v=00001) <-> CO2(X,v=03301) + CO2(X,v=01101) | CO2vib | 1, 35.5, -88., 233 |
CO2(X,v=12202) + CO2(X,v=00001) <-> CO2(X,v=11102) + CO2(X,v=01101) | CO2vib | 1, 35.9, -88., 233 |
CO2(X,v=12202) + CO2(X,v=01101) <-> CO2(X,v=11102) + CO2(X,v=02201) | CO2vib | 1, 36.6, -88., 233 |
CO2(X,v=12202) + CO2(X,v=01101) <-> CO2(X,v=11102) + CO2(X,v=10002) | CO2vib | 1, 36.6, -88., 233 |
CO2(X,v=12202) + CO2(X,v=02201) <-> CO2(X,v=03301) + CO2(X,v=03301) | CO2vib | 1, 36.6, -88., 233 |
CO2(X,v=12202) + CO2(X,v=02201) <-> CO2(X,v=11102) + CO2(X,v=03301) | CO2vib | 1, 37.5, -88., 233 |
CO2(X,v=12202) + CO2(X,v=02201) <-> CO2(X,v=11102) + CO2(X,v=11102) | CO2vib | 1, 37., -88., 233 |
CO2(X,v=12202) + CO2(X,v=03301) <-> CO2(X,v=03301) + CO2(X,v=04401) | CO2vib | 1, 36.9, -88., 233 |
CO2(X,v=12202) + CO2(X,v=03301) <-> CO2(X,v=11102) + CO2(X,v=04401) | CO2vib | 1, 37.3, -88., 23 |
CO2(X,v=12202) + CO2(X,v=03301) <-> CO2(X,v=11102) + CO2(X,v=12202) | CO2vib | 1, 37.3, -88., 233 |
CO2(X,v=12202) + CO2(X,v=10002) <-> CO2(X,v=02201) + CO2(X,v=20003) | CO2vib | 1, 34.9, -89., 234 |
CO2(X,v=12202) + CO2(X,v=10002) <-> CO2(X,v=03301) + CO2(X,v=11102) | CO2vib | 1, 36.9, -88., 233 |
CO2(X,v=12202) + CO2(X,v=10002) <-> CO2(X,v=11102) + CO2(X,v=11102) | CO2vib | 1, 37.3, -88., 233 |
CO2(X,v=12202) + CO2(X,v=11102) <-> CO2(X,v=03301) + CO2(X,v=12202) | CO2vib | 1, 37.3, -88., 233 |
CO2(X,v=12202) + CO2(X,v=11102) <-> CO2(X,v=03301) + CO2(X,v=20003) | CO2vib | 1, 37.3, -88., 233 |
CO2(X,v=12212) + CO2(X,v=00011) <-> CO2(X,v=02211) + CO2(X,v=10012) | CO2vib | 1, 33.8, -88., 233 |
CO2(X,v=12212) + CO2(X,v=00011) <-> CO2(X,v=03311) + CO2(X,v=01111) | CO2vib | 1, 35.5, -88., 233 |
CO2(X,v=12212) + CO2(X,v=00011) <-> CO2(X,v=11112) + CO2(X,v=01111) | CO2vib | 1, 35.9, -88., 233 |
CO2(X,v=12212) + CO2(X,v=01111) <-> CO2(X,v=11112) + CO2(X,v=02211) | CO2vib | 1, 36.6, -88., 233 |
CO2(X,v=12212) + CO2(X,v=01111) <-> CO2(X,v=11112) + CO2(X,v=10012) | CO2vib | 1, 36.6, -88., 233 |
CO2(X,v=12212) + CO2(X,v=02211) <-> CO2(X,v=03311) + CO2(X,v=03311) | CO2vib | 1, 36.6, -88., 233 |
CO2(X,v=12212) + CO2(X,v=02211) <-> CO2(X,v=11112) + CO2(X,v=03311) | CO2vib | 1, 37.5, -88., 233 |
CO2(X,v=12212) + CO2(X,v=02211) <-> CO2(X,v=11112) + CO2(X,v=11112) | CO2vib | 1, 37., -88., 233 |
CO2(X,v=12212) + CO2(X,v=03311) <-> CO2(X,v=03311) + CO2(X,v=04411) | CO2vib | 1, 36.9, -88., 233 |
CO2(X,v=12212) + CO2(X,v=03311) <-> CO2(X,v=11112) + CO2(X,v=04411) | CO2vib | 1, 37.3, -88., 23 |
CO2(X,v=12212) + CO2(X,v=03311) <-> CO2(X,v=11112) + CO2(X,v=12212) | CO2vib | 1, 37.3, -88., 233 |
CO2(X,v=12212) + CO2(X,v=10012) <-> CO2(X,v=02211) + CO2(X,v=20013) | CO2vib | 1, 34.9, -89., 234 |
CO2(X,v=12212) + CO2(X,v=10012) <-> CO2(X,v=03311) + CO2(X,v=11112) | CO2vib | 1, 36.9, -88., 233 |
CO2(X,v=12212) + CO2(X,v=10012) <-> CO2(X,v=11112) + CO2(X,v=11112) | CO2vib | 1, 37.3, -88., 233 |
CO2(X,v=12212) + CO2(X,v=11112) <-> CO2(X,v=03311) + CO2(X,v=12212) | CO2vib | 1, 37.3, -88., 233 |
CO2(X,v=12212) + CO2(X,v=11112) <-> CO2(X,v=03311) + CO2(X,v=20013) | CO2vib | 1, 37.3, -88., 233 |
CO2(X,v=12222) + CO2(X,v=00021) <-> CO2(X,v=02221) + CO2(X,v=10022) | CO2vib | 1, 33.8, -88., 233 |
CO2(X,v=12222) + CO2(X,v=00021) <-> CO2(X,v=03321) + CO2(X,v=01121) | CO2vib | 1, 35.5, -88., 233 |
CO2(X,v=12222) + CO2(X,v=00021) <-> CO2(X,v=11122) + CO2(X,v=01121) | CO2vib | 1, 35.9, -88., 233 |
CO2(X,v=12222) + CO2(X,v=01121) <-> CO2(X,v=11122) + CO2(X,v=02221) | CO2vib | 1, 36.6, -88., 233 |
CO2(X,v=12222) + CO2(X,v=01121) <-> CO2(X,v=11122) + CO2(X,v=10022) | CO2vib | 1, 36.6, -88., 233 |
CO2(X,v=12222) + CO2(X,v=02221) <-> CO2(X,v=03321) + CO2(X,v=03321) | CO2vib | 1, 36.6, -88., 233 |
CO2(X,v=12222) + CO2(X,v=02221) <-> CO2(X,v=11122) + CO2(X,v=03321) | CO2vib | 1, 37.5, -88., 233 |
CO2(X,v=12222) + CO2(X,v=02221) <-> CO2(X,v=11122) + CO2(X,v=11122) | CO2vib | 1, 37., -88., 233 |
CO2(X,v=12222) + CO2(X,v=03321) <-> CO2(X,v=03321) + CO2(X,v=04421) | CO2vib | 1, 36.9, -88., 233 |
CO2(X,v=12222) + CO2(X,v=03321) <-> CO2(X,v=11122) + CO2(X,v=04421) | CO2vib | 1, 37.3, -88., 23 |
CO2(X,v=12222) + CO2(X,v=03321) <-> CO2(X,v=11122) + CO2(X,v=12222) | CO2vib | 1, 37.3, -88., 233 |
CO2(X,v=12222) + CO2(X,v=10022) <-> CO2(X,v=02221) + CO2(X,v=20023) | CO2vib | 1, 34.9, -89., 234 |
CO2(X,v=12222) + CO2(X,v=10022) <-> CO2(X,v=03321) + CO2(X,v=11122) | CO2vib | 1, 36.9, -88., 233 |
CO2(X,v=12222) + CO2(X,v=10022) <-> CO2(X,v=11122) + CO2(X,v=11122) | CO2vib | 1, 37.3, -88., 233 |
CO2(X,v=12222) + CO2(X,v=11122) <-> CO2(X,v=03321) + CO2(X,v=12222) | CO2vib | 1, 37.3, -88., 233 |
CO2(X,v=12222) + CO2(X,v=11122) <-> CO2(X,v=03321) + CO2(X,v=20023) | CO2vib | 1, 37.3, -88., 233 |
CO2(X,v=12232) + CO2(X,v=00031) <-> CO2(X,v=02231) + CO2(X,v=10032) | CO2vib | 1, 33.8, -88., 233 |
CO2(X,v=12232) + CO2(X,v=00031) <-> CO2(X,v=03331) + CO2(X,v=01131) | CO2vib | 1, 35.5, -88., 233 |
CO2(X,v=12232) + CO2(X,v=00031) <-> CO2(X,v=11132) + CO2(X,v=01131) | CO2vib | 1, 35.9, -88., 233 |
CO2(X,v=12232) + CO2(X,v=01131) <-> CO2(X,v=11132) + CO2(X,v=02231) | CO2vib | 1, 36.6, -88., 233 |
CO2(X,v=12232) + CO2(X,v=01131) <-> CO2(X,v=11132) + CO2(X,v=10032) | CO2vib | 1, 36.6, -88., 233 |
CO2(X,v=12232) + CO2(X,v=02231) <-> CO2(X,v=03331) + CO2(X,v=03331) | CO2vib | 1, 36.6, -88., 233 |
CO2(X,v=12232) + CO2(X,v=02231) <-> CO2(X,v=11132) + CO2(X,v=03331) | CO2vib | 1, 37.5, -88., 233 |
CO2(X,v=12232) + CO2(X,v=02231) <-> CO2(X,v=11132) + CO2(X,v=11132) | CO2vib | 1, 37., -88., 233 |
CO2(X,v=12232) + CO2(X,v=03331) <-> CO2(X,v=03331) + CO2(X,v=04431) | CO2vib | 1, 36.9, -88., 233 |
CO2(X,v=12232) + CO2(X,v=03331) <-> CO2(X,v=11132) + CO2(X,v=04431) | CO2vib | 1, 37.3, -88., 23 |
CO2(X,v=12232) + CO2(X,v=03331) <-> CO2(X,v=11132) + CO2(X,v=12232) | CO2vib | 1, 37.3, -88., 233 |
CO2(X,v=12232) + CO2(X,v=10032) <-> CO2(X,v=02231) + CO2(X,v=20033) | CO2vib | 1, 34.9, -89., 234 |
CO2(X,v=12232) + CO2(X,v=10032) <-> CO2(X,v=03331) + CO2(X,v=11132) | CO2vib | 1, 36.9, -88., 233 |
CO2(X,v=12232) + CO2(X,v=10032) <-> CO2(X,v=11132) + CO2(X,v=11132) | CO2vib | 1, 37.3, -88., 233 |
CO2(X,v=12232) + CO2(X,v=11132) <-> CO2(X,v=03331) + CO2(X,v=12232) | CO2vib | 1, 37.3, -88., 233 |
CO2(X,v=12232) + CO2(X,v=11132) <-> CO2(X,v=03331) + CO2(X,v=20033) | CO2vib | 1, 37.3, -88., 233 |
CO2(X,v=12242) + CO2(X,v=00041) <-> CO2(X,v=02241) + CO2(X,v=10042) | CO2vib | 1, 33.8, -88., 233 |
CO2(X,v=12242) + CO2(X,v=00041) <-> CO2(X,v=03341) + CO2(X,v=01141) | CO2vib | 1, 35.5, -88., 233 |
CO2(X,v=12242) + CO2(X,v=00041) <-> CO2(X,v=11142) + CO2(X,v=01141) | CO2vib | 1, 35.9, -88., 233 |
CO2(X,v=12242) + CO2(X,v=01141) <-> CO2(X,v=11142) + CO2(X,v=02241) | CO2vib | 1, 36.6, -88., 233 |
CO2(X,v=12242) + CO2(X,v=01141) <-> CO2(X,v=11142) + CO2(X,v=10042) | CO2vib | 1, 36.6, -88., 233 |
CO2(X,v=12242) + CO2(X,v=02241) <-> CO2(X,v=03341) + CO2(X,v=03341) | CO2vib | 1, 36.6, -88., 233 |
CO2(X,v=12242) + CO2(X,v=02241) <-> CO2(X,v=11142) + CO2(X,v=03341) | CO2vib | 1, 37.5, -88., 233 |
CO2(X,v=12242) + CO2(X,v=02241) <-> CO2(X,v=11142) + CO2(X,v=11142) | CO2vib | 1, 37., -88., 233 |
CO2(X,v=12242) + CO2(X,v=03341) <-> CO2(X,v=03341) + CO2(X,v=04441) | CO2vib | 1, 36.9, -88., 233 |
```

```
CO2(X,v=12242) + CO2(X,v=03341) <-> CO2(X,v=11142) + CO2(X,v=04441) | CO2vib | 1, 37.3, -88., 23 |
CO2(X,v=12242) + CO2(X,v=03341) <-> CO2(X,v=11142) + CO2(X,v=12242) | CO2vib | 1, 37.3, -88., 233 |
CO2(X,v=12242) + CO2(X,v=10042) <-> CO2(X,v=02241) + CO2(X,v=20043) | CO2vib | 1, 34.9, -89., 234 |
CO2(X,v=12242) + CO2(X,v=10042) <-> CO2(X,v=03341) + CO2(X,v=11142) | CO2vib | 1, 36.9, -88., 233 |
CO2(X,v=12242) + CO2(X,v=10042) <-> CO2(X,v=11142) + CO2(X,v=11142) | CO2vib | 1, 37.3, -88., 233 |
CO2(X,v=12242) + CO2(X,v=11142) <-> CO2(X,v=03341) + CO2(X,v=12242) | CO2vib | 1, 37.3, -88., 233 |
CO2(X,v=12242) + CO2(X,v=11142) <-> CO2(X,v=03341) + CO2(X,v=20043) | CO2vib | 1, 37.3, -88., 233 |
CO2(X,v=12252) + CO2(X,v=00051) <-> CO2(X,v=02251) + CO2(X,v=10052) | CO2vib | 1, 33.8, -88., 233 |
CO2(X,v=12252) + CO2(X,v=00051) <-> CO2(X,v=03351) + CO2(X,v=01151) | CO2vib | 1, 35.5, -88., 233 |
CO2(X,v=12252) + CO2(X,v=00051) <-> CO2(X,v=11152) + CO2(X,v=01151) | CO2vib | 1, 35.9, -88., 233 |
CO2(X,v=12252) + CO2(X,v=01151) <-> CO2(X,v=11152) + CO2(X,v=02251) | CO2vib | 1, 36.6, -88., 233 |
CO2(X,v=12252) + CO2(X,v=01151) <-> CO2(X,v=11152) + CO2(X,v=10052) | CO2vib | 1, 36.6, -88., 233 |
CO2(X,v=12252) + CO2(X,v=02251) <-> CO2(X,v=03351) + CO2(X,v=03351) | CO2vib | 1, 36.6, -88., 233 |
CO2(X,v=12252) + CO2(X,v=02251) <-> CO2(X,v=11152) + CO2(X,v=03351) | CO2vib | 1, 37.5, -88., 233 |
CO2(X,v=12252) + CO2(X,v=02251) <-> CO2(X,v=11152) + CO2(X,v=11152) | CO2vib | 1, 37., -88., 233 |
CO2(X,v=12252) + CO2(X,v=03351) <-> CO2(X,v=03351) + CO2(X,v=04451) | CO2vib | 1, 36.9, -88., 233 |
CO2(X,v=12252) + CO2(X,v=03351) <-> CO2(X,v=11152) + CO2(X,v=04451) | CO2vib | 1, 37.3, -88., 23 |
CO2(X,v=12252) + CO2(X,v=03351) <-> CO2(X,v=11152) + CO2(X,v=12252) | CO2vib | 1, 37.3, -88., 233 |
CO2(X,v=12252) + CO2(X,v=10052) <-> CO2(X,v=02251) + CO2(X,v=20053) | CO2vib | 1, 34.9, -89., 234 |
CO2(X,v=12252) + CO2(X,v=10052) <-> CO2(X,v=03351) + CO2(X,v=11152) | CO2vib | 1, 36.9, -88., 233 |
CO2(X,v=12252) + CO2(X,v=10052) <-> CO2(X,v=11152) + CO2(X,v=11152) | CO2vib | 1, 37.3, -88., 233 |
CO2(X,v=12252) + CO2(X,v=11152) <-> CO2(X,v=03351) + CO2(X,v=12252) | CO2vib | 1, 37.3, -88., 233 |
CO2(X,v=12252) + CO2(X,v=11152) <-> CO2(X,v=03351) + CO2(X,v=20053) | CO2vib | 1, 37.3, -88., 233 |
CO2(X,v=13302) + CO2(X,v=00001) <-> CO2(X,v=04401) + CO2(X,v=01101) | CO2vib | 1, 35.7, -88., 233 |
CO2(X,v=13302) + CO2(X,v=00001) <-> CO2(X,v=12202) + CO2(X,v=01101) | CO2vib | 1, 36.2, -88., 233 |
CO2(X,v=13302) + CO2(X,v=01101) <-> CO2(X,v=04401) + CO2(X,v=02201) | CO2vib | 1, 36.4, -88., 233 |
CO2(X,v=13302) + CO2(X,v=01101) <-> CO2(X,v=04401) + CO2(X,v=10002) | CO2vib | 1, 36.4, -88., 233 |
CO2(X,v=13302) + CO2(X,v=01101) <-> CO2(X,v=12202) + CO2(X,v=02201) | CO2vib | 1, 36.9, -88., 233 |
CO2(X,v=13302) + CO2(X,v=01101) <-> CO2(X,v=12202) + CO2(X,v=10002) | CO2vib | 1, 36.9, -88., 233 |
CO2(X,v=13302) + CO2(X,v=02201) <-> CO2(X,v=04401) + CO2(X,v=03301) | CO2vib | 1, 36.8, -88., 233 |
CO2(X,v=13302) + CO2(X,v=02201) <-> CO2(X,v=04401) + CO2(X,v=11102) | CO2vib | 1, 36.8, -88., 233 |
CO2(X,v=13302) + CO2(X,v=02201) <-> CO2(X,v=12202) + CO2(X,v=03301) | CO2vib | 1, 37.5, -88., 233 |
CO2(X,v=13302) + CO2(X,v=02201) <-> CO2(X,v=12202) + CO2(X,v=11102) | CO2vib | 1, 37.3, -88., 233 |
CO2(X,v=13302) + CO2(X,v=10002) <-> CO2(X,v=04401) + CO2(X,v=11102) | CO2vib | 1, 36.4, -88., 233 |
CO2(X,v=13302) + CO2(X,v=10002) <-> CO2(X,v=12202) + CO2(X,v=11102) | CO2vib | 1, 37.6, -88., 233 |
CO2(X,v=13312) + CO2(X,v=00011) <-> CO2(X,v=04411) + CO2(X,v=01111) | CO2vib | 1, 35.7, -88., 233 |
CO2(X,v=13312) + CO2(X,v=00011) <-> CO2(X,v=12212) + CO2(X,v=01111) | CO2vib | 1, 36.2, -88., 233 |
CO2(X,v=13312) + CO2(X,v=01111) <-> CO2(X,v=04411) + CO2(X,v=02211) | CO2vib | 1, 36.4, -88., 233 |
CO2(X,v=13312) + CO2(X,v=01111) <-> CO2(X,v=04411) + CO2(X,v=10012) | CO2vib | 1, 36.4, -88., 233 |
CO2(X,v=13312) + CO2(X,v=01111) <-> CO2(X,v=12212) + CO2(X,v=02211) | CO2vib | 1, 36.9, -88., 233 |
CO2(X,v=13312) + CO2(X,v=01111) <-> CO2(X,v=12212) + CO2(X,v=10012) | CO2vib | 1, 36.9, -88., 233 |
CO2(X,v=13312) + CO2(X,v=02211) <-> CO2(X,v=04411) + CO2(X,v=03311) | CO2vib | 1, 36.8, -88., 233 |
CO2(X,v=13312) + CO2(X,v=02211) <-> CO2(X,v=04411) + CO2(X,v=11112) | CO2vib | 1, 36.8, -88., 233 |
CO2(X,v=13312) + CO2(X,v=02211) <-> CO2(X,v=12212) + CO2(X,v=03311) | CO2vib | 1, 37.5, -88., 233 |
CO2(X,v=13312) + CO2(X,v=02211) <-> CO2(X,v=12212) + CO2(X,v=11112) | CO2vib | 1, 37.3, -88., 233 |
CO2(X,v=13312) + CO2(X,v=10012) <-> CO2(X,v=04411) + CO2(X,v=11112) | CO2vib | 1, 36.4, -88., 233 |
CO2(X,v=13312) + CO2(X,v=10012) <-> CO2(X,v=12212) + CO2(X,v=11112) | CO2vib | 1, 37.6, -88., 233 |
CO2(X,v=13322) + CO2(X,v=00021) <-> CO2(X,v=04421) + CO2(X,v=01121) | CO2vib | 1, 35.7, -88., 233 |
CO2(X,v=13322) + CO2(X,v=00021) <-> CO2(X,v=12222) + CO2(X,v=01121) | CO2vib | 1, 36.2, -88., 233 |
CO2(X,v=13322) + CO2(X,v=01121) <-> CO2(X,v=04421) + CO2(X,v=02221) | CO2vib | 1, 36.4, -88., 233 |
CO2(X,v=13322) + CO2(X,v=01121) <-> CO2(X,v=04421) + CO2(X,v=10022) | CO2vib | 1, 36.4, -88., 233 |
CO2(X,v=13322) + CO2(X,v=01121) <-> CO2(X,v=12222) + CO2(X,v=02221) | CO2vib | 1, 36.9, -88., 233 |
CO2(X,v=13322) + CO2(X,v=01121) <-> CO2(X,v=12222) + CO2(X,v=10022) | CO2vib | 1, 36.9, -88., 233 |
CO2(X,v=13322) + CO2(X,v=02221) <-> CO2(X,v=04421) + CO2(X,v=03321) | CO2vib | 1, 36.8, -88., 233 |
CO2(X,v=13322) + CO2(X,v=02221) <-> CO2(X,v=04421) + CO2(X,v=11122) | CO2vib | 1, 36.8, -88., 233 |
CO2(X,v=13322) + CO2(X,v=02221) <-> CO2(X,v=12222) + CO2(X,v=03321) | CO2vib | 1, 37.5, -88., 233 |
CO2(X,v=13322) + CO2(X,v=02221) <-> CO2(X,v=12222) + CO2(X,v=11122) | CO2vib | 1, 37.3, -88., 233 |
CO2(X,v=13322) + CO2(X,v=10022) <-> CO2(X,v=04421) + CO2(X,v=11122) | CO2vib | 1, 36.4, -88., 233 |
CO2(X,v=13322) + CO2(X,v=10022) <-> CO2(X,v=12222) + CO2(X,v=11122) | CO2vib | 1, 37.6, -88., 233 |
CO2(X,v=13332) + CO2(X,v=00031) <-> CO2(X,v=04431) + CO2(X,v=01131) | CO2vib | 1, 35.7, -88., 233 |
CO2(X,v=13332) + CO2(X,v=00031) <-> CO2(X,v=12232) + CO2(X,v=01131) | CO2vib | 1, 36.2, -88., 233 |
CO2(X,v=13332) + CO2(X,v=01131) <-> CO2(X,v=04431) + CO2(X,v=02231) | CO2vib | 1, 36.4, -88., 233 |
CO2(X,v=13332) + CO2(X,v=01131) <-> CO2(X,v=04431) + CO2(X,v=10032) | CO2vib | 1, 36.4, -88., 233 |
CO2(X,v=13332) + CO2(X,v=01131) <-> CO2(X,v=12232) + CO2(X,v=02231) | CO2vib | 1, 36.9, -88., 233 |
CO2(X,v=13332) + CO2(X,v=01131) <-> CO2(X,v=12232) + CO2(X,v=10032) | CO2vib | 1, 36.9, -88., 233 |
CO2(X,v=13332) + CO2(X,v=02231) <-> CO2(X,v=04431) + CO2(X,v=03331) | CO2vib | 1, 36.8, -88., 233 |
CO2(X,v=13332) + CO2(X,v=02231) <-> CO2(X,v=04431) + CO2(X,v=11132) | CO2vib | 1, 36.8, -88., 233 |
CO2(X,v=13332) + CO2(X,v=02231) <-> CO2(X,v=12232) + CO2(X,v=03331) | CO2vib | 1, 37.5, -88., 233 |
CO2(X,v=13332) + CO2(X,v=02231) <-> CO2(X,v=12232) + CO2(X,v=11132) | CO2vib | 1, 37.3, -88., 233 |
CO2(X,v=13332) + CO2(X,v=10032) <-> CO2(X,v=04431) + CO2(X,v=11132) | CO2vib | 1, 36.4, -88., 233 |
CO2(X,v=13332) + CO2(X,v=10032) <-> CO2(X,v=12232) + CO2(X,v=11132) | CO2vib | 1, 37.6, -88., 233 |
CO2(X,v=13342) + CO2(X,v=00041) <-> CO2(X,v=04441) + CO2(X,v=01141) | CO2vib | 1, 35.7, -88., 233 |
CO2(X,v=13342) + CO2(X,v=00041) <-> CO2(X,v=12242) + CO2(X,v=01141) | CO2vib | 1, 36.2, -88., 233 |
CO2(X,v=13342) + CO2(X,v=01141) <-> CO2(X,v=04441) + CO2(X,v=02241) | CO2vib | 1, 36.4, -88., 233 |
CO2(X,v=13342) + CO2(X,v=01141) <-> CO2(X,v=04441) + CO2(X,v=10042) | CO2vib | 1, 36.4, -88., 233 |
CO2(X,v=13342) + CO2(X,v=01141) <-> CO2(X,v=12242) + CO2(X,v=02241) | CO2vib | 1, 36.9, -88., 233 |
CO2(X,v=13342) + CO2(X,v=01141) <-> CO2(X,v=12242) + CO2(X,v=10042) | CO2vib | 1, 36.9, -88., 233 |
CO2(X,v=13342) + CO2(X,v=02241) <-> CO2(X,v=04441) + CO2(X,v=03341) | CO2vib | 1, 36.8, -88., 233 |
CO2(X,v=13342) + CO2(X,v=02241) <-> CO2(X,v=04441) + CO2(X,v=11142) | CO2vib | 1, 36.8, -88., 233 |
CO2(X,v=13342) + CO2(X,v=02241) <-> CO2(X,v=12242) + CO2(X,v=03341) | CO2vib | 1, 37.5, -88., 233 |
CO2(X,v=13342) + CO2(X,v=02241) <-> CO2(X,v=12242) + CO2(X,v=11142) | CO2vib | 1, 37.3, -88., 233 |
CO2(X,v=13342) + CO2(X,v=10042) <-> CO2(X,v=04441) + CO2(X,v=11142) | CO2vib | 1, 36.4, -88., 233 |
CO2(X,v=13342) + CO2(X,v=10042) <-> CO2(X,v=12242) + CO2(X,v=11142) | CO2vib | 1, 37.6, -88., 233 |
CO2(X,v=13352) + CO2(X,v=00051) <-> CO2(X,v=04451) + CO2(X,v=01151) | CO2vib | 1, 35.7, -88., 233 |
CO2(X,v=13352) + CO2(X,v=00051) <-> CO2(X,v=12252) + CO2(X,v=01151) | CO2vib | 1, 36.2, -88., 233 |
CO2(X,v=13352) + CO2(X,v=01151) <-> CO2(X,v=04451) + CO2(X,v=02251) | CO2vib | 1, 36.4, -88., 233 |
CO2(X,v=13352) + CO2(X,v=01151) <-> CO2(X,v=04451) + CO2(X,v=10052) | CO2vib | 1, 36.4, -88., 233 |
CO2(X,v=13352) + CO2(X,v=01151) <-> CO2(X,v=12252) + CO2(X,v=02251) | CO2vib | 1, 36.9, -88., 233 |
CO2(X,v=13352) + CO2(X,v=01151) <-> CO2(X,v=12252) + CO2(X,v=10052) | CO2vib | 1, 36.9, -88., 233 |
CO2(X,v=13352) + CO2(X,v=02251) <-> CO2(X,v=04451) + CO2(X,v=03351) | CO2vib | 1, 36.8, -88., 233 |
CO2(X,v=13352) + CO2(X,v=02251) <-> CO2(X,v=04451) + CO2(X,v=11152) | CO2vib | 1, 36.8, -88., 233 |
CO2(X,v=13352) + CO2(X,v=02251) <-> CO2(X,v=12252) + CO2(X,v=03351) | CO2vib | 1, 37.5, -88., 233 |
CO2(X,v=13352) + CO2(X,v=02251) <-> CO2(X,v=12252) + CO2(X,v=11152) | CO2vib | 1, 37.3, -88., 233 |
CO2(X,v=13352) + CO2(X,v=10052) <-> CO2(X,v=04451) + CO2(X,v=11152) | CO2vib | 1, 36.4, -88., 233 |
```

```
CO2(X,v=13352) + CO2(X,v=10052) <-> CO2(X,v=12252) + CO2(X,v=11152) | CO2vib | 1, 37.6, -88., 233 |
CO2(X,v=20003) + CO2(X,v=00001) <-> CO2(X,v=10002) + CO2(X,v=10002) | CO2vib | 1, 34.9, -89., 234 |
CO2(X,v=20003) + CO2(X,v=00001) <-> CO2(X,v=11102) + CO2(X,v=01101) | CO2vib | 1, 35.9, -88., 233 |
CO2(X,v=20003) + CO2(X,v=01101) <-> CO2(X,v=11102) + CO2(X,v=02201) | CO2vib | 1, 36.6, -88., 233 |
CO2(X,v=20003) + CO2(X,v=01101) <-> CO2(X,v=11102) + CO2(X,v=10002) | CO2vib | 1, 36.7, -88.2, 233 |
CO2(X,v=20003) + CO2(X,v=02201) <-> CO2(X,v=11102) + CO2(X,v=03301) | CO2vib | 1, 37., -88., 233 |
CO2(X,v=20003) + CO2(X,v=02201) <-> CO2(X,v=11102) + CO2(X,v=11102) | CO2vib | 1, 37., -88., 233 |
CO2(X,v=20003) + CO2(X,v=03301) <-> CO2(X,v=11102) + CO2(X,v=04401) | CO2vib | 1, 37.3, -88., 233 |
CO2(X,v=20003) + CO2(X,v=10002) <-> CO2(X,v=11102) + CO2(X,v=11102) | CO2vib | 1, 37.3, -88., 233 |
CO2(X,v=20003) + CO2(X,v=11102) <-> CO2(X,v=11102) + CO2(X,v=12202) | CO2vib | 1, 37.7, -88., 233 |
CO2(X,v=20013) + CO2(X,v=00011) <-> CO2(X,v=10012) + CO2(X,v=10012) | CO2vib | 1, 34.9, -89., 234 |
CO2(X,v=20013) + CO2(X,v=00011) <-> CO2(X,v=11112) + CO2(X,v=01111) | CO2vib | 1, 35.9, -88., 233 |
CO2(X,v=20013) + CO2(X,v=01111) <-> CO2(X,v=11112) + CO2(X,v=02211) | CO2vib | 1, 36.6, -88., 233 |
CO2(X,v=20013) + CO2(X,v=01111) <-> CO2(X,v=11112) + CO2(X,v=10012) | CO2vib | 1, 36.7, -88.2, 233 |
CO2(X,v=20013) + CO2(X,v=02211) <-> CO2(X,v=11112) + CO2(X,v=03311) | CO2vib | 1, 37., -88., 233 |
CO2(X,v=20013) + CO2(X,v=02211) <-> CO2(X,v=11112) + CO2(X,v=11112) | CO2vib | 1, 37., -88., 233 |
CO2(X,v=20013) + CO2(X,v=03311) <-> CO2(X,v=11112) + CO2(X,v=04411) | CO2vib | 1, 37.3, -88., 233 |
CO2(X,v=20013) + CO2(X,v=10012) <-> CO2(X,v=11112) + CO2(X,v=11112) | CO2vib | 1, 37.3, -88., 233 |
CO2(X,v=20013) + CO2(X,v=11112) <-> CO2(X,v=11112) + CO2(X,v=12212) | CO2vib | 1, 37.7, -88., 233 |
CO2(X,v=20023) + CO2(X,v=00021) <-> CO2(X,v=10022) + CO2(X,v=10022) | CO2vib | 1, 34.9, -89., 234 |
CO2(X,v=20023) + CO2(X,v=00021) <-> CO2(X,v=11122) + CO2(X,v=01121) | CO2vib | 1, 35.9, -88., 233 |
CO2(X,v=20023) + CO2(X,v=01121) <-> CO2(X,v=11122) + CO2(X,v=02221) | CO2vib | 1, 36.6, -88., 233 |
CO2(X,v=20023) + CO2(X,v=01121) <-> CO2(X,v=11122) + CO2(X,v=10022) | CO2vib | 1, 36.7, -88.2, 233 |
CO2(X,v=20023) + CO2(X,v=02221) <-> CO2(X,v=11122) + CO2(X,v=03321) | CO2vib | 1, 37., -88., 233 |
CO2(X,v=20023) + CO2(X,v=02221) <-> CO2(X,v=11122) + CO2(X,v=11122) | CO2vib | 1, 37., -88., 233 |
CO2(X,v=20023) + CO2(X,v=03321) <-> CO2(X,v=11122) + CO2(X,v=04421) | CO2vib | 1, 37.3, -88., 233 |
CO2(X,v=20023) + CO2(X,v=10022) <-> CO2(X,v=11122) + CO2(X,v=11122) | CO2vib | 1, 37.3, -88., 233 |
CO2(X,v=20023) + CO2(X,v=11122) <-> CO2(X,v=11122) + CO2(X,v=12222) | CO2vib | 1, 37.7, -88., 233 |
CO2(X,v=20033) + CO2(X,v=00031) <-> CO2(X,v=10032) + CO2(X,v=10032) | CO2vib | 1, 34.9, -89., 234 |
CO2(X,v=20033) + CO2(X,v=00031) <-> CO2(X,v=11132) + CO2(X,v=01131) | CO2vib | 1, 35.9, -88., 233 |
CO2(X,v=20033) + CO2(X,v=01131) <-> CO2(X,v=11132) + CO2(X,v=02231) | CO2vib | 1, 36.6, -88., 233 |
CO2(X,v=20033) + CO2(X,v=01131) <-> CO2(X,v=11132) + CO2(X,v=10032) | CO2vib | 1, 36.7, -88.2, 233 |
CO2(X,v=20033) + CO2(X,v=02231) <-> CO2(X,v=11132) + CO2(X,v=03331) | CO2vib | 1, 37., -88., 233 |
CO2(X,v=20033) + CO2(X,v=02231) <-> CO2(X,v=11132) + CO2(X,v=11132) | CO2vib | 1, 37., -88., 233 |
CO2(X,v=20033) + CO2(X,v=03331) <-> CO2(X,v=11132) + CO2(X,v=04431) | CO2vib | 1, 37.3, -88., 233 |
CO2(X,v=20033) + CO2(X,v=10032) <-> CO2(X,v=11132) + CO2(X,v=11132) | CO2vib | 1, 37.3, -88., 233 |
CO2(X,v=20033) + CO2(X,v=11132) <-> CO2(X,v=11132) + CO2(X,v=12232) | CO2vib | 1, 37.7, -88., 233 |
CO2(X,v=20043) + CO2(X,v=00041) <-> CO2(X,v=10042) + CO2(X,v=10042) | CO2vib | 1, 34.9, -89., 234 |
CO2(X,v=20043) + CO2(X,v=00041) <-> CO2(X,v=11142) + CO2(X,v=01141) | CO2vib | 1, 35.9, -88., 233 |
CO2(X,v=20043) + CO2(X,v=01141) <-> CO2(X,v=11142) + CO2(X,v=02241) | CO2vib | 1, 36.6, -88., 233 |
CO2(X,v=20043) + CO2(X,v=01141) <-> CO2(X,v=11142) + CO2(X,v=10042) | CO2vib | 1, 36.7, -88.2, 233 |
CO2(X,v=20043) + CO2(X,v=02241) <-> CO2(X,v=11142) + CO2(X,v=03341) | CO2vib | 1, 37., -88., 233 |
CO2(X,v=20043) + CO2(X,v=02241) <-> CO2(X,v=11142) + CO2(X,v=11142) | CO2vib | 1, 37., -88., 233 |
CO2(X,v=20043) + CO2(X,v=03341) <-> CO2(X,v=11142) + CO2(X,v=04441) | CO2vib | 1, 37.3, -88., 233 |
CO2(X,v=20043) + CO2(X,v=10042) <-> CO2(X,v=11142) + CO2(X,v=11142) | CO2vib | 1, 37.3, -88., 233 |
CO2(X,v=20043) + CO2(X,v=11142) <-> CO2(X,v=11142) + CO2(X,v=12242) | CO2vib | 1, 37.7, -88., 233 |
CO2(X,v=20053) + CO2(X,v=00051) <-> CO2(X,v=10052) + CO2(X,v=10052) | CO2vib | 1, 34.9, -89., 234 |
CO2(X,v=20053) + CO2(X,v=00051) <-> CO2(X,v=11152) + CO2(X,v=01151) | CO2vib | 1, 35.9, -88., 233 |
CO2(X,v=20053) + CO2(X,v=01151) <-> CO2(X,v=11152) + CO2(X,v=02251) | CO2vib | 1, 36.6, -88., 233 |
CO2(X,v=20053) + CO2(X,v=01151) <-> CO2(X,v=11152) + CO2(X,v=10052) | CO2vib | 1, 36.7, -88.2, 233 |
CO2(X,v=20053) + CO2(X,v=02251) <-> CO2(X,v=11152) + CO2(X,v=03351) | CO2vib | 1, 37., -88., 233 |
CO2(X,v=20053) + CO2(X,v=02251) <-> CO2(X,v=11152) + CO2(X,v=11152) | CO2vib | 1, 37., -88., 233 |
CO2(X,v=20053) + CO2(X,v=03351) <-> CO2(X,v=11152) + CO2(X,v=04451) | CO2vib | 1, 37.3, -88., 233 |
CO2(X,v=20053) + CO2(X,v=10052) <-> CO2(X,v=11152) + CO2(X,v=11152) | CO2vib | 1, 37.3, -88., 233 |
CO2(X,v=20053) + CO2(X,v=11152) <-> CO2(X,v=11152) + CO2(X,v=12252) | CO2vib | 1, 37.7, -88., 233 |
CO2(X,v=21103) + CO2(X,v=00001) <-> CO2(X,v=12202) + CO2(X,v=01101) | CO2vib | 1, 36.2, -88., 233 |
CO2(X,v=21103) + CO2(X,v=00001) <-> CO2(X,v=20003) + CO2(X,v=01101) | CO2vib | 1, 36.3, -88., 233 |
CO2(X,v=21103) + CO2(X,v=01101) <-> CO2(X,v=12202) + CO2(X,v=02201) | CO2vib | 1, 36.9, -88., 233 |
CO2(X,v=21103) + CO2(X,v=01101) <-> CO2(X,v=12202) + CO2(X,v=10002) | CO2vib | 1, 36.9, -88., 233 |
CO2(X,v=21103) + CO2(X,v=01101) <-> CO2(X,v=20003) + CO2(X,v=02201) | CO2vib | 1, 37., -88., 233 |
CO2(X,v=21103) + CO2(X,v=01101) <-> CO2(X,v=20003) + CO2(X,v=10002) | CO2vib | 1, 37., -98., 233 |
CO2(X,v=21103) + CO2(X,v=02201) <-> CO2(X,v=12202) + CO2(X,v=03301) | CO2vib | 1, 37.3, -88., 233 |
CO2(X,v=21103) + CO2(X,v=02201) <-> CO2(X,v=12202) + CO2(X,v=11102) | CO2vib | 1, 37.5, -88., 233 |
CO2(X,v=21103) + CO2(X,v=02201) <-> CO2(X,v=20003) + CO2(X,v=03301) | CO2vib | 1, 37.4, -88., 233 |
CO2(X,v=21103) + CO2(X,v=02201) <-> CO2(X,v=20003) + CO2(X,v=11102) | CO2vib | 1, 37.4, -88., 233 |
CO2(X,v=21103) + CO2(X,v=03301) <-> CO2(X,v=12202) + CO2(X,v=12202) | CO2vib | 1, 37.6, -88., 233 |
CO2(X,v=21103) + CO2(X,v=03301) <-> CO2(X,v=20003) + CO2(X,v=04401) | CO2vib | 1, 37.7, -88., 233 |
CO2(X,v=21103) + CO2(X,v=10002) <-> CO2(X,v=12202) + CO2(X,v=11102) | CO2vib | 1, 37.6, -88., 233 |
CO2(X,v=21103) + CO2(X,v=10002) <-> CO2(X,v=20003) + CO2(X,v=11102) | CO2vib | 1, 37.8, -88., 233 |
CO2(X,v=21103) + CO2(X,v=11102) <-> CO2(X,v=20003) + CO2(X,v=12202) | CO2vib | 1, 38.1, -88., 233 |
CO2(X,v=21103) + CO2(X,v=11102) <-> CO2(X,v=20003) + CO2(X,v=20003) | CO2vib | 1, 38.1, -88., 233 |
CO2(X,v=21113) + CO2(X,v=00011) <-> CO2(X,v=12212) + CO2(X,v=01111) | CO2vib | 1, 36.2, -88., 233 |
CO2(X,v=21113) + CO2(X,v=00011) <-> CO2(X,v=20013) + CO2(X,v=01111) | CO2vib | 1, 36.3, -88., 233 |
CO2(X,v=21113) + CO2(X,v=01111) <-> CO2(X,v=12212) + CO2(X,v=02211) | CO2vib | 1, 36.9, -88., 233 |
CO2(X,v=21113) + CO2(X,v=01111) <-> CO2(X,v=12212) + CO2(X,v=10012) | CO2vib | 1, 36.9, -88., 233 |
CO2(X,v=21113) + CO2(X,v=01111) <-> CO2(X,v=20013) + CO2(X,v=02211) | CO2vib | 1, 37., -88., 233 |
CO2(X,v=21113) + CO2(X,v=01111) <-> CO2(X,v=20013) + CO2(X,v=10012) | CO2vib | 1, 37., -98., 233 |
CO2(X,v=21113) + CO2(X,v=02211) <-> CO2(X,v=12212) + CO2(X,v=03311) | CO2vib | 1, 37.3, -88., 233 |
CO2(X,v=21113) + CO2(X,v=02211) <-> CO2(X,v=12212) + CO2(X,v=11112) | CO2vib | 1, 37.5, -88., 233 |
CO2(X,v=21113) + CO2(X,v=02211) <-> CO2(X,v=20013) + CO2(X,v=03311) | CO2vib | 1, 37.4, -88., 233 |
CO2(X,v=21113) + CO2(X,v=02211) <-> CO2(X,v=20013) + CO2(X,v=11112) | CO2vib | 1, 37.4, -88., 233 |
CO2(X,v=21113) + CO2(X,v=03311) <-> CO2(X,v=12212) + CO2(X,v=12212) | CO2vib | 1, 37.6, -88., 233 |
CO2(X,v=21113) + CO2(X,v=03311) <-> CO2(X,v=20013) + CO2(X,v=04411) | CO2vib | 1, 37.7, -88., 233 |
CO2(X,v=21113) + CO2(X,v=10012) <-> CO2(X,v=12212) + CO2(X,v=11112) | CO2vib | 1, 37.6, -88., 233 |
CO2(X,v=21113) + CO2(X,v=10012) <-> CO2(X,v=20013) + CO2(X,v=11112) | CO2vib | 1, 37.8, -88., 233 |
CO2(X,v=21113) + CO2(X,v=11112) <-> CO2(X,v=20013) + CO2(X,v=12212) | CO2vib | 1, 38.1, -88., 233 |
CO2(X,v=21113) + CO2(X,v=11112) <-> CO2(X,v=20013) + CO2(X,v=20013) | CO2vib | 1, 38.1, -88., 233 |
CO2(X,v=21123) + CO2(X,v=00021) <-> CO2(X,v=12222) + CO2(X,v=01121) | CO2vib | 1, 36.2, -88., 233 |
CO2(X,v=21123) + CO2(X,v=00021) <-> CO2(X,v=20023) + CO2(X,v=01121) | CO2vib | 1, 36.3, -88., 233 |
CO2(X,v=21123) + CO2(X,v=01121) <-> CO2(X,v=12222) + CO2(X,v=02221) | CO2vib | 1, 36.9, -88., 233 |
CO2(X,v=21123) + CO2(X,v=01121) <-> CO2(X,v=12222) + CO2(X,v=10022) | CO2vib | 1, 36.9, -88., 233 |
CO2(X,v=21123) + CO2(X,v=01121) <-> CO2(X,v=20023) + CO2(X,v=02221) | CO2vib | 1, 37., -88., 233 |
CO2(X,v=21123) + CO2(X,v=01121) <-> CO2(X,v=20023) + CO2(X,v=10022) | CO2vib | 1, 37., -98., 233 |
CO2(X,v=21123) + CO2(X,v=02221) <-> CO2(X,v=12222) + CO2(X,v=03321) | CO2vib | 1, 37.3, -88., 233 |
```

```
CO2(X,v=21123) + CO2(X,v=02221) <-> CO2(X,v=12222) + CO2(X,v=11122) | CO2vib | 1, 37.5, -88., 233 |
CO2(X,v=21123) + CO2(X,v=02221) <-> CO2(X,v=20023) + CO2(X,v=03321) | CO2vib | 1, 37.4, -88., 233 |
CO2(X,v=21123) + CO2(X,v=02221) <-> CO2(X,v=20023) + CO2(X,v=11122) | CO2vib | 1, 37.4, -88., 233 |
CO2(X,v=21123) + CO2(X,v=03321) <-> CO2(X,v=12222) + CO2(X,v=12222) | CO2vib | 1, 37.6, -88., 233 |
CO2(X,v=21123) + CO2(X,v=03321) <-> CO2(X,v=20023) + CO2(X,v=04421) | CO2vib | 1, 37.7, -88., 233 |
CO2(X,v=21123) + CO2(X,v=10022) <-> CO2(X,v=12222) + CO2(X,v=11122) | CO2vib | 1, 37.6, -88., 233 |
CO2(X,v=21123) + CO2(X,v=10022) <-> CO2(X,v=20023) + CO2(X,v=11122) | CO2vib | 1, 37.8, -88., 233 |
CO2(X,v=21123) + CO2(X,v=11122) <-> CO2(X,v=20023) + CO2(X,v=12222) | CO2vib | 1, 38.1, -88., 233 |
CO2(X,v=21123) + CO2(X,v=11122) <-> CO2(X,v=20023) + CO2(X,v=20023) | CO2vib | 1, 38.1, -88., 233 |
CO2(X,v=21133) + CO2(X,v=00031) <-> CO2(X,v=12232) + CO2(X,v=01131) | CO2vib | 1, 36.2, -88., 233 |
CO2(X,v=21133) + CO2(X,v=00031) <-> CO2(X,v=20033) + CO2(X,v=01131) | CO2vib | 1, 36.3, -88., 233 |
CO2(X,v=21133) + CO2(X,v=01131) <-> CO2(X,v=12232) + CO2(X,v=02231) | CO2vib | 1, 36.9, -88., 233 |
CO2(X,v=21133) + CO2(X,v=01131) <-> CO2(X,v=12232) + CO2(X,v=10032) | CO2vib | 1, 36.9, -88., 233 |
CO2(X,v=21133) + CO2(X,v=01131) <-> CO2(X,v=20033) + CO2(X,v=02231) | CO2vib | 1, 37., -88., 233 |
CO2(X,v=21133) + CO2(X,v=01131) <-> CO2(X,v=20033) + CO2(X,v=10032) | CO2vib | 1, 37., -98., 233 |
CO2(X,v=21133) + CO2(X,v=02231) <-> CO2(X,v=12232) + CO2(X,v=03331) | CO2vib | 1, 37.3, -88., 233 |
CO2(X,v=21133) + CO2(X,v=02231) <-> CO2(X,v=12232) + CO2(X,v=11132) | CO2vib | 1, 37.5, -88., 233 |
CO2(X,v=21133) + CO2(X,v=02231) <-> CO2(X,v=20033) + CO2(X,v=03331) | CO2vib | 1, 37.4, -88., 233 |
CO2(X,v=21133) + CO2(X,v=02231) <-> CO2(X,v=20033) + CO2(X,v=11132) | CO2vib | 1, 37.4, -88., 233 |
CO2(X,v=21133) + CO2(X,v=03331) <-> CO2(X,v=12232) + CO2(X,v=12232) | CO2vib | 1, 37.6, -88., 233 |
CO2(X,v=21133) + CO2(X,v=03331) <-> CO2(X,v=20033) + CO2(X,v=04431) | CO2vib | 1, 37.7, -88., 233 |
CO2(X,v=21133) + CO2(X,v=10032) <-> CO2(X,v=12232) + CO2(X,v=11132) | CO2vib | 1, 37.6, -88., 233 |
CO2(X,v=21133) + CO2(X,v=10032) <-> CO2(X,v=20033) + CO2(X,v=11132) | CO2vib | 1, 37.8, -88., 233 |
CO2(X,v=21133) + CO2(X,v=11132) <-> CO2(X,v=20033) + CO2(X,v=12232) | CO2vib | 1, 38.1, -88., 233 |
CO2(X,v=21133) + CO2(X,v=11132) <-> CO2(X,v=20033) + CO2(X,v=20033) | CO2vib | 1, 38.1, -88., 233 |
CO2(X,v=21143) + CO2(X,v=00041) <-> CO2(X,v=12242) + CO2(X,v=01141) | CO2vib | 1, 36.2, -88., 233 |
CO2(X,v=21143) + CO2(X,v=00041) <-> CO2(X,v=20043) + CO2(X,v=01141) | CO2vib | 1, 36.3, -88., 233 |
CO2(X,v=21143) + CO2(X,v=01141) <-> CO2(X,v=12242) + CO2(X,v=02241) | CO2vib | 1, 36.9, -88., 233 |
CO2(X,v=21143) + CO2(X,v=01141) <-> CO2(X,v=12242) + CO2(X,v=10042) | CO2vib | 1, 36.9, -88., 233 |
CO2(X,v=21143) + CO2(X,v=01141) <-> CO2(X,v=20043) + CO2(X,v=02241) | CO2vib | 1, 37., -88., 233 |
CO2(X,v=21143) + CO2(X,v=01141) <-> CO2(X,v=20043) + CO2(X,v=10042) | CO2vib | 1, 37., -98., 233 |
CO2(X,v=21143) + CO2(X,v=02241) <-> CO2(X,v=12242) + CO2(X,v=03341) | CO2vib | 1, 37.3, -88., 233 |
CO2(X,v=21143) + CO2(X,v=02241) <-> CO2(X,v=12242) + CO2(X,v=11142) | CO2vib | 1, 37.5, -88., 233 |
CO2(X,v=21143) + CO2(X,v=02241) <-> CO2(X,v=20043) + CO2(X,v=03341) | CO2vib | 1, 37.4, -88., 233 |
CO2(X,v=21143) + CO2(X,v=02241) <-> CO2(X,v=20043) + CO2(X,v=11142) | CO2vib | 1, 37.4, -88., 233 |
CO2(X,v=21143) + CO2(X,v=03341) <-> CO2(X,v=12242) + CO2(X,v=12242) | CO2vib | 1, 37.6, -88., 233 |
CO2(X,v=21143) + CO2(X,v=03341) <-> CO2(X,v=20043) + CO2(X,v=04441) | CO2vib | 1, 37.7, -88., 233 |
CO2(X,v=21143) + CO2(X,v=10042) <-> CO2(X,v=12242) + CO2(X,v=11142) | CO2vib | 1, 37.6, -88., 233 |
CO2(X,v=21143) + CO2(X,v=10042) <-> CO2(X,v=20043) + CO2(X,v=11142) | CO2vib | 1, 37.8, -88., 233 |
CO2(X,v=21143) + CO2(X,v=11142) <-> CO2(X,v=20043) + CO2(X,v=12242) | CO2vib | 1, 38.1, -88., 233 |
CO2(X,v=21143) + CO2(X,v=11142) <-> CO2(X,v=20043) + CO2(X,v=20043) | CO2vib | 1, 38.1, -88., 233 |
CO2(X,v=21153) + CO2(X,v=00051) <-> CO2(X,v=12252) + CO2(X,v=01151) | CO2vib | 1, 36.2, -88., 233 |
CO2(X,v=21153) + CO2(X,v=00051) <-> CO2(X,v=20053) + CO2(X,v=01151) | CO2vib | 1, 36.3, -88., 233 |
CO2(X,v=21153) + CO2(X,v=01151) <-> CO2(X,v=12252) + CO2(X,v=02251) | CO2vib | 1, 36.9, -88., 233 |
CO2(X,v=21153) + CO2(X,v=01151) <-> CO2(X,v=12252) + CO2(X,v=10052) | CO2vib | 1, 36.9, -88., 233 |
CO2(X,v=21153) + CO2(X,v=01151) <-> CO2(X,v=20053) + CO2(X,v=02251) | CO2vib | 1, 37., -88., 233 |
CO2(X,v=21153) + CO2(X,v=01151) <-> CO2(X,v=20053) + CO2(X,v=10052) | CO2vib | 1, 37., -98., 233 |
CO2(X,v=21153) + CO2(X,v=02251) <-> CO2(X,v=12252) + CO2(X,v=03351) | CO2vib | 1, 37.3, -88., 233 |
CO2(X,v=21153) + CO2(X,v=02251) <-> CO2(X,v=12252) + CO2(X,v=11152) | CO2vib | 1, 37.5, -88., 233 |
CO2(X,v=21153) + CO2(X,v=02251) <-> CO2(X,v=20053) + CO2(X,v=03351) | CO2vib | 1, 37.4, -88., 233 |
CO2(X,v=21153) + CO2(X,v=02251) <-> CO2(X,v=20053) + CO2(X,v=11152) | CO2vib | 1, 37.4, -88., 233 |
CO2(X,v=21153) + CO2(X,v=03351) <-> CO2(X,v=12252) + CO2(X,v=12252) | CO2vib | 1, 37.6, -88., 233 |
CO2(X,v=21153) + CO2(X,v=03351) <-> CO2(X,v=20053) + CO2(X,v=04451) | CO2vib | 1, 37.7, -88., 233 |
CO2(X,v=21153) + CO2(X,v=10052) <-> CO2(X,v=12252) + CO2(X,v=11152) | CO2vib | 1, 37.6, -88., 233 |
CO2(X,v=21153) + CO2(X,v=10052) <-> CO2(X,v=20053) + CO2(X,v=11152) | CO2vib | 1, 37.8, -88., 233 |
CO2(X,v=21153) + CO2(X,v=11152) <-> CO2(X,v=20053) + CO2(X,v=12252) | CO2vib | 1, 38.1, -88., 233 |
CO2(X,v=21153) + CO2(X,v=11152) <-> CO2(X,v=20053) + CO2(X,v=20053) | CO2vib | 1, 38.1, -88., 233 |
```